THE HONG KONG
POLYTECHNIC UNIVERSITY
香港理工大學
Pao Yue-kong Library
包玉剛圖書館

Copyright Undertaking

This thesis is protected by copyright, with all rights reserved.

By reading and using the thesis, the reader understands and agrees to the following terms:

1. The reader will abide by the rules and legal ordinances governing copyright regarding the use of the thesis.
2. The reader will use the thesis for the purpose of research or private study only and not for distribution or further reproduction or any other purpose.
3. The reader agrees to indemnify and hold the University harmless from and against any loss, damage, cost, liability or expenses arising from copyright infringement or unauthorized usage.

IMPORTANT

If you have reasons to believe that any materials in this thesis are deemed not suitable to be distributed in this form, or a copyright owner having difficulty with the material being included in our database, please contact lbsys@polyu.edu.hk providing details. The Library will look into your claim and consider taking remedial action upon receipt of the written requests.

Pao Yue-kong Library, The Hong Kong Polytechnic University, Hung Hom, Kowloon, Hong Kong

http://www.lib.polyu.edu.hk

NOVEL BIOSENSING PLATFORMS FOR A FAST SCREENING OF MILK CONTAMINANTS AND PROSTATE CANCER

TSOI TIK HUNG

Ph.D

The Hong Kong Polytechnic University

2017

The Hong Kong Polytechnic University

Department of Applied Biology and Chemical Technology

Novel biosensing platforms for a fast screening of milk contaminants and prostate cancer

Tsoi Tik Hung

A thesis submitted in partial fulfilment of the requirements for the degree of Doctor of Philosophy

March, 2017

Certificate of Originality

I hereby declare that this thesis is my own work and that, to the best of my knowledge and belief, it reproduces no material previously published or written, nor material that has been accepted for the award of any other degree or diploma, except where due acknowledgement has been made in the text.

_____ (Signed)

_____Tsoi Tik Hung_____(Name of student)

Abstract

Throughout the past decades, the rapid and prosperous development in analytical sciences has allowed scientists to take a deeper insight into more difficult multi-disciplinary research problems. One of the best outcomes of such multidimensionality lies in the evolvement of the concept of biosensor, a major research area among contemporary analytical scientists. Some fundamentals on this discipline will be given in Chapter One. Research and development never stop and scientists keep on designing different types of biosensing techniques for addressing different existing analytical problems. Similarly, this work aims to address two important public health concerns, particularly in food-safety and clinical area, by developing rapid biosensing methods through a smart design and application of small particles with specific properties.

The first public concern is related to milk safety. In China, the milk safety issue has aroused citizens' high concern due to the detection of different harmful contaminants present in milk. A recent notorious incident was the adulterant melamine scandal in 2008, which melamine was illegally abused to boost nitrogen levels during protein tests. Other than that, different undesired preservatives, synthetic hormones, antibiotics, bacteria and pathogens were reported to be food hazards to citizens. To ensure milk safety, a lot of monitoring works are needed and therefore a fast and multiplex screening method is in demand by food regulatory units. In Chapter Two, the development of a sensing method towards melamine based on the use of magnetic microspheres and flow cytometric

immunoassay is reported. Detection can be achieved in a simple, sensitive, specific, high-throughput and organic solvent-free manner.

Another public health concern is related to prostate cancer (PCa), one of the commonest male-related cancers in the world with an increasing incidence rate. Hong Kong is no exception in this public health issue. Nevertheless, current screening methods towards PCa are not perfect enough. We have an urgent demand for more sensitive and accurate diagnostic biomarkers or methods to detect early PCa and improve the treatment outcome, given the latency of early, treatable PCa and the lethality of its late, discernible stage. In Chapter Three, it reports and discusses the results of our large-cohort study on urinary polyamine levels of suspected PCa patients. A useful biomarker, urinary spermine, was discovered and its usefulness in PCa detection was demonstrated. Based on this finding, Chapter Four focuses on the development of a rapid sensing method towards this novel biomarker via the use of DNA and gold nanoparticles. Any aggregations of gold nanoparticles induced by spermine would shift its absorption band and results in a distinct color change, which can be observed directly by naked eyes and acts as a mean of simple and indirect sensing of urinary spermine. This design would certainly help in diagnosing PCa in the future.

Overall, this work takes a step towards in tackling the abovementioned public health problems.

Acknowledgements

Hereby I would like to devote my wholehearted gratitude to the following persons:

First and foremost, I sincerely express my thankfulness to my supervisor Prof. Wing-Tak Wong for his generous support, guidance and encouragement during my PhD study. Lots of chances from works, together with his enlightening advices have conferred me invaluable experiences and expanded my horizon no matter in research or personal levels. I dedicate this thesis to him and wish him and his family all the best.

Second, I would like to thank all the former and current Wong's group members: Dr. Ka-Leung Wong, Dr. Ga-Lai Law, Dr. Yan-Juan Gu, Dr. Chi-Tung Yeung, Dr. Wai-Sum Lo, Dr. Chi-Fai Chan and Mr. Yuk-Wang Yip for their valuable discussions and indispensable helping hands.

Third, I express my appreciation to all collaborators for their grateful supports and inspiring discussions to my work presented in this thesis. I thank Dr. Ka-Fung Chiu and Prof. Chi-Fai Ng from The Chinese University of Hong Kong for providing clinical samples and advices on clinical issues.

Equally important is to acknowledge the help from technicians and scientific officers of the Department of Applied Biology and Chemical Technology, especially Dr. Pui-Kin So and Dr. Wai-Ting Wong for their unlimited supports on instrumentation problems.

My special thank also goes to my ex-colleagues Dr. Leung-Shi Cheng, Mr. Yan-Wai Wong and Mr. Kwok-Wai Chan from the Government Laboratory, HKSAR

for their sharing on both working and life experiences, which is influential to my career planning.

Last but not least, I am eternally grateful to my parent, my brother, my sister and girlfriend, who stand by me all the time with endless love and care during my study.

I sincerely wish all the above-mentioned persons have a healthy and joyful life.

TABLE OF CONTENTS

DECLARATION ii

ABSTRACT iii

ACKNOWLEDGMENTS v

TABLE OF CONTENTS vii

LIST OF ABBREVIATIONS x

CHAPTER ONE. INTRODUCTION

1.1 Fundamentals of biosensor 1

1.2 Biosensors for public health applications 5

1.3 Objectives of the dissertation work 8

1.4 References 10

1.5 Appendix 16

CHAPTER TWO. MICROSPHERE-BASED FLOW CYTOMETRIC IMMUNOASSAY FOR MELAMINE DETECTION

2.1 Introduction 19

2.1.1 Background information on melamine 19

2.1.2 Fundamentals of immunoassay 22

2.1.3 Fundamentals of flow cytometry and application example 25

2.1.4 Design of experiment 28

2.2 Experimental section 30

2.2.1 Chemicals, reagents and materials 30

2.2.2 Synthesis of coating antigens 31

2.2.3 Conjugation of coating antigens onto magnetic microspheres 39

2.2.4 Sample pretreatment step for infant formula powder 40

2.2.5 Melamine standards preparation 40

2.2.6 General procedure of immunoassay 40

2.2.7 Instrumentation and data analysis 41

2.3 Results and Discussion 45

2.3.1 Optimization of working conditions 45

2.3.2 In-house validaion of the developed assay 53

2.3.3 Discussion 58

2.4 References 66

2.5 Appendix 77

CHAPTER THREE URINARY POLYAMINES: A PILOT STUDY ON THEIR ROLES AS PROSTATE CANCER DETECTION BIOMARKERS

3.1 Introduction 85

3.1.1 Background information and statistics on prostate cancer 85

3.1.2 Current PCa detection methods and medical situations 87

3.1.3 Background of urinary biomarkers and examples 95

3.1.4 Background of polyamines 97

3.1.5 Fundamentals of UPLC-MS/MS 98

3.1.6 Design of experiment 102

3.2 Experimental section 105

3.2.1 Chemicals, reagents and materials 105

3.2.2 Urine samples collection 105

3.2.3 Creatinine determination 107

3.2.4 Sample preparation for polyamine determination 109

3.2.5 Standard/sample pretreatment for polyamine determination 109

3.2.6 Quality control samples preparation 110

3.2.7 Stability study 110

3.2.8 Instrumentation and statistical analysis 111

3.3 Results and Discussion 114

3.3.1 Urinary polyamine contents 114

3.3.2 Receiver operating characteristics analysis 120

3.3.3 Correlation study 121

3.3.4 Discussion 124

3.4 References 132

3.5 Appendix 145

CHAPTER FOUR. FLEXIBLE GOLD NANOPARTICLES BASED APTASENSOR TOWARDS URINARY SPERMINE FOR CANCER SCREENING

4.1 Introduction 152

4.1.1 Classical techniques for polyamine detection 152

4.1.2 Fundamental of AuNPs 155

4.1.3 Interactions between AuNPs and DNA 165

4.1.4 Design of experiment 167

4.2 Experimental section 168

4.2.1 Materials and instruments 168

4.2.2 Synthesis of citrate-AuNPs 170
4.2.3 Quantitative detection of spermine by AuNPs 172
4.2.4 Optimization of working conditions 172
4.2.5 Sample pretreatment procedures 173
4.2.6 Isothermal titration calorimetry study 173
4.3 Results and discussion 174
4.4 References 201
4.5 Appendix 213
CHAPTER FIVE. CONCLUSIONS AND FUTURE WORKS 236
LIST OF PUBLICATIONS 239

List of Abbreviations

2-B	2-Butylamine
AETT	N^2-(2-aminoethyl)-1,3,5-triazine-2,4,6-triamine
Ag	Agmatine
Arg	Arginine
AUC	Area under curve
AuNPs	Gold nanoparticles
BPH	Benign prostatic hyperplasia
Br	Benzylamine
BR buffer	Britton-Robinson buffer
BSA	Bovine serum albumin
Cad	Cadaverine
Crea	Creatinine
D_2O	Deuterium oxide
Dap	1,5-Diaminopentane
DMSO	Dimethyl sulfoxide
DNA	Deoxyribonucleic acid
DRE	Digital rectal examination
EDC	1-Ethyl-3-(3-dimethyl-aminopropyl) carbodiimide
ELISA	Enzyme linked immunosorbent assay
EPS	Human expressed prostatic secretions
ERSPC	European Randomized Study of Screening for Prostate Cancer

FAO	Food and Agriculture Organization of the United Nations
His	Histamine
$HAuCl_4$	Hydrogen tetrachloroaurate (III)
HC	Healthy control
HFBA	Heptafluorobutyric acid
HPLC	High performance liquid chromatography
HTD	6-hydrazinyl-1,3,5-triazine-2,4-diamine
IC	Inhibitory concentration
Ipt	Isoputrenine
IS	Internal standard
ITC	Isothermal titration calorimetry
IUPAC	International Union of Pure and Applied Chemistry
LOD	Limit of detection
LOQ	Limit of quantitation
Me	Methylamine
MEL	Melamine
MRL	Maximum residual level
MRM	Multiple reaction monitoring
N-actCad	N-acetylcadaverine
N-actPut	N-acetylputrescine
N-actSpm	N-acetylspermine
NEM	No evidence of malignancy

NHS	N-Hydroxysuccinimide
NMR	Nuclear magnetic resonance
n–B	N-butylamine
Orn	Ornithine
PBS	Phosphate buffer saline
PBSBT	Phosphate buffer saline supplemented with BSA and Tween-20
PCa	Prostate cancer
PHI	Prostate health index
PLCO	Prostate, Lung, Colorectal, and Ovarian
ppb	Parts per billion
ppm	Parts per million
PPV	Positive predictive rate
Pr	Propylamine
PSA	Prostate Specific Antigen
Pt	Putrenine
Put	Putrescine
QC	Quality control
RNA	Ribonucleic acid
ROC	Receiver operating characteristics
rpm	Rounds per minute
RSD	Relative standard deviation
SEM	Standard error of mean

Spd	Spermidine
SPE	Solid phase extraction
Spm	Spermine
Spm acid 1	N-(3-aminopropyl)-N-(2-carboxyethyl)-1 4-Diaminobutane
SPO	Spermine oxidase
SPR	Surface plasmon resonance
SSAT	Spermidine/spermine N^1-acetyltransferase
TRUSPB	Transrectal ultrasound guided prostatic biopsy
Tyr	Tyramine
UPLC-MS/MS	Ultra-high performance liquid chromatography coupled with tandem mass spectrometer
WHO	World Health Organization

CHAPTER ONE: INTRODUCTION

1.1 Fundamentals of biosensor

A high demand for an accurate measurement of specific analytes always exists for improving our quality of lives in different ways. For health care, we need to monitor biomarkers that are indicative of diseases, diagnose infectious diseases or monitor any physiological changes inside our body, etc. For environmental purpose, we need to analyze harmful chemicals present in water or soil so as to have a better effluent control or waste disposal. In food-related fields, we need to monitor food's quality and ensure their safety to be consumed. We can also monitor any industrial processes during food production and processing to maximize the production yield. Throughout the past decades in analytical sciences, research and development never stop and scientists keep on designing different types of instrumental techniques to address every analytical problems, not only in the fields abovementioned.

The rapid and prosperous development in analytical sciences allows scientists to take a deeper insight into more difficult multi-disciplinary research problems, and hence triggering more research in this aspect. One of the best outcomes of such multidimensionality lies in the evolvement of the concept of biosensor, a major research area currently among analytical scientists. For your information, Figure 1.1 shows the historical chart illustrating the occurrence of the keyword 'biosensor' in academic publications in recent years. Around two

hundredfold increase in the number of publications can be observed from 1980 to 2015, demonstrating clearly the attractiveness of this broad discipline to scientists.

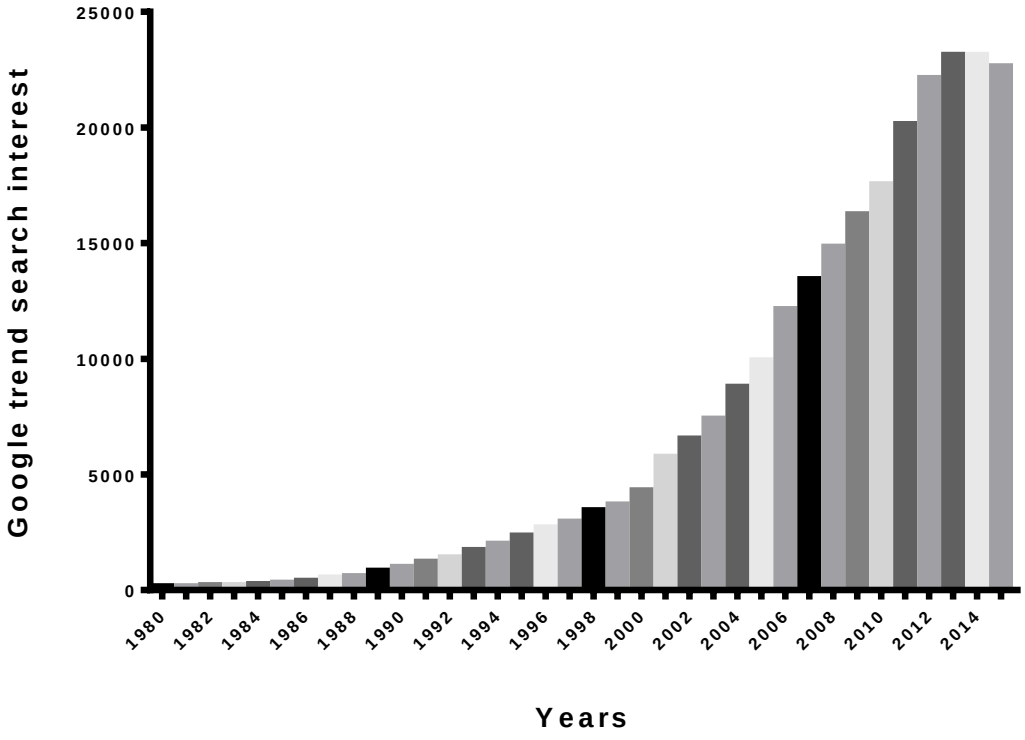

Figure 1.1 Historical chart of the occurrence of the keyword 'biosensor' in academic publications from 1980 to 2015.

To define the term biosensor, probably due to its involvement of scientists from different disciplines, the definition was not that clear initially. Some scientists might view a sensor working in biological samples, no matter physically or chemically, as a type of biosensor. On the other hand, some might only view it as a chemo-sensor working in natural matrices instead. To distinguish between these two types of devices, the most widely adopted definition is the one from the International Union of Pure and Applied Chemistry (IUPAC), where a biosensor is a self-contained integrated device that is able to provide specific quantitative or

semi-quantitative analytical information by employing a biological recognition element placing in a direct spatial contact with a transducing element to provide any types of signals to be recorded, and the signal is proportional to the concentration of a specific chemical or set of chemicals. [1] Under this definition, Figure 1.2 illustrates the typical configuration of a biosensor:

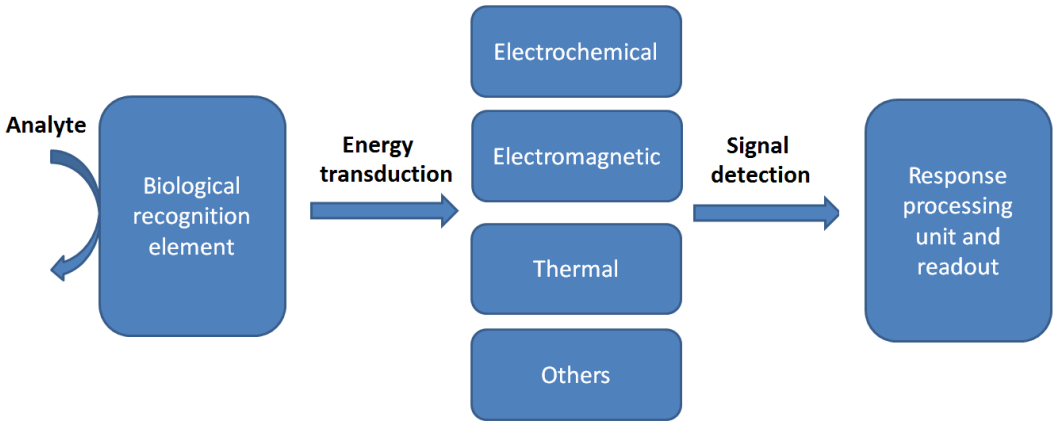

Figure 1.2 Typical configuration of a biosensor.

Briefly, the key principle is the molecular recognition due to any interactions between the bioactive molecules and the target analyte. The transducer, which works intimately with the bio-element, will convert any physical or chemical signals consecutive to that recognition process into a second type of signal. This can be of electrochemical types like amperometric, conductimetric or potentiometric; electromagnetic types like absorbance, fluorescence or chemiluminescence; thermal types like adiabatic or others like bio-magnetic or any mass variations. Finally they are being captured by a detector, and then being processed into some readable formats to users. This final reading is usually

proportional to the chemical/physical/biological events happening with the bio-element, and thus proportional to the concentration of target analyte for a quantitative or semi-quantitative analysis.

Biosensors can be categorized according to the type of bio-element utilized. To name some, but not limiting to, enzymatic biosensor is the commonest type. As the name suggested, it employs enzyme, a macromolecular proteinaceous bio-catalyst, to accelerate specific type of chemical reactions. Antibody, the protein made by our immune system to fight any pathogens, can identify its complementary antigen and it is widely employed in the well-known immunoassay techniques. More discussions on this technique will be given in Chapter Two. Nucleic acids strand like deoxyribonucleic acid (DNA) or ribonucleic acid (RNA) are comparatively more recent advanced biomaterial. They can coil around their complementary strands and form a double helical structure through specific base pairings. We usually call this type of biosensor an aptasensor. In Chapter Four it will describe such an example of our developed aptasensor for clinical application. Receptor proteins can also recognize and respond to its endogenous ligand and cause certain type of cellular response. Other than that, some scientists would even employ microorganisms, cells or tissue samples directly based on their biological activities, e.g. for measuring biochemical oxygen demand. Different designs of novel and inspiring biosensors are being developed and used every day depending on the area where it is going to operate.

Comparing to other conventional techniques, biosensors are envisioned as a device to offer numerous advantages. It is a new option of sensor, providing high

specificity in complex matrices in a real-time, reversible manner without any needs of complicated sample purification steps or a large sample volume. Minimum perturbation would be generated to the sample and keep them in a stable and intact state. It also promises a quick, simple, accurate, sensitive and convenient measurement. From an economic point of view, they can be miniaturized and therefore achieve a low cost of manufacturing and provide portability. Last but not least, owing to the flexibility in its design, it can achieve a good accessibility for any challenging tasks in any types of environment. All of these fascinating characteristics explain well why it is one of the hottest research topics nowadays.

1.2 Biosensors for public health applications

In this sub-chapter some application examples of biosensors for public health purposes will be discussed. These examples will be related to areas that chapters later on focusing on, e.g. for food safety and clinical applications more specifically.

Milk and milk products always make important contributions to humans' diet. They are highly nutritional, providing high quality protein and are supplementary sources of different essential elements to our body, like different metal ions, vitamin A, D, B-12 and also riboflavin. According to the Hong Kong Population-Based Food Consumption Survey commissioned by the Food and Environmental Hygiene Department, Government of Hong Kong SAR, on average 34.23g/day of such milk products are consumed by each citizen. [2] This in-turn

makes milk adulteration a very serious food fraud to citizens, posing serious health hazards, social and economic problems. Most of the times this term refers to an activity which somebody deliberately add some forbidden adulterants into food. Sometimes it can also be due to an improper management during manufacturing or poor detection techniques, and we often more specifically classify it as 'contamination' rather.

A very common example is antibiotics. They are chemical drugs used to treat or prevent any bacterial infections either by killing or inhibiting bacterial growth. In the case of dairy cattle, antibiotics are widely applied to treat mastitis, a very common persistent and inflammatory reaction of their breast or udder tissues. Therefore antibiotics residues are sometimes found in milk, potentially bringing undesired effects including its immune-pathological effects, carcinogenicity, nephropathy, hepatotoxicity, reproductive disorders, allergy and possible transfer of antibiotic resistant bacteria to human. [3]

Biosensors are therefore employed for monitoring the residual level of contaminants in food for safety purposes. To give a few examples without mentioning exact details, Liu *et al.* reported their developed bio-layer interferometry for a rapid detection of β-lactam antibiotic residue in milk employing its antibiotic receptor for recognition. [4] Employing a similar detection scheme, Maragos *et al.* developed another immunosensor for the mycotoxin deoxynivalenol. [5] Another novel example was an amperometric affinity disposable magnetosensor developed by Gamella *et al.* for a simultaneous detection of penicillin G sodium salt, amoxicillin, ampicillin sodium salt, cefapirin,

oxacillin and cloxacillin. [6] Last but not least, Taranova *et al.* reported an interesting immunochromatographic strip for monitoring ofloxacin, chloramphenicol and streptomycin. [7] Signals are presented in a 'traffic light' format due to the use of multi-color quantum dots on the line. Table A1.1 in Appendix gives more example of biosensor application on milk-related contaminants.

The next hot area biosensors being applied and developed is in clinical area, especially on biomarker-related topics. Briefly, a biomarker refers to a traceable indicator of certain biological conditions, which can be any biological processes, pathogenic processes or therapeutic reactions. Depending on the types of events they are indicating, biomarkers can be further classified in different ways. More information will be given in Chapter Three.

One of a biomarker example is uric acid, an important metabolite of purine nucleotides in our bodies. If its concentration is high in blood, it usually indicates several kinds of diseases like gout and hyperuricemia. [8] Besides, it is also associated with medical conditions like the formation of kidney stones and diabetes. [9] To monitor this metabolite, Pieramarini *et al.* used uricase, an enzyme that catalyzes the breakdown of uric acid, as the bio-element and developed a screen-printed electrode based electrochemical biosensor for use in blood serum matrices. [8] Another biomarker example was from Liu *et al.*, which they reported a dual functional electrochemical biosensor for prostate specific antigen (PSA) and telomerase activity. [10] The former one is a widely applied biomarker for prostate cancer (PCa), a cancerous disease of high concern in recent years. This dissertation

work also focuses on this kind of cancer and more details can be found in Chapter Three and Four. Alpha-fetoprotein is another cancer-indicating biomarker. Elevated level in plasma may indicate hepatocellular cancer, yolk sac cancer or liver metastasis. [11] Based on this observation, Li *et al.* have published their biomarker design combining properties of gold nanoparticles (AuNPs) and ultra-thin optical microfibers. [12] Chen *et al.* reported their SPR biosensor for fetal fibronectin, an informative glycoprotein for predicting the risk of preterm birth. [13] The last example was a graphene oxide based biosensor fabricated by Kailashiya *et al.* for detection of platelet-derived micro-particles in blood, a biomarker associating with coronary diseases. [14] Table A1.2 summarizes more example of biosensor for clinical applications:

1.3 Objectives of the dissertation work

Similar to the above shortlisted literatures, in this dissertation we plan to address several analytical problems in milk safety and clinical field. In China, the milk safety issue has aroused citizens' high concern after the notorious melamine scandal in 2008, in which melamine has been illegally abused to boost nitrogen levels during protein tests. Other than that, different undesired preservatives, synthetic hormones, antibiotics, bacteria and pathogens were reported to be food hazards threating citizens. To ensure milk safety for consumption, a lot of monitoring works need to be performed and therefore an ideal multiplex screening method is demanded by food regulatory units. In Chapter Two, the development of

a sensitive and selective sensing method towards melamine based on the use of magnetic microspheres and flow cytometric immunoassay is reported.

For clinical side, I concern the current medical status of PCa, which is one of the most common male-related cancers in the world with a continuous increasing incidence rate. Hong Kong is no exception in this public health issue. Nevertheless, current screening methods towards PCa are not perfect enough. We have an urgent demand for more sensitive and accurate diagnostic biomarkers or methods to detect early PCa and improve treatment outcome, given the latency of early, treatable PCa and the lethality of its late, discernible stage. In Chapter Three, the results of our large-cohort study on urinary polyamine levels of potential PCa patients is reported and discussed. A useful biomarker, urinary spermine, was discovered and it demonstrated usefulness in PCa detection. Based on this finding, Chapter Four focuses on the development of a rapid sensing method towards this novel biomarker via the use of DNA and AuNPs. Any aggregation of AuNPs induced by spermine would show a color change in solution. This visual change can be observed directly by naked eyes, which acts as a mean of simple and indirect sensing of urinary spermine.

Through exploring more new biosensor designs, hopefully this dissertation work can contribute, even a little bit, to solve the concerned analytical problems in the future and inspire more novel ideas from scientists in this field.

1.4 References

1. Thévenot, D. R., Toth, K., Durst, R. A., & Wilson, G. S. (2001). Electrochemical biosensors: recommended definitions and classification. *Biosensors and Bioelectronics*, 16(1), 121-131.
2. Food and Environmental Hygiene Department, Government of HKSAR. (2010) Hong Kong population-based food consumption survey 2005-2007 Final Report. http://www.cfs.gov.hk/english/programme/programme_firm/files/FCS_final_report.pdf
3. Nisha, A. R. (2008). Antibiotic residues-a global health hazard. *Vet World*, 1(12), 375-377.
4. Liu, X., Fu, H., Xue, F., Ma, T., Zeng, X., & Zhu, H. (2014). Rapid detection of [Beta]-lactam antibiotic residue in milk using biolayer interferometry. *Agricultural Biotechnology*, 3(1), 9.
5. Maragos, C. M. (2012). Signal amplification using colloidal gold in a biolayer interferometry-based immunosensor for the mycotoxin deoxynivalenol. *Food Additives & Contaminants: Part A*, 29(7), 1108-1117.
6. Gamella, M., Campuzano, S., Conzuelo, F., Esteban-Torres, M., De Las Rivas, B., Reviejo, A. J., ... & Pingarrón, J. M. (2013). An amperometric affinity penicillin-binding protein magnetosensor for the detection of β-lactam antibiotics in milk. *Analyst*, 138(7).
7. Taranova, N. A., Berlina, A. N., Zherdev, A. V., & Dzantiev, B. B. (2015). ‘Traffic light’immunochromatographic test based on multicolor quantum dots

for the simultaneous detection of several antibiotics in milk. *Biosensors and Bioelectronics*, 63, 255-261.

8. Piermarini, S., Migliorelli, D., Volpe, G., Massoud, R., Pierantozzi, A., Cortese, C., & Palleschi, G. (2013). Uricase biosensor based on a screen-printed electrode modified with Prussian blue for detection of uric acid in human blood serum. *Sensors and Actuators B: Chemical*, 179, 170-174.
9. Chen, X., Chen, J., Wang, F., Xiang, X., Luo, M., Ji, X., & He, Z. (2012). Determination of glucose and uric acid with bienzyme colorimetry on microfluidic paper-based analysis devices. *Biosensors and Bioelectronics*, 35(1), 363-368.
10. Liu, J., Lu, C. Y., Zhou, H., Xu, J. J., Wang, Z. H., & Chen, H. Y. (2013). A dual-functional electrochemical biosensor for the detection of prostate specific antigen and telomerase activity. *Chemical Communications*, 49(59), 6602-6604.
11. Tamura, Y., Yamagiwa, S., Aoki, Y., Kurita, S., Suda, T., Ohkoshi, S., ... & Niigata Liver Disease Study Group. (2009). Serum alpha-fetoprotein levels during and after interferon therapy and the development of hepatocellular carcinoma in patients with chronic hepatitis C. *Digestive diseases and sciences*, 54(11), 2530-2537.
12. Li, K., Liu, G., Wu, Y., Hao, P., Zhou, W., & Zhang, Z. (2014). Gold nanoparticle amplified optical microfiber evanescent wave absorption biosensor for cancer biomarker detection in serum. *Talanta*, 120, 419-424.

13. Chen, C. Y., Chang, C. C., Yu, C., & Lin, C. W. (2012). Clinical application of surface plasmon resonance-based biosensors for fetal fibronectin detection. *Sensors*, 12(4), 3879-3890.

14. Kailashiya, J., Singh, N., Singh, S. K., Agrawal, V., & Dash, D. (2015). Graphene oxide-based biosensor for detection of platelet-derived microparticles: A potential tool for thrombus risk identification. *Biosensors and Bioelectronics*, 65, 274-280.

15. Ezhilan, M., Gumpu, M. B., Ramachandra, B. L., Nesakumar, N., Babu, K. J., Krishnan, U. M., & Rayappan, J. B. B. (2016). Design and development of electrochemical biosensor for the simultaneous detection of melamine and urea in adulterated milk samples. *Sensors and Actuators B: Chemical*, 238, 1283-1292.

16. Kumar, P., Lambadi, P. R., & Navani, N. K. (2015). Non-enzymatic detection of urea using unmodified gold nanoparticles based aptasensor. *Biosensors and Bioelectronics*, 72, 340-347.

17. Ramesh, R., Puhazhendi, P., Kumar, J., Gowthaman, M. K., D'Souza, S. F., & Kamini, N. R. (2015). Potentiometric biosensor for determination of urea in milk using immobilized Arthrobacter creatinolyticus urease. *Materials Science and Engineering: C*, 49, 786-792.

18. Chávez, N. A., Jauregui, J., Palomares, L. A., Macías, K. E., Jiménez, M., & Salinas, E. (2012). A highly sensitive sandwich ELISA for the determination of glycomacropeptide to detect liquid whey in raw milk. *Dairy science & technology*, 92(2), 121-132.

19. Indyk, H. E., Gill, B. D., & Woollard, D. C. (2015). An optical biosensor-based immunoassay for the determination of bovine serum albumin in milk and milk products. *International Dairy Journal*, 47, 72-78.

20. Jasti, L. S., Dola, S. R., Fadnavis, N. W., Addepally, U., Daniels, S., & Ponrathnam, S. (2014). Co-immobilized glucose oxidase and β-galactosidase on bovine serum albumin coated allyl glycidyl ether (AGE)–ethylene glycol dimethacrylate (EGDM) copolymer as a biosensor for lactose determination in milk. *Enzyme and microbial technology*, 64, 67-73.

21. Mishra, R. K., Dominguez, R. B., Bhand, S., Muñoz, R., & Marty, J. L. (2012). A novel automated flow-based biosensor for the determination of organophosphate pesticides in milk. *Biosensors and Bioelectronics*, 32(1), 56-61.

22. Yan, X., Li, H., Han, X., & Su, X. (2015). A ratiometric fluorescent quantum dots based biosensor for organophosphorus pesticides detection by inner-filter effect. *Biosensors and Bioelectronics*, 74, 277-283.

23. Yi, Y., Zhu, G., Liu, C., Huang, Y., Zhang, Y., Li, H., ... & Yao, S. (2013). A label-free silicon quantum dots-based photoluminescence sensor for ultrasensitive detection of pesticides. *Analytical chemistry*, 85(23), 11464-11470.

24. Kaur, H., Kumar, S., & Verma, N. (2014). Enzyme-based colorimetric and potentiometric biosensor for detecting Pb (II) ions in milk. *Brazilian Archives of Biology and Technology*, 57(4), 613-619.

25. Verma, N., Kumar, S., & Kaur, H. (2010). Fiber optic biosensor for the detection of Cd in milk. *Journal of Biosensors & Bioelectronics*, 2010.

26. Hardeep, K., & Verma, N. (2015). High throughput optical biosensor for monitoring Pb (II) Ions in milk through fluorescence based microarray approach. *Journal of Biosensors & Bioelectronics*, 6(2), 1.

27. Riedel, T., Rodriguez-Emmenegger, C., de los Santos Pereira, A., Bědajánková, A., Jinoch, P., Boltovets, P. M., & Brynda, E. (2014). Diagnosis of Epstein–Barr virus infection in clinical serum samples by an SPR biosensor assay. *Biosensors and Bioelectronics*, 55, 278-284.

28. Xu, H., Gu, D., He, J. A., Shi, L., Yao, J., Liu, C., ... & Long, J. (2015). Multiplex biomarker analysis biosensor for detection of hepatitis B virus. *Bio-Medical Materials and Engineering*, 26(s1), S2091-S2100.

29. Bisoffi, M., Severns, V., Branch, D. W., Edwards, T. L., & Larson, R. S. (2013). Rapid detection of human immunodeficiency virus types 1 and 2 by use of an improved piezoelectric biosensor. *Journal of clinical microbiology*, 51(6), 1685-1691.

30. Baca, J. T., Severns, V., Lovato, D., Branch, D. W., & Larson, R. S. (2015). Rapid detection of Ebola virus with a reagent-free, point-of-care biosensor. *Sensors*, 15(4), 8605-8614.

31. Shojaei, T. R., Salleh, M. A. M., Tabatabaei, M., Ekrami, A., Motallebi, R., Rahmani-Cherati, T., ... & Jorfi, R. (2014). Development of sandwich-form biosensor to detect Mycobacterium tuberculosis complex in clinical sputum specimens. *Brazilian Journal of Infectious Diseases*, 18(6), 600-608.

32. Luo, C., Tang, H., Cheng, W., Yan, L., Zhang, D., Ju, H., & Ding, S. (2013). A sensitive electrochemical DNA biosensor for specific detection of

Enterobacteriaceae bacteria by Exonuclease III-assisted signal amplification. *Biosensors and Bioelectronics*, 48, 132-137.

33. Phaneuf, C. R., Mangadu, B., Piccini, M. E., Singh, A. K., & Koh, C. Y. (2016). Rapid, portable, multiplexed detection of bacterial pathogens directly from clinical sample matrices. *Biosensors,* 6(4), 49.

1.5 Appendix

Concerned analytes	Biosensing techniques	Reference
Antibiotics	Biolayer Interferometry for βeta-lactam	[4]
	Biolayer Interferometry for deoxynivalenol	[5]
	Amperometric affinity magnetosensor for six antibiotics residues	[6]
	Immunochromatographic test for ofloxacin, chloramphenicol and streptomycin	[7]
Urea	Cyclic voltammetric biosensor based on zinc oxide nanospheres modified Platinum electrode	[15]
	Gold nanoparticles based aptasensor	[16]
	Arthrobacter creatinolyticus urease on modified poly(acrylonitrile–methylmethacrylate–sodium vinylsulfonate) membrane	[17]
Wheat	Enzyme-linked immunosorbent assay (ELISA)	[18]
	Surface plasmon resonance (SPR) based immunoassay	[19]
	Glucose oxidase and βeta-galactosidase immobilized copolymer	[20]
Pesticides	Automated flow-based biosensor for organophosphate pesticides	[21]

	Ratiometric fluorescent quantum dots based for organophosphate pesticides	[22]
	Label-Free Silicon Quantum Dots-Based Photoluminescence Sensor for organophosphate pesticides	[23]
Metal ion	Urease based Colorimetric and Potentiometric Biosensor for Lead(II) ion detection	[24]
	Fiber optic biosensor for cadmium detection	[25]
	Optical biosensor employing Bacillus sphaericus for Lead(II) ion detection	[26]

Table A1.1 Recent advances of biosensors for milk contaminants-related applications.

Analyte type	Biosensing techniques	Reference
Biomarker	Screen-printed electrode for uric acid	[8]
	Dual-functional electrochemical biosensor for PSA and telomerase activity	[10]
	Biofunctionalized AuNPs for α-fetoprotein	[12]
	SPR-Based Biosensors for fetal fibronectin	[13]
	Graphene oxide-based biosensor for platelet-derived microparticles	[14]
Virus	SPR biosensor assay for *Epstein–Barr* virus	[27]
	Protein microarray-based biosensor for hepatitis B virus	[28]
	Piezoelectric Biosensor for human immunodeficiency virus type 1 & 2	[29]
	Surface acoustic wave biosensors for *Ebola* virus	[30]
Bacterial pathogens	Quantum dots and AuNPs conjunct with specific oligonucleotides for Mycobacterium tuberculosis complex	[31]
	Electrochemical DNA biosensor for *Enterobacteriaceae* bacteria	[32]
	Microfluidic platform for *E. coli*, *Listeria*, *Salmonella*, and *Shigella*.	[33]

Table A1.2 Recent advances of biosensors for clinical applications.

CHAPTER TWO: MICROSPHERE-BASED FLOW CYTOMETRIC IMMUNOASSAY FOR MELAMINE DETECTION

2.1 Introduction

2.1.1 Background information on melamine

1,3,5-triazine-2,4,6-triamine, or more famously known as melamine (MEL), is an organic base with six nitrogen atoms in each molecule, which constitute two-third of its total molecular weight. (Figure 2.1) Other less common names include cyanurotriamide, cyanurotriamine and cyanuramide. MEL is commercially synthesized from urea in a large scale manner to obtain MEL-formaldehyde resins, which is a widely used chemical in industrial processes for the manufacturing of laminates, plastics, commercial filters, coatings, glues or adhesives and flame retardant. [1] Other than that, it is sometimes used as a non-protein nitrogenous source for feeding cattle. However, it was shown to be ineffective and inappropriate for ruminants' consumption due to its slow hydrolysis process, as observed from the poor solubility data in Table 2.1. [2] Therefore according to Food and Agriculture Organization of the United Nations (FAO) / World Health Organization (WHO) Codex Alimentarius, which is a harmonized international food standard, MEL is not approved to be added into foods or food products. Nevertheless, melamine food contamination is still possible through the wide usage of MEL resin tableware in our daily lives. MEL also exists as a metabolite product of cyromazine, a commonly used insecticide on animals or crops.

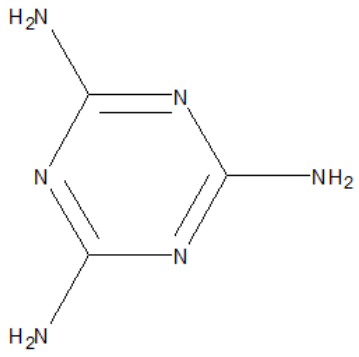

Figure 2.1 Chemical structure of MEL.

Property	Description
Appearance at room temperature	Colorless to white crystals
Molecular weight	126.12g/mol
Melting point	354˚C
Solubility	Partially soluble in water
	3.1g/L in water at 20˚C
	13.4g/L in water at 50˚C
	25g/L in water at boiling point

Table 2.1 Summary of the general properties of MEL. [2]

Except being a contaminant existing in the environment, more seriously is its abuse as an illegal adulterant in infant formula milk powder to elevate falsely the protein contents detected by the Kjeldahl method. Kjeldahl method is a classical nitrogen content determination approach consisting of steps like

degradation of organic matters in samples, liberation and capturing of ammonia and a back-titration step. It is not able to distinguish nitrogen content from protein or non-protein source. In early September 2008, the Chinese government announced that twenty-two manufacturers of powdered infant formula were selling products tainted with this industrial chemical. [3] Some government-sanctioned "Chinese National Brands" were also included, and nearly 20% of all available infant formula powder in market of China were harmful. [3] This milk scandal in 2008 finally led to the formation of kidney stones in approximately 300,000 infants. Six deaths were reported. [4] After this incident, the acceptable limit of 1mg/kg for infant formula milk powder and 2.5mg/kg for other foods containing more than 15% milk, as recommended by WHO/FAO, are adopted in many countries. [5] Public confidence towards the safety of infant formula milk powder or food from China is still not recovered even several years after that incident. [6] Therefore it is of paramount importance to develop effective food hazard detection methods, especially for MEL, for regulatory units and public health purpose. Also it is a popular research area among scientists in analytical fields towards this high-concerning analyte. [7-8]

Amongst these developed analytical methods, chromatographic instruments coupling with mass spectrometer based detector are the most popular detection methods to be employed due to their strong power in both analyte separation and identity confirmation. [9-10] However, these techniques are usually complicated and require trained technical staffs for handling the tedious procedures for pre-treatment, clean-up of samples or even derivatization steps. The

long time for each run also limits their applications in high-throughput analysis. Apparently we need a better method which is simple and quick such that we can achieve a cost-effective preliminary MEL-screening before we pass any suspicious samples to mass spectrometer-based techniques for further confirmatory analysis. Table A2.1 and A2.2 give more information about the published classical techniques and recent advances in MEL detection techniques respectively.

2.1.2 Fundamentals of immunoassay

Amongst all MEL detection approaches, immunoassay is one of the commonest biochemical techniques employed nowadays. After being developed firstly by Yalow and Benson in 1960s, who were also being awarded the Nobel Prize for this powerful technique, for over 50 years no matter in life-science research for tracking proteins or hormones, food monitoring for detecting contaminants or clinical diagnostics for improving treatment outcomes, they are still the standard method for detection of biomolecules. Enzyme linked immunosorbent assay (ELISA) is the most widely used configuration of immunoassay where enzyme conjugated antibody is employed as the basis of detection. Fluorescence tagged antibody is another common choice to provide signals.

The basic principle of ELISA is to capture an analyte or antibody on a solid support, usually a microtiter plate, via their specific complementary interactions between epitope and antigen-binding site both in structural and spatial

configuration. Another antigen or antibody molecule which is usually linked with an enzyme will be incubated subsequently to generate and amplify signals during the final substrate addition step. ELISA tests are viewed as rapid, highly sensitive and selective when compared with other methods. Quantitation usually can be achieved at micro- or nano- level within an hour. Moreover, the method is simple to perform without the need of high technical requirements, and no harmful reagents are usually involved. All of these properties make it a desirable technique for food safety monitoring.

Format of ELISA:

There are five types of configurations frequently being employed in ELISA: Direct, indirect, sandwich, competitive and immunocapture. (Figure A2.1-A2.5)

In the direct format, antigens inside samples are directly attached onto the solid support. Subsequently enzyme labeled antibody and substrate will be added to provide signals. This format is quick with the fewest steps, and it is free from the cross-reactivity problem caused by secondary antibody. However, the assay is often not sensitive as others due to the absence of signal amplification steps. The existence of interfering proteins in crude samples may also affect the assay performance significantly by competing for the binding sites of solid support.

The indirect format is usually employed to detect specific antibody in sera. With the use of secondary antibody for binding on several epitopes of the primary

one, sensitivity is increased compared to that perform in its absence. The compensation is an extra incubating step which lengthens the procedural time.

The sandwich format requires the use of two types of antibodies. One is for capturing and the other one is for detection, whereas the antigen is 'sandwiched' between them. Due to its comparably better sensitivity and robustness, it is the commonest ELISA approach. But a requirement is that the antigen should not be too small so as to be bound by two antibodies.

Opposite to the sandwich format, the competitive format is a good choice when the antigen is having a low molecular weight. In this approach, a competing enzyme labeled analyte is added together with sample to compete for the sites of antibody being coated on the solid support. The performance of this assay is easily influenced by any matrix interferences or factors during incubation, like time and the amount of competing ligands so it requires a careful handling.

The immunocapture format is another format for detecting specific Immunoglobulin M antibody, the type of antibody produced instantly by our bodies to fight bacteria or viruses. After being captured by an anti-IgM antibody, we add enzyme-linked antigen or antigen/antibody pair to provide signals. Depending on the property of target analyte and type of antibodies available, users can easily tailor-make their own in-house immunoassay kit.

2.1.3 Fundamentals of microsphere-based flow cytometric immunoassay

To improve the analytical performance of immunoassay, for instance, to confer it an ability of multiplexing and to further simplify the procedures, one advance is to replace the solid support from plate wells to various tiny particles with different properties. In the flow cytometric immunoassay to be discussed below, two categories of such small microspheres are classified: the non-magnetic and magnetic one. They are polymeric particles, usually made of polystyrene, with surface functionalized with another polymer to provide reactive sites like carboxylate or amine groups for further conjugation. These two types only differ in whether an extra magnetite layer is present in the magnetic one (Figure 2.2). Through this ~5% iron content doping, magnetic property is therefore provided, conferring the particles advantages like ease of analyte isolation through facilitating washing steps, and ease of automation by using a magnetic plate for manipulation. [11]

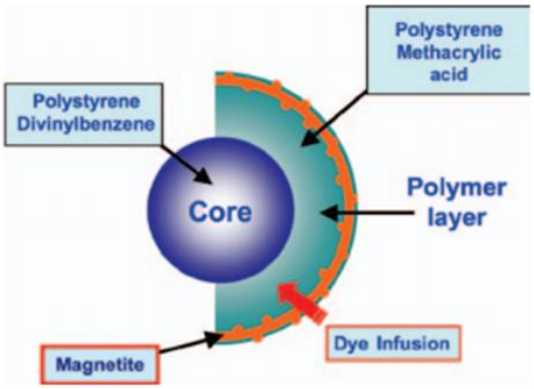

Figure 2.2 Microsphere structure. (Size: ~5.6μm and ~6.5μm for non-magnetic and magnetic beads respectively) [11]

Another important feature is that these microspheres are stained with two or three types of fluorescence dyes internally for them to exhibit fluorescence. This is achieved by first, swelling inside dyes-containing solution for infusion to take place and second, shrinking and letting the dye molecules being trapped inside the polymer coating or core. [11] Dyes' ratios are precisely controlled to make up a 100- or even 500-membered family in a two-dimensional or three-dimensional bead map respectively. (Figure 2.3) By spectrally distinguishing different beads according to the dyes' ratio, this technology, more specifically the xMAP® technology, enables users to develop their own assays in a fast and multiplex manner.

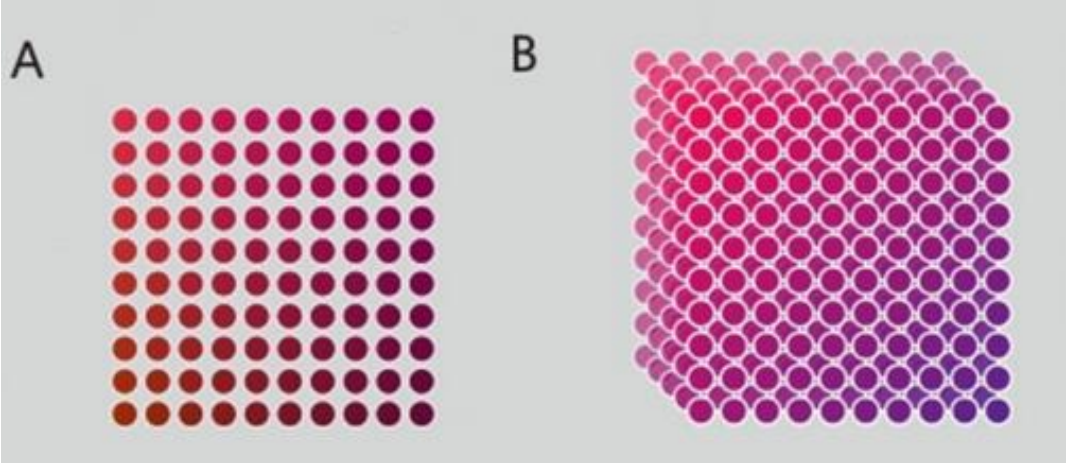

Figure 2.3 (A) Two-dimensional representation of 100 different sets of microsphere in specific dyes' ratio. (B) Three-dimensional representation of 500 different sets of microsphere in specific dyes' ratio. [Reproduced from 12]

To tell more about the spectral distinguishing part, it is achieved by a suspension array system based on the principle of flow cytometry. Flow cytometry has long been a unique technique for specifically resolving and quantifying distinct cells or organelles' populations based on their fluorescence characteristics or physical properties. There are three main components in a typical flow cytometer: the fluidics part, the optical part and the electronic part. The flow system brings cells to an interrogation region under the action of sheath fluid for creating a laminar flow. Lasers will be excited onto them as they pass through this narrow region one by one for individual analysis. This is termed as a 'hydrodynamic focusing' process. Different kinds of information related to the cells can be obtained here, e.g. forward-angle scatter intensity gives us information about the cell diameter while the side scatter intensity reveals information about granular structures within the cell or its surface. [12] Any fluorescence tag antibodies will also be excited here by a suitable laser for quantitation purpose. (Figure 2.4) In the case of microsphere based flow cytometric analysis, similar to typical flow cytometry, xMAP® microspheres will be analyzed sequentially and their specific spectral addresses will be determined here to allow multiplexing. Finally the signals will be processed by an electronic system for readout.

While the basic principle is similar to that of ELISA, microsphere based flow cytometric immunoassay is believed to offer several advantages: enhanced reproducibility, excellent sensitivity due to the effective use of larger surface areas of microspheres, and ability to monitor multi-analytes. Over 14,000 peer-reviewed

articles described the use of xMAP® platform for different applications, emphasizing its versatility and flexibility.

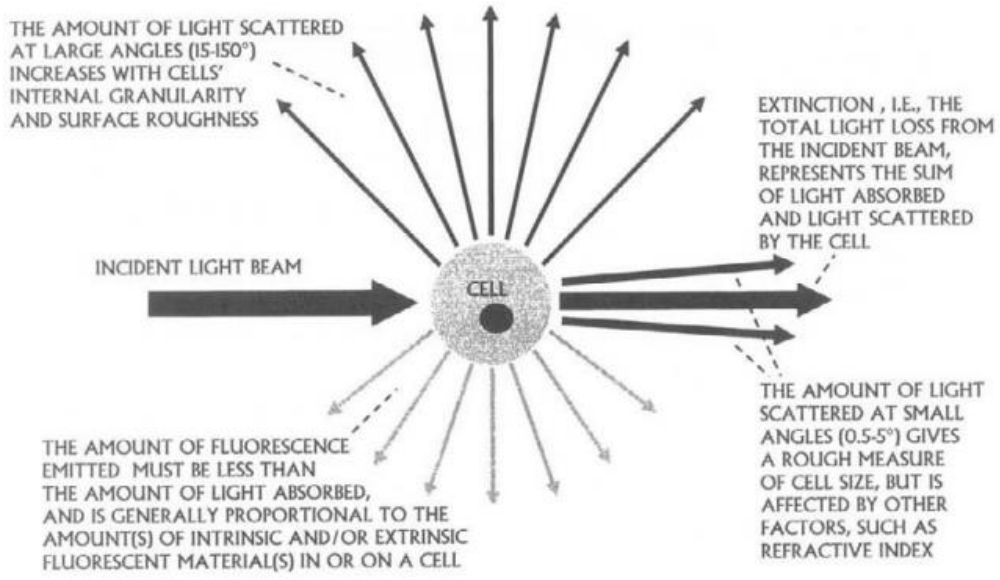

Figure 2.4 Interaction of a cell with light beam in a flow cytometer. [13]

2.1.4 Design of experiment

In this chapter, we will describe the development of a microsphere based flow cytometric immunoassay for MEL detection. Figure 2.5 illustrates the schematic diagram. A novel MEL derivative was synthesized and conjugated to the carboxylated microsphere surface via covalent bonding. The surface decorated beads were then utilized for detection of MEL in infant formula milk powders through an indirect competitive inhibitory format immunoassay. With a higher concentration of MEL in the sample for competition, less MEL primary antibodies would therefore be captured by those microspheres bound with MEL derivative. So as the secondary antibody which was labeled with a well-known bright

fluorescent reporter protein phycoerythrin. Less amount can bind to the attached MEL primary antibody during the subsequent incubation. From the extent of fluorescence quenching we could indirectly quantified the MEL content in samples. Validation of this developed method was performed strictly, showing its capability for tainted infant formula powder analysis according to the legislated MEL tolerance level; superior advantages were also demonstrated to be simple, high throughput, fast and organic solvent-free when compared with other MEL targeting methods listed in Table A2.1 and A2.2.

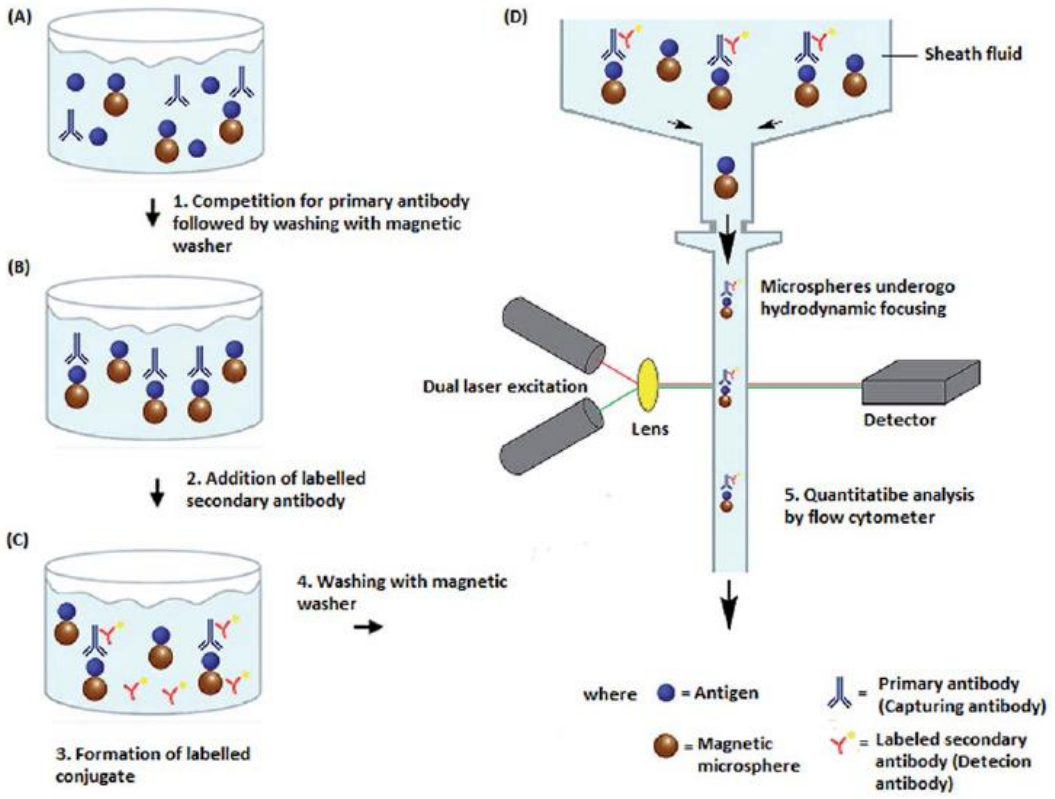

Figure 2.5 Schematic diagram of designed method.

2.2 Experimental section

2.2.1 Chemicals, reagents and materials

MEL was bought from Meryer Chemical Technology Ltd. Co. (Shanghai, China). Melamine analogs including atrazine and ammelide were obtained from TCI (Shanghai, China), while ammeline was obtained from Lancaster Synthesis (Massachusetts, USA). Cyanuric chloride, ethylenediamine, sodium chloride, sodium hydroxide, sodium phosphate monobasic, sodium phosphate dibasic, potassium chloride, Tween-20, Bovine serum albumin (BSA), cyromazine, N-hydroxysuccinimide (NHS) and 1-Ethyl-3-(3-dimethyl-aminopropyl) carbodiimide hydrochloride (EDC) were all purchased from Sigma-Aldrich (Hong Kong, China). Ammonium hydroxide solution (25%) and hydrochloride acid were from reagent grade commercial sources.

Mouse Monoclonal antibody towards MEL was bought from Creative Diagnostics (New York, USA). Phycoerythrin Goat Anti-Mouse Ig was obtained from SantaCruz Biotechnology (Hong Kong, China). xMAP® technology related stuffs such as the magnetic carboxylated microsphere (MC10026-01), sheath fluid for flow cytometry, 96-wells flat bottom plates, calibration and verification kit, amine coupling kit and handheld magnetic washer were obtained from Biorad (Hong Kong, China). Magnetic Particle Separator was obtained from Invitrogen (Hong Kong, China). A 96-wells plate shaker was obtained from IKA (Hong Kong, China). Refrigerated centrifuge 5417R was obtained from Eppendorf (Hong Kong, China). An ELISA kit for MEL was obtained from Romer Labs (Redhill, Singapore) for comparison of analytical performance.

0.1M phosphate buffer saline (PBS) buffer was self-prepared by adding 80g sodium chloride, 12.8g sodium phosphate monobasic and 4.5g sodium phosphate dibasic dehydrate into 1000mL deionized water. pH was then tuned to 7.4. 0.01M PBS was prepared by dilution from 0.1M PBS again with pH tuned to 7.4. PBSBT was prepared by supplementing 0.01M PBS with both BSA and Tween-20 (0.1% weight to volume ratio) respectively.

2.2.2 Synthesis of coating antigens

Three types of coating antigens were tested: MEL itself, 6-hydrazinyl-1,3,5-triazine-2,4-diamine (HTD) and N^2-(2-aminoethyl)-1,3,5-triazine-2,4,6-triamine (AETT). The latter two were not commercial available so they were synthesized ourselves according to the reaction pathways below: (Figure 2.6)

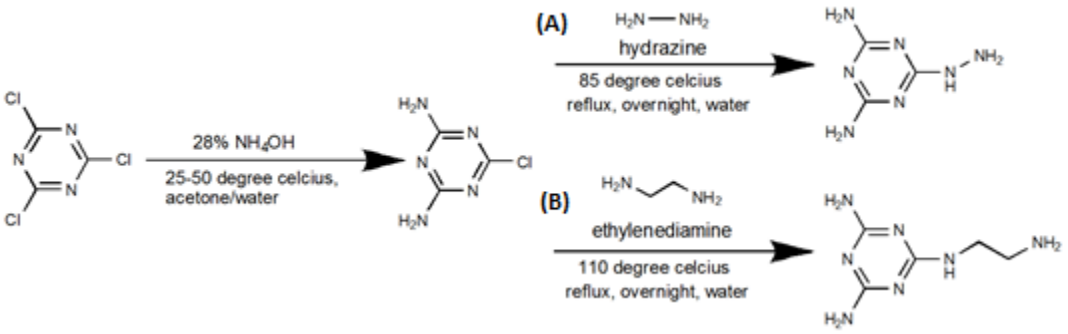

Figure 2.6 Two-steps reaction pathways for the synthesis of (A) HTD and (B) AETT.

The first step was to replace two chlorine atoms of cyanuric chloride with amine groups by Saito's approach [14]: Cyanuric chloride (17.9g) was dissolved in 100ml acetone, and 100ml water was subsequently added. The mixture was cooled to 0˚C in an ice bath. 32ml 25% aqueous ammonium hydroxide solution was added in a dropwise manner for amination to take place. The solution was kept and stirred at 25 ˚C overnight. Finally the mixture was filtered and washed with 30ml tetrahydrofuran for three times. After further drying by vacuum, we obtained a pure white solid of the chlorodiamino-triazine intermediate. (13.2g, 93.1%) Characterization was done by Nuclear Magnetic Spectroscopy (NMR): ^{1}H NMR (400MHz, DMSO-d_6): δ (ppm) 7.108-7.181(doublet), ^{13}C NMR (100MHz, DMSO-d_6): δ (ppm) 167.47, 169.11. (Figure 2.7-2.8)

After obtaining the intermediate, HTD and AETT were synthesized from it by Baliani and Zhou's method respectively. [15-16] For HTD, excess hydrazine monohydrate (4.20mL) was added dropwise to the intermediate solution (2.50g in 20mL water) and refluxed at 85 ˚C overnight. The final white solid was filtered, washed with water and vacuum-dried. (1.60g, 65.6%) ^{1}H NMR (400MHz, DMSO-d_6): δ (ppm) 4.008 (s, 2H), 6.119 (s, 4H) & 7.580 (s, 1H), ^{13}C NMR (100MHz, DMSO-d_6): δ (ppm) 167.40, 168.93. (Figure 2.9-2.10)

For AETT, briefly ethylenediamine (3.1g) was dissolved in water, followed by adding chlorodiamino-triazine intermediate (1.45g). The mixture was heated to reflux at 110˚C overnight. Afterwards it was cooled in an ice bath for precipitating and filtering any insoluble white solids. The remaining filtrate was vacuum-concentrated to obtain a yellow oily mixture, which was further distilled to remove

the excess ethylenediamine and yielded a yellow solid. Ethanol was employed to wash this yellow solid for three times, which was eventually vacuum-dried to obtain a pure white solid product. (1.00g, 30%) ^{1}H NMR (400MHz, DMSO-d_6): δ (ppm) 2.905 (t, 1H), 3.37 (q, 4H), 6.164-6.306 (doublet, 4H), 6.690 (t, 1H), 8.181(b, 2H) ^{13}C NMR (100MHz, D_2O): δ (ppm) 37.75, 40.00, 166.31, 166.60. (Figure 2.11-2.14) An intense m/z peak at 170 was found by which corresponds to $[M-H]^+$.

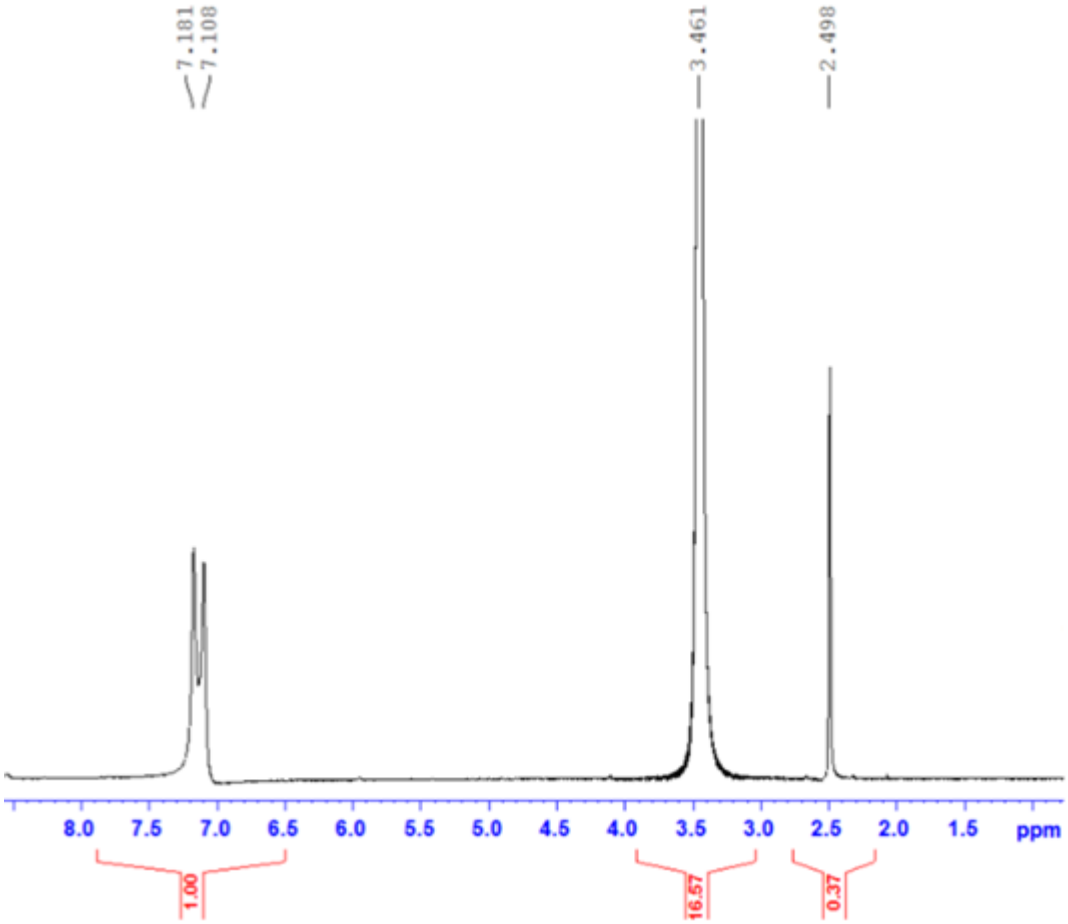

Figure 2.7. ^{1}H NMR spectrum of chlorodiamino-triazine in DMSO-d_6.

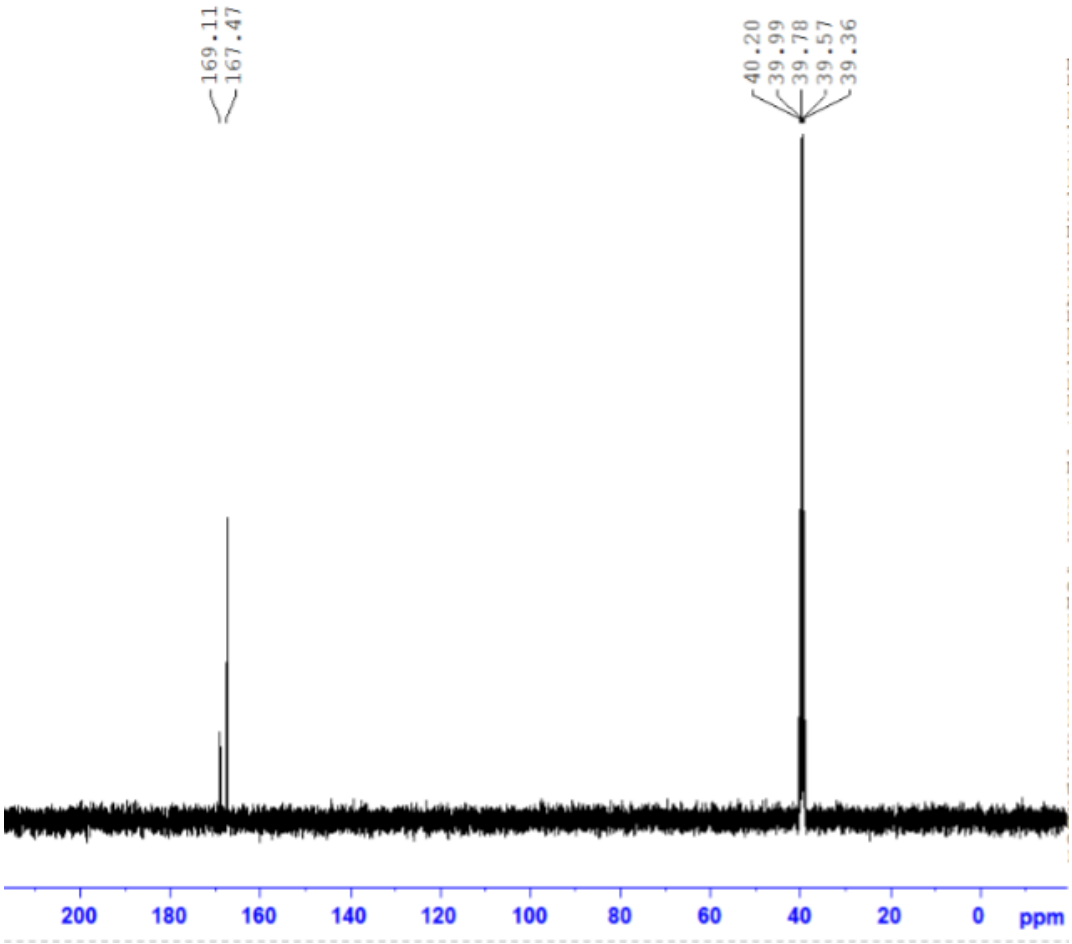

Figure 2.8. ^{13}C NMR spectrum of chlorodiamino-triazine in DMSO-d_6.

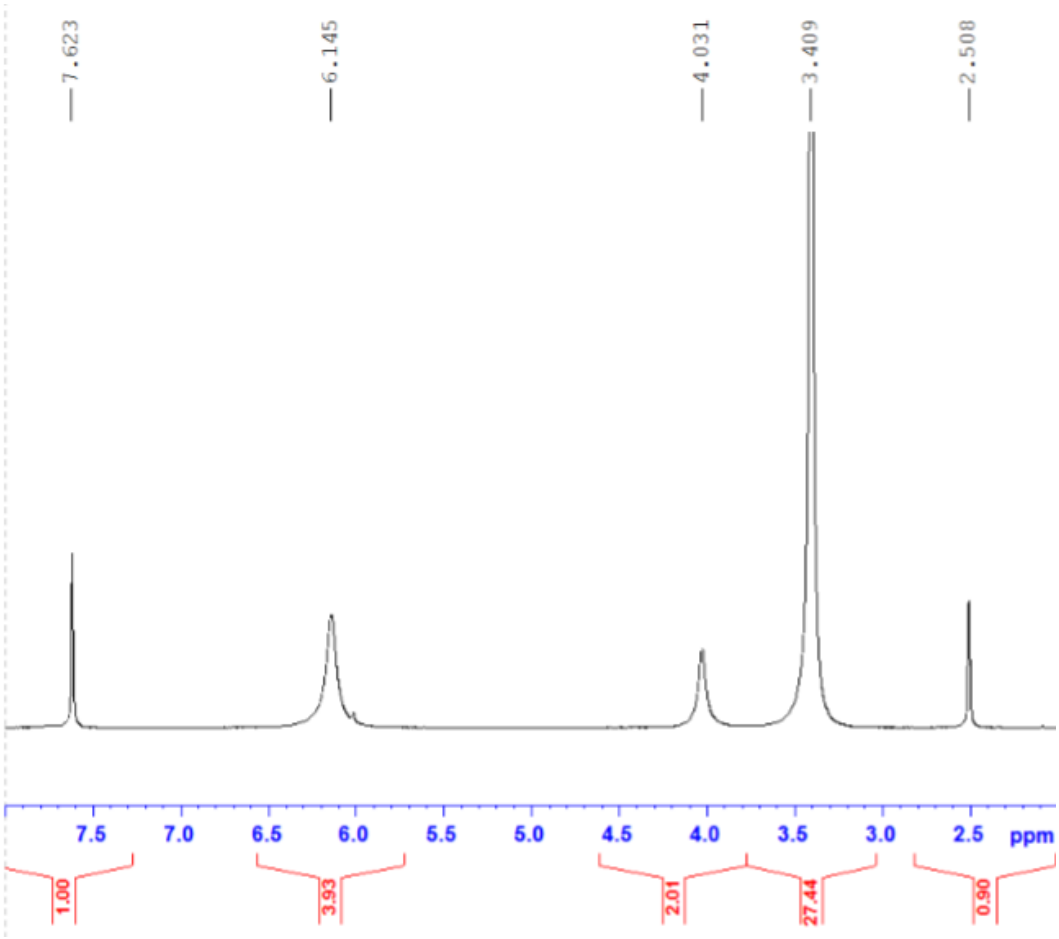

Figure 2.9 ^{1}H NMR spectrum of HTD in DMSO-d$_6$.

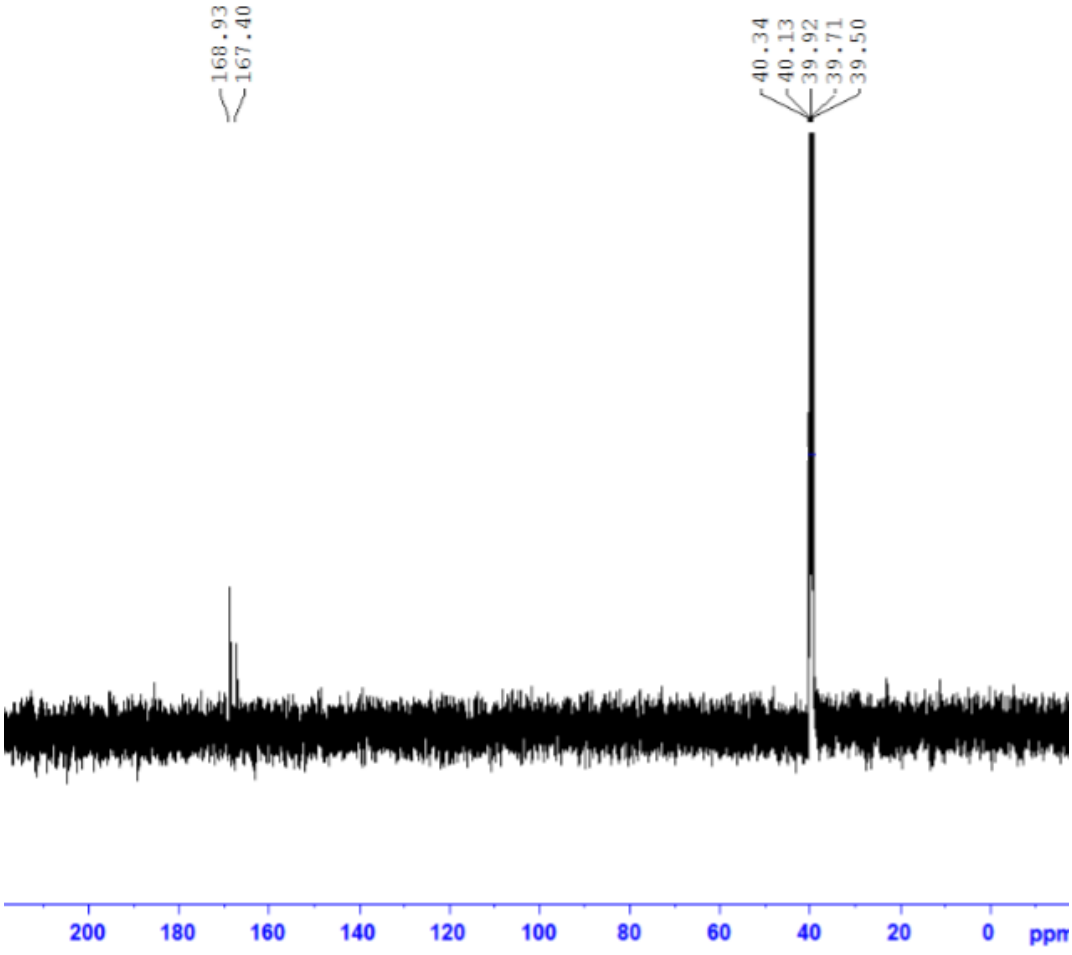

Figure 2.10 ^{13}C NMR spectrum of HTD in DMSO-d$_6$.

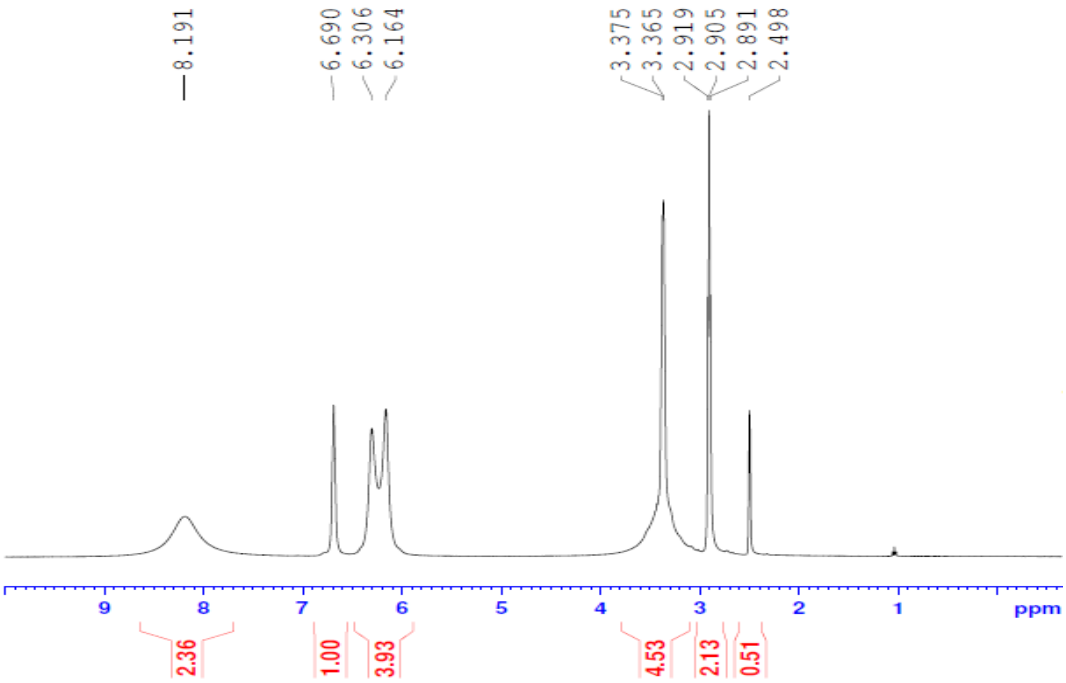

Figure 2.11 ^{1}H NMR spectrum of AETT in DMSO-d$_6$.

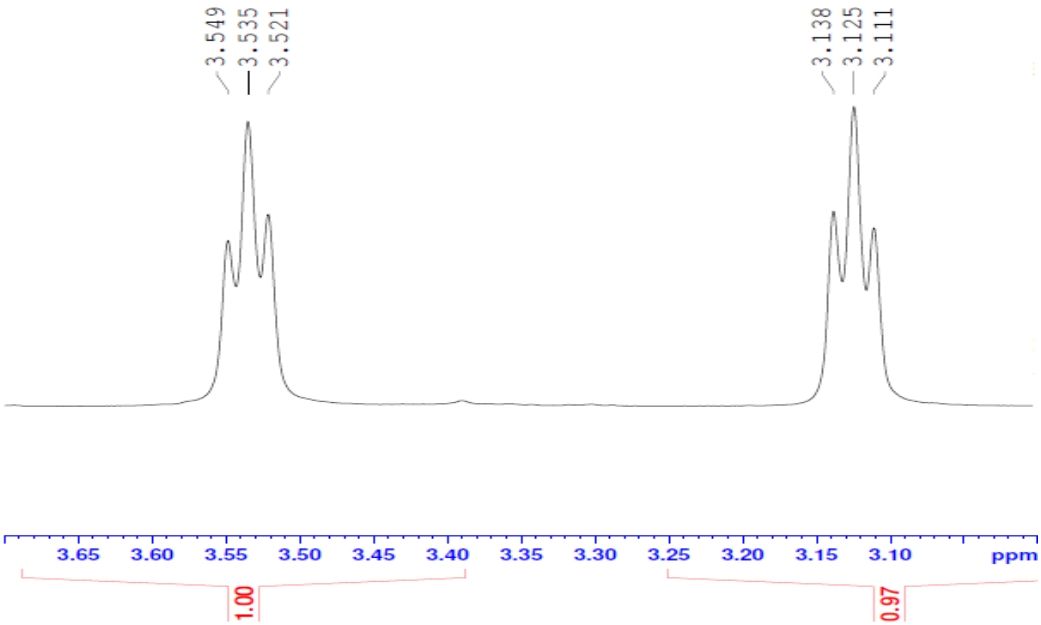

Figure 2.12 ^{1}H NMR spectrum of AETT in D$_2$O (focusing on 3.0-3.7ppm only).

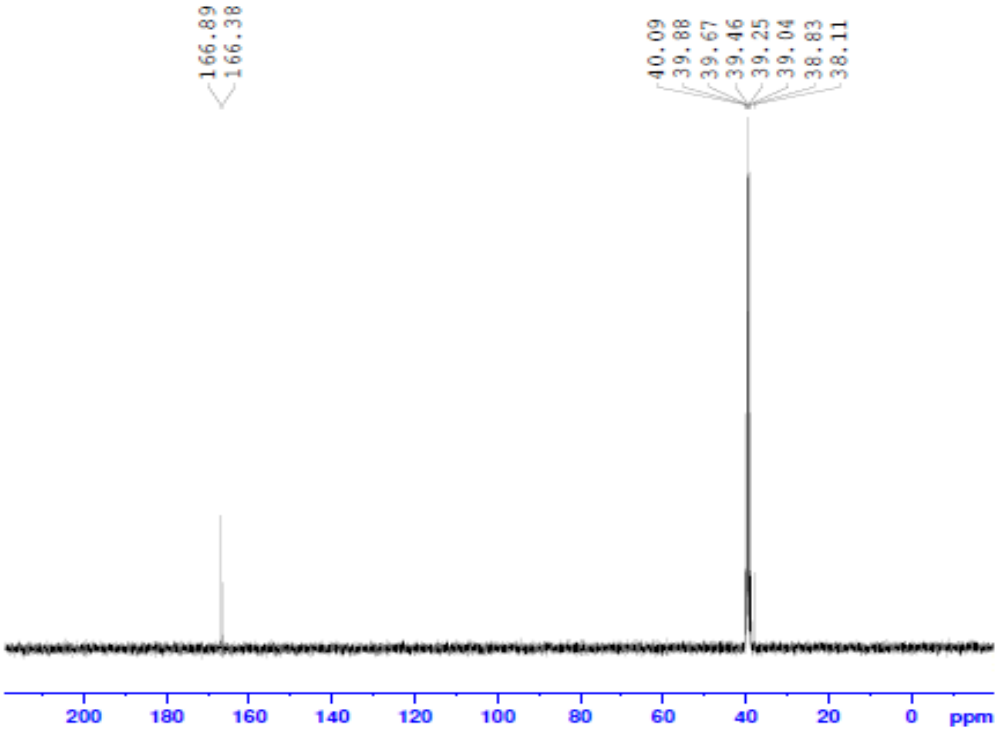

Figure 2.13 ^{13}C NMR spectrum of AETT in DMSO-d$_6$.

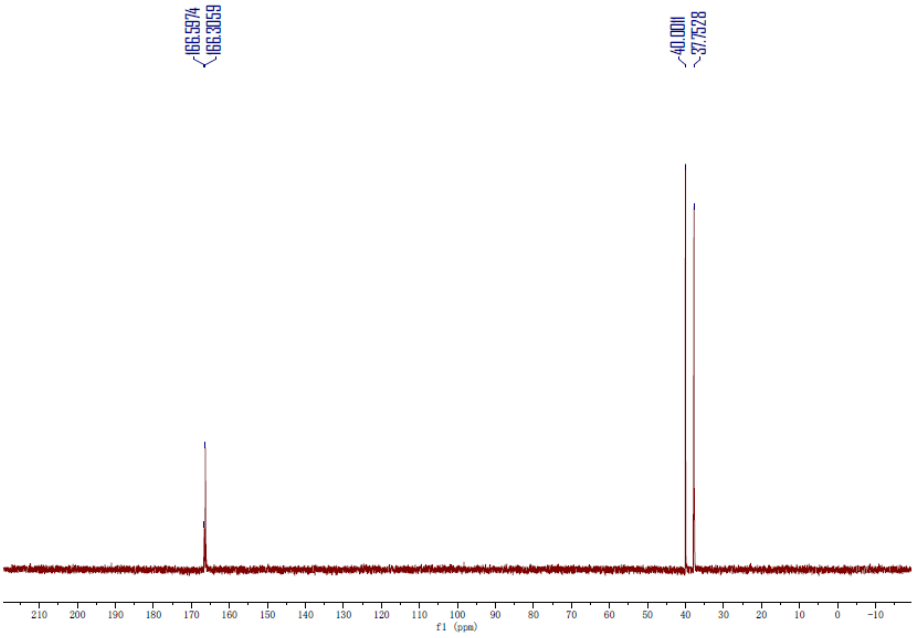

Figure 2.14 ^{13}C NMR spectrum of AETT in D$_2$O.

2.2.3 Conjugation of coating antigens onto magnetic microspheres

The three coating antigens were immobilized separately onto carboxylated microspheres by the standard NHS/EDC conjugation approach according to the protocol of amine coupling kit. [17-18] The effect of BSA as an intermediate linker was also studied. In short, inside an Eppendorf tube, $5x10^5$ microspheres were washed by bead-wash buffer (PBS, 0.05% Tween-20, pH 7.4) and activated by 10µl 50mg/ml NHS/EDC mixture for 20 minutes at room temperature inside activation buffer (0.1M NaH_2PO_4, pH 6.2). An excess of BSA (100µg) was then incubated with the activated microspheres for 2 hours at room temperature for binding to occur. After BSA coupling, the carboxylate groups of the coupled BSA were further activated by the same approach again at pH 6.0, and incubated with 100µg individual coating antigen overnight. Blocking buffer (PBS-TBN: PBS containing 0.1% BSA, 0.02% Tween-20 and 0.05% sodium azide, pH 7.4) was used to block the remaining unreacted carboxylate groups. Finally it was re-suspended and stored in storage buffer (PBS, 0.1% BSA, 0.02% Tween-20, 0.05% sodium azide) at 4˚C. All of the incubation steps and final storage were performed in the absence of light to prevent any photo-bleaching processes of microspheres. Separation was done by placing the Eppendorf tube inside the magnetic particle separator. The final concentration of microsphere was determined by a hemocytometer, where microspheres per unit area were counted with the aid of a microscope.

2.2.4 Sample pretreatment step for infant formula powder

To clean up the sample, infant formula powder (0.2g) was mixed with 1g of sodium chloride. 10mL of 0.1M PBS was added to dissolve the powder and salt. Afterwards, it was centrifuged at 13000rpm at room temperature for 10 minutes. The clear fraction in-between was used directly for immunoassay detection.

2.2.5 Melamine standards preparation

Infant formula powder is well known to have a complex matrix, and therefore a matrix-match calibration was essential to address this issue for an accurate quantitation. To perform such type of calibration, firstly we confirmed the absence of MEL in the selected milk powders of different brands by a commercial available ELISA kit. They were then mixed together in equal portions and prepared according to the procedures abovementioned. This pooled solution was used as diluent for preparing MEL standards from a stock MEL solution (1000µg/ml), which was prepared by dissolving 0.05g MEL in 50mL 0.01M PBS.

2.2.6 General procedure of immunoassay

All of the incubations were performed inside wells of a 96-wells flat bottom plate. General workflows were as-follows: In each well 2000 microspheres were utilized. Supernatant solution was removed by a handheld magnetic washer while keeping the magnetic microspheres inside wells. 100µl of MEL standards/sample and 50µl of the mouse monoclonal anti-MEL primary antibody

(0.58μg/ml) prepared in 0.01M PBS were then added for 1 hour incubation. Coating antigens on the microsphere surface and free MEL in samples would compete for the binding sites of primary antibodies. Afterwards supernatant solution was removed and the wells were washed with 150μl PBSBT for three times. After washing, 50μl phycoerythrin-linked goat anti-mouse Ig secondary antibody (3μg/ml) prepared in 0.01M PBS was added and incubated for 30 minutes for providing fluorescence signals to those bound primary antibody. Each well was further washed with another 150μl PBSBT for three times to remove any unbound antibodies, and finally being reconstituted with 125μl PBSBT for measurement. All of the incubation steps were performed in the absence of light with constant shaking (750rpm) at room temperature.

2.2.7 Instrumentation and data analysis

The fluorophore attaching to the secondary antibody and microsphere was quantified using a Luminex 200 analyzer for an indirect quantitation of MEL. Inside the laser region of the instrument, there were two lasers: a red laser (635nm) for classifying the internal dyes' ratio of microspheres and a green laser (532nm) for exciting the reporter phycoerythrin to give fluorescence signal. Fluorescence intensity was then detected at 565-585nm, which suited the emission range of phycoerythrin. The doublet discriminator gate, which was used to control the sampling particle size and avoid any clumped or aggregated microspheres, was optimized and set at 6300-22000. (Figure 2.15) The target number of minimum bead count was set to be 100, a suggested value by the protocol for giving a

representable result. 75µl was set as the sample acquisition volume. Figure 2.16 shows the typical results obtained from different calibration points of MEL standard curve. The calibration points were fitted using GraphPad Prism 6.0 by a modified Logistic-5PL equation set inside the Bio-Plex Software Manager (Brendan Scientific, Carlsbad, CA, USA) by a non-linear regression fitting procedure:

$$y = d + \frac{a - d}{[1 + \left(\frac{x}{c}\right)^{b}]^{g}}$$

where x is the concentration, y is the response, a is the estimated response at zero concentration, b is the slope of the tangent at midpoint, c is the midrange concentration or midpoint, d is the estimated response at infinite concentration, and g is an asymmetry factor. [19]

All measurements in every experiment were recorded at least twice, and results were expressed as the mean value ± SEM (standard error of the mean).

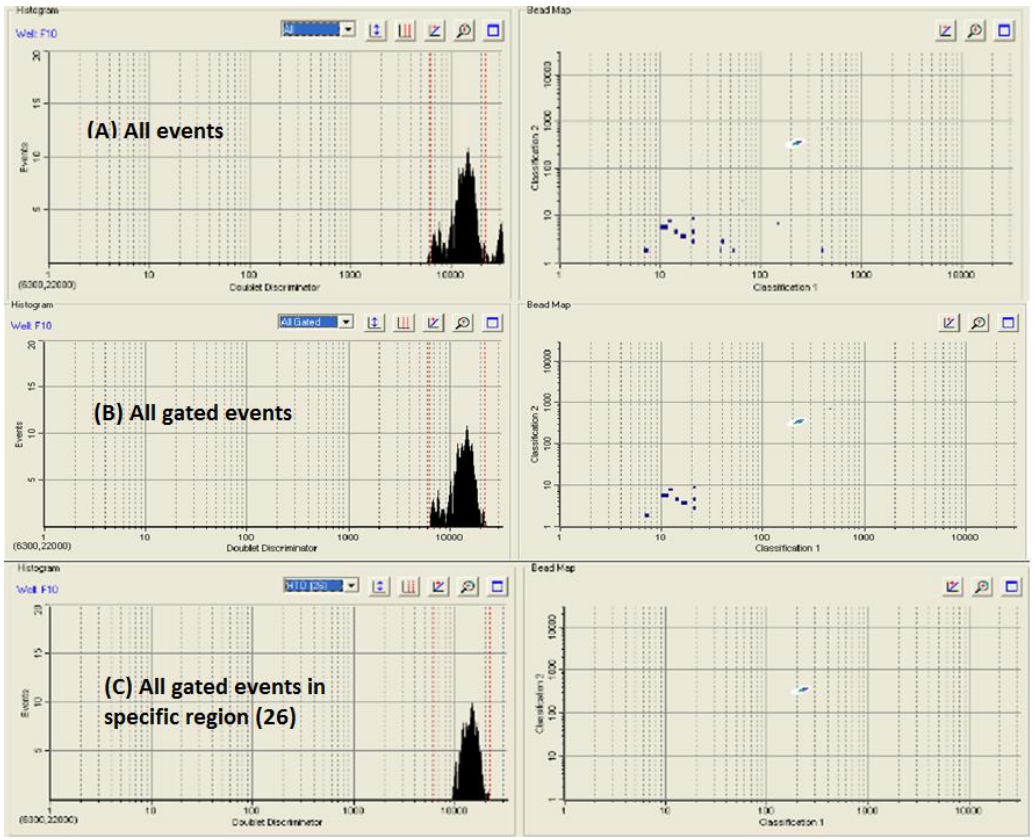

Figure 2.15 Selection of target events to be monitored by gating and bead-map region selection.

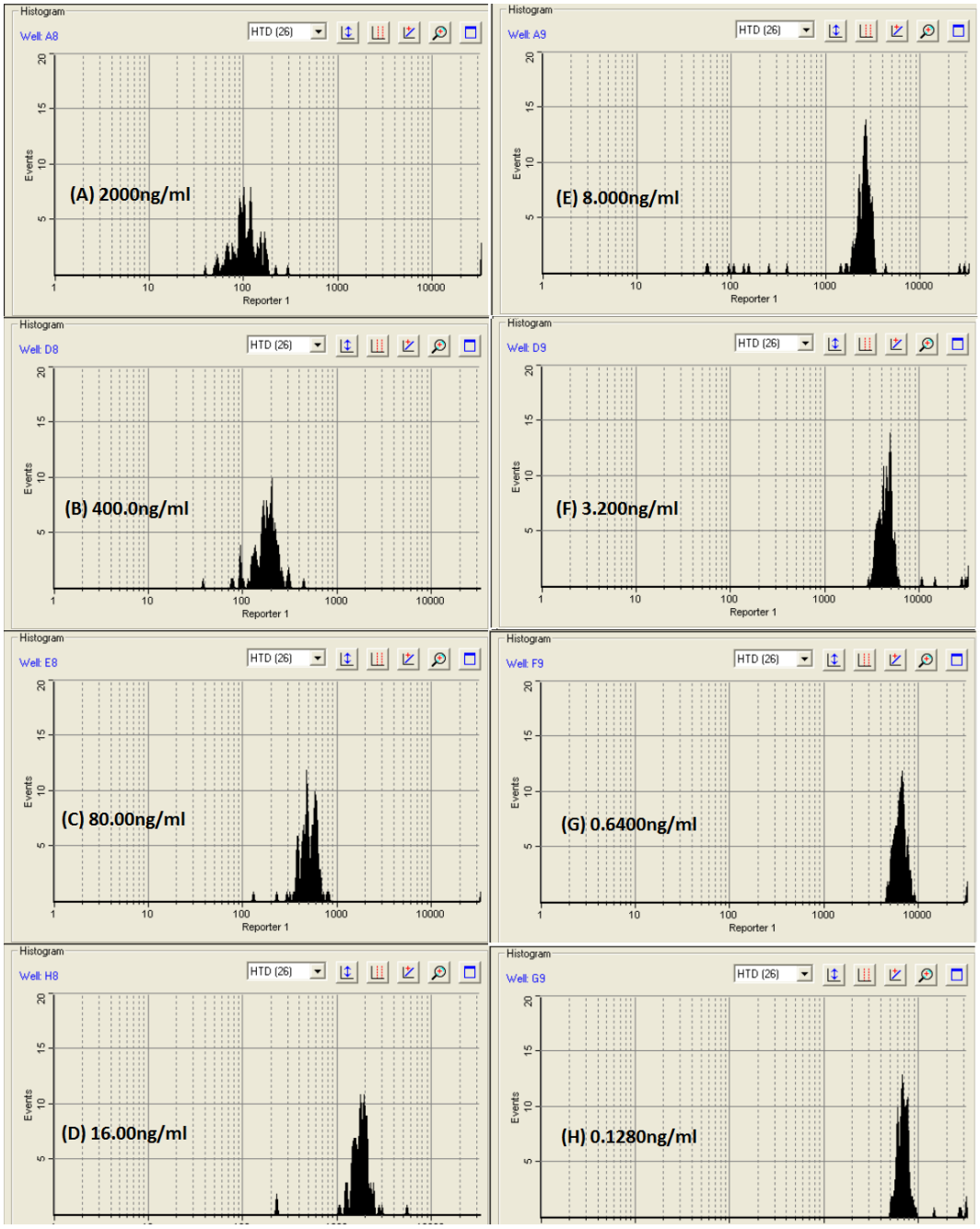

Figure 2.16 Histogram plot of fluorescence intensity of different calibration points of MEL standard curve. (0.1280-2000ng/ml)

2.3 Results & discussion

2.3.1 Optimization of working conditions

To search for the best working conditions for spike analysis, different parameters were optimized and they are discussed in the following section:

Type of coating antigen:

The efficiencies of MEL, HTD and AETT as coating antigens were compared. They were all directly conjugated onto microspheres under the same conditions and similar procedures as above. The decorated microspheres were then titrated against different concentration of primary antibody and fixed amount of secondary antibody. The corresponding fluorescence intensity was measured and plotted. (Figure 2.17) We can observe an increasing trend in both cases, implying their successful immobilization onto surfaces of microspheres. However, comparing the three cases, when employing AETT as coating antigens the given fluorescence intensity was apparently much greater than in other two cases. Therefore AETT was chosen as the coating antigen for the final real samples analysis.

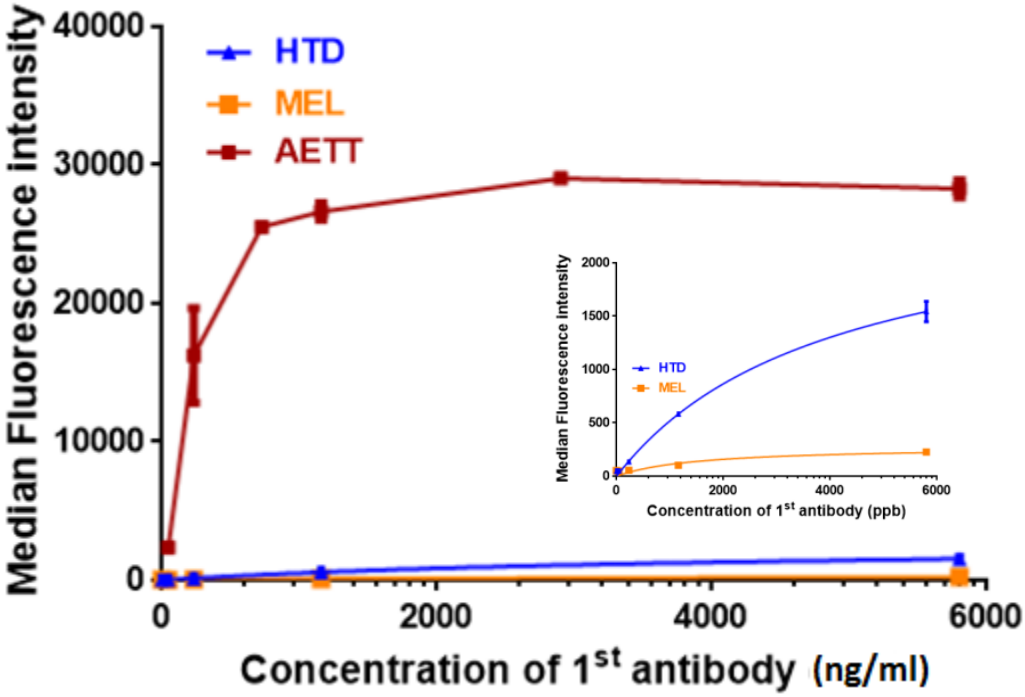

Figure 2.17 Titration of microspheres of different coating antigens against primary antibody. (0-5800ng/ml) Inset: y-axis re-adjusted for HTD and MEL.

Amount of coating antigen for immobilization:

Three concentrations of AETT (10, 50 and 100µg) were tested to investigate how the sensitivity was being affected by plotting and comparing the calibration graphs for these three batches of microspheres. (Figure 2.18) It we demonstrated that the three curves overlapped to each other when expressed in percentage inhibition versus concentration curve, implying them having a similar sensitivity. When expressed in terms of median fluorescence intensity, a higher immobilization concentration gave higher median fluorescence intensity under the same conditions. Therefore the highest tested concentration of AETT (100µg) was selected for a higher resolution.

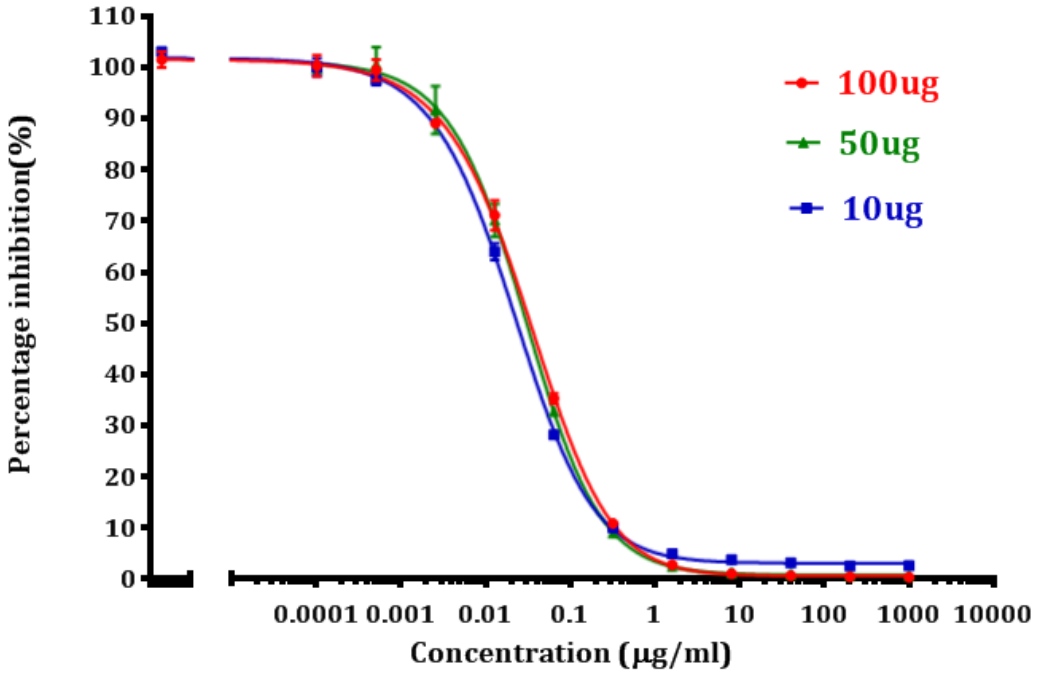

Figure 2.18 MEL calibration curve obtained with three batches of microspheres, with each being coated with 10, 50 or 100µg of AETT separately. All data points are expressed as the percentage inhibition in the absence of any MEL (mean ± SEM, n=2)

Competition format:

In previous literatures, different types of incubation procedures, including both one-step and two-steps incubation have been reported among coupled microsphere, primary antibody and sample solution. [20-24] It was believed the sequence and approach of incubation were critical to the method's performance, so three types of competitive formats and their corresponding calibration curves were compared in this study. As observed in Figure 2.19, the format in green curve in

which the primary antibody was incubated with microsphere first, it was having the poorest sensitivity. For the other two formats, again the calibration curves nearly superimposed implying a similar sensitivity when expressed in terms of percentage inhibition. But when looking into their median fluorescence intensity, the format in blue curve gave higher signal and better resolution. Moreover, such a one-step incubation format was much more simple and convenient.

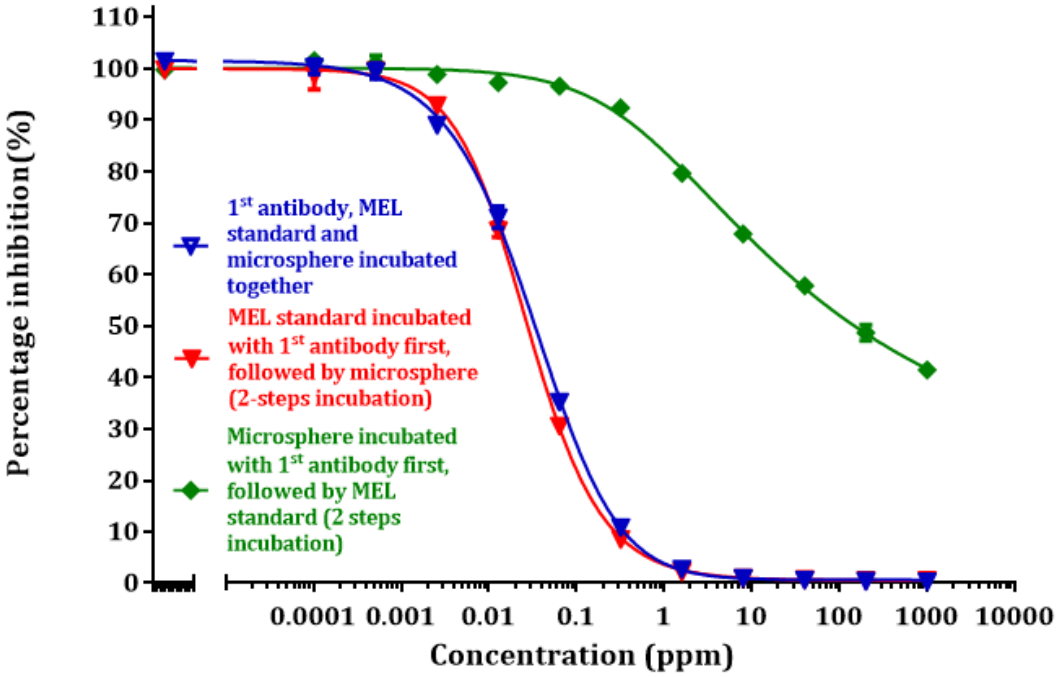

Figure 2.19 MEL calibration curve obtained with three different competition formats. For one-step incubation (blue curve), the total incubation time was 1 hour. For two-steps incubation (red and green curves), each step was incubated for 30 minutes. All data points are expressed as the percentage inhibition in the absence of any MEL (mean ± SEM, n=2)

Incubation time with primary antibody:

The incubation time with the primary antibody is also having a critical effect on the extent of competition between microsphere and MEL in sample and thus the sensitivity of the method. Different incubation durations from 15-120 minutes were compared. As shown in Figure 2.20, shortening the incubation time from 120 to 15 minutes gradually shifted the calibration curve from right to the left. It means it would be more sensitive for low concentration analysis. But the compensation compromise was weaker median fluorescence intensity as well as a poorer resolution and precision. This was due to not having sufficient time for reaching the equilibrium state. Since the method was designed to be a simple and fast screening method, 60 minutes was chosen which is reasonably fast and demonstrating a good precision along its dynamic range. Moreover, this incubation time is long enough for minimizing any incubation time delay when handling large batch analysis.

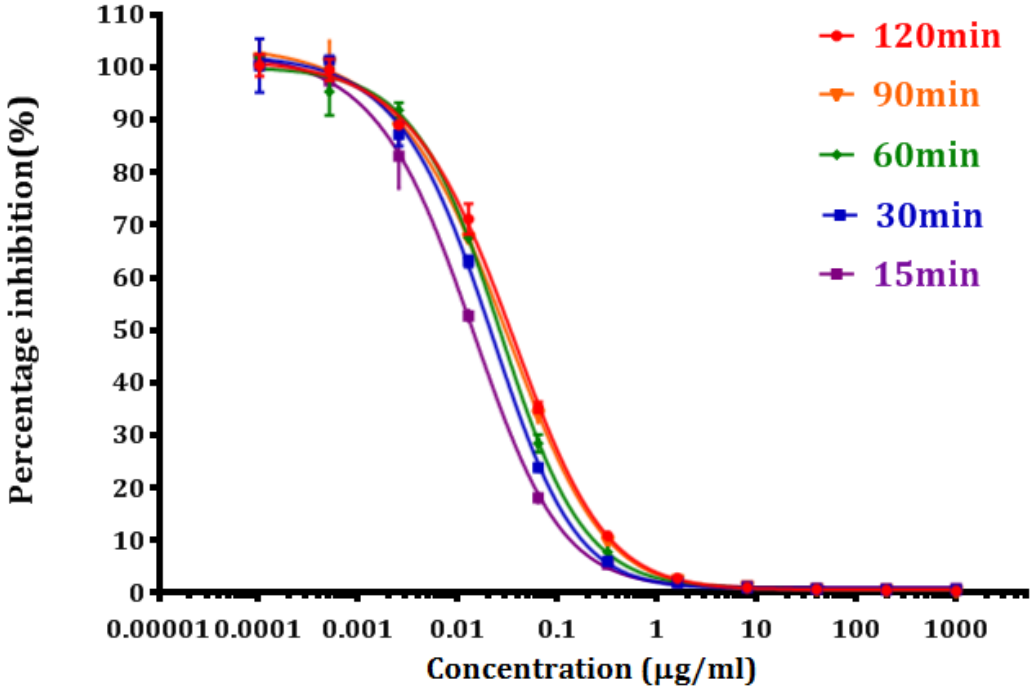

Figure 2.20 MEL calibration curve obtained with five different incubation times. (15-120 minutes) All data points are expressed as the percentage inhibition in the absence of any MEL (mean ± SEM, n=2)

Antibody concentration:

There were two factors we needed to make a balance when optimizing antibody concentration: the given fluorescence intensity and cost. For MEL primary antibody, fluorescence leveled off at around 0.58µg/ml, so this level was employed for further tests. (Figure 2.21) For secondary antibody, as the concentration increased from 50 to 3000 ng/ml, the median fluorescence intensity kept increasing, since more secondary antibodies had been successfully bound to the microsphere. (Figure 2.22) Higher concentrations were not tested due to the

high cost incurred and therefore the highest level being tested (3000ng/ml) was employed for the spiked sample analysis afterwards.

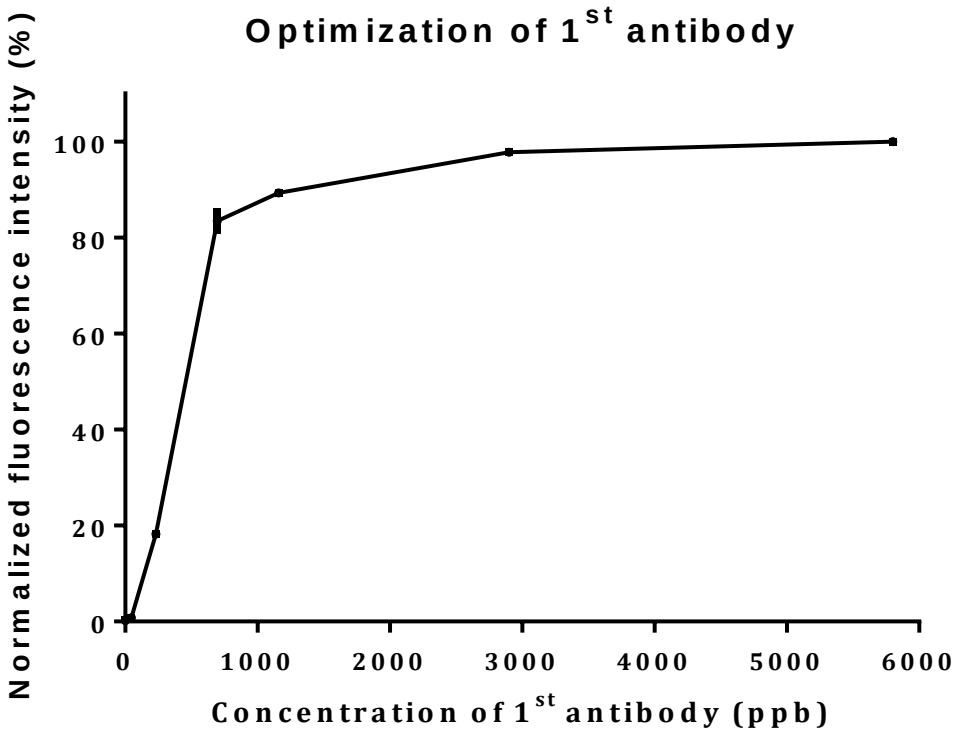

Figure 2.21 Optimization of primary antibody concentration. Each data point was obtained under different concentrations of 1st antibody in the absence of MEL. (0.37-5800ng/ml) The signals were normalized to the highest signal measured (5800ng/ml) and expressed as normalized fluorescence intensity (mean ± SEM, n=2)

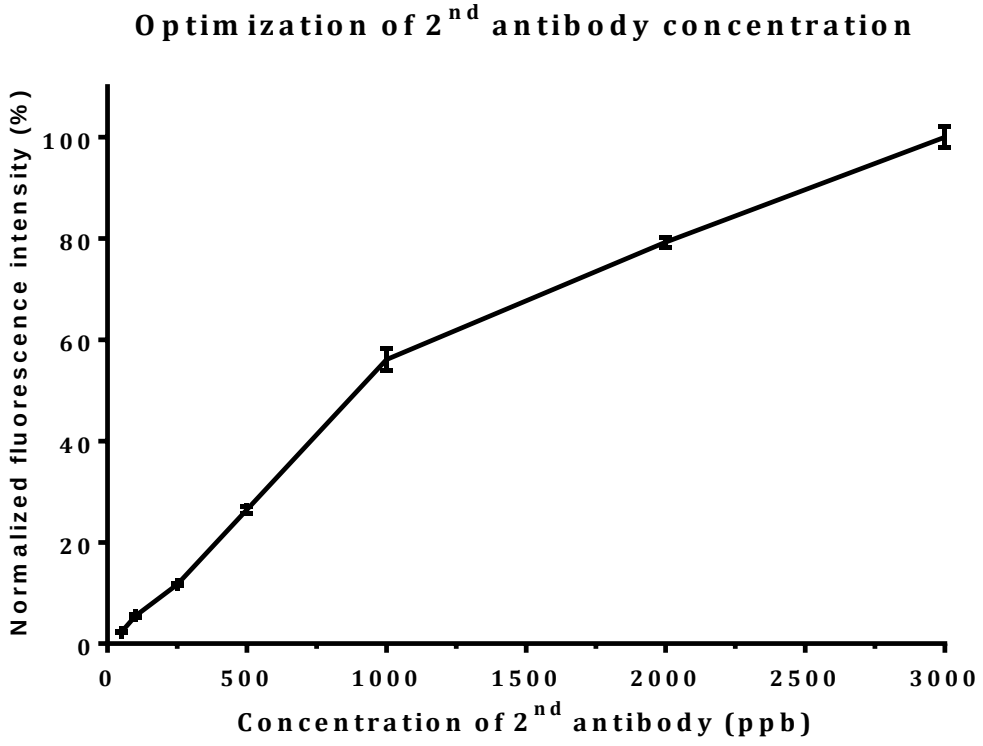

Figure 2.22 Optimization of secondary antibody concentration. Each data point was obtained under different concentrations of 2nd antibody in the absence of MEL. (50-3000ng/ml) The signals were normalized to the highest signal measured (3000ng/ml) and expressed as normalized fluorescence intensity (mean ± SEM, n=2)

After optimization, the calibration graph of MEL with maximized sensitivity was obtained (Figure 2.23). Concentration required to cause a 50% inhibitory on the highest fluorescence intensity, or IC_{50} which defined the sensitivity of the assay, was found to be 7.58ng/ml. IC_{10} - IC_{90}, which defined the dynamic range of the method, were from 1.01ng/ml to 94.30ng/ml. [22] Limit of

detection (LOD) was calculated by subtracting three times the standard deviation of median fluorescence intensity of blank (n=16) from the maximum fluorescence signal of the curve, which was determined to be 0.70ng/ml. The method was more sensitive towards MEL when compared with most MEL detection methods. (Table A2.1-A2.2)

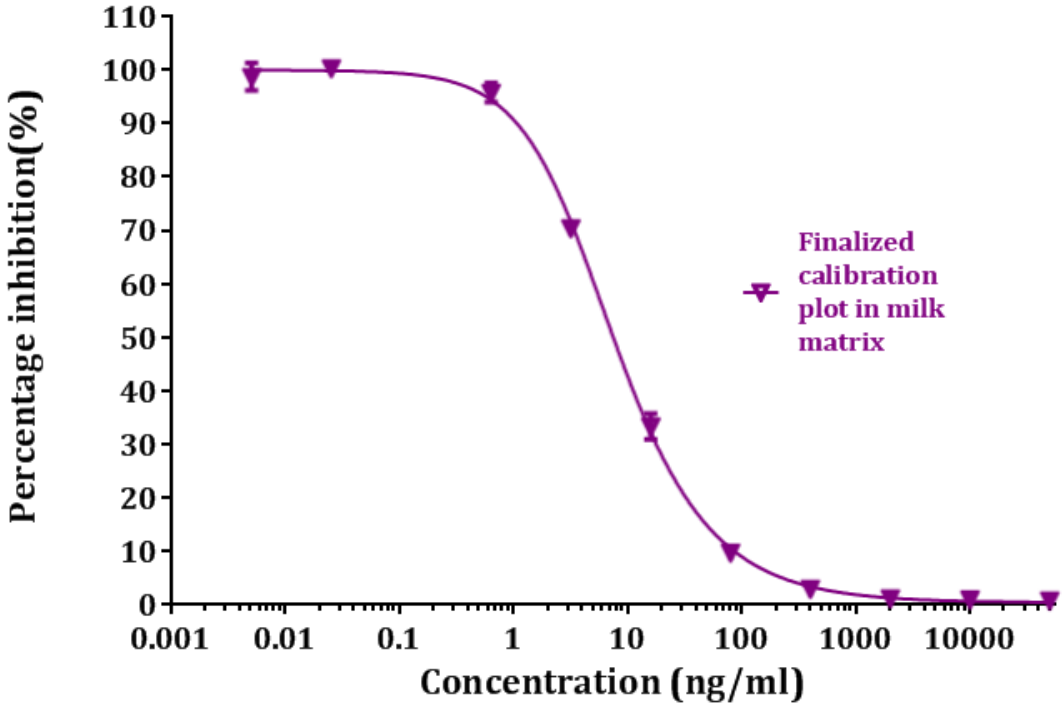

Figure 2.23 Calibration curve of MEL in milk matrix after optimization.

2.3.2 In-house validation of the developed assay

Reproducibility:

To demonstrate the reproducibility and robustness of the developed assay, MEL calibration curves were plotted and compared using either the same batch of

immobilized microspheres on three different days or three independent batches of immobilized microspheres on the same day. IC_{20}, IC_{50} and IC_{80} values were then compared to see if the shape of the calibration curves were significantly different from each other. (Figure 2.24 and 2.25) Student's t-test demonstrated that there were no significant differences for the three trials in either inter-batch or intra-batch reproducibility at 95% confidence interval ($p < 0.05$). Performance is stable and easy to be reproduced, showing a good robustness of the developed assay.

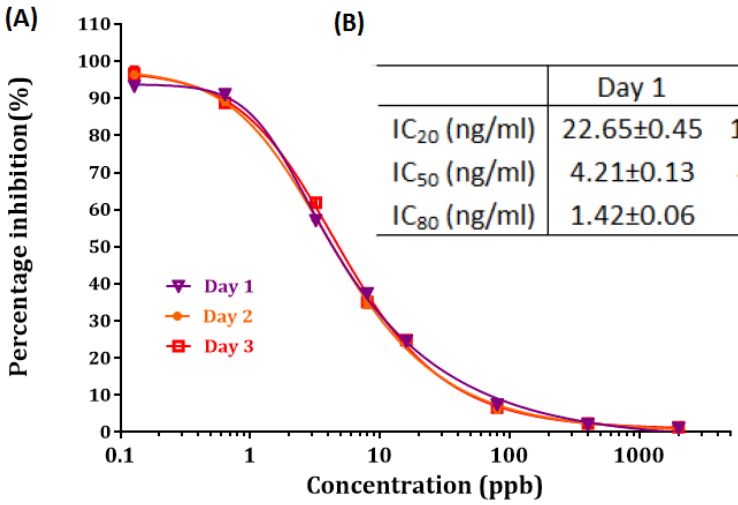

	Day 1	Day 2	Day 3
IC_{20} (ng/ml)	22.65±0.45	19.30±0.40	19.50±0.20
IC_{50} (ng/ml)	4.21±0.13	4.13±0.05	4.76±0.05
IC_{80} (ng/ml)	1.42±0.06	1.18±0.03	1.35±0.15

Figure 2.24 (A) MEL Calibration curves plotted on different days using the same batch of immobilized microspheres under the same conditions (range: 0.128–2000ng/ml). Each data point was expressed as the percentage inhibition in the absence of MEL (mean ± SEM, n=2). (B) IC_{20}, IC_{50} and IC_{80} of the corresponding three calibration curves (mean ± SEM, n=2).

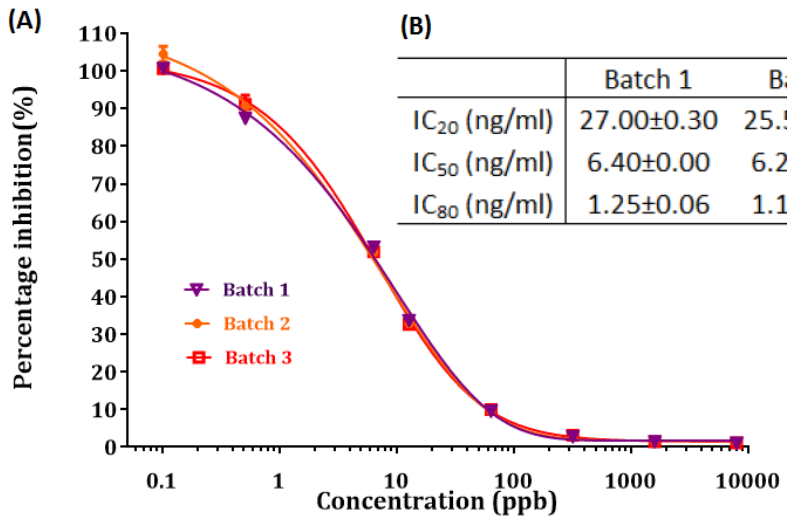

(B)

	Batch 1	Batch 2	Batch 3
IC_{20} (ng/ml)	27.00±0.30	25.55±1.75	27.35±1.85
IC_{50} (ng/ml)	6.40±0.00	6.27±0.43	6.41±0.15
IC_{80} (ng/ml)	1.25±0.06	1.13±0.07	1.51±0.26

Figure 2.25 (A) MEL Calibration curves plotted on the same day using three independent batches of immobilized microspheres under the same conditions (range: 0.128–10000ng/ml). Each data point was expressed as the percentage inhibition in the absence of MEL (mean ± SEM, n=2). (B) IC_{20}, IC_{50} and IC_{80} of the corresponding three calibration curves (mean ± SEM, n=2).

Selectivity:

To test for the selectivity of the method, four MEL analogs were employed and being tested in the place of MEL. (Figure 2.26) In each case the corresponding calibration graphs were constructed. (Figure 2.27) Cross-reactivity values were then calculated based on the IC_{50} value using the following equation:

$$CR\% = IC_{50} \text{ of MEL} / IC_{50} \text{ of compound X } 100$$

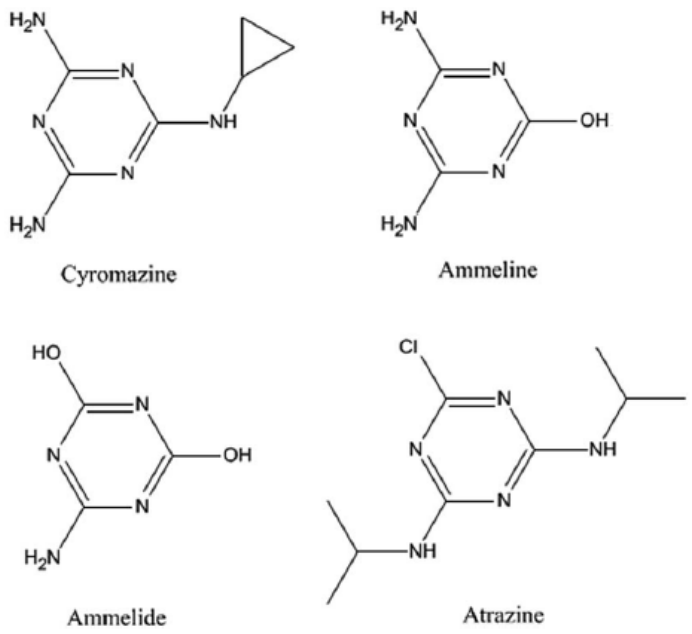

Figure 2.26 Chemical structures of four MEL analogs.

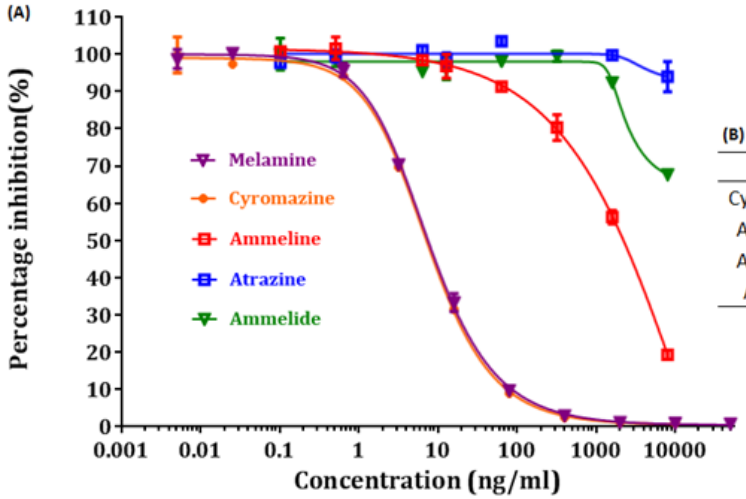

(B)

	Cross-Reactivity (%)
Cyromazine	100
Ammelide	<0.5
Ammeline	<0.5
Atrazine	<0.5

Figure 2.27 (A) Calibration curves of MEL, cyromazine, ammeline, atrazine and ammelide. Each data point was expressed as the percentage inhibition in the absence of that compound. (mean ± SEM, n=2) (B) Cross-reactivity values to MEL.

Comparison of performance to a commercial available ELISA kit:

Spike analysis was finally performed to check if the recoveries of fortified MEL at four concentration levels (0.1, 0.5, 1.5 and 10μg/g) could be reproduced in six brands of infant formula powders, which had been analyzed by a commercial ELISA kit confirming the absence of any MEL. Spiked samples were then measured by both the developed method and the commercial ELISA kit. The results are summarized in Table 2.2:

Infant formula powder	Concentration fortified (μg/g)	Mean recovery(%) obtained from microsphere-based method	RSD(%)	Mean recovery(%) obtained from a commercial ELISA kit	RSD(%)
Brand 1	0.1	102.5	2.13	Nil (out of detection range)	
	0.5	102.0	0.26	124.6	15.99
	1.5	97.8	5.94	83.5	5.09
	10	122.6	4.60	111.2	5.43
Brand 2	0.1	120.3	5.88	Nil (out of detection range)	
	0.5	117.8	2.67	110.2	5.79
	1.5	103.7	3.41	80.6	24.61
	10	111.6	4.85	86.1	12.81
Brand 3	0.1	99.5	3.30	Nil (out of detection range)	
	0.5	91.7	2.34	127.3	9.81
	1.5	94.5	2.18	79.9	5.15
	10	102.3	2.10	127.4	5.85
Brand 4	0.1	77.7	7.41	Nil (out of detection range)	
	0.5	89.2	1.10	134.3	6.11
	1.5	97.2	2.72	80.9	5.85
	10	89.8	7.18	115.9	7.90
Brand 5	0.1	105.5	2.84	Nil (out of detection range)	
	0.5	120.0	2.30	120.8	0.44
	1.5	115.7	7.81	80.4	16.51
	10	123.1	6.23	116.8	7.31
Brand 6	0.1	109.5	3.95	Nil (out of detection range)	
	0.5	127.0	2.50	170.2	9.88
	1.5	108.3	6.57	88.3	12.02
	10	123.1	5.70	125.3	15.01

Table 2.2 Spike analysis results in six brands of fortified infant formula powder samples as determined by the developed microsphere-based method and a commercial ELISA kit (n=3).

2.3.3 Discussion

At the early stage of assay development, designing the coating antigen was the first thing to start with. Apart from using MEL as its homogeneous coating antigen, HTD and AETT were synthesized and proposed to be a heterogeneous coating antigen for being immobilized onto the carboxylated microsphere. The former one was previously reported to be a structural mimic for MEL, and it was demonstrated to be a good hapten for antibody production and good coating antigen on the sensor chip of an optical surface plasmon resonance biosensor. [25] The latter was designed by us, and it possesses the following characteristics: Firstly it has a similar structure to MEL with only one NH_2 group being modified into an ethylenediamine spacer arm; the other amine groups as well as the triazine core remain unchanged to keep the melamine moiety for forming an epitope to be recognized by MEL monoclonal antibody. Secondly, when AETT molecules are immobilized onto the microsphere in a high concentration, strong steric hindrance might be brought by the bulky triazine rings. It was believed the ethylenediamine spacer arm can help to alleviate it and therefore allow more molecules to be coupled onto the microsphere. This was proved by another experiment carried out using linkers with various lengths to bridge HTD and microspheres. (Figure 2.28 and 2.29) Data showed that with a longer linker, steric hindrance could be minimized. More coating antigens and antibodies could therefore effectively bind onto the bead. Thirdly, the terminal NH_2 group on ethylenediamine spacer arm can provide a reactive amine for further conjugation with carboxylate groups on microspheres via typical NHS/EDC chemistry. And finally the results showed that

our designed MEL analog was the best coating antigen compared to HTD or MEL itself under described conditions. For the low conjugation efficiency of HTD and MEL, probably working pH was needed to be further optimized, e.g. to a more acidic condition as previous procedures suggested. [25]

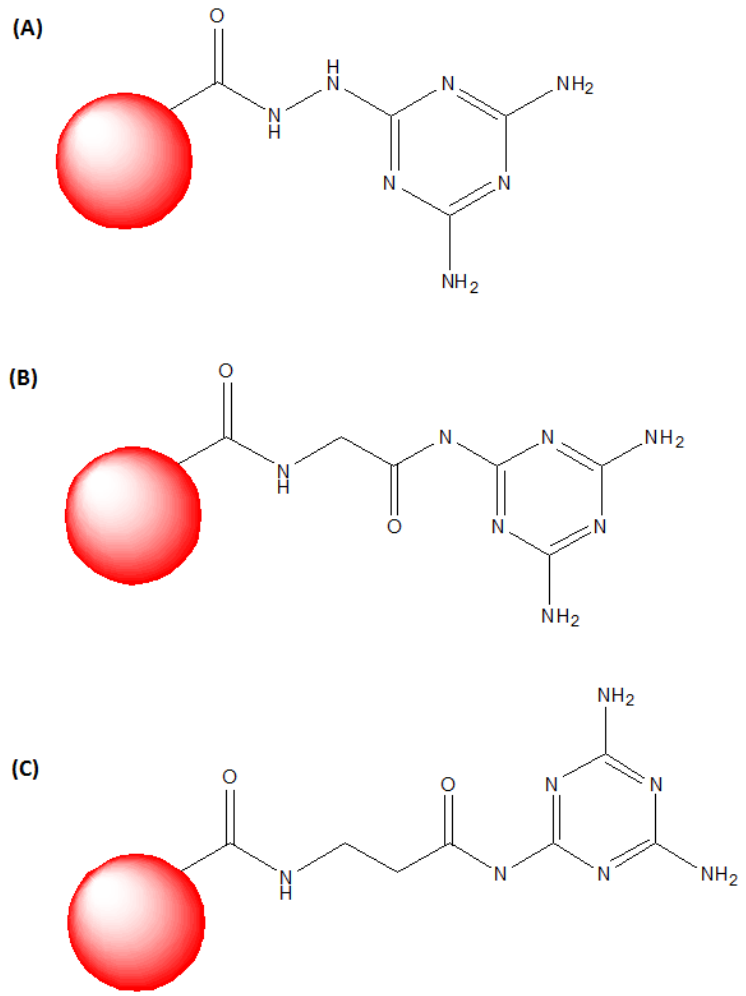

Figure 2.28 Schematic diagram of conjugated HTD with (A) no linker, (B) glycine (NH_2CH_2COOH) as linker, (C) β-alanine ($NH_2CH_2CH_2COOH$) as linker.

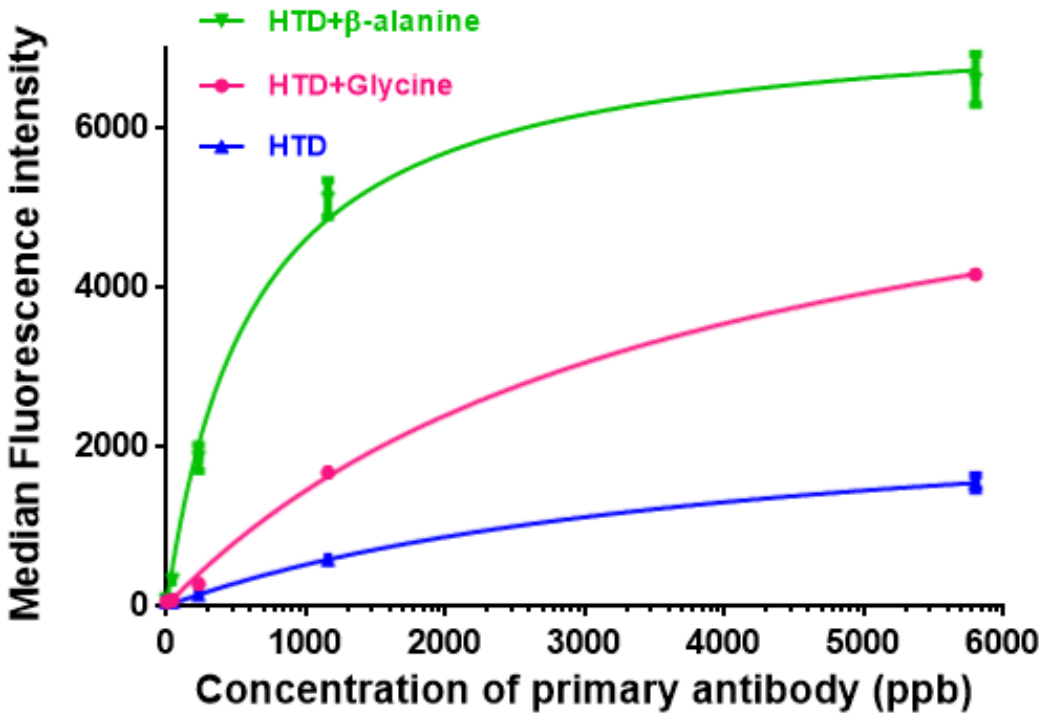

Figure 2.29 Titration of HTD coupled microspheres with different linkers against MEL primary antibody.

AETT was initially immobilized onto the microsphere directly without any linkers. However, it was demonstrated to have a poor reproducibility. RSD for certain calibration points could reach up to 25% which was not desirable. (Figure 2.30) To address this problem, BSA protein was used as another linker between the microsphere and AETT molecules. Compared to glycine and β-alanine employed in previous preliminary study on linkers' length, BSA is having a larger molecular size (~67kDa) and a lot of carboxylate and amine groups. During immobilization, the carboxylate groups on microspheres were activated and reacted with the amine groups on BSA. Afterwards, the carboxylate groups on

BSA were activated once again for reacting with the amine groups on AETT this time. Overall AETT was coupled via such a two-steps coupling scheme. One thing to notice was that the pH of solution during coupling of AETT onto adhered BSA needed to be conducted at pH 6 for preventing any possible self-conjugation of BSA through its carboxylate and amine groups and therefore the aggregation of microspheres. [26] With the use of BSA, the reproducibility improved with RSD<10% in all calibration points. Furthermore, it was discovered that BSA indeed provided more conjugation sites for AETT and led to stronger fluorescence intensity. (Figure 2.30)

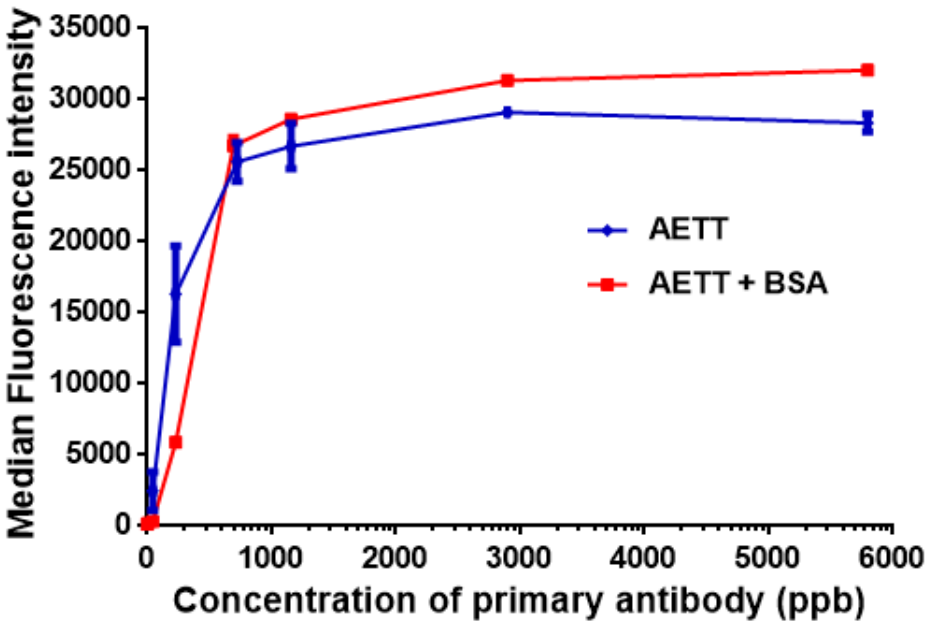

Figure 2.30 Comparison of titration results against primary antibody using AETT-microspheres in the present or absence of BSA linker.

It was observed at first that the number of beads successfully being counted by the instrument was very small to give reproducible results (less than 30), despite 2000 beads had been added into each well. Meimaridou *et al.* suggested that this problem was possibly due to the physical adsorption of polystyrene microspheres onto the plate well surface. [27] Therefore we changed the washing solvent and diluent from typical PBS to PBSBT. On one hand, the plenty amount of BSA inside could act as a scarified protein and saturate all binding sites. On the other hand, Tween-20 is a non-ionic surfactant well known to minimize any non-specific protein adsorption in immunoassay. Both supplements worked together and helped addressing the problem. Finally the number of beads could be counted easily and reached the target value 100.

The spiked real infant powder samples could not be easily quantitated by standards prepared in blank solvent due to the complexity of matrices in infant formula milk powder, which resulted in a significant difference in the median fluorescence intensity of calibration curves especially at the low concentration region. (Figure 2.31) The simple pre-treatment steps abovementioned were not sufficient to completely reduce such matrix interferences. As results, for an accurate quantitative analysis a matrix-match calibration approach was essential by preparing all standard solutions inside a pooled milk matrix. However, different brands of infant formulas are having different composition of constituents, resulting in a different matrix effect. We guessed a different protein profile would be the major difference by analyzing their contents. Salting out technique was therefore employed by using a more concentrated PBS (0.1M) during sample

preparation. This technique is an easy way to remove proteins inside without complicating or lengthening the sample preparation procedures. Compared to 0.01M PBS we used at first, a more similar milk matrix environment was maintained in each case. The spike analysis of all the six brands of infant formula powder could at last give good recoveries in each spiked level.

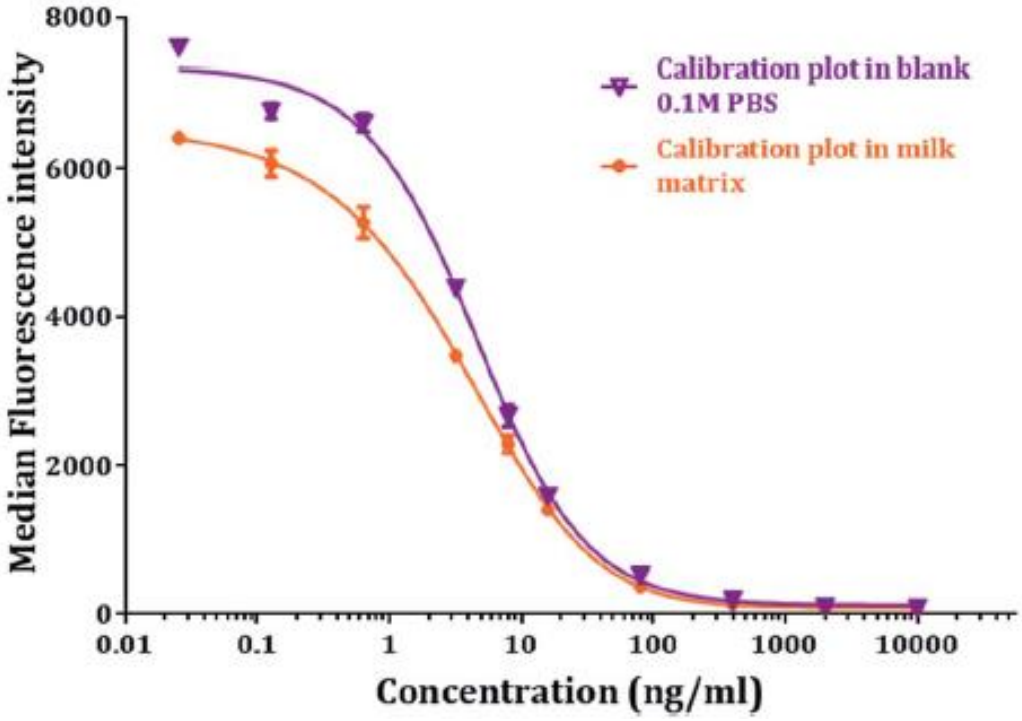

Figure 2.31 Calibration plot of melamine prepared in blank 0.1 M PBS buffer and in milk matrix.

The validation of the performance of the developed assay was achieved by a spike analysis in six different brands of infant formula powders designed for different ages of infants. Four difference concentration levels were tested: 0.1, 0.5, 1.5 and 10μg/g where the legislated acceptable level was 1μg/g. Results proved

that, not only did it give satisfactory spike recoveries; the relative standard deviations of all tested fortified levels were all also acceptable and smaller than 8%.

When comparing with the results obtained from the ELISA kit, which failed to detect accurately at low concentration level and failed to give precise results as observed from the RSDs (up to 24.61%), apparently our developed method showed superiority no matter in sensitivity, precision, accuracy and suitability for analysis of large batch of samples. More importantly, it can be transformed into a multiplex method easily for a simultaneous detection of other classes of milk contaminants/adulterants. That is a feature that conventional ELISA cannot achieve.

To test for the specificity of the method, cross-reactivity values to other MEL analogs were explored. An insignificant cross-reactivity value to MEL (<0.5%) were demonstrated in most cases, only with cyromazine being an exception. It responded exactly identical as MEL to the primary antibody with CR value equal to 100%. It could therefore be deduced that the targeted epitope of the chosen MEL primary antibody consists of two NH_2 groups and one N atom attaching to the triazine ring. An extra lone pair of electrons, for example from the hydroxyl group in ammeline, could already affect the binding of antibody. Unfortunately the monoclonal antibody towards MEL was a limiting resource to this study and only one type of commercially available antibody was being tested. Other types of antibodies need to be tested if higher specificity towards MEL is

desired. For example, Cao *et al.* has reported their production of a novel MEL monoclonal antibody which showed a very good selectivity targeting MEL. [1]

Nevertheless, we should also notice that the cross-reactivity to cyromazine should not be viewed as a drawback. The developed method was designed as a primary screening technique to ensure milk safety. Cyromazine is actually a commonly used pesticide for controlling fry in cattle manure, field crops, vegetables and fruits by inhibiting insect growth. [28] MEL is one of its degradation products or metabolite. A Maximum Residue Level (MRL) of 0.05 mg/kg of cyromazine was also established by the Chinese Agriculture Department in 2001 in any foods of animal edible tissues. [29] This developed method would still be sensitive enough to screen for it at the same time according to the MRL level established. This method could therefore fulfil users' concerns when they want to detect MEL and cyromazine together, similar to other previously published literatures describing such dual-analytes detection. [30-32]

To further improve the performance of the assay in the future, polyclonal antibody, which is believed to exhibit a wider recognizing ability towards any structurally similar compounds to MEL, might be more suitable to be employed than monoclonal antibody to screen for any similar milk adulterants. A higher sensitivity was also expected.

2.4 References

1. Cao, B., Yang, H., Song, J., Chang, H., Li, S., & Deng, A. (2013). Sensitivity and specificity enhanced enzyme-linked immunosorbent assay by rational hapten modification and heterogeneous antibody/coating antigen combinations for the detection of melamine in milk, milk powder and feed samples. *Talanta*, 116, 173-180.
2. Hau, A. K. C., Kwan, T. H., & Li, P. K. T. (2009). Melamine toxicity and the kidney. *Journal of the American Society of Nephrology*, 20(2), 245-250.
3. Xiaojing, L. (2011). The cause and effect analysis of the melamine incident in China'. *Asian Journal of Agricultural Research*, 5(3), 176-85.
4. Sun, F., Ma, W., Xu, L., Zhu, Y., Liu, L., Peng, C., ... & Xu, C. (2010). Analytical methods and recent developments in the detection of melamine. *TrAC Trends in Analytical Chemistry*, 29(11), 1239-1249.
5. Yin, W., Liu, J., Zhang, T., Li, W., Liu, W., Meng, M., ... & Lu, X. (2010). Preparation of monoclonal antibody for melamine and development of an indirect competitive ELISA for melamine detection in raw milk, milk powder, and animal feeds. *Journal of agricultural and food chemistry*, 58(14), 8152-8157.
6. Ji, A. L., Wong, Y. L. I., Cai, T. J., & Liu, J. (2014). Infant formula safety concerns and consequences in China. *World journal of pediatrics: WJ*P, 10(1), 7.

7. Chu, P. W., Chan, K. M., Cheung, S. T., & Wong, Y. C. (2010). Review of analytical techniques used in proficiency-testing programs for melamine in animal feed and milk. *TrAC Trends in Analytical Chemistry*, 29(9), 1014-1026.
8. Tittlemier, S. A. (2010). Methods for the analysis of melamine and related compounds in foods: a review. *Food Additives and Contaminants*, 27(2), 129-145.
9. Nochetto, C. B., Stine, C. B., & Reimschuessel, R. (2013). Development and validation of a method for the simultaneous determination and confirmation of melamine and cyanuric acid in fish kidney by LC/MS/MS. *Journal of AOAC International*, 96(3), 663-669.
10. Hong, M., Sai, F., Yong-Ning, W. U., Zhang, L., Ping-Ping, Z. H. O. U., Hui-Jing, C. H. E. N., ... & Jing-Guang, L. I. (2009). Simultaneous determination of melamine, ammelide, ammeline, and cyanuric acid in milk and milk products by gas chromatography-tandem mass spectrometry. *Biomedical and Environmental Sciences*, 22(2), 87-94.
11. Houser, B. (2012). Bio-Rad's Bio-Plex® suspension array system, xMAP technology overview. *Archives of Physiology and Biochemistry*, 118(4), 192-196.
12. Angeloni, S., Cordes, R., Dunbar, S., Garcia, C., Gibson, G., Martin, C., & Stone, V. (2014). *xMAP cookbook. A collection of methods and protocols for developing multiplex assays with xMAP technology*, ed, 2.
13. Shapiro, H. M. (2005). *Practical flow cytometry*. John Wiley & Sons.
14. Saito, K., Nishimura, N., Sasaki, S., Oishi, Y., & Shibasaki, Y. (2013). Synthesis of polyguanamines from 2-N, N-dibutylamino-4, 6-dichloro-1, 3, 5-

triazine with aromatic diamines. *Reactive and Functional Polymers*, 73(5), 756-763.

15. Baliani, A., Peal, V., Gros, L., Brun, R., Kaiser, M., Barrett, M. P., & Gilbert, I. H. (2009). Novel functionalized melamine-based nitroheterocycles: synthesis and activity against trypanosomatid parasites. *Organic & Biomolecular Chemistry*, 7(6), 1154-1166.
16. Zhou, Z., & Bong, D. (2012). Small-molecule/polymer recognition triggers aqueous-phase assembly and encapsulation. *Langmuir*, 29(1), 144-150.
17. Bjerre, M., Hansen, T. K., Flyvbjerg, A., & Tønnesen, E. (2009). Simultaneous detection of porcine cytokines by multiplex analysis: development of magnetic bioplex assay. *Veterinary Immunology and Immunopathology*, 130(1), 53-58.
18. Vignali, D. A. (2000). Multiplexed particle-based flow cytometric assays. *Journal of Immunological Methods*, 243(1), 243-255.
19. Gottschalk, P. G., & Dunn, J. R. (2005). The five-parameter logistic: a characterization and comparison with the four-parameter logistic. *Analytical Biochemistry*, 343(1), 54-65.
20. Fraga, M., Vilariño, N., Louzao, M. C., Campbell, K., Elliott, C. T., Kawatsu, K., ... & Botana, L. M. (2012). Detection of paralytic shellfish toxins by a solid-phase inhibition immunoassay using a microsphere-flow cytometry system. *Analytical Chemistry*, 84(10), 4350-4356.
21. Anderson, G. P., Kowtha, V. A., & Taitt, C. R. (2010). Detection of fumonisin B1 and ochratoxin A in grain products using microsphere-based fluid array immunoassays. *Toxins*, 2(2), 297-309.

22. Fraga, M., Vilariño, N., Louzao, M. C., Rodríguez, P., Campbell, K., Elliott, C. T., & Botana, L. M. (2013). Multidetection of paralytic, diarrheic, and amnesic shellfish toxins by an inhibition immunoassay using a microsphere-flow cytometry system. *Analytical Chemistry*, 85(16), 7794-7802.
23. Rodríguez, L. P., Vilariño, N., Louzao, M. C., Dickerson, T. J., Nicolaou, K. C., Frederick, M. O., & Botana, L. M. (2014). Microsphere-based immunoassay for the detection of azaspiracids. *Analytical Biochemistry*, 447, 58-63.
24. Li, Y., Wu, H., Guo, L., Zheng, Y., & Guo, Y. (2012). Microsphere-based flow cytometric immunoassay for the determination of citrinin in red yeast rice. *Food Chemistry*, 134(4), 2540-2545.
25. Fodey, T. L., Thompson, C. S., Traynor, I. M., Haughey, S. A., Kennedy, D. G., & Crooks, S. R. (2011). Development of an optical biosensor based immunoassay to screen infant formula milk samples for adulteration with melamine. *Analytical Chemistry*, 83(12), 5012-5016.
26. Hermanson, G. T. (2013). *Bioconjugate techniques*. Academic press.
27. Meimaridou, A., Haasnoot, W., Noteboom, L., Mintzas, D., Pulkrabova, J., Hajslová, J., & Nielen, M. W. (2010). Color encoded microbeads-based flow cytometric immunoassay for polycyclic aromatic hydrocarbons in food. *Analytica Chimica Act*a, 672(1), 9-14.
28. Sancho, J. V., Ibanez, M., Grimalt, S., Pozo, O. J., & Hernandez, F. (2005). Residue determination of cyromazine and its metabolite melamine in chard samples by ion-pair liquid chromatography coupled to electrospray tandem mass spectrometry. *Analytica Chimica Acta*, 530(2), 237-243.

29. Wei, R., Wang, R., Zeng, Q., Chen, M., & Liu, T. (2009). High-performance liquid chromatographic method for the determination of cyromazine and melamine residues in milk and pork. *Journal of Chromatographic Science*, 47(7), 581-584.

30. Wang, S., Li, D., Hua, Z., & Zhao, M. (2011). Molecularly imprinted monolith coupled on-line with high performance liquid chromatography for simultaneous quantitative determination of cyromazine and melamine. *Analyst*, 136(18), 3672-3679.

31. Wang, H., Lin, L., Sun, Q., Lin, Q., Xiong, X., Wu, K., & Yu, C. P. (2014). Simultaneous determination of cyromazine, melamine and their biodegradation products by ion-pair high-performance liquid chromatography. *International Journal of Environmental Analytical Chemistry*, 94(12), 1173-1182.

32. Le, T., Yan, P., Xu, J., & Hao, Y. (2013). A novel colloidal gold-based lateral flow immunoassay for rapid simultaneous detection of cyromazine and melamine in foods of animal origin. *Food Chemistry*, 138(2), 1610-1615.

33. Panuwet, P., Nguyen, J. V., Wade, E. L., D'Souza, P. E., Ryan, P. B., & Barr, D. B. (2012). Quantification of melamine in human urine using cation-exchange based high performance liquid chromatography tandem mass spectrometry. *Journal of Chromatography B*, 887, 48-54.

34. Wu, Q., Fan, K., Sha, W., Ruan, H., Zeng, R., & Shieh, C. (2009). Highly sensitive detection of melamine based on reversed phase liquid chromatography mass spectrometry. *Chinese Science Bulletin*, *54*(5), 732-737.

35. Ibáñez, M., Sancho, J. V., & Hernández, F. (2009). Determination of melamine in milk-based products and other food and beverage products by ion-pair liquid chromatography–tandem mass spectrometry. *Analytica Chimica Acta*, *649*(1), 91-97.

36. Filigenzi, M. S., Puschner, B., Aston, L. S., & Poppenga, R. H. (2008). Diagnostic determination of melamine and related compounds in kidney tissue by liquid chromatography/tandem mass spectrometry. *Journal of Agricultural and Food Chemistry*, *56*(17), 7593-7599.

37. Andersen, W. C., Turnipseed, S. B., Karbiwnyk, C. M., Clark, S. B., Madson, M. R., Gieseker, C. M., ... & Reimschuessel, R. (2008). Determination and confirmation of melamine residues in catfish, trout, tilapia, salmon, and shrimp by liquid chromatography with tandem mass spectrometry. *Journal of Agricultural and Food Chemistry*, *56*(12), 4340-4347.

38. Filigenzi, M. S., Tor, E. R., Poppenga, R. H., Aston, L. A., & Puschner, B. (2007). The determination of melamine in muscle tissue by liquid chromatography/tandem mass spectrometry. *Rapid Communications in Mass Spectrometry*, *21*(24), 4027-4032.

39. Tittlemier, S. A., Lau, B. P. Y., Ménard, C., Corrigan, C., Sparling, M., Gaertner, D., ... & Feeley, M. (2009). Melamine in infant formula sold in Canada: occurrence and risk assessment. *Journal of Agricultural and Food Chemistry*, *57*(12), 5340-5344.

40. Varelis, P., & Jeskelis, R. (2008). Preparation of [13 C 3]-melamine and 13 C 3]-cyanuric acid and their application to the analysis of melamine and cyanuric

acid in meat and pet food using liquid chromatography-tandem mass spectrometry. *Food Additives and Contaminants*, *25*(10), 1208-1215.

41. Filazi, A., Sireli, U. T., Ekici, H., Can, H. Y., & Karagoz, A. (2012). Determination of melamine in milk and dairy products by high performance liquid chromatography. *Journal of Dairy Science*, *95*(2), 602-608.
42. Sun, H., Wang, L., Ai, L., Liang, S., & Wu, H. (2010). A sensitive and validated method for determination of melamine residue in liquid milk by reversed phase high-performance liquid chromatography with solid-phase extraction. *Food Control*, *21*(5), 686-691.
43. Muñiz-Valencia, R., Ceballos-Magaña, S. G., Rosales-Martinez, D., Gonzalo-Lumbreras, R., Santos-Montes, A., Cubedo-Fernandez-Trapiella, A., & Izquierdo-Hornillos, R. C. (2008). Method development and validation for melamine and its derivatives in rice concentrates by liquid chromatography. Application to animal feed samples. *Analytical and Bioanalytical Chemistry*, *392*(3), 523-531.
44. Kim, B., Perkins, L. B., Bushway, R. J., Nesbit, S., Fan, T., Sheridan, R., & Greene, V. (2008). Determination of melamine in pet food by enzyme immunoassay, high-performance liquid chromatography with diode array detection, and ultra-performance liquid chromatography with tandem mass spectrometry. *Journal of AOAC International*, *91*(2), 408-413.
45. Venkatasami, G., & Sowa, J. R. (2010). A rapid, acetonitrile-free, HPLC method for determination of melamine in infant formula. *Analytica Chimica Acta*, *665*(2), 227-230.

46. Zheng, X. L., Yu, B. S., Li, K. X., & Dai, Y. N. (2012). Determination of melamine in dairy products by HILIC-UV with NH_2 column. *Food Control*, *23*(1), 245-250.

47. Ehling, S., Tefera, S. H. O. I. P., & Ho, I. P. (2007). High-performance liquid chromatographic method for the simultaneous detection of the adulteration of cereal flours with melamine and related triazine by-products ammeline, ammelide, and cyanuric acid. *Food Additives and Contaminants*, *24*(12), 1319-1325.

48. Finete, V. D. L. M., Gouvêa, M. M., de Carvalho Marques, F. F., & Netto, A. D. P. (2015). Validation of a method of high performance liquid chromatography with fluorescence detection for melamine determination in UHT whole bovine milk. *Food Control*, *51*, 402-407.

49. Hong, M., Sai, F., Yong-Ning, W. U., Zhang, L., Ping-Ping, Z. H. O. U., Hui-Jing, C. H. E. N., ... & Jing-Guang, L. I. (2009). Simultaneous determination of melamine, ammelide, ammeline, and cyanuric acid in milk and milk products by gas chromatography-tandem mass spectrometry. *Biomedical and Environmental Sciences*, *22*(2), 87-94.

50. Xia, X., Ding, S., Li, X., Gong, X., Zhang, S., Jiang, H., ... & Shen, J. (2009). Validation of a confirmatory method for the determination of melamine in egg by gas chromatography–mass spectrometry and ultra-performance liquid chromatography–tandem mass spectrometry. *Analytica Chimica Acta*, *651*(2), 196-200.

51. Zhu, X., Wang, S., Liu, Q., Xu, Q., Xu, S., & Chen, H. (2009). Determination of residues of cyromazine and its metabolite, melamine, in animal-derived

food by gas chromatography− mass spectrometry with derivatization. *Journal of Agricultural and Food Chemistry*, *57*(23), 11075-11080.

52. Yokley, R. A., Mayer, L. C., Rezaaiyan, R., Manuli, M. E., & Cheung, M. W. (2000). Analytical method for the determination of cyromazine and melamine residues in soil using LC-UV and GC-MSD. *Journal of Agricultural and Food Chemistry*, *48*(8), 3352-3358.
53. Mauer, L. J., Chernyshova, A. A., Hiatt, A., Deering, A., & Davis, R. (2009). Melamine detection in infant formula powder using near-and mid-infrared spectroscopy. *Journal of Agricultural and Food Chemistry*, *57*(10), 3974-3980.
54. Yang, S., Ding, J., Zheng, J., Hu, B., Li, J., Chen, H., ... & Qiao, X. (2009). Detection of melamine in milk products by surface desorption atmospheric pressure chemical ionization mass spectrometry. *Analytical Ahemistry*, *81*(7), 2426-2436.
55. Chen, Z., & Yan, X. (2009). Simultaneous determination of melamine and 5-hydroxymethylfurfural in milk by capillary electrophoresis with diode array detection. *Journal of Agricultural and Food Chemistry*, *57*(19), 8742-8747.
56. Lachenmeier, D. W., Humpfer, E., Fang, F., Schütz, B., Dvortsak, P., Sproll, C., & Spraul, M. (2009). NMR-spectroscopy for nontargeted screening and simultaneous quantification of health-relevant compounds in foods: the example of melamine. *Journal of Agricultural and Food Chemistry*, *57*(16), 7194-7199.
57. Beltrán-Martinavarro, B., Peris-Vicente, J., Marco-Peiró, S., Esteve-Romero, J., Rambla-Alegre, M., & Carda-Broch, S. (2012). Use of micellar mobile

phases for the chromatographic determination of melamine in dietetic supplements. *Analyst*, *137*(1), 269-274.

58. Beltrán-Martinavarro, B., Peris-Vicente, J., Carda-Broch, S., & Esteve-Romero, J. (2014). Development and validation of a micellar liquid chromatography-based method to quantify melamine in swine kidney. *Food Control*, *46*, 168-173.
59. Pietrzyk, A., Kutner, W., Chitta, R., Zandler, M. E., D'Souza, F., Sannicolo, F., & Mussini, P. R. (2009). Melamine acoustic chemosensor based on molecularly imprinted polymer film. *Analytical Chemistry*, *81*(24), 10061-10070.
60. Liang, R., Zhang, R., & Qin, W. (2009). Potentiometric sensor based on molecularly imprinted polymer for determination of melamine in milk. *Sensors and Actuators B: Chemical*, *141*(2), 544-550.
61. Li, L., Li, B., Cheng, D., & Mao, L. (2010). Visual detection of melamine in raw milk using gold nanoparticles as colorimetric probe. *Food Chemistry*, *122*(3), 895-900.
62. Han, C., & Li, H. (2010). Visual detection of melamine in infant formula at 0.1 ppm level based on silver nanoparticles. *Analyst*, *135*(3), 583-588.
63. Liu, Y. T., Deng, J., Xiao, X. L., Ding, L., Yuan, Y. L., Li, H., ... & Wang, L. L. (2011). Electrochemical sensor based on a poly (para-aminobenzoic acid) film modified glassy carbon electrode for the determination of melamine in milk. *Electrochimica Acta*, *56*(12), 4595-4602.
64. Xu, Q., Wei, H. P., Du, S., Li, H. B., Ji, Z. P., & Hu, X. Y. (2013). Detection of subnanomolar melamine based on electrochemical accumulation coupled

with enzyme colorimetric assay. *Journal of Agricultural and Food Chemistry*, *61*(8), 1810-1817.

65. Akter, H., Shaikh, A. A., Chowdhury, T. R., Rahman, M. S., Bakshi, P. K., & Ahammad, A. S. (2013). Gold nanoparticle-modified indium tin oxide electrode for highly sensitive electrochemical detection of melamine. *ECS Electrochemistry Letters*, *2*(8), B13-B15.
66. Liao, C. W., Chen, Y. R., Chang, J. L., & Zen, J. M. (2011). A sensitive electrochemical approach for melamine detection using a disposable screen printed carbon electrode. *Electroanalysis*, *23*(3), 573-576.
67. Fodey, T. L., Thompson, C. S., Traynor, I. M., Haughey, S. A., Kennedy, D. G., & Crooks, S. R. (2011). Development of an optical biosensor based immunoassay to screen infant formula milk samples for adulteration with melamine. *Analytical Chemistry*, *83*(12), 5012-5016.
68. Zeng, H. J., Yang, R., Wang, Q. W., Li, J. J., & Qu, L. B. (2011). Determination of melamine by flow injection analysis based on chemiluminescence system. *Food chemistry*, *127*(2), 842-846.
69. Shen, S. F., Zhao, H. W., Xu, D., Wu, L. P., & Huang, C. Z. (2011). Colorimetric assay of melamine based on the aggregation of gold nanoparticles. *Journal of Biomedical Nanotechnology*, *7*(5), 691-695.
70. Wild, D. (Ed.). (2013). *The immunoassay handbook: theory and applications of ligand binding, ELISA and related techniques*. Newnes.

2.5 Appendix

Method	Matrix	Detection limit	Reference
LC–MS/MS	Human urine	0.00066mg/kg	[33]
LC–MS/MS	Rat plasma, liver, kidney, spleen, bladder, and brain	0.00560–0.0083lmg/kg	[34]
LC–MS/MS	Milk-based products and other food and beverage products	0.01–0.10mg/kg	[35]
LC–MS/MS	Kidney tissue	0.092–0.140mg/kg	[36]
LC–MS/MS	Catfish, trout, tilapia, salmon, and shrimp	0.0032mg/kg	[37]
LC–MS/MS	Porcine muscle	0.0017mg/kg	[38]
LC–MS/MS	Infant formula	4ng/g	[39]
LC–MS	Catfish, pork, chicken, and pet food	0.01mg/kg	[40]
HPLC–DAD	Milk and dairy products	0.035–0.110mg/kg	[41]
HPLC–DAD	Liquid milk	0.018mg/kg	[42]
HPLC–DAD	Rice protein concentrate feeds	55–113mg/kg	[43]
HPLC–DAD	Pet food	0.1μg/ml	[44]

HPLC–UV	Infant formula	0.1mg/kg	[45]
HPLC–UV	Dairy products	0.003mg/kg	[46]
HPLC–UV	Cereal flours	5–90mg/kg	[47]
HPLC-Fluo	Bovine UHT whole milk	0.0081μg/mL	[48]
GC–MS/MS	Milk and milk products	0.002mg/kg	[49]
GC–MS	Eggs	0.01mg/kg	[50]
GC–MS	Muscle	10μg/kg	[51]
LC–GC–MS	Soil	2.5ppb, 0.05ppb	[52]
NIR/FTIR	Infant formula powder	1ppm	[53]
DAPCI-MS	Milk	0.08mg/kg	[54]
CE-DAD	Milk	0.047μg/mL	[55]
NMR	Milk product	0.69mg/kg	[56]
MLC	Liquid and powdered milk samples	9ng/ml	[57]
MLC	Swine kidney	5ppb	[58]

Table A2.1 Summary of published classical methods for detection of melamine in food products.

Method	LOD	References
Chemosensor based on MIP film	5nM	[59]
Potentiometric sensor based on a MIP	6.0μM	[60]
Colorimetric sensor based on unmodified Gold NPs	0.4μg/mL	[61]
Colorimetric sensor based on silver NPs	0.1μg/g	[62]
Electrochemical sensor based on para-aminobenzoic acid	0.36μM	[63]
Glassy carbon electrode by chemical coupling of horseradish peroxidase	1.0×10^{-11}M	[64]
Indium tin oxide electrode modified by gold NPs	0.13ppb	[65]
Screen printed carbon electrode	98.3ppb	[66]
Optical biosensor based on polyclonal antibody	0.5μg/mL	[67]
Chemiluminescenc based on Luminal–H_2O_2	0.12μg/mL	[68]
Aptamers (poly-T10) based on AuNPs	41.7nM	[69]

Table A2.2 List of recent advances in MEL detection techniques.

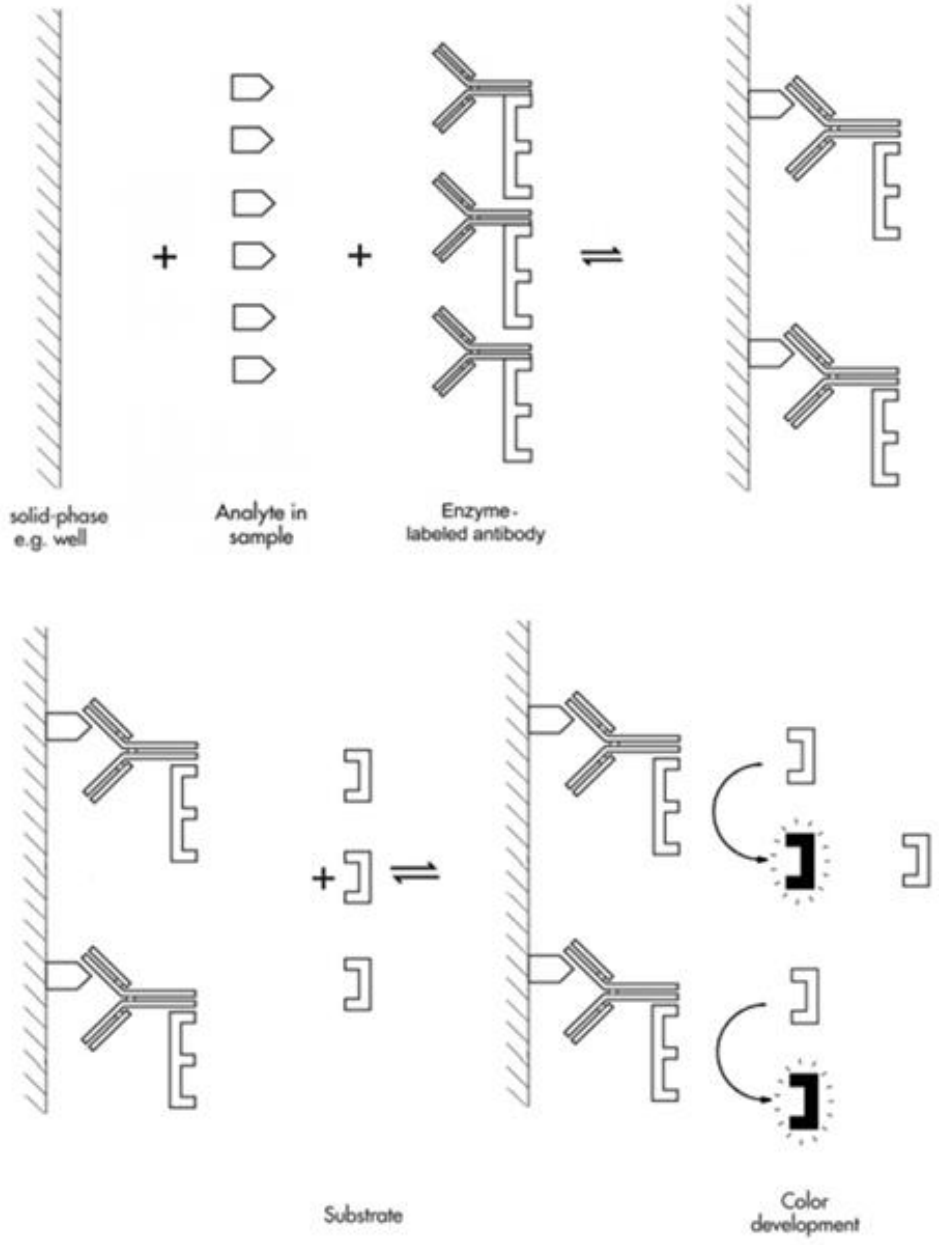

Figure A2.1 Direct format ELISA. [Reproduce from 70]

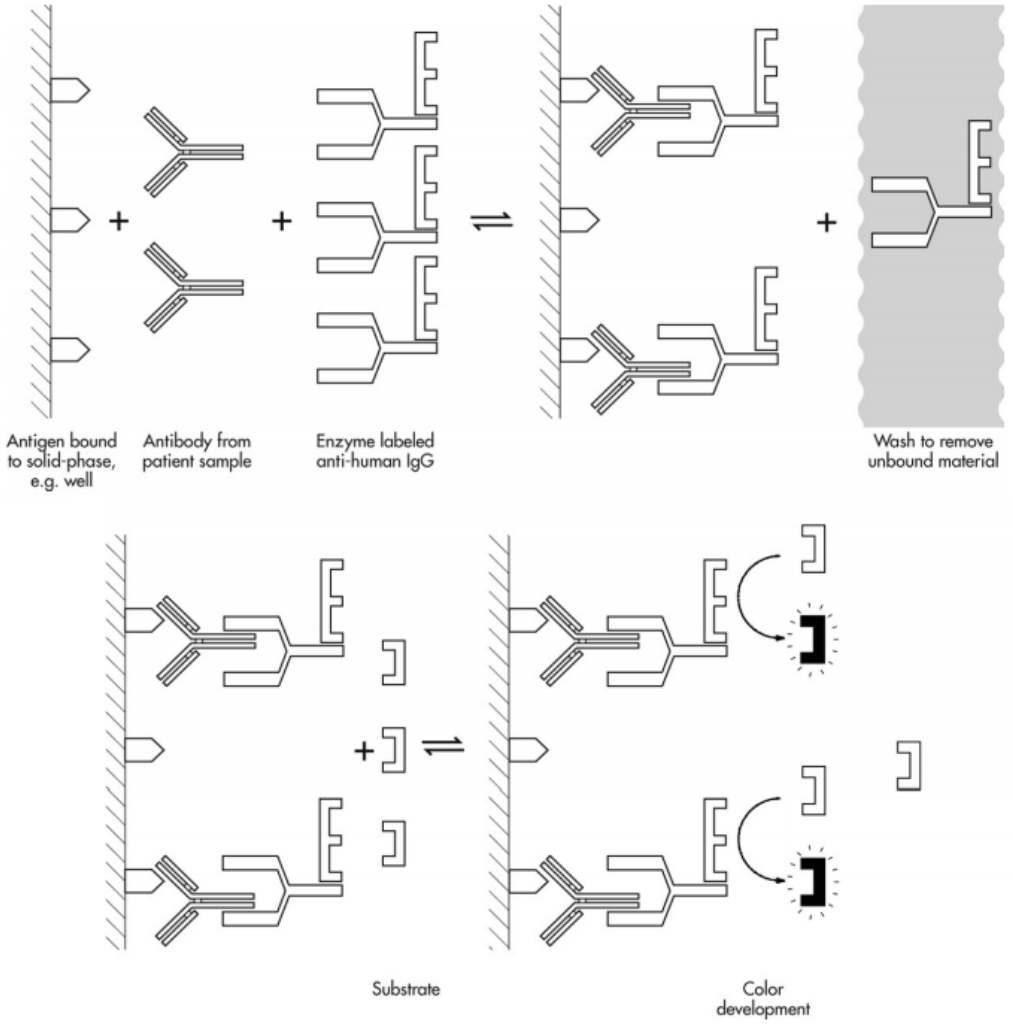

Figure A2.2 Indirect format ELISA. [70]

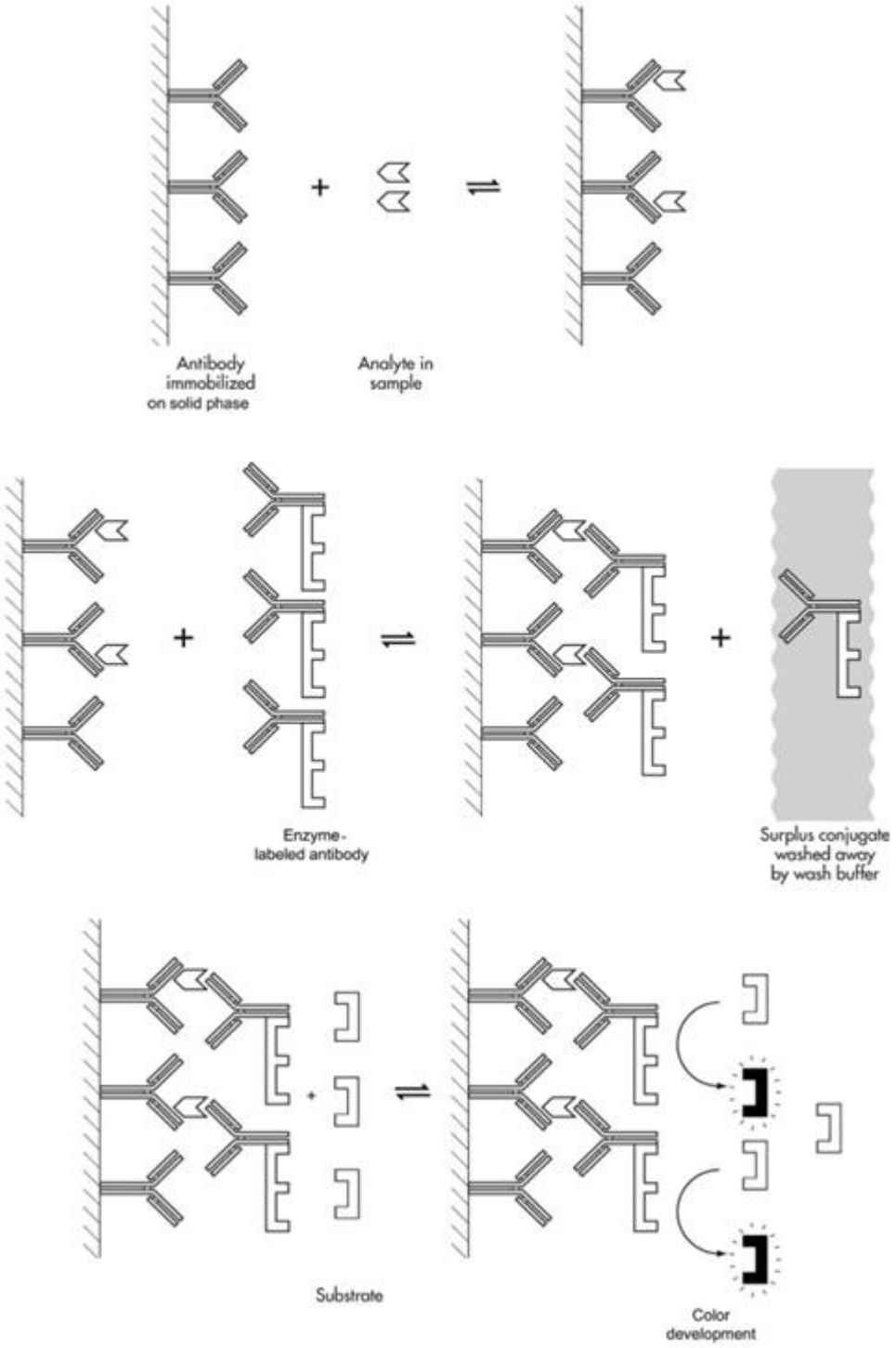

Figure A2.3 Sandwich format ELISA. [70]

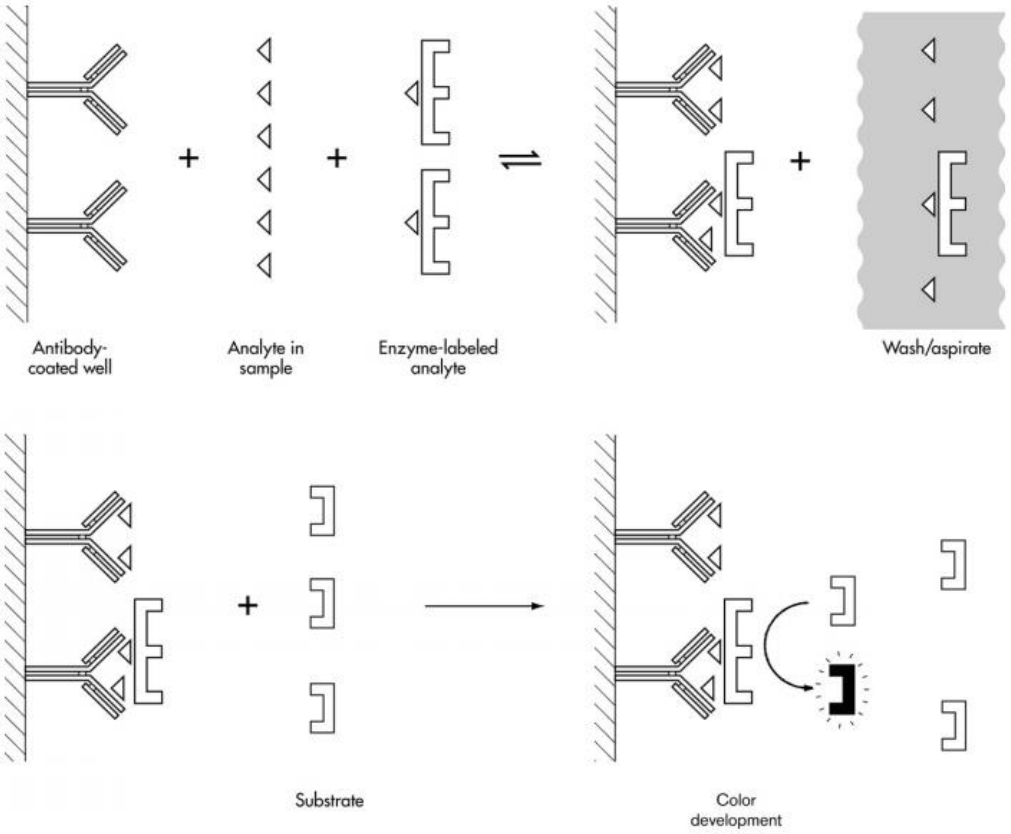

Figure A2.4 Competitive format ELISA. [70]

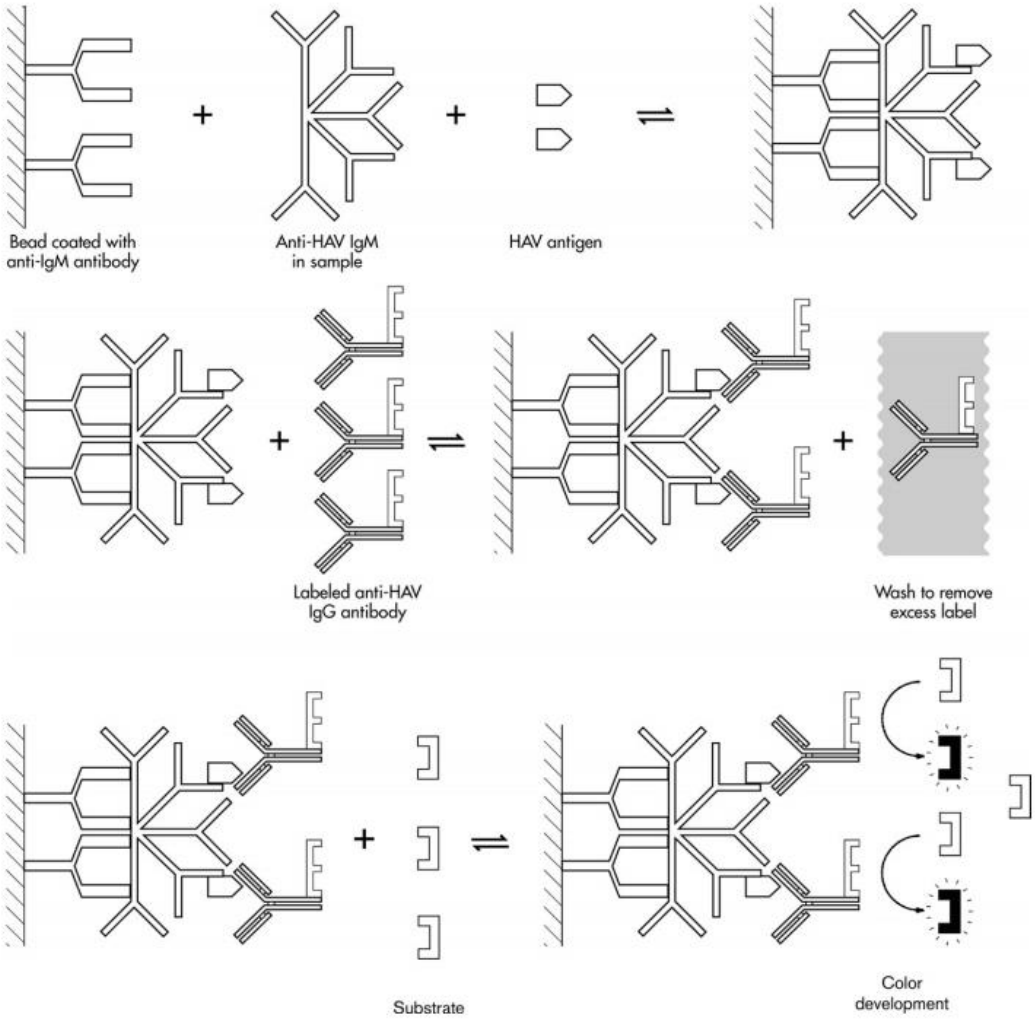

Figure A2.5 Immunocapture format ELISA. [70]

CHAPTER THREE: URINARY POLYAMINES: A PILOT STUDY ON THEIR ROLES AS PROSTATE CANCER DETECTION BIOMARKERS

3.1 Introduction

3.1.1 Background information and statistics on prostate cancer

Prostate cancer (PCa) refers to an abnormal, malignant growth and disorder of glandular cells of the prostate. These cells gradually grow into a lump which can be of a benign or malignant form. The former usually won't spread to other parts of body and cause minimal harm. On the other hand, the latter one can spread to surrounding tissues or organs to develop metastasis, a very painful and functionally limiting stage of this killing disease. In America it is the most commonly diagnosed cancer and ranks 2nd in the most fatal cancers. [1] On average, approximately 1/6 men in America will be diagnosed with this disease in his lifetime. For your reference, 220800 new PCa cases were diagnosed and 1/8 of them were estimated to be killed by it. [2]

No exception is Hong Kong regarding this public health issue of high concern. With reference to the statistics of Hong Kong Cancer Registry, Hospital Authority, HKSAR, PCa ranked 3rd and 5th in the most common and fatal cancers respectively in 2013. [3] Figure 3.1 shows the age-standardized incidence and mortality rate of PCa from 1981 to 2014 in Hong Kong. A distinct three- and two-fold increase could be observed in its incidence and mortality rate respectively when comparing 1981 with 2013.

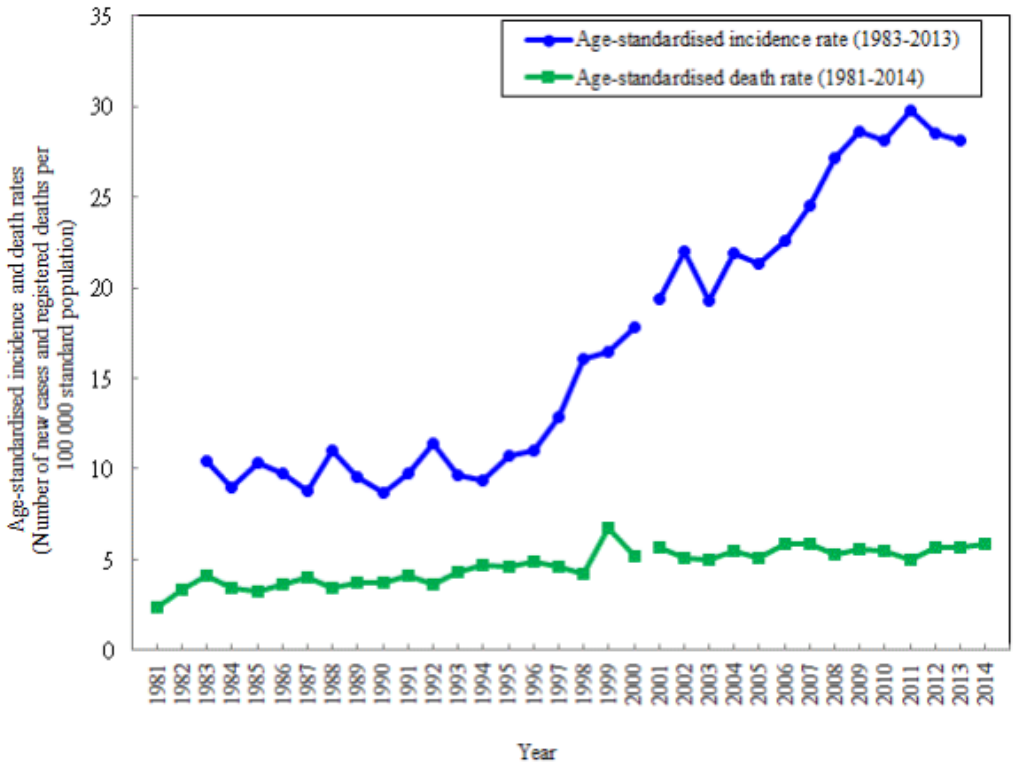

Figure 3.1 Age-standardized incidence and mortality rate of PCa from 1981 to 2014 in Hong Kong. [3]

PCa is reported to be greatly associated with patients' age. For example, comparing the incidence rate, 40-59 years is only 1/6 of that of 60-79, and it was believed oxidative stress caused by aging was the main factor leading to accumulated DNA damages and an imbalance of intracellular pro-oxidant and anti-oxidant level. [5] All of these lead to cancer formation in the prostate. As results, PCa is becoming a major health problem threatening developed countries, in which citizens are expected to have a longer life expectancy. Other potential influencing risk factors include race, familial aggregation, hormones, diet and smoking habit, etc. [6-9]

It was also reported that early PCa cases were associated with a significant lower probability of PCa-related mortality in ten years follow-up than a late one (30-50% for Gleason 7 and 50-80% for 8-10). [4] Given this statistics, the analytical problem presents here is in what ways we can achieve a sensitive and accurate diagnosis to detect early PCa, such that the treatment outcome can be significantly improved during this latency and curable period, and avoided progressing into the late and lethal stage for saving more lives.

3.1.2 Current PCa detection methods and medical situation

Nowadays the diagnosis of PCa relied mainly on three approaches: firstly is the clinical suspiciousness raised by digital rectal examination (DRE) and serum prostate specific antigen (PSA) screening test, followed by transrectal ultrasound guided prostatic biopsy (TRUSPB) for confirmation.

DRE

DRE is a simple procedure involving a doctor inserting his gloved finger into the rectum and directly feel any abnormalities of the prostate. (Figure 3.2) These abnormalities can be any nodules, asymmetries or hard mass. However, it brings a discomfort feeling to patients, and at the same time it is also a strongly investigator-dependent technique, lacking a high sensitivity and specificity towards PCa diagnosis. [10] Therefore DRE is not recommended as a sole screening test for the early detection of PCa. When working alone, the positive

predictive value (PPV) is low as 8% only. [5] Also most DRE positive PCa results are of advanced staging.

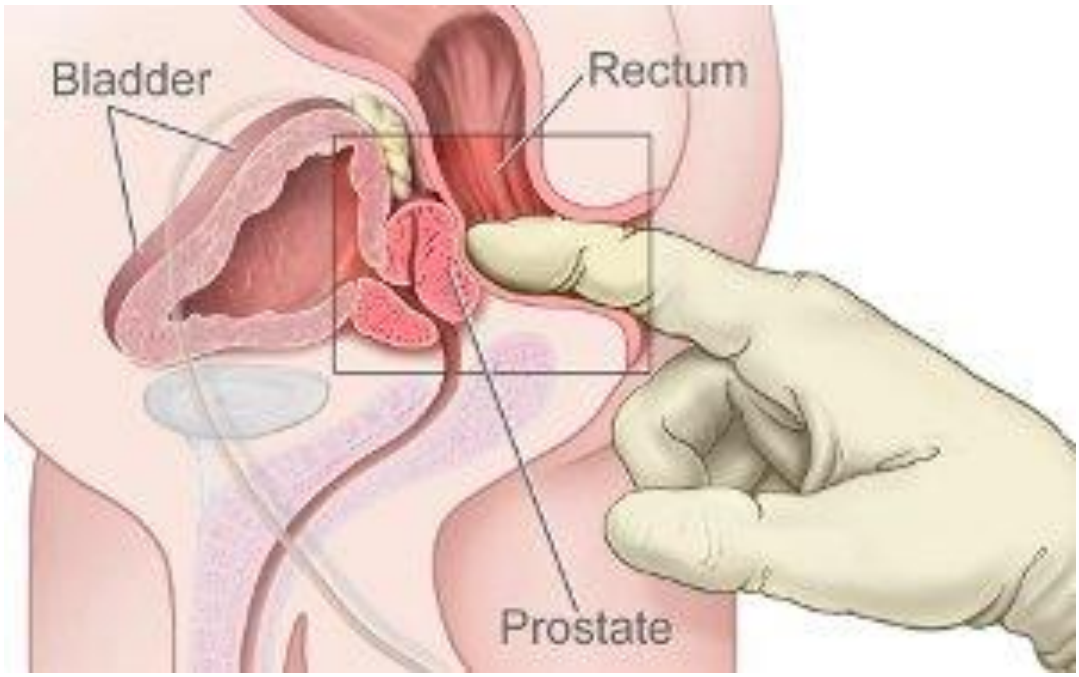

Figure 3.2 DRE of the prostate. [11]

Serum PSA test

PSA is an androgen-regulated protein primarily produced by the prostatic epithelial cells every day. More specifically, it is the major protease in semen which is responsible for breaking down any high molecular weight proteins of the seminal coagulum into smaller polypeptides such that the semen becomes more fluidic. Normal serum PSA level ranges from 0.0 to 4.0ng/ml. It is believed that cancer, although not completely specific, can temporarily increase this serum level, making serum PSA test still the most commonly employed biomarker for PCa for almost two decades.

Despite PSA test's simplicity and commonness, elevated PSA levels had also been observed in patients with other conditions including benign prostatic hyperplasia (BPH), prostatitis, urological interventions or outcomes of certain pharmacological therapies, etc. It means it has a poor specificity towards PCa. The general adopted 4.0ng/ml cut-off point fails to distinguish PCa clearly from healthy cases. For reference, within the grey zone of 4-10ng/ml, the PPV has a small mean value of 21%. [12] Usually doctors will supplement serum PSA test with DRE results to improve the performance. When working together as a screening tool, the PPV increases to around 32%, which is still far from satisfactory. [5]

A wide variety of PSA concepts were introduced and tried to improve the performance of PSA measurement. For example, owing to the observation that PCa increases more PSA per unit of prostate volume than other interfering diseases like BPH, PSA density of transition zone has been suggested to be a potential biomarker, which is defined as the total serum PSA level divided by the prostate volume [13-14]. PSA velocity is the second example which indicates the rate of increase in serum PSA over a period of time. It is calculated by the formula PSA velocity = (2nd PSA – 1st PSA/$Time_1$) + (3rd PSA – 2nd PSA/$Time_2$). At least three measurements are needed to be performed within 2-years' period of time. Other interpretations like free to total PSA (total PSA = free PSA + α-1-Antichymotrypsin bound PSA + α-1-protease inhibitor) ratio [14-15], PSA isoform [−2] proenzyme PSA (p2PSA) and Prostate Health Index (PHI) [16-17] were all reported by scientists for improving PCa diagnosis performance. For your

information, the Hong Kong East Cluster of Hospital Authority has just started to apply PHI as a PCa biomarker in early 2016, which is a combination of PSA, free PSA and p2PSA tests.

TRUSPB

Rather than being a convenient screening tool, TRUSPB is currently the main diagnostic approach for histological confirmation of PCa. The procedures are tedious: an ultrasound probe guided by a needle will be gently inserted into the rectum and emit sound waves for subsequent scanning. (Figure 3.3) Any abnormal situations like PCa will alter the wave reflection pattern and therefore the ultrasound image of suspicious area. Afterwards, these dark suspicious area or hypoechoic lesions will be biopsied usually at least six to eight times from different location of the prostate for further microscopic evaluation. Depending on the case, it is not uncommon to ask for more biopsies.

Despite its strong power in PCa confirmation; however, its procedures are tedious and lead to significant discomfort and complications to patients. [18-20] These includes hematuria in between 6 to 13%, urinary tract infection in 0.3 to 4% and serious infections in less than 2% of PCa patients. [21-23] Other harms include pain, fever, urinary difficulty or any other issues requiring further follow up or hospitalization.

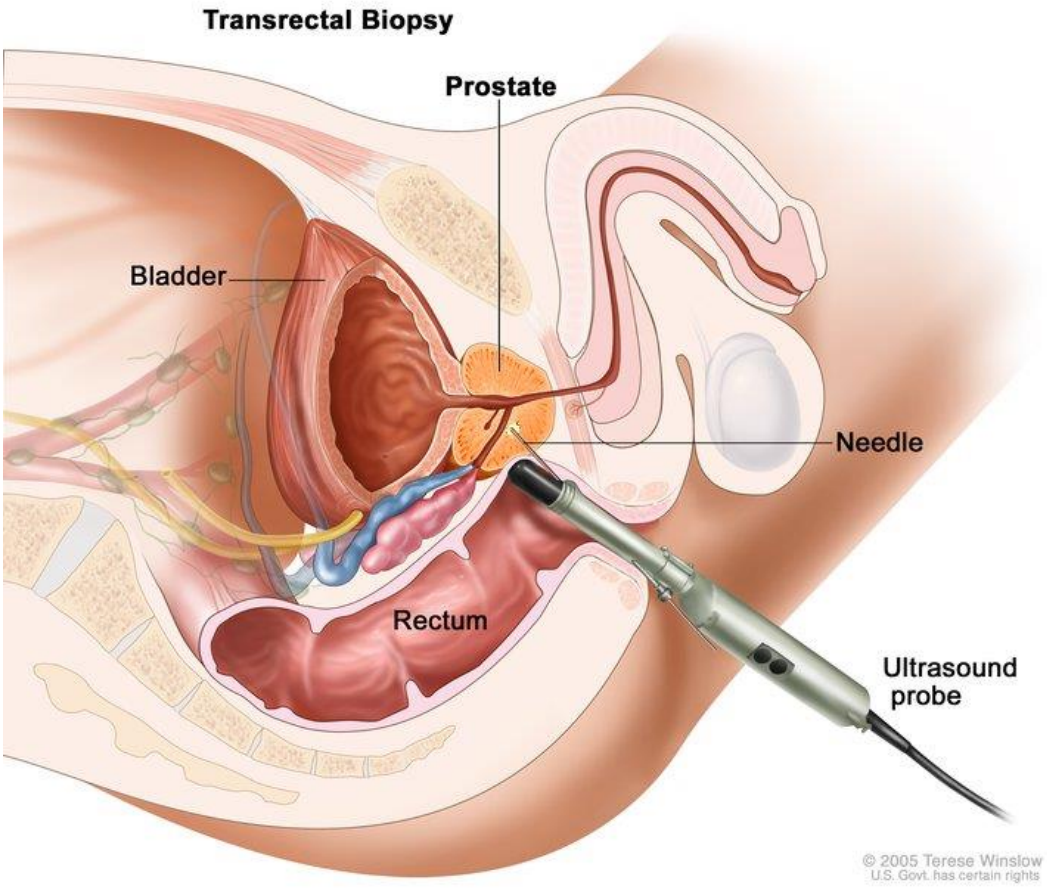

Figure 3.3 TRUSPB of the prostate. [11]

Current medical situations on PCa screening

Nowadays the above-discussed three methods remain widely employed for PCa screening and diagnosis, especially serum PSA test which is easy, convenient, minimally invasive and acceptable to general population. In Figure 3.1 we can observe the sudden increase in PCa incidence rate starting from early 1990s, and it was due to the development and advocate of the serum PSA test. While substantive advances had been achieved on PSA, the accuracy and its significance to affect the outcome of disease are still far from satisfactory. This makes the role

of PSA/DRE-oriented early PCa screening remain uncertain whether the overall value has a likelihood of benefit to citizens.

The debate remains controversial over decades, and two landmark literatures tried to answer this question by performing an unprecedented large scale randomized study on the overall outcome of PCa screening. Their contributions to the understanding of PCa screening are very significant even after seven years of publishing and a short summary on their results is given below:

The first one was conducted and published by the European Randomized Study of Screening for Prostate Cancer (ERSPC) in 2009. [24] 162,243 PCa patients were sampled from seven different European countries. They were assigned either to the screening group or control group. With an average follow-up time up to 8.8 years on all the participants with age of 55-69, the cancer incidence and mortality rate were determined. (Table 3.1) Their results showed that the mortality rate was significantly decreased, albeit to a little extent, through PCa screening.

Participants	Number (%)	PCa incidence (%)	PCa mortality (%)
Screening group	72890 (44.9)	5990 (8.2)	214 (0.29)
Control group	89353 (55.1)	4307 (4.8)	326 (0.36)
Total	162243 (100)	10297 (13.0)	540 (0.33)

Table 3.1 ERSPC results on the effect of PCa screening.

Nevertheless, another remarkable literature published by the US-based Prostate, Lung, Colorectal, and Ovarian (PLCO) Cancer Screening Trial in the same year did not give coincident results as ERSPC. [25] After seven years of follow up on participants with age of 55-74, screening could not demonstrate its ability to reduce PCa mortality rate.

Participants	Number (%)	PCa incidence (%)	PCa mortality (%)
Screening group	38343 (50.0)	3452 (9.0)	92 (0.24)
Control group	38350 (50.0)	2974 (7.8)	82 (0.21)
Total	76693 (100)	6426 (8.4)	174 (0.23)

Table 3.2 PLCO results on the effect of PCa screening.

The analyses on the results of the two trials were highly complex. They triggered more new questions in this field and failed to resolve the controversy. There is a need for further assessment on PCa screening and its efficiency, especially its relationship with treatment outcome and the quality of life of citizens from a macroscopic viewpoint. Nevertheless, their results are still remarkable to the PCa world. Different organizations have their own interpretations on them and suggested different guidelines to clinicians. (Table A3.1)

While most organizations stand in the middle ground on the effect of PCa screening, the guideline from the USPSTF was the most influential one. After appraisal of the data from different sources, they decisively publish a Grade D

recommendation on PCa screening, which means that they do not encourage the continuation of PCa screening activity. They believe that most likely the high false-positive rate of PSA test carries more harms than benefits. Besides the potentials risks brought by TRUSPB abovementioned, more importantly is the harms from over-diagnosis. It has been estimated that between 23 and 42% of the PCa cases would remain asymptomatic for their whole lives and won't be diagnosed without screening. [27] When they are treated with those unnecessary treatments, they are subjected to their risks, e.g. in 1000 men, 5 men receiving PCa surgery can be killed while 10-70 will have serious complications; radiotherapy can result in urinary incontinence, erectile and bowel dysfunction; androgen deprivation therapy can lead to erectile dysfunction, gynecomastia and hot flashes while this therapy is yet to show their effect in decreasing mortality rate; last but not least is the persistent worry about the disease. [28]

This statement had drawn a lot of awareness from clinicians and the lay public upon publication. Together with the extensive media coverage, this guideline has an immediate impact on clinical practice. Two studies have proved that after its publication, a significant decrease on the number of biopsies performed based on the referrals from PSA screening was noticed. [29-30] While it is good to hear that fewer low risk PCa cases are being screened out, a sudden drop in the detection rate of high risk PCa becomes another concern. In view of this, the USPSTF was thought to be too polarized, and most clinicians think that USPSTF need to clarify its recommendation to avoid further confusing practitioners and the public with the misunderstanding that PSA test was no longer

accurate and useful [31] Most urologists still persist in the truth that PSA test has its value in decreasing mortality rate. The most widely accepted way to handle PCa screening currently, as most organizations suggested, is to establish a shared decision-making and well inform suspected patients with the currently existing limitations and potential risks before performing any screening activities.

3.1.3 Background of urinary biomarkers

Apparently the message delivered by the current medical situation is that we need a better biomarker for PCa screening, and it should possess advantages like non-invasive, accurate, simple to perform and can significantly improve the outcome of screening using mortality as the end point.

Urine-based assays present an important area for biomarker research due to the advance in proteomic and metabolomics. Urine collection behaves as an ideal source for biomarker investigation because it is non-invasive and readily available; more importantly, it is closely related to the urological organs including the prostate. It may contain information from kidney, urinary tracts or even distant organs through the action of glomerular filtration. It also affords detection samples for either malignancy-related metabolites excreted in urine, directly exfoliated PCa cells or prostatic products secreted into the genitourinary tract. [32] Many urinary PCa specific biomarkers have been reported and under clinical review. (Table 3.3) While some of them showed good values in both sensitivity and specificity, the testing sample size was usually not large enough to reach a definite conclusion

confirming their biomarker roles. Further decisive evaluation was usually suggested.

Biomarker	**Sensitivity (%)**	**Specificity (%)**	**Reference**
DNA marker			
GSTP1	46	56	[33]
8-OHdG	31	100	[34]
Loss of heterozygosity	86.7	44	[35]
RNA marker			
uPM3	74	91	[36]
hTERT RNA	36	66	[33]
TERT activity	100	88.6	[37]
PCA3	66	89	[36]
Protein marker			
AMACR gene	100	58	[38]
Telomerase activity	58	100	[39]
Urinary tissue factor	65	75	[40]
Transferrin	75	30	[41]

Table 3.3 Summary of representative potential urinary PCa biomarkers.

3.1.4 Background of polyamines

One example of such cancer biomarkers are natural polyamines. Research on this group of analytes could date back several centuries and had proven their effects through regulating specific gene expression and ion channels, associating with different nucleic acids and maintaining chromatin conformation, membrane stability and free-radical scavenging. (Figure 3.4) [42-47] Owing to their active participation into these metabolic pathways, their contents, especially urinary contents, were considered as potential biomarkers for monitoring different types of growing tumors and for following medical treatment of cancer patients. One of the most promising finding was reported by Russell's group in the late 1960s, which reported a considerable increase of ornithine decarboxylase, a key enzyme for polyamine production, as well as urinary polyamines contents in patients with various types of solid tumors and leukemia. [48-49] Afterwards, polyamine studies focusing on specific cancers never stop, and these include cervical, colorectal and breast cancer, etc. [50-52] Nevertheless, very scanty articles tried to explore the predictive relationship between urinary polyamines levels and PCa. The prostate indeed is one of the human organs having the highest concentration of polyamines, especially spermine that we will focus on. [53] Clinical relevance of polyamines in PCa related processes, like PCa cells' proliferation, differentiation under the control of androgens had been shown. Besides, an interference with homeostasis may serve as a target for PCa chemotherapy. [53] Previous literatures also suggested monitoring prostatic spermine concentration as a biomarker for diagnosing PCa based on the observation of significantly different levels in

cancerous and non-cancerous prostate tissues. [54] All of these evidences supported the idea of monitoring urinary polyamines concentration to be a means for PCa diagnosis.

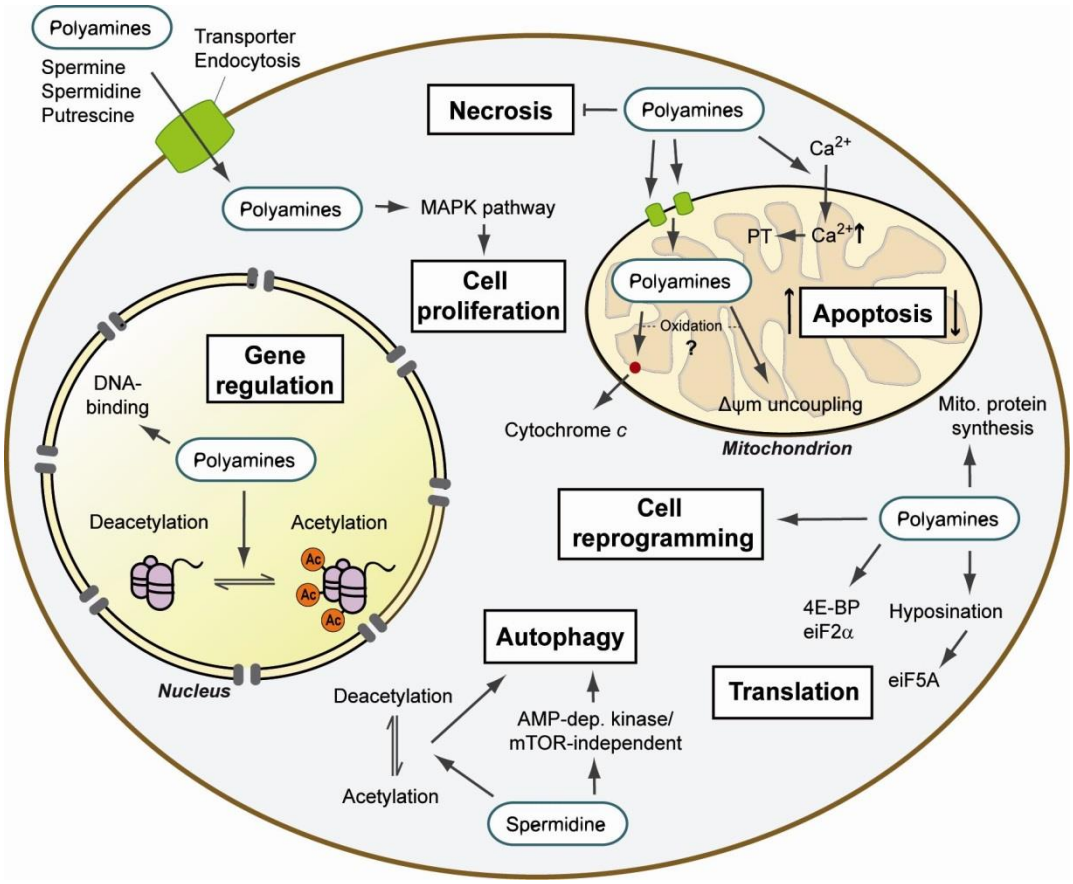

Figure 3.4 Cellular mechanisms of polyamines actions. [55]

3.1.5 Fundamentals of ultrahigh performance liquid chromatography coupled with tandem mass spectrometer (UPLC-MS/MS)

To achieve an accurate and reliable quantitation in biomarker research, UPLC-MS/MS is one of the most powerful instruments to complete the task. It is composed of two parts as describe below:

UPLC

Liquid chromatography is the component to achieve analyte separation based on their different extents of interaction between single solvent/solvent mixture (mobile phase) and column (stationary phase). It is composed of the mobile phase treatment and supply system, pumping system, sample injection system, chromatographic column for separation and finally one or more detectors. (Figure 3.5) While the usual version of liquid chromatography, the high performance liquid chromatography (HPLC), has been proven and widely accepted to be one of the most predominant technology with ready adaptability for analyte separation in different types of samples, the new advance UPLC presents an even further improved version taking advantage of the advances in particle chemistry, system optimization, detector design, and data processing and control. [57] Comparing to the usual column particle size packed in HPLC column, in UPLC it decreases from 3-10µm to below 3µm. According to the Van Deemter curve, with a smaller particle size, the height equivalent of theoretical plates becomes steadier under condition of high flow rate. (Figure 3.6) Also the pressure can reach up to 15000-20000psi compared to 5800-7000psi in HPLC. Therefore separation of analytes can now be achieved in a faster manner with higher resolution and sensitivity.

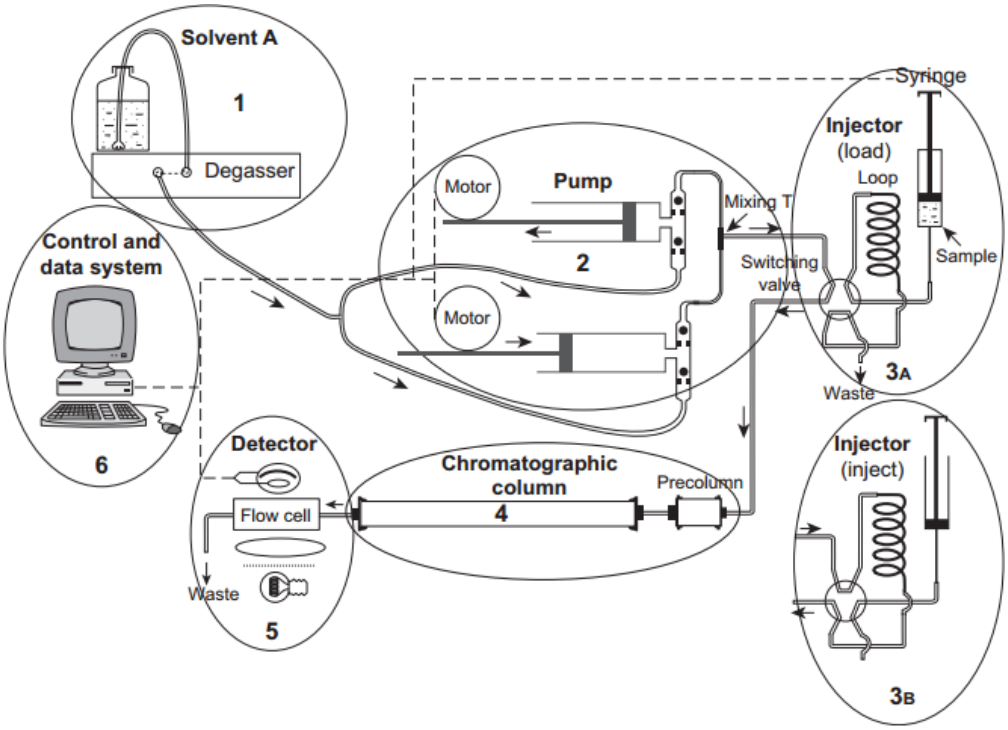

Figure 3.5 Block diagram of a typical LC system. [56]

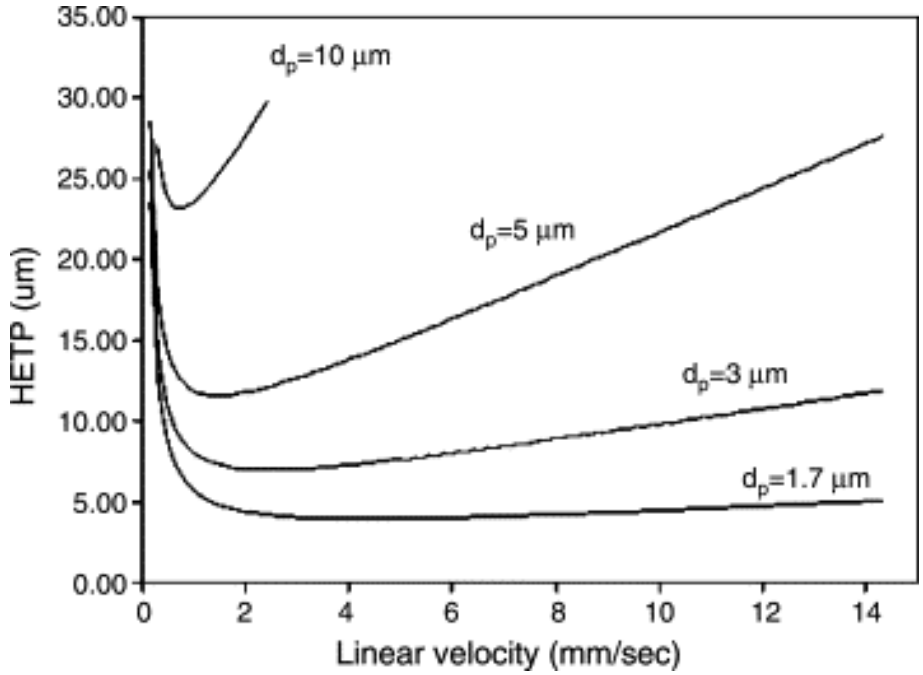

Figure 3.6 Van Deemter curves at different column particle sizes. [57]

Tandem mass spectrometer

Tandem mass spectrometer is a smart design that allows users to obtain mass spectrums of selected ions. Figure 3.7 shows the typical components of it. When being coupled with UPLC, the analyte eluted out from the column will enter the mass spectrometer sequentially depending on their retention times spending in the column.

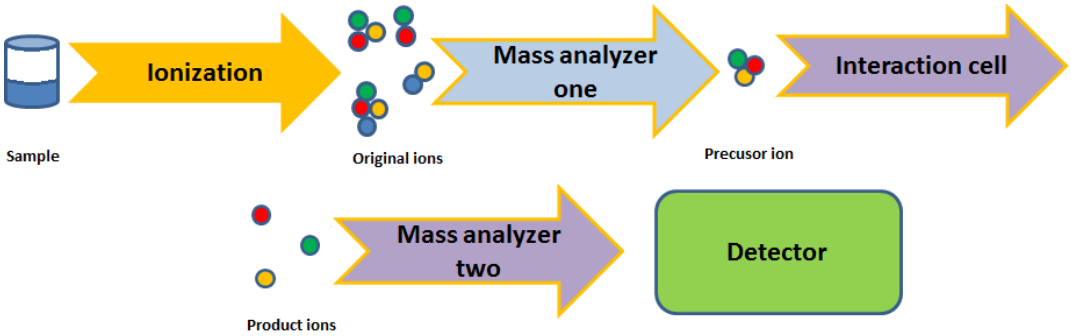

Figure 3.7 Block diagram of a tandem mass spectrometer.

Upon arrival to the mass spectrometer, they are firstly being ionized and fragmented. Subsequently the ions enter into the first quadrupole, which is a mass analyzer for selecting specific ions according to our settings. These precursor ions are then sent to the second quadrupole, an interaction cell where the precursor ions are further decomposed by different means. Afterwards, the product ions reach the third quadrupole which is another mass analyzer for selecting final target ion for detection. This tandem-in-space mass spectrometer, or sometimes called a triple quadrupole mass spectrometer allows users to obtain different types of mass spectrums, like a product ion spectrum, precursor ion or neutral loss spectrum by

varying the mass each analyzer is monitoring. By choosing a suitable pair of precursor and product ions for a target analyte in the multiple reaction monitoring (MRM) mode, the selectivity provided overcomes the problem brought by elution of co-eluted matrix components, allowing sufficient sensitivity for surveillance monitoring studies or other quantitative analyses when compared with the single selected ion monitoring mode.

3.1.6 Design of experiment

To explore new PCa biomarkers that can replace or at least supplement the serum PSA test, in this chapter it describes our effort to evaluate the potential of three main urinary polyamines as PCa biomarkers by comparing the levels among diagnosed PCa, BPH patients and healthy control (HC). These three polyamines are putrescine (Put), spermidine (Spd) and spermine (Spm). (Figure 3.8) And the method for their accurate quantitation was developed on a UPLC-MS/MS using separated deuterated internal standards (IS) for each of them. (Figure 3.9) Statistical tools like Student t's test and receiver operating characteristics (ROC) were used to assess the significance of difference, sensitivity and specificity of each proposed analyte. Results were also tried to be matched with different clinico-pathologic characteristics of participants to see if there are any significant correlations.

Putrescine
Chemical Formula: $C_4H_{12}N_2$
Molecular Weight: 88.15

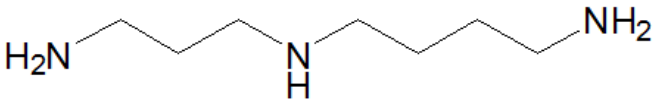

Spermidine
Chemical Formula: $C_7H_{19}N_3$
Molecular Weight: 145.25

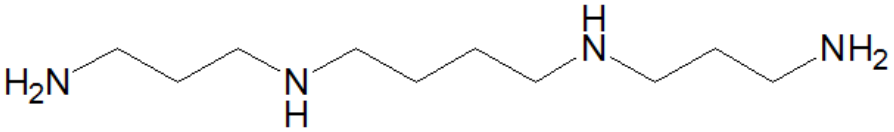

Spermine
Chemical Formula: $C_{10}H_{26}N_4$
Molecular Weight: 202.34

Figure 3.8 Structures of Put, Spd and Spm.

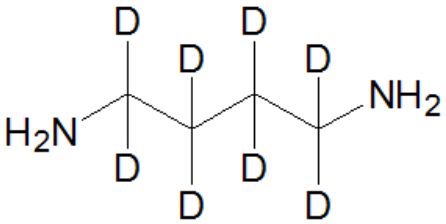

Putrescine-d_8
Chemical Formula: $C_4H_4D_8N_2$
Molecular Weight: 96.20

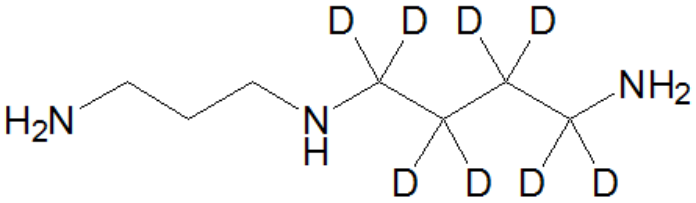

Spermidine-d_8
Chemical Formula: $C_7H_{11}D_8N_3$
Molecular Weight: 153.30

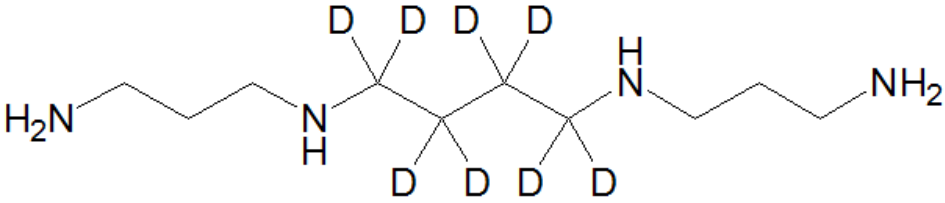

Spermine-d_8
Chemical Formula: $C_{10}H_{18}D_8N_4$
Molecular Weight: 210.39

Figure 3.9 Structures of Put-d_8, Spd-d_8 and Spm-d_8.

3.2 Experimental section

3.2.1 Chemicals, reagents and materials

For the mobile phases, water was purified in a Milli-Q Direct Water Purification System (Millipore, USA). Acetonitrile was obtained from ACS (HPLC grade, ≥ 99.9%).

All chemical standards, including 1,4-Diaminobutane (Put, 99%), spermidine (Spd, ≥99.0%), spermine (Spm, ≥99.0%), 1,4-Diamino(butane-d_8) dihydrochloride (98 atom % D), spermidine–(butane-d_8) trihydrochloride (98 atom % D, 95% CP), spermine–(butane-d_8) tetrahydrochloride (97 atom % D, 95% CP) and heptafluorobutyric acid (HFBA, ≥99.0%) were purchased from Sigma-Aldrich (Hong Kong, China) and used without further purification.

Strong Anion Exchange solid phase extraction (SPE) cartridges were used for urine clean-up, and they were brought from Phenomenex (Strata, 100mg/3mL, USA). Centrifugation was performed using a Refrigerated centrifuge obtained from Eppendorf (5417R, Hong Kong, China). The creatinine concentration inside urine samples were determined by LabAssayTM Creatinine assay (Wako, Japan). Methanol was used for pre-condition and it was obtained from TEDIA (HPLC/Spectro grade, ≥ 99.9%).

3.2.2 Urine samples collection

This study was collaborated with the Chinese University of Hong Kong. The collection of urine samples from participants was reviewed and approved by the Clinical Research Ethical Committee of the Chinese University of Hong Kong,

and we followed strictly to the guidelines developed by that committee. Written consent was acquired from all of the patients who agreed to participate into the study. Basically, between Oct-2014 and Mar-2016 we obtained urine samples at noon time after lunch prior to TRUSPB from 165 male patients with age greater or equal to 50. They were all having a serum PSA level over 4.0ng/ml. These patients' urine samples were accepted only when they didn't have clinically active urinary tract infection which might be biasing to the outcome of our study. When patients did not consent to take part in the current study, or if they showed clinical evidence of other types of cancers other than PCa, they were excluded from our sampling scheme.

Amongst these 165 patients, three subsets could be classified for the clinical samples enrolled in the current study. 66 were diagnosed to have PCa and the remaining 99 were having no evidence of malignancy (NEM) by using TRUSPB as the reference diagnostic method. To further categorize these 99 NEM patients, using the criteria whether the prostate volume was larger than 30ml, 88 were found to have BPH. Others were considered as HC. (Figure 3.10)

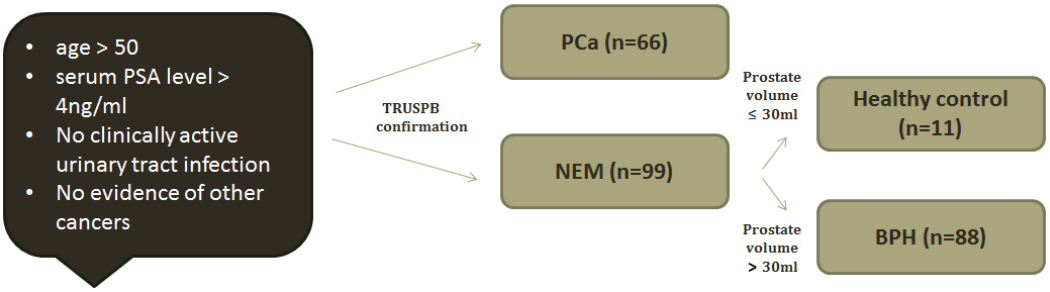

Figure 3.10 Participants' enrolment criteria and categorization.

All pathological examinations were conducted at Prince of Wales Hospital, The Chinese University of Hong Kong, Hong Kong under supervision of experienced uro-pathologists. Table 3.4 shows all the clinic-pathologic characteristics of samples. All samples were stored at -20˚C until measurement which was conducted within three months after collection.

3.2.3 Creatinine determination

Briefly, urine samples and standards were thawed and centrifuged. The supernatant was then separated, deproteinized and reacted with picric acid in an alkaline condition to produce an orange Janovsky complex through the Jaffe reaction. [58] (Figure 3.11) Quantitation of total creatinine inside urine was achieved indirectly by measuring the absorbance of the orange complex at 520nm by a Clariostar Monochromator Microplate Reader (BMG Labtech, Hong Kong). If the creatinine level was too concentrated inside urine samples and exceeded the highest calibration points, they were diluted with water with appropriate dilution factors before sample preparation and analyzed again. Each sample was determined at least twice and RSD should be less than 15%.

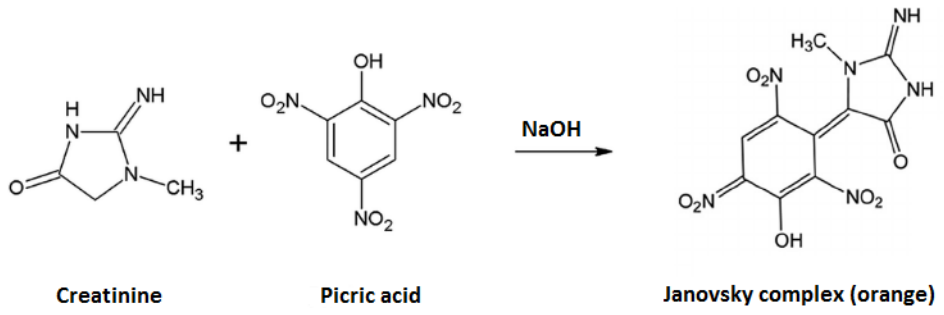

Figure 3.11 The Jaffe reaction between creatinine and picric acid.

Characteristics	PCa (n=66)	BPH (n=88)	HC (n=11)	*p* value (PCa vs BPH)	*p* value (PCa vs HC)	*p* value (BPH vs HC)
Age (years)						
Mean(SEM)	69.6(0.8)	66.9(0.6)	64.9(1.1)	0.018	0.027	0.245
Median	69	66	65			
Range	54-86	51-79	59-74			
Preoperative PSA (ng/ml)						
Mean(SEM)	46.39(8.61)	12.39(1.57)	26.54(7.51)	<0.0001	0.350	0.007
Median	15.60	8.60	8.50			
Range	4.20-299.00	4.40-98.50	4.3-66.00			
Gleason score (GS)		Nil	Nil			
5	1					
6	26					
7	15					
8	10					
9	12					
10	2					
Prostate volume (ml)						
Mean(SEM)	43.81(2.44)	67.28(2.98)	17.46(2.67)	<0.0001	<0.0001	<0.0001
Median	40.00	56.50	20.40			
Range	16.60-87.80	32.20-162.00	4.60-30.00			

Table 3.4 Clinico-pathologic characteristics of all participants.

3.2.4 Sample preparation for polyamine determination

Stock solutions (5000µg/ml) of the three polyamines were prepared in water individually. An intermediate standard of 50µg/ml was prepared by mixing the three stock solutions with appropriate dilution factors. It was then used to prepare a series of working standards with seven different polyamine concentrations ranging from 10-1000ng/ml in water. (10, 25, 50, 100, 250, 500 and 1000ng/ml) For IS, similarly the stock solutions (5000µg/ml) of each deuterated polyamines were prepared in water separately. The three stock solutions were mixed and diluted to give an IS working solution (1µg/ml) in water.

3.2.5 Standard/sample pretreatment for polyamine determination

We followed the sample preparation procedures published before with little modifications. [59] Urine samples/standards were thawed naturally and centrifuged at 13000 rpm and room temperature for 5 minute. 120µL of urine sample/standard supernatant were mixed with 60µL of IS working solution and 420µL of water. Of this well-vortexed solution, 550µL was passed through the strong anion exchange SPE cartridges, which had been conditioned and equilibrated with 1mL of methanol and water respectively. 450µL of water was passed through the cartridge afterwards to elute out all polyamines and make up a 1ml solution. Finally 400µL of this SPE-treated sample was mixed with 100µL of 10% HFBA solution in water, well vortexed for instrumental analysis. If the urine samples were too concentrated which exceeded the highest calibration points, they

were diluted with water with suitable dilution factors before sample preparation and analyzed again.

3.2.6 Quality control (QC) samples preparation

For each batch of sample analysis, every time three QC working solutions were analyzed to verify the accuracy of calibration curves and guarantee the comparability from batch to batch. QC solutions were prepared using analyzed control urine samples from colleagues of our research group. Firstly, the polyamines concentrations of each controls' urine samples were determined. They were then mixed equally to give a pooled urine sample. Afterwards, three QC working solutions with different polyamine concentration ranges (low, medium and high) were prepared by mixing this pooled urine sample with standard solutions. For low QC working solution, the SPE-treated pooled urine sample was mixed with SPE-treated 10ng/ml standard at a 1:7 ratio. For medium QC working solution, the SPE-treated pooled urine samples were mixed with SPE-treated 100ng/ml standard at a 1:1 ratio. For high QC working solution, the SPE-treated pooled urine sample was mixed with SPE-treated 1000ng/ml standard at a 1:1 ratio.

3.2.7 Stability study

To study whether the samples and standards were stable during storage or sample preparation, Häkkinen *et al.* had previously demonstrated that they were all having a good short-term, long-term and freeze thaw stability, which were the

stability after storing at six hours at room temperature, after storage at -20˚C and -80˚C for two months and after running through three cycles of freezing and thawing before sample preparation respectively. [59] We further verified by analyzing both the content of polyamines and creatinine inside standards and selected urine samples. We found that even went through five cycles of freeze and thaw, all the contents were still stable in six months' time when being stored at -20˚C. For the SPE-treated samples, they were stable for at least two days when being stored at 4 ˚C and up to a year when being stored at -20 ˚C.

3.2.8 Instrumentation and statistical analysis

The quantitation of polyamines was performed with UPLC-MS/MS. UPLC separation was done by an Agilent 1290 Infinity Quaternary LC System while mass analyzing was done by an Agilent 6460 Triple Quadrupole mass spectrometer equipped with an Agilent Jet Stream technology electrospray ionization source. The column used was an Agilent EclipsePlus C18 RRHD (2.1x50 mm, 1.8 µm) protected with an Agilent SB-C18 guard column (2.1x5 mm, 1.8 µm).

The choices and elution profiles of mobile phases were optimized as follows: Eluent A was water with 0.1% HFBA while eluent B was acetonitrile with 0.1% HFBA. Eluent A was decreased from 95% to 60% in 10 minutes, and from 60% to 10% in 1 minute. Afterwards the gradient was held constant for another 5 minutes. The gradient was then increased from 10% to 95% in 1 minute,

and held constant for additional 8 minutes. The total run-time was 25 minutes per injection.

The auto-sampler and column temperatures were set at 4 and 35˚C respectively. Injection was achieved by 5-second needle wash in Flush Port mode for 3 times with eluent B. Each time 10 μL of sample solution was injected.

For the parameters of the source, the drying gas (nitrogen) temperature was optimized as 300˚C with 5 L/min flow rate. Nebulizer pressure was set as 45psi. Sheath gas temperature was 250˚C with 11 L/min flow rate. Capillary voltage was set as 3500V. For mass detection, scheduled MRM mode was used to enhance sensitivity. All of the information about the optimized MRM transitions can be found in Table 3.5.

Quantitation results were calculated using Agilent MassHunter Workstation software pre-installed in the computer linked to the UPLC-MS/MS. Calibration curves were fitted by linear regression without any weighing. Each time the correlation coefficient should be at least 0.995. Acceptance values for each calibration point and quality control working solution were ±30% to ensure a good accuracy. For precision verification, a 250ng/ml standard was injected after every 10-samples injection to check if it could be reproduced. The criterion was ±15%.

	Precursor ion	Daughter ion	Dwell time (ms)	Fragmentor Voltage (V)	Collision energy (V)	Cell Accelerator Voltage (V)
Put	89	72*	100	70	6	3
Put-d_8	97	80*	100	70	6	3
Spd	146	112	100	90	10	3
	146	72*	100	90	15	3
Spd-d_8	154	120	100	90	10	3
	154	80*	100	90	15	3
Spm	203	129	100	90	10	3
	203	112*	100	90	15	3
Spm-d_8	211	137	100	90	10	3
	211	120*	100	90	15	3

Table 3.5 MRM transitions, dwell time, fragmentor, collision energy and cell accelerator voltage for Put, Spd, Spm and their corresponding internal standards (*Denoted the quantifier transitions)

For the statistical analysis, the ROC curves and the area under curve (AUC) values were calculated using GraphPad Prism 6 software (GraphPad Software, San Diego, CA, USA). Any *p* values smaller than 0.05 (two-tailed) were considered as statistically significant during comparison based on Student's t-test.

3.3 Results and discussions

3.3.1 Urinary polyamines contents

Put, Spd, Spm together with their corresponding deuterated internal standards were successfully being separated and quantified from all samples by the developed method in UPLC-MS/MS. (Figure 3.12) The calibration curves were all satisfactory with R^2 not less than 0.995 (Figure 3.13). All QC solutions' polyamine contents gave accurate results according to the mixing ratios and guaranteed the comparability between samples of different batches. Mean urinary polyamines concentration for each participant was then normalized to their urinary creatinine levels and expressed as μmol/g of creatinine. Table 3.6 shows the summarized creatinine results of all participants. This normalization process was necessary to compensate for any diuresis processes or differences in urinary flow rate hindering actual quantity measurements. [60] The assumption here was that the creatinine excretion was constant across and within individuals, and normalization to it would help reflecting the true changes in biomarker excretion. More discussions will be given in the following discussion part.

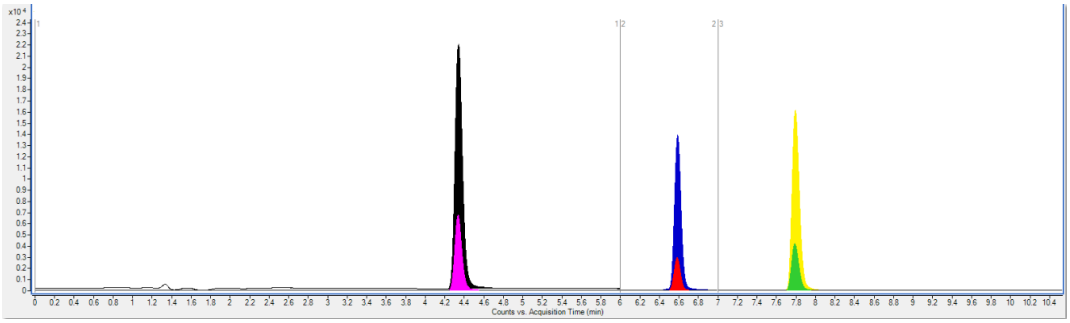

Figure 3.12 Overlaid UPLC-MS/MS SRM chromatograms of 1000ng/ml mixed polyamines standard (focusing on 0-10min only). Put (Black peak, t_R = 4.3 min), Put-d_8 (Pink peak, t_R = 4.3 min), Spd (Blue peak, t_R = 6.6 min), Spd-d_8 (Red peak, t_R = 6.6 min), Spm (Yellow peak, t_R = 7.9 min) and Spm-d_8 (Green peak, t_R = 7.9 min).

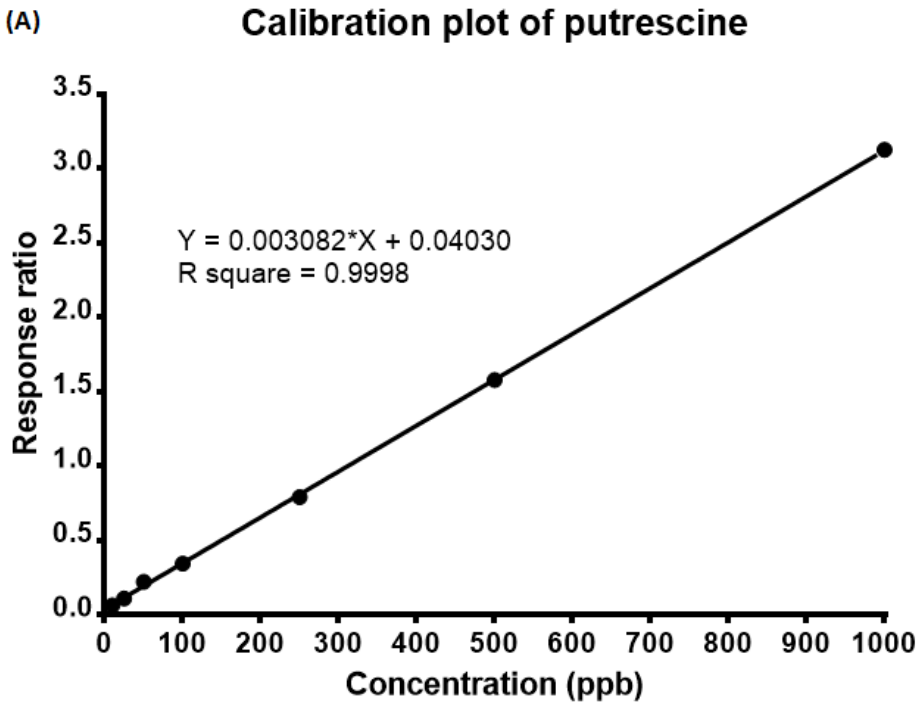

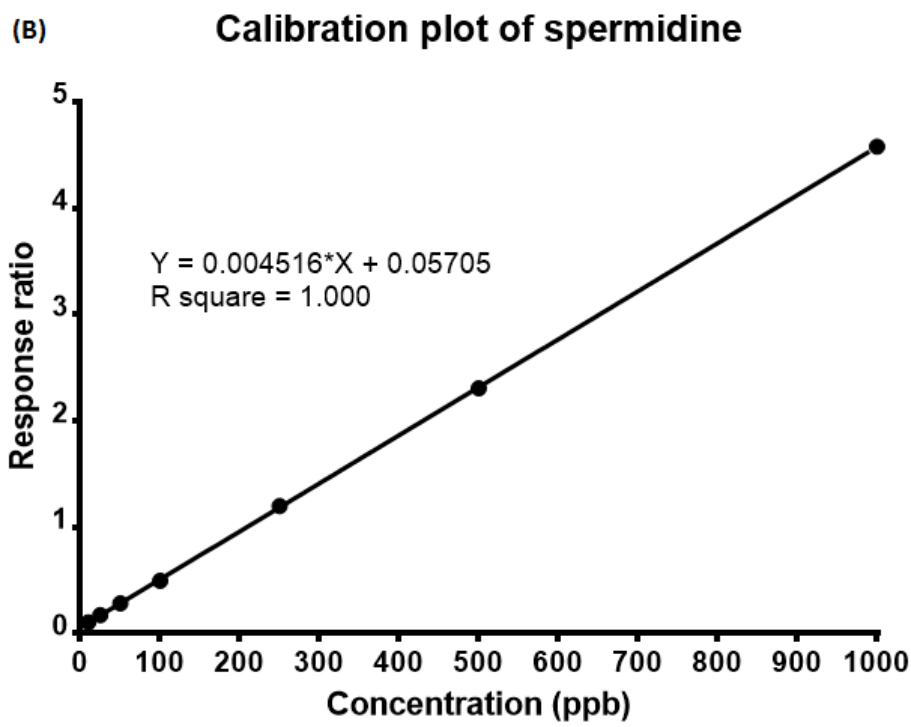

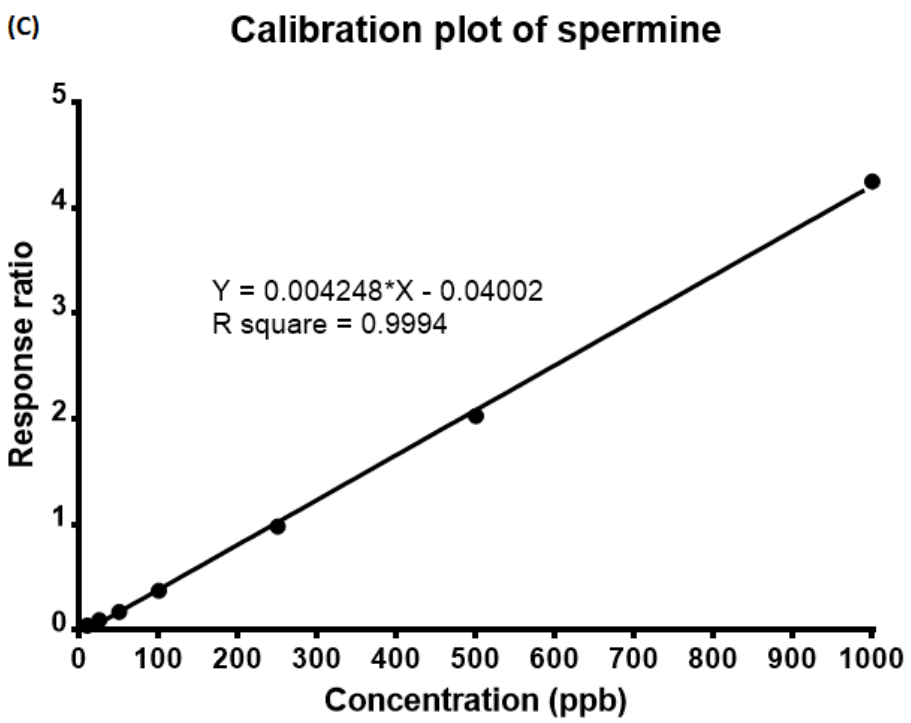

Figure 3.13 Calibration graphs of polyamines. (A) Put (r^2 = 0.9998) (B) Spd (r^2 = 1.000) (C) Spm (r^2 = 0.9994)

	PCa (n=66)	BPH (n=88)	HC (n=11)	*p* value (PCa vs BPH)	*p* value (PCa vs HC)	*p* value (BPH vs HC)
Creatinine (ppm)						
Mean(SEM)	828.30(76.82)	970.40(69.06)	1143(269.40)	0.173	0.151	0.427
Median	671.31	751.80	951.98			
Range	119.57-3102.61	171.43-3025.24	174.16-3183.77			

Table 3.6 Summarized urinary creatinine results from participants of different subsets.

Figure 3.14 and Table 3.7 shows the graphical comparison of data and tabulates different subsets' normalized polyamines levels respectively:

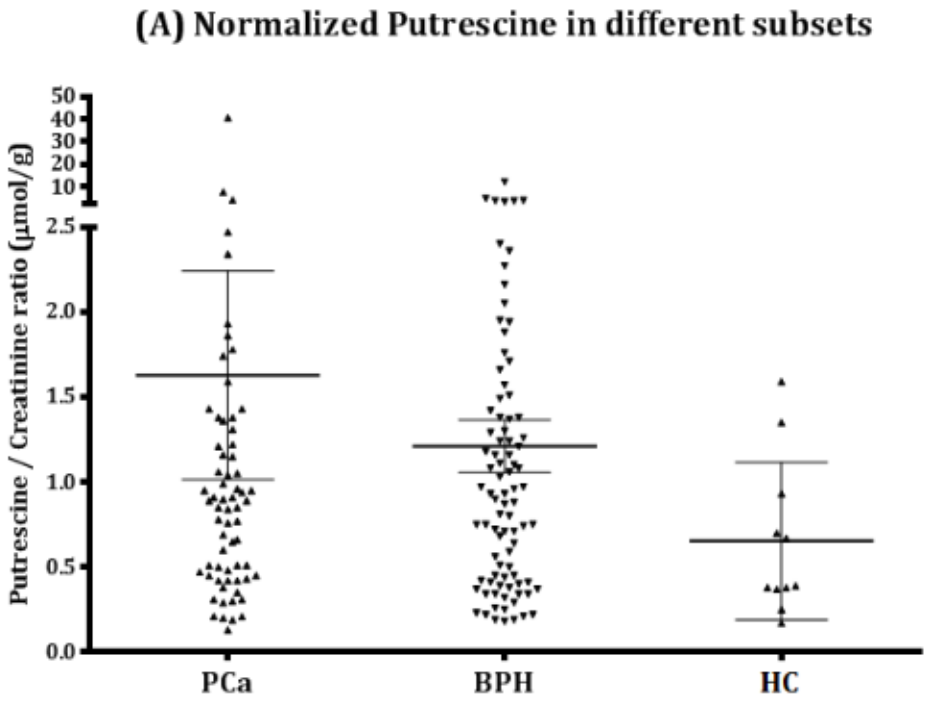

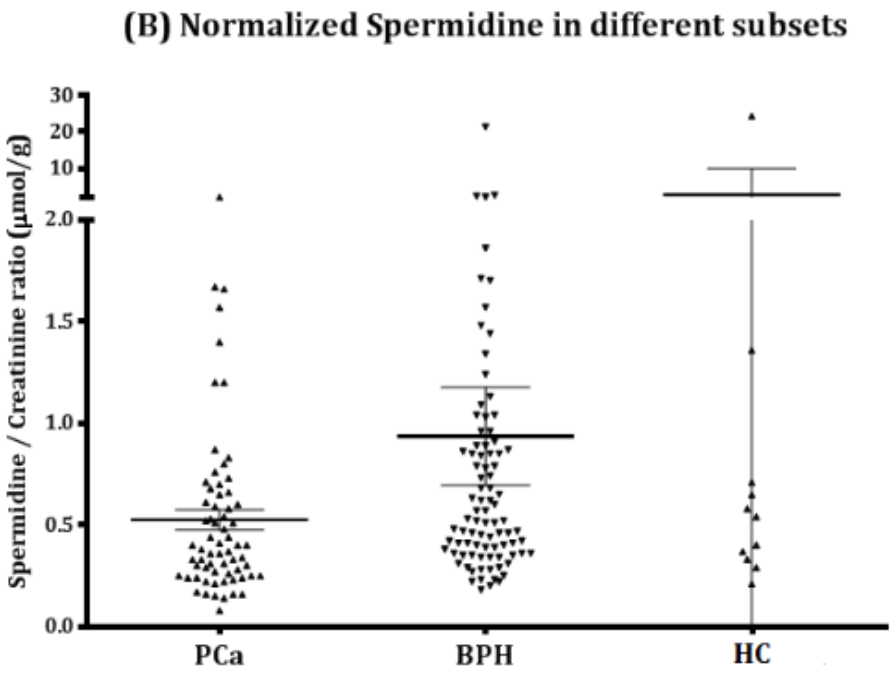

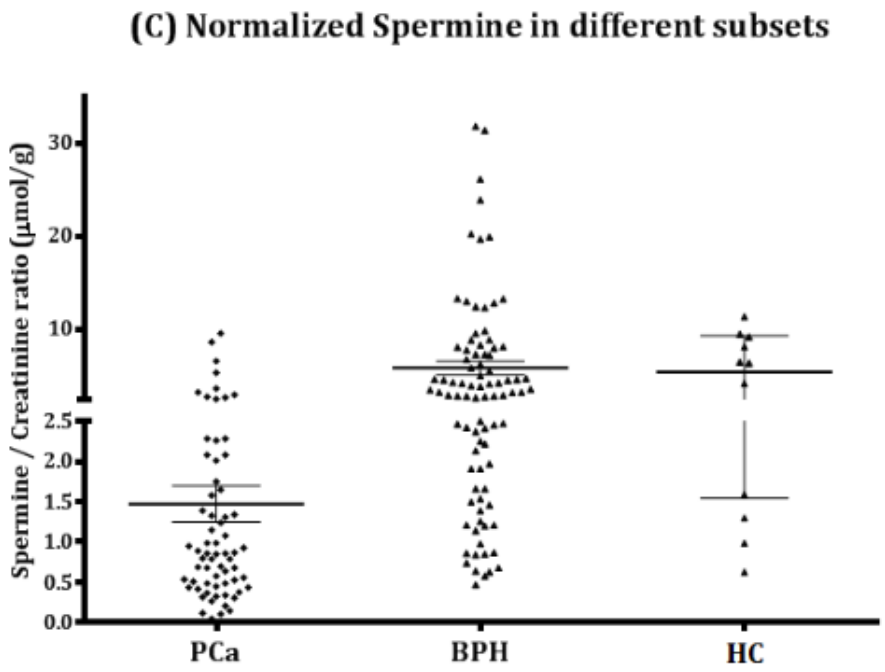

Figure 3.14 Graphical distribution of (A) normalized Put, (B) normalized Spd, (C) normalized Spm values in PCa, BPH and HC. The black bar in the figures indicates the mean value of each subset while the error bar indicates the corresponding SEM.

	PCa	BPH	HC	*p* value (PCa vs BPH)	*p* value (PCa vs HC)	*p* value (BPH vs HC)
Normalized Put						
Mean (SEM)	1.63(0.61)	1.21(0.16)	0.65(0.14)	0.459	0.522	0.212
Median	0.87	0.92	0.39			
Range	0.13-40.64	0.18-12.04	0.17-1.59			
25% Percentile	0.45	0.41	0.37			
75% Percentile	1.24	1.38	0.93			
Normalized Spd						
Mean (SEM)	0.52(0.05)	0.94(0.24)	2.71(2.17)	0.147	0.014	0.081
Median	0.39	0.52	0.54			
Range	0.08 - 2.09	0.18 - 21.42	0.21- 24.40			
25% Percentile	0.25	0.36	0.33			
75% Percentile	0.65	0.89	0.71			
Normalized Spm						
Mean (SEM)	1.47(0.22)	5.87(0.71)	5.43(1.17)	<0.0001	<0.0001	0.833
Median	0.86	3.25	6.37			
Range	0.05 - 9.57	0.47 - 31.78	0.63- 11.36			
25% *P*ercentile	0.48	1.72	1.30			
75% Percentile	1.82	7.65	9.18			

**SEM represents the standard error of the mean.*

Table 3.7 Column statistics of normalized polyamine contents (µmol/g of creatinine) in different subsets.

Among the three polyamines monitored, normalized Spm showed a remarkable decrease in PCa patients compared to non-cancerous cases including BPH patients and HC in terms of statistical means (Unpaired student's t-test). The mean value was 1.47 in PCa vs 5.87 in BPH vs 5.43 in HC. *P* values were <0.0001 in t-test, which means the difference was significant at the 95% confidence interval. For normalized Put and Spd, no obvious enhancement or suppression could be observed neither by looking at their distributions nor comparing their mean values by t-test. (Put: 1.63 in PCa vs 1.21 in BPH vs 0.65 in HC; Spd: 0.52 in PCa vs 0.94 in BPH vs 2.71 in HC)

3.3.2 Receiver operating characteristics analysis

Figure 3.15 shows the ROC curves of the three normalized polyamines for evaluating the diagnostic power of the selected polyamines for PCa diagnosis. The AUC for normalized Put, Spd and Spm were found to be 0.63±0.05, 0.65±0.05 and 0.83±0.03 respectively. The threshold values for Spm with the corresponding sensitivity and specificity are listed in Table A3.2. The one with the maximum sum of sensitivity and specificity is 2.325μmol/g of creatinine, giving corresponding sensitivity and specificity values of 84.85% and 67.68% respectively.

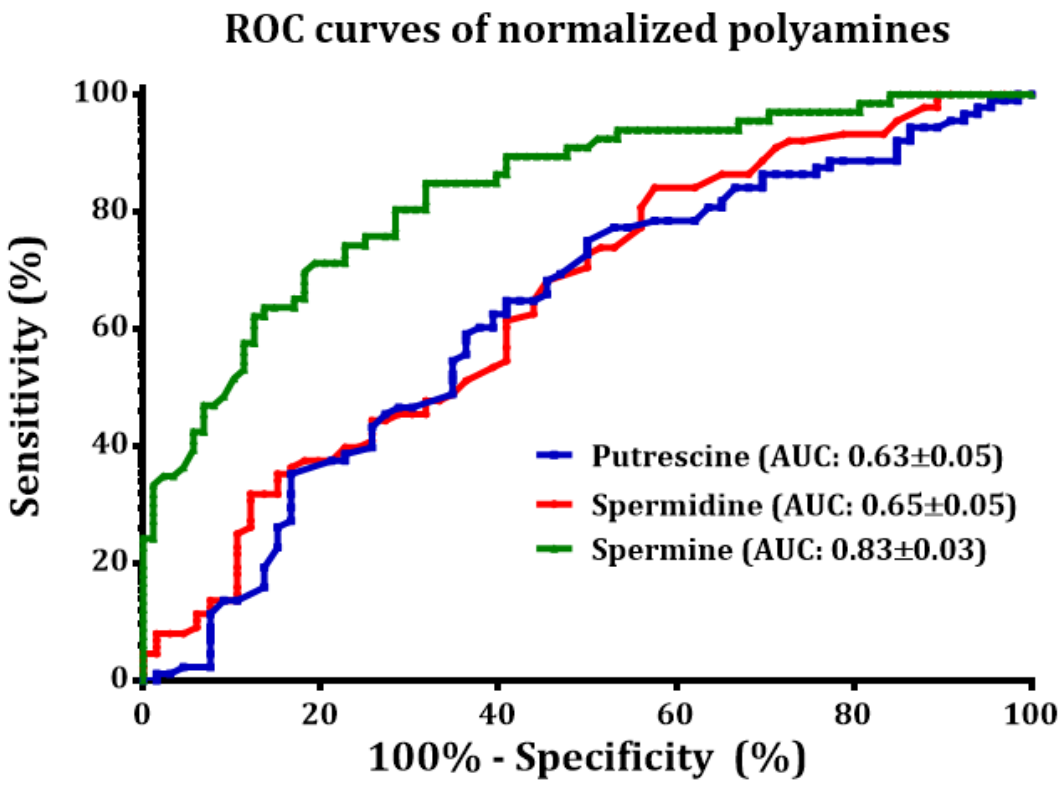

Figure 3.15 Receiver operating characteristic analysis for normalized Put, Spd and Spm values.

3.3.3 Correlation study

Correlations between urinary Spm had also been performed with participants' clinic-pathologic characteristics including their ages, serum PSA values, creatinine contents and prostate volumes to check if its drop was related to any of these factors. Our results showed that all of them demonstrated weak correlations with correlation coefficient smaller than 0.2. (Figure 3.16) However, it is interesting to observe that for serum PSA, participants with high serum PSA values were usually accompanied with a low urinary Spm value, and vice versa.

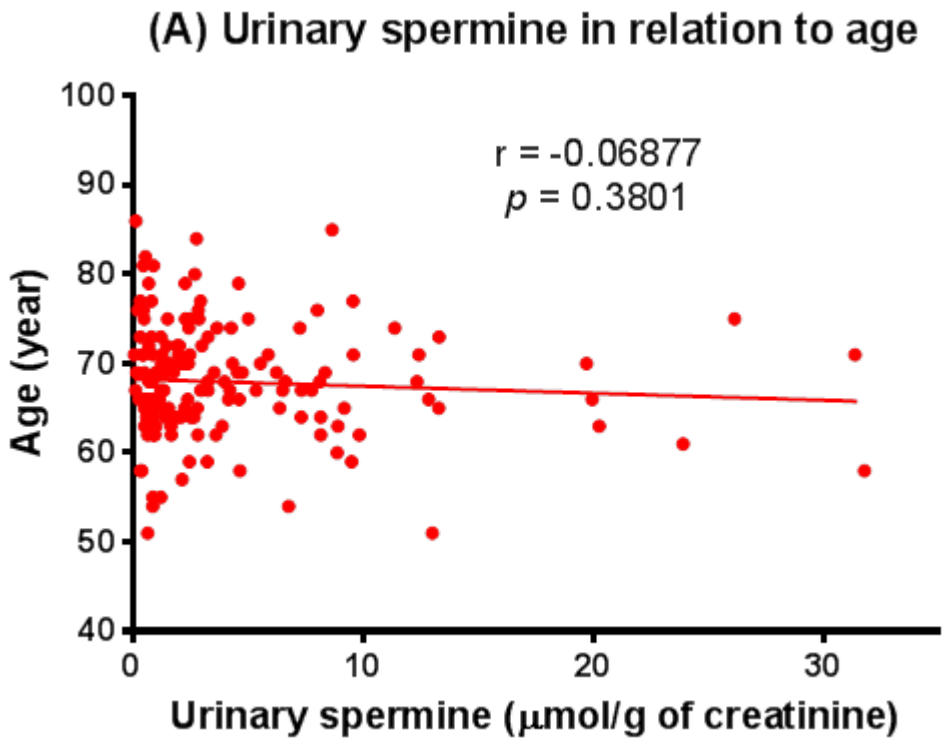
(A) Urinary spermine in relation to age
r = -0.06877
p = 0.3801
Age (year)
100
90
80
70
60
50
40
0
10
20
30
Urinary spermine (μmol/g of creatinine)

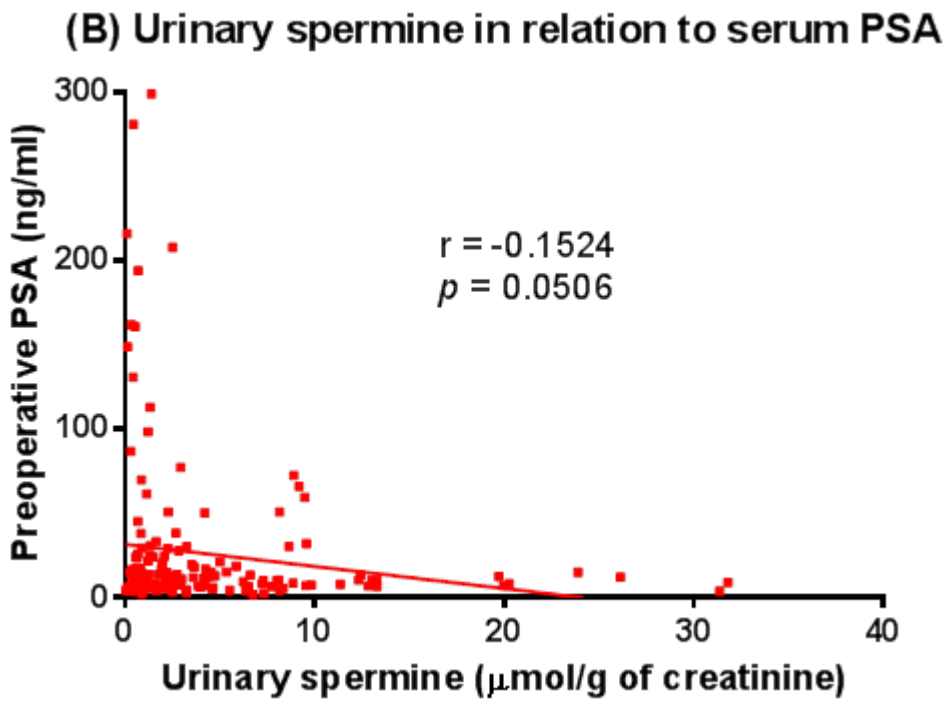
(B) Urinary spermine in relation to serum PSA
r = -0.1524
p = 0.0506
Preoperative PSA (ng/ml)
300
200
100
0
0
10
20
30
40
Urinary spermine (μmol/g of creatinine)

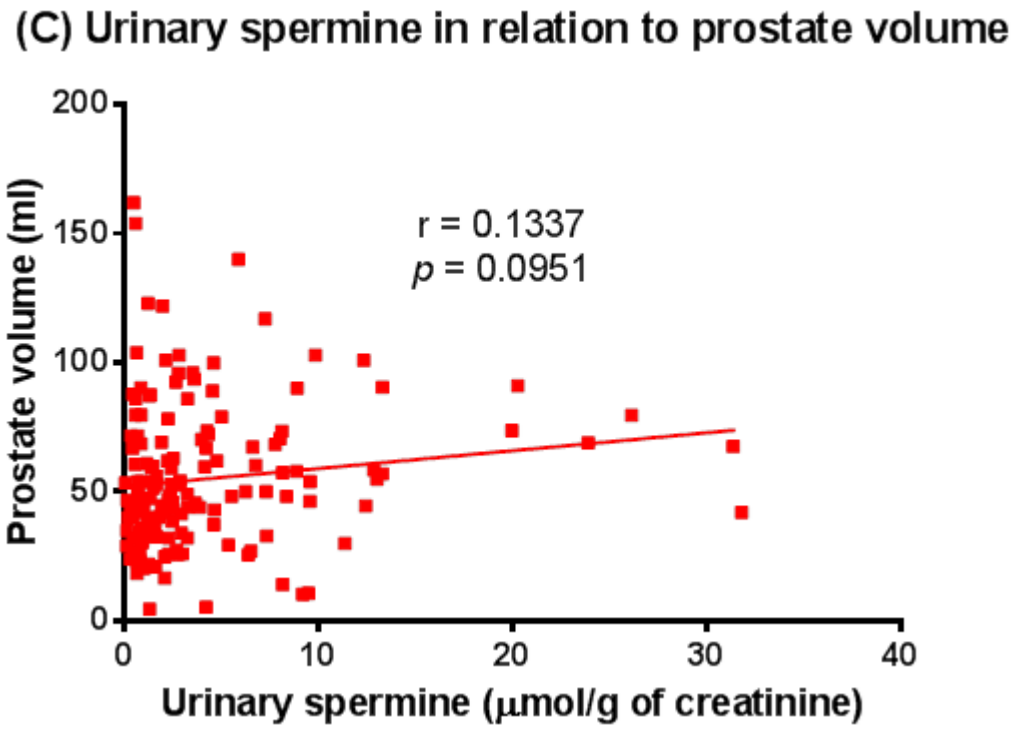

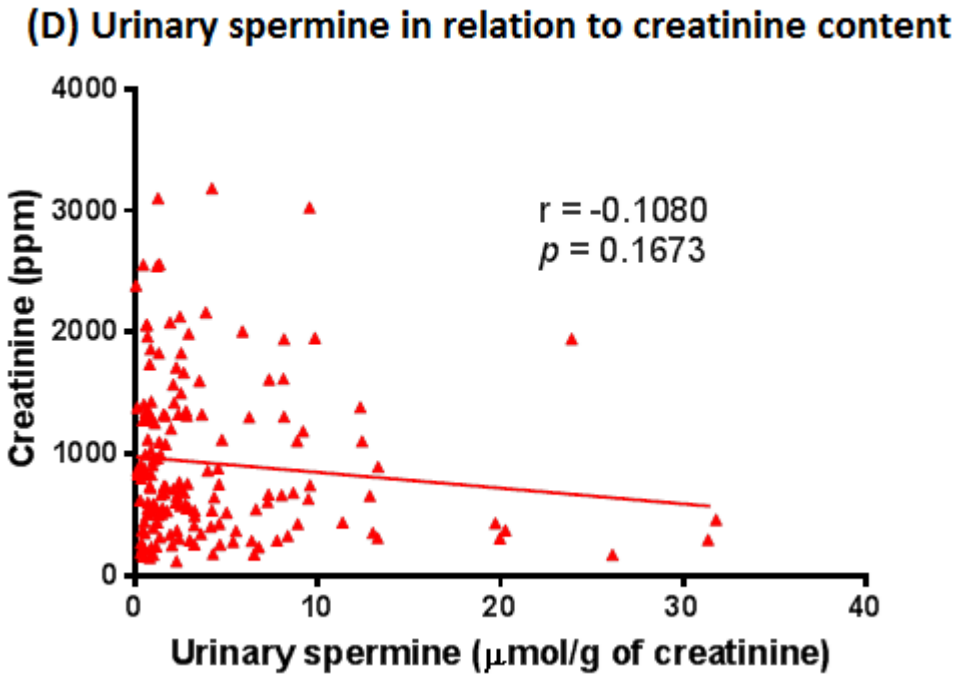

Figure 3.16 Correlation studies of urinary Spm with (A) age, (B) serum PSA, (C) prostate volume and (D) creatinine content.

3.3.4 Discussion

The relationship between polyamines and cancer has long been studied by scientists. The general concept believed was that an increase of polyamine levels in serum/urine usually reflects an enhanced levels of polyamine synthesis caused by the rapid-growing cancer tissues/cells, which can be associated with an increased cell proliferation, decreased apoptosis and increased expression of genes affecting tumor invasion and metastasis. [61-63] Russell *et al.* from USA firstly reported the increase of urinary polyamines levels in various solid tumors, including ovarian teratoma, rectal carcinoma, lymphosarcoma, osteogenic sarcoma and acute myelocytic leukaemia. [64] Japan was another country with numerous scientists participating actively in polyamine studies, and she is the only country officially recognizing urinary polyamines as tumor markers. [63] For example, Kyoko Hiramatsu *et al.* reported an elevation N^1, N^{12}–Diacetylspermine in patients with early and late stage colorectal and breast cancers and established its role to be a novel marker for these cancers. [65] Detection kit is even commercially available for its detection. In cases of cervical cancer, Lee and his groupmates had shown a significant elevation in polyamines level in Put, Spd and Spm gradually from non-cancerous to benign cervical diseases and cervical cancer cases. [66] For hepatic cancer, Liu *et al.* had monitored the level differences between polyamines, polyamine precursors and catabolites in both patients' plasma and urines using UPLC coupled with tandem mass spectrometer similar to our study. [67] Analyzing all of their results carefully, we can see that different kinds of polyamines in fact showed different variations depending on the type of cancers.

The statement of elevated urinary polyamine levels in cancer cases is just not specific enough.

Very scanty reports focused on exploring the outcome of PCa on urinary polyamines levels, which in turn might provide a potential diagnostic tool for this highly incident cancer. Forty years before in 1975, Fair *et al.* had reported a significant elevation of urinary Spd content in PCa patients by electrophoresis, but not Put and Spm. [68] Horn *et al.* analyzed urinary Spd and Put contents in patients with tumors in either breast, stomach, prostate, female genital tract, or metastatic carcinomas of unknown origins by LC coupled with fluorometric detector in 1984, yet yielding an indeterminate conclusion on their biomarker roles. [69] With the recent advance in analytical field, we can now achieve a more accurate quantitative analysis for analytes inside more complicated matrices. As demonstrated in the current pilot study, we re-evaluated the potential abilities of three natural polyamines, Put, Spd and Spm, as urinary biomarkers for PCa screening by the more powerful and reliable UPLC-MS/MS. Through a well validated method using separate deuterated internal standards for correcting matrix effects for each polyamine, we can have a clearer understanding on their roles. Our results demonstrated that Spm was the best and only polyamine able to be employed as such a PCa diagnostic biomarker. A significant decrease in its urinary level was observed, providing it ability for PCa monitoring. For Put and Spd, hardly could we find any differences between two subsets by statistical means.

The observation of such a declined level in urinary Spm actually was reasonable and being supported by results of previous literature regarding PCa and

polyamines studies. To give some examples, the observation of lower Spm contents in prostatic cell lines with less degree of differentiation were reported by van der Graaf *et al.* in both PCa cell lines with various differentiation extent as well as biopsied samples. Despite examining only a limited number of tissue specimens, a reduced Spm level in tumor prostatic tissues compared to normal and benign hyperplastic prostatic tissues was reported using the instrument of HPLC with a fluorometric detector. [54] Such a decrease of prostatic Spm content was therefore suggested to indicate a conversion of PCa phenotype. Similarly Swanson *et al.* reported a declined Spm level in prostate tissue samples using the technique of Proton high-resolution magic angle spinning nuclear magnetic resonance spectroscopy and quantitative histopathology. [70] High grade cancer prostate tissue could even be distinguished from low grade cancer tissue by the gradual decreasing concentration of Spm and citrate, as reported by Giskeødegård *et al*. [71] Other than a direct and complicated monitoring of prostate tissues, other easily accessible biological fluids were also of high concern. Serkova *et al.* reported that in human expressed prostatic secretions (EPS), citrate, myo-inositol and Spm are potentially important markers of PCa, and all of them showed a significant dropped level in PCa patients compared to healthy control samples. The AUC value reported for Spm in EPS is 0.87, a value close to what we discovered in this research, in spite of the fact we only studied participants having serum PSA value over 4.0ng/ml. [72] With respect to these previous literatures on PCa, a decrease in urinary Spm content could be expected as urine represents a biological fluid closely related to exfoliated cancer cells and secreted prostatic products from the prostate. [32] In essence, numerous advantages of urine like its ready

availability and non-invasive character are things that the prostate tissue samples and EPS cannot compare with. Therefore the discovery of a useful urine PCa biomarker can be inspiring to the current PCa world for reducing unnecessary biopsies and treatments that can be harmful or even fatal.

To explain the declined level of Spm in PCa patients, the exact mechanism is still under research and lacks definite evidence. Schipper *et al.* suggested a possible explanation that the changes in cell organization caused by cancer cells proliferation would eventually result in a decreased luminal volume, which in turn reduces the amount of secreted compounds into the prostate tissue, prostatic fluid or even urine. [53] But this could hardly explain why only urinary Spm level declined. Cheng *et al.* reported that Spm was a proposed endogenous inhibitor to PCa growth, and a linear correlation was found between Spm content and the volume percentage of normal prostatic epithelial cells as quantified by histopathology. [73] Smith *et al.* also reported that Spm can inhibit the growth of prostatic carcinoma both in vitro and in vivo after they observed a slow growth of prostatic carcinoma within the prostate gland, a microenvironment with a very high localized Spm content. [74] And in recent studies it was suggested that dysregulation of polyamine metabolism, or more specifically the polyamine catabolism, may be involved in PCa. Increases in spermine oxidase (SMO) and spermidine/spermine N^1-acetyltransferase (SSAT) expression were observed in both precursor prostatic inflammatory atrophy lesions and early prostatic intraepithelial neoplastic lesions, which can result in a depletion of Spm content. (Figure 3.17) [75-77] This hypothesis also matches well with the observation of a

significant increase in urinary diacetylspermine content in patients with urogenital malignancies resulted from the enzymatic action of SSAT, as reported by Hiramatsu *et al*. [78] Therefore our observation of a decrease in urinary Spm is in line with previous findings and suggested mechanisms. For Spd, we hypothesized the action of SMO and SSAT counteracted each other so no significant changes were found.

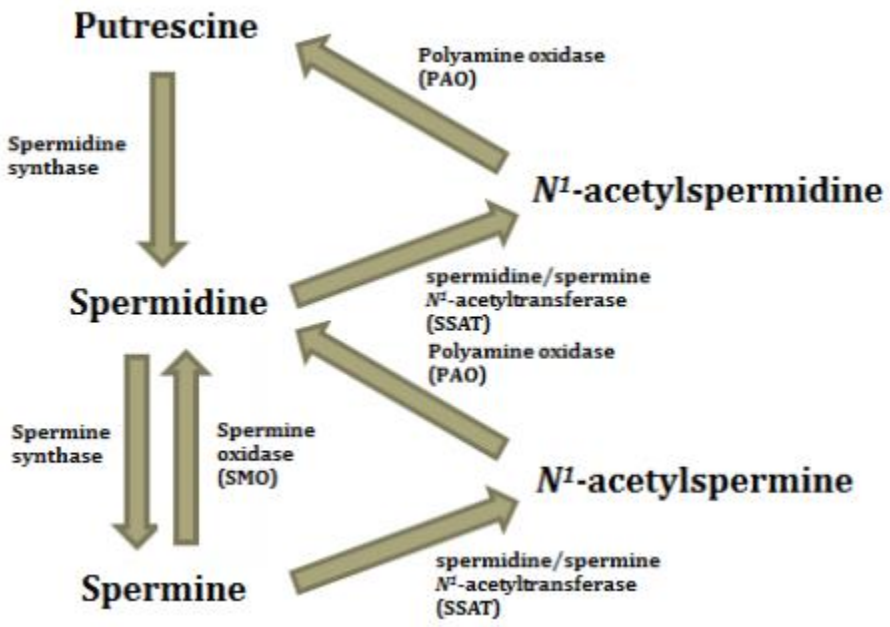

Figure 3.17 Polyamine metabolic pathway (focusing on Put, Spd and Spm only).

Nevertheless, unlike what Giskeødegård *et al.* reported that prostatic Spm content could act as a biomarker to assess PCa aggressiveness [71], we could not give a determinate conclusion if urinary Spm possesses a similar cancer grade-differentiating ability. From our results, a drop in high grade cancer (GS=8-10)

could be observed compared to low grade cancer (GS≤6), albeit not that significant. (1.23 in High grade vs 1.47 in low grade; p=0.611) Instead, it acts like a diagnostic biomarker working in accordance with TRUSPB for PCa diagnosis.

Compare to the currently adopted serum PSA test, it is generally accepted that it leaves much to be desired as a primary screening test. As above-mentioned it had been shown to cause over-diagnosis and over-treatment especially to patients showing PSA value in the grey zone. The outcome of it is still controversial if it is a blessing or a curse to PCa suspects. To give more information, serum PSA alone demonstrated a fair sensitivity and specificity of 65% and 47% respectively. [79] Li *et al.* reported an even poorer sensitivity and specificity for it in their study (Sensitivity = 54.8%, Specificity = 57.1%, AUC = 0.684). [80] Another large-scale study by Ferro *et al.* showed that total PSA only gave AUC value of 0.52±0.07. [81] Our data, which focused on patients with PSA>4.0ng/ml, shows a better screening performance with AUC value equal to 0.73±0.04 (Figure 3.18), but it is still poorer than that of urinary Spm. The best sensitivity and specificity were only 67.05% and 68.75% respectively. Therefore urinary Spm seems can act as a secondary screening test to screen out those non-cancerous cases with elevated serum PSA. Even compared with the recently adopted PHI test for PCa screening, which shows a specificity of 43.1% at 90% sensitivity and AUC value of 0.76, urinary Spm is still a superior biomarker. [82]

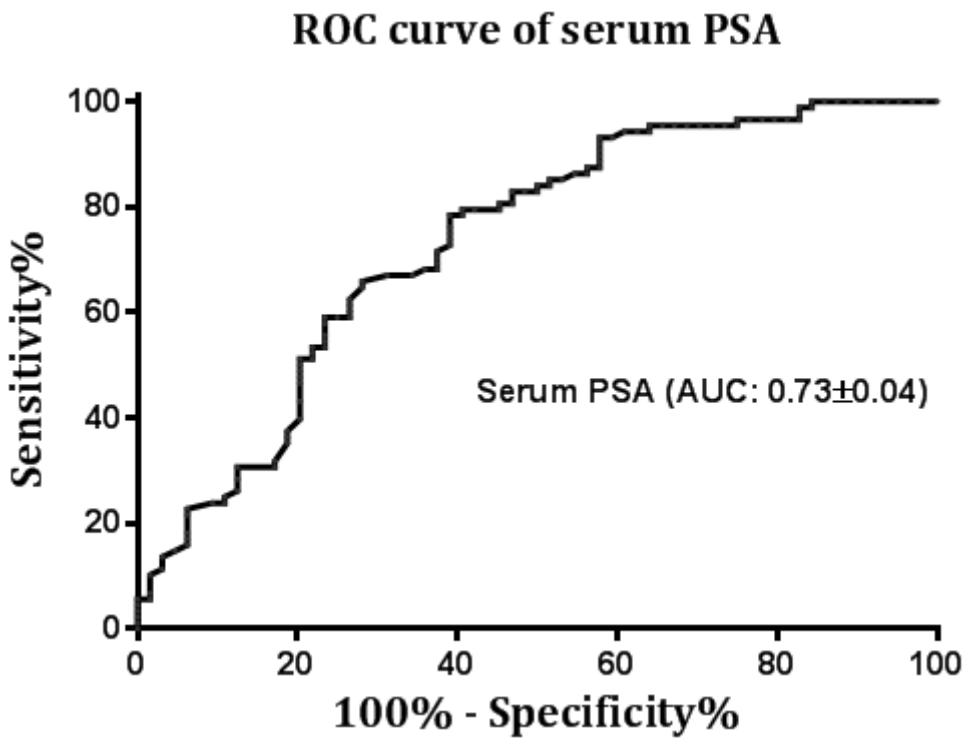

Figure 3.18 ROC curve of serum PSA in the current study.

The current research is not without limitations. One of the biggest problems might be brought by the urinary creatinine normalization process in the results of the current study. In urinary biomarker research, when we want to assess the complete profile of concerning urinary biomarker, the 'gold standard' approach is to collect all urines in 24-hr and pool them together. This is generally considered as the most accurate method; however, this collection method which can be expensive and time consuming is not easy to implement in large-cohort study. [83] A widely accepted method in biomarker research is by normalizing to the content of creatinine, which is a freely filtered metabolite with a relatively constant excretion rate per day relating to our muscle mass. Most of the previous

reported literatures relied on using creatinine as a valid index of complete urine. Hou *et al.* before reported the creatinine-normalized value on cotinine in smokers' urines correlated well with the total cotinine in their 24-hr urine, which further supports its usage. [84] By this mean we can correct any fluid intake factors that may dilute the urine and the biomarker concentration inside, and estimate the urine sample integrity. Nevertheless, some scientists also reported the potential of over- or under-estimation in excretion rate of biomarkers like polyphenols or urinary protein. [83, 85] It is because external stressor like kidney failure can have impacts on the excretion rates. Also glomerular filtration rates can vary across or within individuals at different time period. [86] The implicit assumption that creatinine normalization helps to overview complete urine profiles might be problematic when being applied in large population study. The big challenge to have an easy and accurate urine overview in urinary biomarker research is still waiting to be solved.

On the other hand, all patients sample were obtained from one hospital in Hong Kong. Collecting samples from multi-center and multi-country should strengthen the outcome of our study. Diet control had not been performed to completely exclude any food habit effects. However, Vargas *et al.* reported before no significant association relationship was observed between urinary polyamines measured and dietary polyamine intake. [87] Finally, as a pilot study, the number of samples being analyzed was still limited. Larger scale study is needed to further confirm the observation and mechanism in the future. A long-term follow-up

monitoring of urinary Spm on specific PCa patients should also provide us more useful information on the role of this biomarker.

3.4 References

1. Alberts, A. R., Schoots, I. G., & Roobol, M. J. (2015). Prostate-specific antigen-based prostate cancer screening: Past and future. *International Journal of Urology*, 22(6), 524-532.
2. Siegel, R. L., Miller, K. D., & Jemal, A. (2015). Cancer statistics, 2015. *CA: a Cancer Journal for Clinicians*, 65(1), 5-29.
3. Census and Statistics Department, Department of Health, Hong Kong Cancer Registry, Hospital Authority, Government of Hong Kong SAR. http://www.chp.gov.hk/en/content/9/25/5781.html
4. Albertsen, P. C., Hanley, J. A., & Fine, J. (2005). 20-year outcomes following conservative management of clinically localized prostate cancer. *Jama*, 293(17), 2095-2101.
5. Abdel-Wahab, M., & Silva, O. E. (2008). Prostate cancer: a practical guide. Saunders.
6. Cotter, M. P., Gern, R. W., Ho, G. Y., Chang, R. Y., & Burk, R. D. (2002). Role of family history and ethnicity on the mode and age of prostate cancer presentation. *The Prostate*, 50(4), 216-221.
7. Henderson, B. E., Ross, R. K., Pike, M. C., & Casagrande, J. T. (1982). Endogenous hormones as a major factor in human cancer. *Cancer Research*, 42(8), 3232-3239.

8. Howell, M. A. (1974). Factor analysis of international cancer mortality data and per capita food consumption. *British Journal of Cancer*, 29(4), 328.
9. Hickey, K., Do, K. A., & Green, A. (2001). Smoking and prostate cancer. *Epidemiologic Reviews*, 23(1), 115-125.
10. Schröder, F. H., Kruger, A. B., Rietbergen, J., Kranse, R., van der Maas, P., Beemsterboer, P., & Hoedemaeker, R. (1998). Evaluation of the digital rectal examination as a screening test for prostate cancer. *Journal of the National Cancer Institute*, 90(23), 1817-1823.
11. National Cancer Institute, USA https://visuals.nci.nih.gov/
12. Rigau, M., Olivan, M., Garcia, M., Sequeiros, T., Montes, M., Colás, E., ... & Cooper, C. (2013). The present and future of prostate cancer urine biomarkers. *International Journal of Molecular Sciences*, 14(6), 12620-12649.
13. Benson, M. C., Whang, I. S., Pantuck, A., Ring, K., Kaplan, S. A., Olsson, C., & Cooner, W. H. (1992). Prostate specific antigen density: a means of distinguishing benign prostatic hypertrophy and prostate cancer. *The Journal of Urology*, 147(3 Pt 2), 815-816.
14. Djavan, B., Zlotta, A., Kratzik, C., Remzi, M., Seitz, C., Schulman, C. C., & Marberger, M. (1999). PSA, PSA density, PSA density of transition zone, free/total PSA ratio, and PSA velocity for early detection of prostate cancer in men with serum PSA 2.5 to 4.0 ng/mL. *Urology*, 54(3), 517-522.
15. Van Cangh, P. J., De Nayer, P., De Vischer, L., Sauvage, P., Tombal, B., Lorge, F., ... & Opsomer, R. (1996). Free to total prostate-specific antigen (PSA) ratio improves the discrimination between prostate cancer and benign

prostatic hyperplasia (BPH) in the diagnostic gray zone of 1.8 to 10 ng/mL total PSA. *Urology*, 48(6), 67-70.

16. Catalona, W. J., Partin, A. W., Sanda, M. G., Wei, J. T., Klee, G. G., Bangma, C. H., ... & Shin, S. S. (2011). A multicenter study of [-2] pro-prostate specific antigen combined with prostate specific antigen and free prostate specific antigen for prostate cancer detection in the 2.0 to 10.0 ng/ml prostate specific antigen range. *The Journal of Urology*, 185(5), 1650-1655.
17. Ng, C. F., Chiu, P. K., Lam, N. Y., Lam, H. C., Lee, K. W., & Hou, S. S. (2014). The Prostate Health Index in predicting initial prostate biopsy outcomes in Asian men with prostate-specific antigen levels of 4–10 ng/mL. *International Urology and Nephrology*, 46(4), 711-717.
18. Wu, C. L., Carter, H. B., Naqibuddin, M., & Fleisher, L. A. (2001). Effect of local anesthetics on patient recovery after transrectal biopsy. *Urology*, 57(5), 925-929.
19. Chan, E. S., Lo, K. L., Ng, C. F., Hou, S. M., & Yip, S. K. (2012). Randomized controlled trial of antibiotic prophylaxis regimens for transrectal ultrasound-guided prostate biopsy. *Chinese Medical Journal*, 125(14), 2432-2435.
20. Wagenlehner, F. M., Van Oostrum, E., Tenke, P., Tandogdu, Z., Çek, M., Grabe, M., ... & Weidner, W. (2013). Infective complications after prostate biopsy: outcome of the Global Prevalence Study of Infections in Urology (GPIU) 2010 and 2011, a prospective multinational multicentre prostate biopsy study. *European Urology*, 63(3), 521-527.

21. Ecke, T. H., Gunia, S., Bartel, P., Hallmann, S., Koch, S., & Ruttloff, J. (2008, October). Complications and risk factors of transrectal ultrasound guided needle biopsies of the prostate evaluated by questionnaire. *In Urologic Oncology: Seminars and Original Investigations* (Vol. 26, No. 5, pp. 474-478). Elsevier.
22. Roberts, R. O., Bergstralh, E. J., Besse, J. A., Lieber, M. M., & Jacobsen, S. J. (2002). Trends and risk factors for prostate biopsy complications in the pre-PSA and PSA eras, 1980 to 1997. *Urology*, 59(1), 79-84.
23. Cam, K., Kayikci, A., Akman, Y., & Erol, A. (2008). Prospective assessment of the efficacy of single dose versus traditional 3-day antimicrobial prophylaxis in 12-core transrectal prostate biopsy. *International journal of urology*, 15(11), 997-1001.
24. Schröder, F. H., Hugosson, J., Roobol, M. J., Tammela, T. L., Ciatto, S., Nelen, V., ... & Denis, L. J. (2009). Screening and prostate-cancer mortality in a randomized European study. *New England Journal of Medicine,* 360(13), 1320-1328.
25. Andriole, G. L., Crawford, E. D., Grubb III, R. L., Buys, S. S., Chia, D., Church, T. R., ... & Weissfeld, J. L. (2009). Mortality results from a randomized prostate-cancer screening trial. *New England Journal of Medicine,* 360(13), 1310-1319.
26. Eckersberger, E., Finkelstein, J., Sadri, H., Margreiter, M., Taneja, S. S., Lepor, H., & Djavan, B. (2009). Screening for prostate cancer: a review of the ERSPC and PLCO trials. *Reviews in Urology*, 11(3), 127.

27. Draisma, G., Etzioni, R., Tsodikov, A., Mariotto, A., Wever, E., Gulati, R., ... & de Koning, H. (2009). Lead time and overdiagnosis in prostate-specific antigen screening: importance of methods and context. *Journal of the National Cancer Institute*, 101(6), 374-383.
28. Moyer, V. A. (2012). Screening for prostate cancer: US Preventive Services Task Force recommendation statement. *Annals of Internal Medicine*, 157(2), 120-134.
29. Bhindi, B., Mamdani, M., Kulkarni, G. S., Finelli, A., Hamilton, R. J., Trachtenberg, J., ... & Fleshner, N. E. (2015). Impact of the US Preventive Services Task Force recommendations against prostate specific antigen screening on prostate biopsy and cancer detection rates. *The Journal of urology*, 193(5), 1519-1524.
30. Drazer, M. W., Huo, D., & Eggener, S. E. (2015). National Prostate Cancer Screening Rates After the 2012 US Preventive Services Task Force Recommendation Discouraging Prostate-Specific Antigen–Based Screening. *Journal of Clinical Oncology*, 33(22), 2416-2423.
31. Taneja, S. S. (2016). Re: National Prostate Cancer Screening Rates after the 2012 US Preventive Services Task Force Recommendation Discouraging Prostate-Specific Antigen-Based Screening. *The Journal of Urology*, 195(2), 350-351.
32. Downes, M. R., Byrne, J. C., Pennington, S. R., Dunn, M. J., Fitzpatrick, J. M., & Watson, R. W. G. (2007). Urinary markers for prostate cancer. *British Journal of Urology International*, 99(2), 263-268.

33. Crocitto, L. E., Korns, D., Kretzner, L., Shevchuk, T., Blair, S. L., Wilson, T. G., ... & Smith, S. S. (2004). Prostate cancer molecular markers GSTP1 and hTERT in expressed prostatic secretions as predictors of biopsy results. *Urology*, 64(4), 821-825.

34. Chiou, C. C., Chang, P. Y., Chan, E. C., Wu, T. L., Tsao, K. C., & Wu, J. T. (2003). Urinary 8-hydroxydeoxyguanosine and its analogs as DNA marker of oxidative stress: development of an ELISA and measurement in both bladder and prostate cancers. *Clinica Chimica Acta*, 334(1), 87-94.

35. Thuret, R., Chantrel-Groussard, K., Azzouzi, A. R., Villette, J. M., Guimard, S., Teillac, P., ... & Cussenot, O. (2005). Clinical relevance of genetic instability in prostatic cells obtained by prostatic massage in early prostate cancer. *British Journal of Cancer*, 92(2), 236-240.

36. Fradet, Y., Saad, F., Aprikian, A., Dessureault, J., Elhilali, M., Trudel, C., ... & Chypre, C. (2004). uPM3, a new molecular urine test for the detection of prostate cancer. *Urology*, 64(2), 311-315.

37. Botchkina, G. I., Kim, R. H., Botchkina, I. L., Kirshenbaum, A., Frischer, Z., & Adler, H. L. (2005). Noninvasive detection of prostate cancer by quantitative analysis of telomerase activity. *Clinical Cancer Research*, 11(9), 3243-3249.

38. Rogers, C. G., YAN, G., ZHA, S., GONZALGO, M. L., ISAACS, W. B., LUO, J., ... & PAVLOVICH, C. P. (2004). Prostate cancer detection on urinalysis for α methylacyl coenzyme a racemase protein. *The Journal of Urology*, 172(4), 1501-1503.

39. MEID, F. H., GYGI, C. M., Leisinger, H. J., BOSMAN, F. T., & BENHATTAR, J. (2001). The use of telomerase activity for the detection of prostatic cancer cells after prostatic massage. *The Journal of Urology*, 165(5), 1802-1805.

40. Lwaleed, B. A., Francis, J. L., & Chisholm, M. (2000). Urinary tissue factor levels in patients with bladder and prostate cancer. *European Journal of Surgical Oncology*, 26(1), 44-49.

41. van Dieijen-Visser, M. P., Hendriks, M. W. G., Delaere, K. P. J., Gijzen, A. H. J., & Brombacher, P. J. (1988). The diagnostic value of urinary transferrin compared to serum prostatic specific antigen (PSA) and prostatic acid phosphatase (PAP) in patients with prostatic cancer. *Clinica Chimica Acta*, 177(1), 77-80.

42. Gerner, E. W., & Meyskens, F. L. (2004). Polyamines and cancer: old molecules, new understanding. *Nature Reviews Cancer*, 4(10), 781-792.

43. Ha, H. C., Sirisoma, N. S., Kuppusamy, P., Zweier, J. L., Woster, P. M., & Casero, R. A. (1998). The natural polyamine spermine functions directly as a free radical scavenger. *Proceedings of the National Academy of Sciences*, 95(19), 11140-11145.

44. Igarashi, K., & Kashiwagi, K. (2010). Modulation of cellular function by polyamines. *The International Journal of Biochemistry & Cell Biology*, 42(1), 39-51.

45. Kurata, H. T., Marton, L. J., & Nichols, C. G. (2006). The polyamine binding site in inward rectifier K+ channels. *The Journal of General Physiology*, 127(5), 467-480.

46. Lopatin, A. N., Makhina, E. N., & Nichols, C. G. (1994). Potassium channel block by cytoplasmic polyamines as the mechanism of intrinsic rectification. *Nature*, 372(6504), 366-369.

47. Williams, K. (1997). Modulation and block of ion channels: a new biology of polyamines. *Cellular Signalling*, 9(1), 1-13.

48. Russell, D., & Snyder, S. H. (1968). Amine synthesis in rapidly growing tissues: ornithine decarboxylase activity in regenerating rat liver, chick embryo, and various tumors. *Proceedings of the National Academy of Sciences*, 60(4), 1420-1427.

49. Russell, D. H., Levy, C. C., Schimpff, S. C., & Hawk, I. A. (1971). Urinary polyamines in cancer patients. *Cancer Research*, 31(11), 1555-1558.

50. Lee, S. H., Yang, Y. J., Kim, K. M., & Chung, B. C. (2003). Altered urinary profiles of polyamines and endogenous steroids in patients with benign cervical disease and cervical cancer. *Cancer Letters*, 201(2), 121-131.

51. Löser, C., Fölsch, U. R., Paprotny, C., & Creutzfeldt, W. (1990). Polyamines in colorectal cancer. Evaluation of polyamine concentrations in the colon tissue, serum, and urine of 50 patients with colorectal cancer. *Cancer*, 65(4), 958-966.

52. Levêque, J., Foucher, F., Bansard, J. Y., Havouis, R., Grall, J. Y., & Moulinoux, J. P. (2000). Polyamine profiles in tumor, normal tissue of the homologous breast, blood, and urine of breast cancer sufferers. *Breast Cancer Research and Treatment*, 60(2), 99-105.

53. Schipper, R. G., Romijn, J. C., Cuijpers, V. M. J. I., & Verhofstad, A. A. J. (2003). Polyamines and prostatic cancer. *Biochemical Society Transactions*, 31(2), 375-380.

54. van der Graaf, M., Schipper, R. G., Oosterhof, G. O., Schalken, J. A., Verhofstad, A. A., & Heerschap, A. (2000). Proton MR spectroscopy of prostatic tissue focused on the detection of spermine, a possible biomarker of malignant behavior in prostate cancer. *Magnetic Resonance Materials in Physics, Biology and Medicine*, 10(3), 153-159.

55. Minois, N., Carmona-Gutierrez, D., & Madeo, F. (2011). Polyamines in aging and disease. *Aging (Albany NY)*, 3(8), 716-732.

56. Moldoveanu, S. C., & David, V. (2012). Essentials in modern HPLC separations. Newnes.

57. Swartz, M. E. (2005). UPLC™: an introduction and review. *Journal of Liquid Chromatography & Related Technologies*, 28(7-8), 1253-1263.

58. Bonsnes, R. W., & Taussky, H. H. (1945). On the colorimetric determination of creatinine by the Jaffe reaction. *Journal of Biological Chemistry*, 158(3), 581-591.

59. Häkkinen, M. R., Roine, A., Auriola, S., Tuokko, A., Veskimäe, E., Keinänen, T. A., ... & Vepsäläinen, J. (2013). Analysis of free, mono-and diacetylated polyamines from human urine by LC–MS/MS. *Journal of Chromatography B*, 941, 81-89.

60. Jung, K. (1991). Enzyme activities in urine. How should we express their excretion? *European Journal of Clinical Chemistry and Clinical Biochemistry*, 29, 725-729.

61. Soda, K. (2011). The mechanisms by which polyamines accelerate tumor spread. *Journal of Experimental & Clinical Cancer Research*, *30*(1), 1.

62. Thomas, T., & Thomas, T. J. (2003). Polyamine metabolism and cancer. *Journal of Cellular and Molecular Medicine*, *7*(2), 113-126.

63. Bachrach, U. (2004). Polyamines and cancer: minireview article. *Amino acids*, *26*(4), 307-309.

64. Russell, D. H. (1971). Increased polyamine concentrations in the urine of human cancer patients. *Nature*, *233*(39), 144-145.

65. Hiramatsu, K., Takahashi, K., Yamaguchi, T., Matsumoto, H., Miyamoto, H., Tanaka, S., ... & Toi, M. (2005). N1, N12-Diacetylspermine as a sensitive and specific novel marker for early-and late-stage colorectal and breast cancers. *Clinical Cancer Research*, *11*(8), 2986-2990.

66. Lee, S. H., Yang, Y. J., Kim, K. M., & Chung, B. C. (2003). Altered urinary profiles of polyamines and endogenous steroids in patients with benign cervical disease and cervical cancer. *Cancer Letters*, *201*(2), 121-131.

67. Liu, R., Li, Q., Ma, R., Lin, X., Xu, H., & Bi, K. (2013). Determination of polyamine metabolome in plasma and urine by ultrahigh performance liquid chromatography–tandem mass spectrometry method: application to identify potential markers for human hepatic cancer. *Analytica Chimica Acta*, *791*, 36-45.

68. Fair, W. R., Wehner, N., & Brorsson, U. (1975). Urinary polyamine levels in the diagnosis of carcinoma of the prostate. *The Journal of Urology*, *114*(1), 88-92.

69. Horn, Y., Beal, S. L., Walach, N., Lubich, W. P., Spigel, L., & Marton, L. J. (1984). Relationship of urinary polyamines to tumor activity and tumor volume in patients. *Cancer Research*, *44*(10), 4675-4678.

70. Swanson, M. G., Vigneron, D. B., Tabatabai, Z. L., Males, R. G., Schmitt, L., Carroll, P. R., ... & Kurhanewicz, J. (2003). Proton HR-MAS spectroscopy and quantitative pathologic analysis of MRI/3D-MRSI-targeted postsurgical prostate tissues. *Magnetic Resonance in Medicine*, *50*(5), 944-954.

71. Giskeødegård, G. F., Bertilsson, H., Selnæs, K. M., Wright, A. J., Bathen, T. F., Viset, T., ... & Tessem, M. B. (2013). Spermine and citrate as metabolic biomarkers for assessing prostate cancer aggressiveness. *PloS One*, *8*(4), e62375.

72. Serkova, N. J., Gamito, E. J., Jones, R. H., O'Donnell, C., Brown, J. L., Green, S., ... & Crawford, E. D. (2008). The metabolites citrate, myo-inositol, and spermine are potential age-independent markers of prostate cancer in human expressed prostatic secretions. *The Prostate*, *68*(6), 620-628.

73. Cheng, L. L., Wu, C. L., Smith, M. R., & Gonzalez, R. G. (2001). Non-destructive quantitation of spermine in human prostate tissue samples using HRMAS 1H NMR spectroscopy at 9.4 T. *FEBS Letters*, *494*(1-2), 112-116.

74. Smith, R. C., Litwin, M. S., Lu, Y., & Zetter, B. R. (1995). Identification of an endogenous inhibitor of prostatic carcinoma cell growth. *Nature Medicine*, *1*(10), 1040-1045.

75. Battaglia, V., Shields, C. D., Murray-Stewart, T., & Casero Jr, R. A. (2014). Polyamine catabolism in carcinogenesis: potential targets for chemotherapy and chemoprevention. *Amino Acids*, *46*(3), 511-519.

76. Casero, R. A., & Pegg, A. E. (2009). Polyamine catabolism and disease. *Biochemical Journal*, *421*(3), 323-338.

77. Goodwin, A. C., Jadallah, S., Toubaji, A., Lecksell, K., Hicks, J. L., Kowalski, J., ... & Casero, R. A. (2008). Increased spermine oxidase expression in human prostate cancer and prostatic intraepithelial neoplasia tissues. *The Prostate*, *68*(7), 766-772.

78. Hiramatsu, K., Sugimoto, M., Kamei, S., Hoshino, M., Kinoshita, K., Iwasaki, K., & Kawakita, M. (1997). Diagnostic and prognostic usefulness of N 1, N 8-diacetylspermidine and N 1, N 12-diacetylspermine in urine as novel markers of malignancy. *Journal of Cancer Research and Clinical Oncology*, *123*(10), 539-545.

79. van Gils, M. P., Hessels, D., van Hooij, O., Jannink, S. A., Peelen, W. P., Hanssen, S. L., ... & Dijkman, G. A. (2007). The time-resolved fluorescence-based PCA3 test on urinary sediments after digital rectal examination; a Dutch multicenter validation of the diagnostic performance. *Clinical Cancer Research*, *13*(3), 939-943.

80. Li, J., Veltri, R. W., Yuan, Z., Christudass, C. S., & Mandecki, W. (2015). Macrophage inhibitory cytokine 1 biomarker serum immunoassay in combination with PSA is a more specific diagnostic tool for detection of prostate cancer. *PloS Oone*, *10*(4), e0122249.

81. Ferro, M., Bruzzese, D., Perdona, S., Marino, A., Mazzarella, C., Perruolo, G., ... & Musi, G. (2013). Prostate Health Index (Phi) and Prostate Cancer Antigen 3 (PCA3) significantly improve prostate cancer detection at initial biopsy in a total PSA range of 2–10 ng/ml. *PloS One*, *8*(7), e67687.

82. Tsu, H. L. J., Ma, W. K., Tsang, C. F., Poon, V. Y., Wong, C. K., Ip, W. K., ... & Cheung, F. K. (2016). Prospective study on the performance of the prostate-specific antigen isoform P2PSA and its derivative Prostate Health Index in prediction of prostate cancer in local Chinese men with total prostate-specific antigen levels of 4-10 ng/mL (Abstract and Poster Presentation). In *14th Urological Association of Asia Congress, Singapore, 20-24 July 2016*.

83. Zamora-Ros, R., Rabassa, M., Cherubini, A., Urpi-Sarda, M., Llorach, R., Bandinelli, S., ... & Andres-Lacueva, C. (2011). Comparison of 24-h volume and creatinine-corrected total urinary polyphenol as a biomarker of total dietary polyphenols in the Invecchiare InCHIANTI study. *Analytica Chimica Acta*, *704*(1), 110-115.

84. Hou, H., Xiong, W., Zhang, X., Song, D., Tang, G., & Hu, Q. (2012). LC-MS-MS measurements of urinary creatinine and the application of creatinine normalization technique on cotinine in smokers' 24 hour urine. *Journal of Analytical Methods in Chemistry, 2012*.

85. Yang, C. Y., Chen, F. A., Chen, C. F., Liu, W. S., Shih, C. J., Ou, S. M., ... & Yang, A. H. (2015). Diagnostic Accuracy of Urine Protein/Creatinine Ratio Is Influenced by Urine Concentration. *PloS One*, *10*(9), e0137460.

86. Waikar, S. S., Sabbisetti, V. S., & Bonventre, J. V. (2010). Normalization of urinary biomarkers to creatinine during changes in glomerular filtration rate. *Kidney International*, *78*(5), 486-494.

87. Vargas, A. J., Ashbeck, E. L., Thomson, C. A., Gerner, E. W., & Thompson, P. A. (2014). Dietary polyamine intake and polyamines measured in urine. *Nutrition and Cancer*, *66*(7), 1144-1153.

3.5 Appendix

Organization	Suggestion on PCa screening	Screening intervial
American Cancer Society	Not recommend for asymptomatic men who has a life expectancy under 10-years, especially for those >50 years old	Every year if ≥2.5ng/ml, Every 2 years if <2.5ng/ml
U.S. Preventive Services Task Force (USPSTF)	Discourage PCa screening. There is moderate or high certainty that the screening is not beneficial or the harms outweigh the benefits	Nil
American Urological Association	Recommend for men of 55-69 years old	Every 2 years
European Association of Urology	Recommend for men with life expectancy ≥ 10-years	Every 2-4 years if >1ng/ml, Every 8 years if <1ng/ml
American College of Physicians	Recommend for men of 50-69 years old	Every year if ≥ 2.5ng/ml
National Comprehensive Cancer Network	Recommend for men of 50-70 years old and 70-75 years if life expectancy is longer than 10-years	Every 1-2 years

Table A3.1 Summary of international guidelines on PCa screening. [26]

Threshold	Sensitivity (%)	95%CI	Specificity (%)	95%CI
< 0.0800	1.515	0.03835% to 8.155%	100.	96.34% to 100.0%
< 0.1150	3.03	0.3691% to 10.52%	100	96.34% to 100.0%
< 0.1350	4.545	0.9474% to 12.71%	100	96.34% to 100.0%
< 0.1800	6.061	1.676% to 14.80%	100	96.34% to 100.0%
< 0.2400	7.576	2.506% to 16.80%	100	96.34% to 100.0%
< 0.2900	9.091	3.410% to 18.74%	100	96.34% to 100.0%
< 0.3150	10.61	4.372% to 20.64%	100	96.34% to 100.0%
< 0.3250	12.12	5.381% to 22.49%	100	96.34% to 100.0%
< 0.3350	13.64	6.430% to 24.31%	100	96.34% to 100.0%
< 0.3550	15.15	7.512% to 26.10%	100	96.34% to 100.0%
< 0.3750	16.67	8.625% to 27.87%	100	96.34% to 100.0%
< 0.4000	18.18	9.763% to 29.61%	100	96.34% to 100.0%
< 0.4300	19.7	10.93% to 31.32%	100	96.34% to 100.0%
< 0.4450	22.73	13.31% to 34.70%	100	96.34% to 100.0%
< 0.4600	24.24	14.54% to 36.36%	100	96.34% to 100.0%
< 0.4800	24.24	14.54% to 36.36%	98.99	94.50% to 99.97%
< 0.5000	27.27	17.03% to 39.64%	98.99	94.50% to 99.97%
< 0.5200	28.79	18.30% to 41.25%	98.99	94.50% to 99.97%
< 0.5350	30.3	19.59% to 42.85%	98.99	94.50% to 99.97%
< 0.5500	31.82	20.89% to 44.44%	98.99	94.50% to 99.97%
< 0.5700	33.33	22.20% to 46.01%	98.99	94.50% to 99.97%
< 0.6050	34.85	23.53% to 47.58%	97.98	92.89% to 99.75%
< 0.6350	34.85	23.53% to 47.58%	95.96	89.98% to 98.89%
< 0.6600	36.36	24.87% to 49.13%	94.95	88.61% to 98.34%
< 0.6850	39.39	27.58% to 52.19%	93.94	87.27% to 97.74%
< 0.6950	40.91	28.95% to 53.71%	93.94	87.27% to 97.74%

< 0.7200	42.42	30.34% to 55.21%	93.94	87.27% to 97.74%
< 0.7650	42.42	30.34% to 55.21%	92.93	85.97% to 97.11%
< 0.7950	45.45	33.14% to 58.19%	92.93	85.97% to 97.11%
< 0.8200	46.97	34.56% to 59.66%	92.93	85.97% to 97.11%
< 0.8450	46.97	34.56% to 59.66%	91.92	84.70% to 96.45%
< 0.8550	48.48	35.99% to 61.12%	90.91	83.44% to 95.76%
< 0.8650	51.52	38.88% to 64.01%	89.9	82.21% to 95.05%
< 0.8800	53.03	40.34% to 65.44%	88.89	80.99% to 94.32%
< 0.9100	54.55	41.81% to 66.86%	88.89	80.99% to 94.32%
< 0.9400	56.06	43.30% to 68.26%	88.89	80.99% to 94.32%
< 0.9650	57.58	44.79% to 69.66%	88.89	80.99% to 94.32%
< 0.9850	57.58	44.79% to 69.66%	87.88	79.78% to 93.58%
< 1.035	60.61	47.81% to 72.42%	86.87	78.59% to 92.82%
< 1.110	62.12	49.34% to 73.78%	86.87	78.59% to 92.82%
< 1.145	62.12	49.34% to 73.78%	85.86	77.41% to 92.05%
< 1.175	63.64	50.87% to 75.13%	85.86	77.41% to 92.05%
< 1.205	63.64	50.87% to 75.13%	84.85	76.24% to 91.26%
< 1.225	63.64	50.87% to 75.13%	82.83	73.94% to 89.67%
< 1.250	65.15	52.42% to 76.47%	82.83	73.94% to 89.67%
< 1.280	65.15	52.42% to 76.47%	81.82	72.80% to 88.85%
< 1.305	65.15	52.42% to 76.47%	80.81	71.66% to 88.03%
< 1.320	66.67	53.99% to 77.80%	80.81	71.66% to 88.03%
< 1.335	68.18	55.56% to 79.11%	80.81	71.66% to 88.03%
< 1.365	69.7	57.15% to 80.41%	80.81	71.66% to 88.03%
< 1.425	71.21	58.75% to 81.70%	79.8	70.54% to 87.20%
< 1.480	71.21	58.75% to 81.70%	78.79	69.42% to 86.36%
< 1.520	71.21	58.75% to 81.70%	77.78	68.31% to 85.52%
< 1.560	71.21	58.75% to 81.70%	76.77	67.21% to 84.67%

< 1.585	72.73	60.36% to 82.97%	76.77	67.21% to 84.67%
< 1.620	72.73	60.36% to 82.97%	75.76	66.11% to 83.81%
< 1.655	74.24	61.99% to 84.22%	75.76	66.11% to 83.81%
< 1.705	74.24	61.99% to 84.22%	73.74	63.93% to 82.07%
< 1.830	75.76	63.64% to 85.46%	73.74	63.93% to 82.07%
< 1.940	75.76	63.64% to 85.46%	71.72	61.78% to 80.31%
< 1.990	75.76	63.64% to 85.46%	70.71	60.71% to 79.43%
< 2.045	77.27	65.30% to 86.69%	70.71	60.71% to 79.43%
< 2.105	80.3	68.68% to 89.07%	70.71	60.71% to 79.43%
< 2.175	80.3	68.68% to 89.07%	69.7	59.64% to 78.53%
< 2.235	80.3	68.68% to 89.07%	68.69	58.59% to 77.64%
< 2.255	80.3	68.68% to 89.07%	67.68	57.53% to 76.73%
< 2.270	81.82	70.39% to 90.24%	67.68	57.53% to 76.73%
< 2.325	84.85	73.90% to 92.49%	67.68	57.53% to 76.73%
< 2.390	84.85	73.90% to 92.49%	66.67	56.48% to 75.82%
< 2.415	84.85	73.90% to 92.49%	65.66	55.44% to 74.91%
< 2.435	84.85	73.90% to 92.49%	64.65	54.40% to 73.99%
< 2.455	84.85	73.90% to 92.49%	63.64	53.36% to 73.07%
< 2.465	84.85	73.90% to 92.49%	62.63	52.33% to 72.15%
< 2.485	84.85	73.90% to 92.49%	61.62	51.30% to 71.22%
< 2.510	84.85	73.90% to 92.49%	60.61	50.28% to 70.28%
< 2.585	86.36	75.69% to 93.57%	60.61	50.28% to 70.28%
< 2.665	86.36	75.69% to 93.57%	59.6	49.26% to 69.34%
< 2.715	87.88	77.51% to 94.62%	59.6	49.26% to 69.34%
< 2.770	89.39	79.36% to 95.63%	59.6	49.26% to 69.34%
< 2.800	89.39	79.36% to 95.63%	58.59	48.24% to 68.40%
< 2.820	89.39	79.36% to 95.63%	57.58	47.23% to 67.45%
< 2.845	89.39	79.36% to 95.63%	56.57	46.23% to 66.50%

< 2.895	89.39	79.36% to 95.63%	55.56	45.22% to 65.55%
< 2.935	89.39	79.36% to 95.63%	54.55	44.22% to 64.59%
< 2.965	89.39	79.36% to 95.63%	53.54	43.23% to 63.62%
< 3.110	90.91	81.26% to 96.59%	53.54	43.23% to 63.62%
< 3.235	90.91	81.26% to 96.59%	52.53	42.24% to 62.66%
< 3.245	90.91	81.26% to 96.59%	51.52	41.25% to 61.68%
< 3.380	92.42	83.20% to 97.49%	50.51	40.27% to 60.71%
< 3.555	92.42	83.20% to 97.49%	49.49	39.29% to 59.73%
< 3.625	92.42	83.20% to 97.49%	48.48	38.32% to 58.75%
< 3.760	93.94	85.20% to 98.32%	48.48	38.32% to 58.75%
< 3.920	93.94	85.20% to 98.32%	47.47	37.34% to 57.76%
< 4.055	93.94	85.20% to 98.32%	46.46	36.38% to 56.77%
< 4.170	93.94	85.20% to 98.32%	45.45	35.41% to 55.78%
< 4.205	93.94	85.20% to 98.32%	44.44	34.45% to 54.78%
< 4.235	93.94	85.20% to 98.32%	43.43	33.50% to 53.77%
< 4.290	93.94	85.20% to 98.32%	42.42	32.55% to 52.77%
< 4.430	93.94	85.20% to 98.32%	41.41	31.60% to 51.76%
< 4.560	93.94	85.20% to 98.32%	40.4	30.66% to 50.74%
< 4.595	93.94	85.20% to 98.32%	39.39	29.72% to 49.72%
< 4.625	93.94	85.20% to 98.32%	38.38	28.78% to 48.70%
< 4.695	93.94	85.20% to 98.32%	37.37	27.85% to 47.67%
< 4.880	93.94	85.20% to 98.32%	36.36	26.93% to 46.64%
< 5.180	93.94	85.20% to 98.32%	35.35	26.01% to 45.60%
< 5.440	95.45	87.29% to 99.05%	35.35	26.01% to 45.60%
< 5.700	95.45	87.29% to 99.05%	34.34	25.09% to 44.56%
< 6.055	95.45	87.29% to 99.05%	33.33	24.18% to 43.52%
< 6.305	95.45	87.29% to 99.05%	32.32	23.27% to 42.47%
< 6.435	95.45	87.29% to 99.05%	31.31	22.36% to 41.41%

< 6.555	95.45	87.29% to 99.05%	30.3	21.47% to 40.36%
< 6.685	96.97	89.48% to 99.63%	30.3	21.47% to 40.36%
< 7.000	96.97	89.48% to 99.63%	29.29	20.57% to 39.29%
< 7.270	96.97	89.48% to 99.63%	28.28	19.69% to 38.22%
< 7.310	96.97	89.48% to 99.63%	27.27	18.80% to 37.15%
< 7.540	96.97	89.48% to 99.63%	26.26	17.93% to 36.07%
< 7.885	96.97	89.48% to 99.63%	25.25	17.06% to 34.98%
< 8.060	96.97	89.48% to 99.63%	24.24	16.19% to 33.89%
< 8.130	96.97	89.48% to 99.63%	23.23	15.33% to 32.79%
< 8.245	96.97	89.48% to 99.63%	21.21	13.64% to 30.58%
< 8.495	96.97	89.48% to 99.63%	20.2	12.80% to 29.46%
< 8.755	98.48	91.84% to 99.96%	20.2	12.80% to 29.46%
< 8.880	98.48	91.84% to 99.96%	19.19	11.97% to 28.34%
< 9.040	98.48	91.84% to 99.96%	18.18	11.15% to 27.20%
< 9.335	98.48	91.84% to 99.96%	17.17	10.33% to 26.06%
< 9.520	98.48	91.84% to 99.96%	16.16	9.530% to 24.91%
< 9.560	98.48	91.84% to 99.96%	15.15	8.736% to 23.76%
< 9.700	100	94.56% to 100.0%	15.15	8.736% to 23.76%
< 10.60	100	94.56% to 100.0%	14.14	7.953% to 22.59%
< 11.85	100	94.56% to 100.0%	13.13	7.181% to 21.41%
< 12.38	100	94.56% to 100.0%	12.12	6.423% to 20.22%
< 12.63	100	94.56% to 100.0%	11.11	5.679% to 19.01%
< 12.93	100	94.56% to 100.0%	10.1	4.951% to 17.79%
< 13.15	100	94.56% to 100.0%	9.091	4.242% to 16.56%
< 13.29	100	94.56% to 100.0%	8.081	3.553% to 15.30%
< 16.50	100	94.56% to 100.0%	7.071	2.890% to 14.03%
< 19.83	100	94.56% to 100.0%	6.061	2.256% to 12.73%
< 20.11	100	94.56% to 100.0%	5.051	1.660% to 11.39%

< 22.08	100	94.56% to 100.0%	4.04	1.112% to 10.02%
< 25.01	100	94.56% to 100.0%	3.03	0.6293% to 8.601%
< 28.75	100	94.56% to 100.0%	2.02	0.2456% to 7.108%
< 31.57	100	94.56% to 100.0%	1.01	0.02557% to5.500%

Table A3.2 Sensitivity and Specificity for normalized Spm at different threshold values.

CHAPTER FOUR: FLEXIBLE GOLD NANO-PARTICLES BASED APTASENSOR TOWARDS URINARY SPERMINE FOR CANCER SCREENING

4.1 Introduction

4.1.1 Overview of polyamines detection methods

In Chapter three the importance of polyamines in human cellular metabolism as well as their biomarker roles in biological fluids has been discussed. To supplement these physiological essential elements for supporting cellular growth and renewal, dietary polyamines contents in food are also of high concern and should be well controlled. Polyamines in food can be detected in wide variety of foods, especially foods of animal origin like fish, eggs or meats. The production usually occurs via several chemical processes: hydrolyzing nitrogenous compounds, decarboxylating or thermal decomposing amino acids and transamination of carbonyl compounds by the biochemical actions of enzymes produced by microorganisms. [1] The concentration can sometimes be higher than expected in food depending on the food nature, its storage and the variety of microorganisms present, and it is able to induce deleterious health effects including headaches, migraines, cardiac palpitations and anaphylactic shock. [2] One example is the histamine intoxication in fishes caused by microbial actions. This chemical can neither be destroyed by freezing nor cooking, and the only effective way to minimize its formation is by a proper storage of the fishes. [3] Other than being a foodborne hazard, polyamines in food were also reported as different quality indexes to reflect the quality of raw materials or sanitary

condition during food processing. For example, they were suggested as quality indicators of fresh chicken meat and bread spoilage, poor storage of wine of Abruzzo and tuna, etc. [4-7]

All of these evidences emphasize the importance of an accurate detection of polyamines content. To detect this group of analytes, classical techniques prevail and Table A4.1 summarizes different classical techniques, derivatization involved and their target polyamines.

Chromatographic and electro-migration methods coupling with different detectors remain the most widely employed method for assay of polyamines, especially mass spectrometer based methods. The advance achieved using classical polyamine detection method was mainly in omitting the need of time-consuming derivatization for generating necessary chromophores or other chemical groups for detection. However, these techniques still involve very expensive instruments. Well-trained technical staffs are needed to operate them properly as well as the tedious sample preparation steps. The throughput rate is also not high enough. There are still many rooms to get improved to make them become rapid screening approaches for polyamine levels in different kinds of biological or food samples.

More new advances in polyamine detection, especially for the concerning Spm, were being developed by analytical scientists in recent years to improve the recognition and transduction process. Some examples are summarized in Table A4.2.

Most of these new techniques are based on the interactions between their novel design of inorganic complexes or nanoparticles with polyamines. Such an interaction would give rise to an immediate change in fluorescence/absorbance and allow a comparatively rapid detection to classical methods. For example, Tu *et al.* designed a novel self-assembly platform using micelles of a pyrene derivative as the shell and squaraine as the nucleus. [22] Addition of Spm would change the morphology of the host micelles and affect the guest aggregation of squaraine. Finally its fluorescence was being turned on which allowed an indirect quantitation of Spm. Chopra *et al.* synthesized a Schiff-base receptor from dipicolinic acid hydrazide, which can be processed into the nanoaggregate form in aqueous medium. [23] These nanoaggregates, when being complexed with copper (II) ion, were able to detect Spm and resulted in a red-shift of its absorption peak. Chow *et al.* prepared a Ruthenium (II)/Europium (III) heterobimetallic complex. Upon binding with gaseous polyamines, spectrofluorometric changes were induced to give a brighter emission. [29] The complex was also being successfully applied in real fish samples to examine their freshness.

Another popular detection platform for polyamine sensing is conjugated polymer which relies on polyamines' multi-cationic nature. Satrijo *et al.* reported their poly-anionic poly (p-phenylene ethynylene) doped with anthryl units. [30] Polyamines including putrescine, spermidine and spermine were able to induce the aggregation process and hence the visually noticeable solution color change. Kim *et al.* also made use of an anionic sulfonated probe for polyamines sensing. [24] The resulting analyte induced formation of emissive excimers turned on the

fluorescence process. Another example is by Malik *et al.*, who made use of polymer-surfactant nanoaggregates with their emission being quenched upon addition of Spm. [26]

Last but not least is the use of AuNPs for sensing, another common approach employing not only for polyamines detection. Kim *et al.* adsorbed boron-dipyrromethene dyes onto the AuNPs' surface and their fluorescence was being quenched through an efficient energy transfer to AuNPs. [27] Addition of polyamines could displace the dyes out and restore their fluorescence emission. Jornet-Martínez *et al.* employed naked AuNPs, which provided a large surface for the amine groups to bind with, for Spm sensing. [22] Rawat *et al.* used tyrosine capped AuNPs to act as both a colorimetric and fluorimetric sensor for Spd and Spm. [28] In this chapter, our works also focuses on the use of AuNPs. More fundamentals about AuNPs are given in the next part.

4.1.2 Fundamentals of gold nanoparticles

Properties of AuNPs:

Under the periodic classification, gold is the third element in Group IB with unique physical, chemical and optical properties that cannot be easily predicted from the trend with other group members like copper and silver. When existing in the form of nanoparticles, these properties further deviated from that of the bulk material. The origin of such deviation is owing to the confinement of unbound electrons' motion which therefore quantizes their energy set and changes

the band gap width. This quantum size confinement effect is important for scientists to tune and make use of gold's properties by varying its size and shape.

For example, bulk gold's color, density, melting point, mechanical strength and conductivity are all sensitive to its size and shape. It is also regarded as chemically inert, having an excellent resistance to corrosion and undesired reactions. As the size approaches smaller and smaller down to 2nm, its metallic character disappears due to the narrowing of the conduction and valence bands. A smaller size also increases the proportion of surface gold atoms up to 60% comparing to the core one. [31] These surface atoms are usually more active and having different chemical properties. Such a loss of chemical inertness in AuNPs confers them potential to be utilized for various applications, e.g. electronic conductor and catalysis. Moreover, both melting point and conductivity decreases due to the decrease in coordination number and interatomic distance of surface atoms.

More important and interesting thing lies in the optical property of AuNPs. It is known that AuNPs solution shows various color based on its intense absorption in the visible range. The origin of the solution color can be attributed to the phenomenon known as the Localized Surface Plasmon Resonance. It describes the collective coherent oscillations of free conduction electrons inside AuNPs and the incoming electromagnetic wave when its wavelength is greater than that of the particle size. (Figure 4.1) The interaction between the free electrons and the electric component of the wave would give rise to a charge separation on opposite ends of the particles. This polarization would create another electric field,

generating a restoring force and leading to the plasmon waves of particles. Such formations of dipole and wave-like oscillations of free electrons, which make up the conduction band, can affect its properties of conductivity and optical reflectivity.

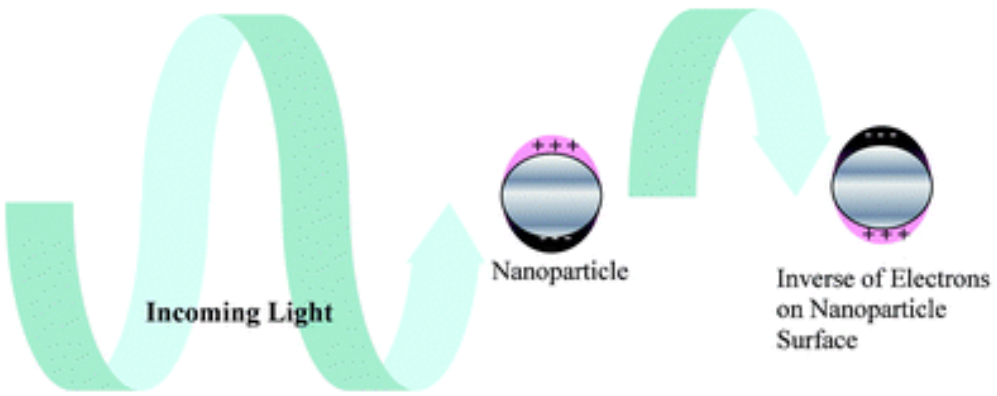

Figure 4.1 Origin of Localized Surface Plasmon Resonance of metal nanoparticle by the oscillation its free conduction electrons. [32]

At the resonant frequency of the electromagnetic wave, such oscillations reach the maximum amplitude and cause a strong absorption in the visible region. This absorption which accounts for the red color formation originates from the intra-band excitation of 6sp electrons. This intense absorption peak can even be 5-6 orders of magnitude stronger than common organic dyes molecules. [33] The resonance frequency is dependent on parameters like the size, shape, structure, composition, type of metal and the surrounding medium of AuNPs. Therefore, as Figure 4.2 shows, AuNPs can exhibit a range of colors from pale red to blue when the particle size and aggregation extent are tuned manually by the above

parameters. UV-Vis absorption spectroscopy also shows the gradual red-shift and broadening of absorption band, as described by Mie theory being established in 1908. [34] These properties make AuNPs a potentially flexible platform for developing different kinds of colorimetric sensor or imaging probes based on any interactions happening on its surface for causing a change in the refractive index and the resonant frequency.

Synthesis of AuNPs:

To synthesize AuNPs, top down and bottom up approaches are two commonly employed strategies to build AuNPs either from bulk physically or individual atoms chemically. (Figure 4.3) Comparatively the bottom up approach is more widely employed and a wide variety of synthetic methods have been developed which are beyond detailed discussion one by one here. Basically they involve two key steps: firstly the chemical reduction process using suitable reducing agents and secondly the stabilization step by surfactants usually possessing electronegative groups, e.g. carboxylate, nitrogen-based, phosphorous, sulfur or oxygen based ligands.

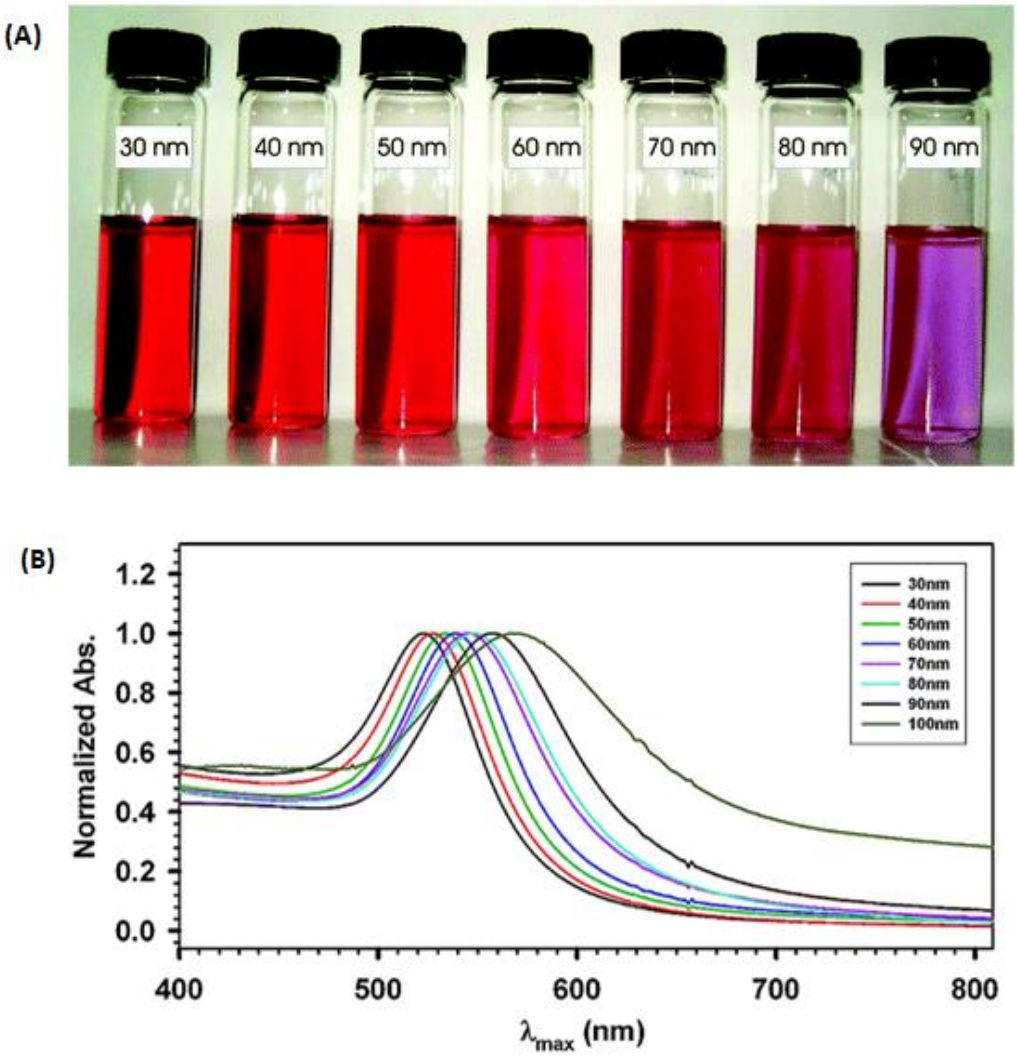

Figure 4.2 (A) Different AuNPs' solution color at different particle sizes. (B) Combined normalized UV-Vis absorption spectra of AuNPs solution at different particle sizes. [35]

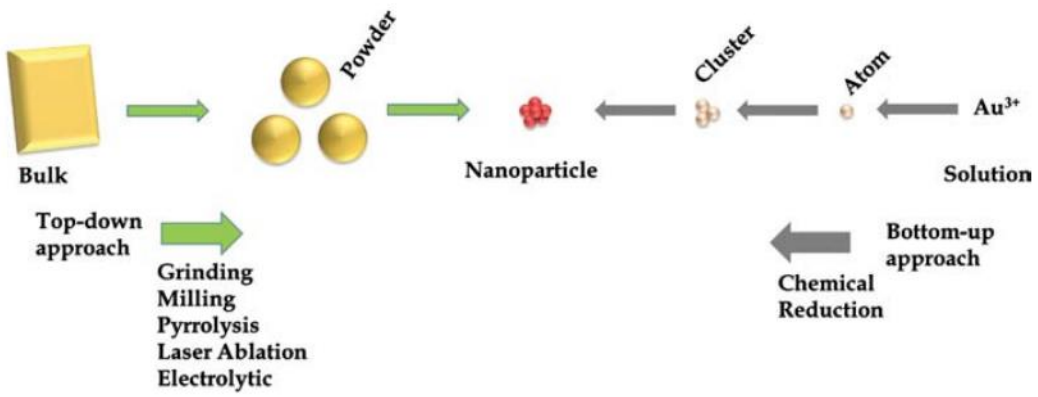

Figure 4.3 Synthesis of AuNPs from top-down or bottom up approaches. [36]

One of the most common synthetic approaches for preparation AuNPs is the Turkevich method developed in 1951, which made use of trisodium citrate as both the reducing agent of gold ions and stabilization agent of colloidal AuNPs. [37] Figure 4.4 shows the schematic illustration of the AuNPs growing process:

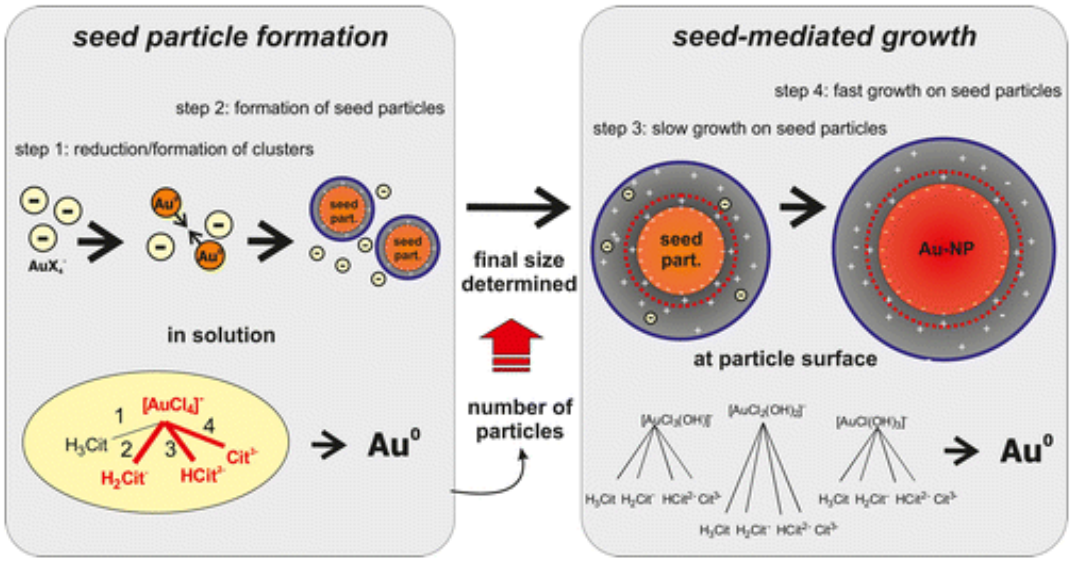

Figure 4.4 Schematic illustration of the AuNPs growing mechanism. [38]

It is a two-steps process involving the seed particle formation and seed-mediated growth. [39] Within the first few seconds of the synthesis, it is regarded as the seed formation stage during which the precursor hydrogen tetrachloroaurate (III) ($HAuCl_4$) is being partially reduced by different citrate species (mainly $HCit^{2-}$) to gold atom in solution. The Au^0 particles then grow due to coalescence and form stable seed particles with a radius of around 1.5 nm. This is the end of the first stage. In the second seed-mediated growth step, any remaining precursors are subsequently reduced and grow on top of the seed until being consumed completely. Finally the citrate ligands bind to the AuNPs surface through inner sphere complexation. Negative charges on carboxylate groups would render AuNPs the same charge for repelling against each other to avoid aggregation. To tailor-make AuNPs with different sizes, numerous reports have described ways to achieve size-tuning from 15 to 150nm by controlling parameters like pH, reaction temperature and precursor concentration which governs the ratio of $[AuCl_4]^-$and $[AuCl_{4-x}(OH)_x]^-$. [39-40]

Although an enormous number of publications regarding use of citrate capped AuNPs are being reported, the conformations of citrate ions on AuNPs are not fully studied. The view of its existing as a fully deprotonated $citrate^{3-}$ form is oversimplified. Some scientists suggested the role of dicarboxyacetone, an oxidation product of citrate, having a key role in nucleation as well as size-control. [41] Only until recent years did surface chemists make some breakthroughs to this question to be answered. By using attenuated total reflectance infrared spectroscopy and X-ray photoelectron spectroscopy, Park *et al.* proposed several

possible coordination forms of adsorbed citrate on Au(111) facet. (Figure 4.5) [42] They also reported the presence of dangling dihydrogen citrate anions which make up a citrate layer of around 8-10Å on the surface. (Figure 4.6) Dicarboxyacetone was also confirmed to have no significant effects on the reduction mechanism of the seed particle formation stage as well as the final AuNPs size under the Turkevich method. These findings provide a foundation for further studies on coordination of other surfactants onto AuNPs or other nanoparticles.

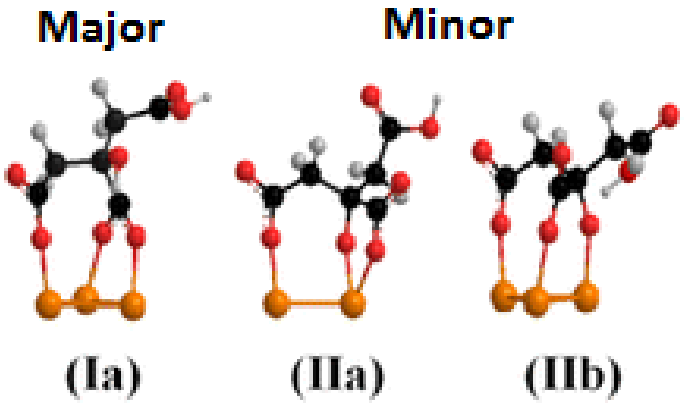

Figure 4.5 Proposed conformations of adsorbed citrate on AuNPs. Orange: gold (representative of the gold surface), red: oxygen, black: carbon, gray: hydrogen. [42]

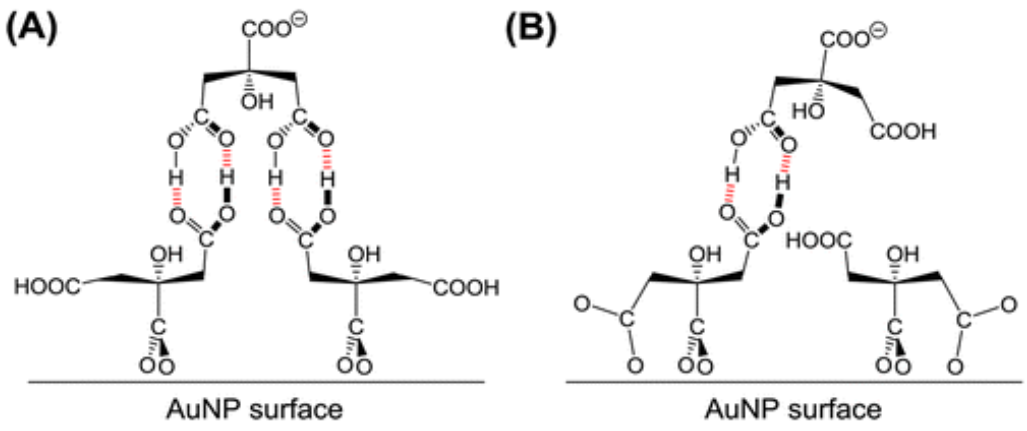

Figure 4.6 Two proposed configurations of a citrate trimer unit as building blocks of surface citrate layers on AuNPs. (A) An organized form where adsorbed citrate anions are linked with adjacent adsorbed anions through formation of hydrogen bonds with acyclic COOH dimers. (B) A disordered form where the citrate trimer is associated with non-interacting terminal COOH and η^1-COO^-groups. [42]

This Turkevich method had been further studied by several groups, e.g. over the effect of pH, temperature, use of fluorescence irradiation and heavy water (D_2O) on the final morphology and size of AuNPs. [43-46] Synthesis using reducing agents other than citrate solution were also studied. [47-49] For example, in this chapter our developed AuNPs aptasensor was based on synthesis using sodium borohydride as reducing agent. This approach was developed by Natan's group, utilizing its much stronger reducing agent than sodium citrate. Comparatively we can get small AuNPs with size around 4nm without any heating processes. [50] Stabilization of AuNPs can also be achieved through different

ligands, like thiolate in Brust-Schiffrin method, polymers, dedrimers or macromolecules with different heteroatoms (N, O, P, S) for interacting with AuNPs surface. [40] All in all, AuNPs are quite comprehensively studied and resulted in various interesting morphologies (spherical, sea-urchin, triangular, rod, cubic, tetragonal, bowl-liked, star-liked, octahedral, decahedral, hexagonal and truncated tetrahedral, etc.) having different photo-physical properties for wide range of applications. (Figure 4.7)

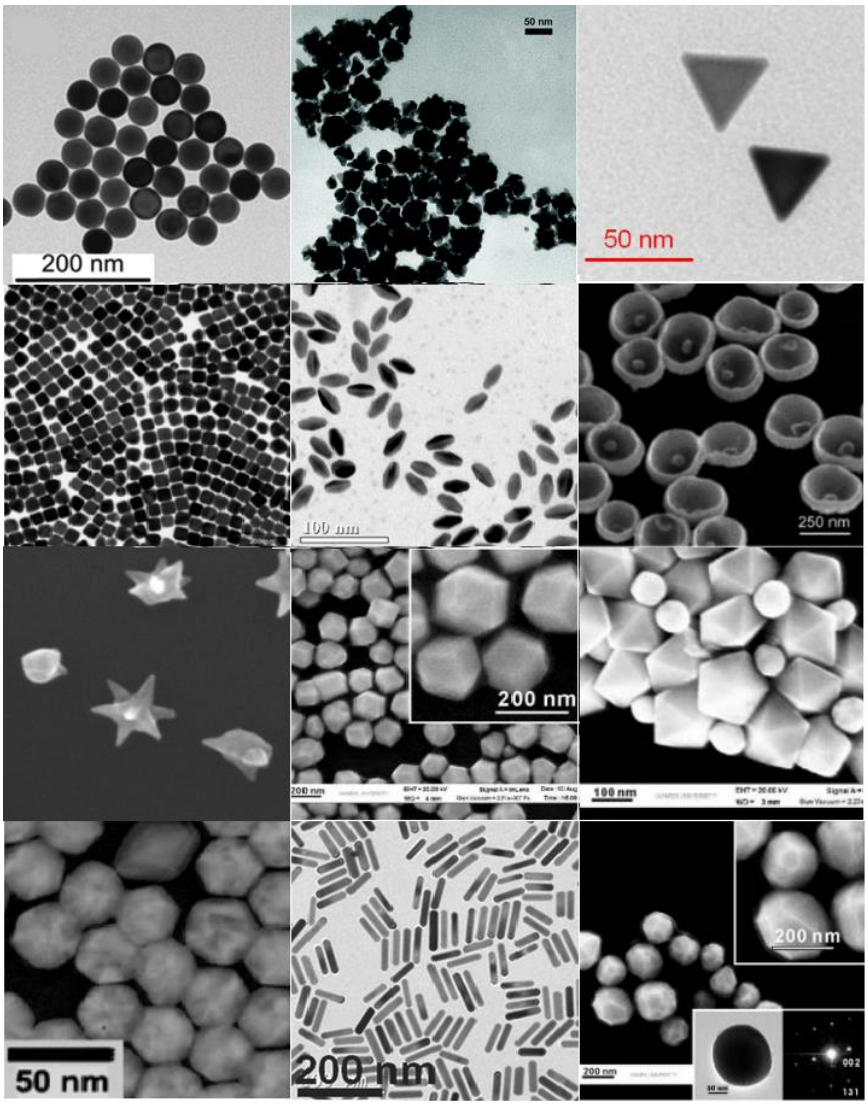

Figure 4.7 AuNPs with different shapes. (Adapted from [51-60])

4.1.3 Interactions between AuNPs and DNA

Deoxyribonucleic acid (DNA) is a block copolymer composing of a series of nucleotides, which is made from a sugar phosphate backbone and a nitrogen containing nucleobase. (Figure 4.8) It is the key molecule for life, encoding the genetic information in living organisms.

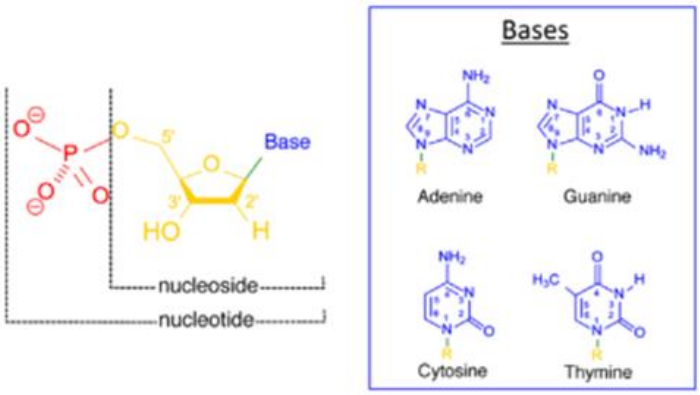

Figure 4.8 Structure of DNA. [61]

With the advance in DNA chemical synthesis, now we can prepare the DNAs with specific nucleotides sequences easily and they have been very common and popular molecules for developing biosensor. [62]

It was reported long time before that single stranded DNA can adsorb onto the surface of AuNPs. This process is often triggered by the addition of salt to screen the negative charge repulsion between the negatively charged citrate-AuNPs and phosphate backbones of DNA. Many articles have already shown the interaction of nucleobases with gold surface non-covalently through non-specific interactions following the order of Cytosine > Guanine > Adenine > Thymine.

(Figure 4.9) [63] Based on this finding, Li *et al.* designed a hybridization assay to detect single base pair mismatch within 5min based on the solution color change upon aggregation. [64]

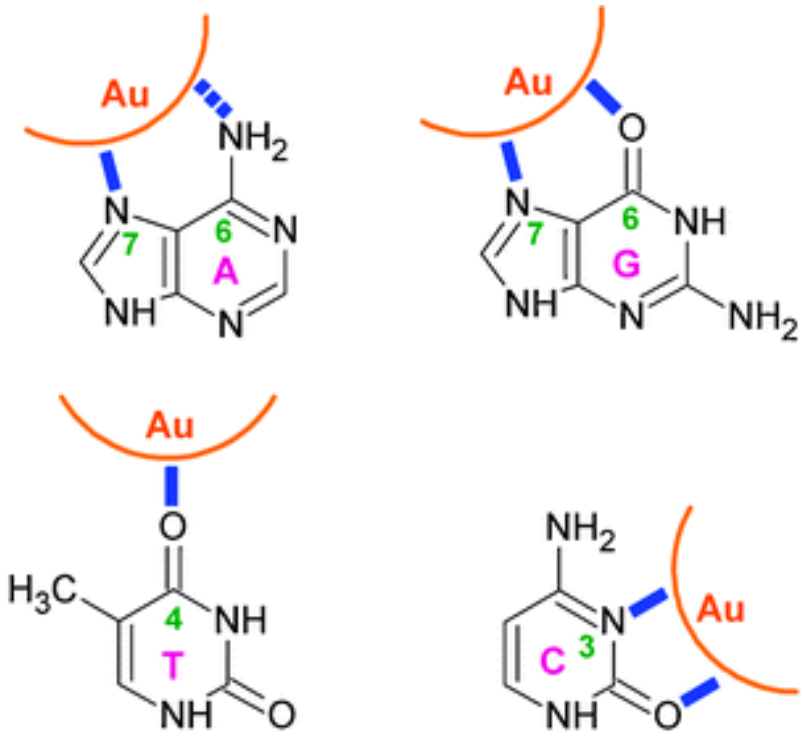

Figure 4.9 Strong chemical bonding between adenine, guanine, thymine, cytosine and gold surface. [65]

Different adsorption models have been suggested to explain the binding isotherms. The latest study on this issue was reported by Zhang *et al.* where the adsorption was proposed to start firstly by surface citrate being displaced by DNA molecules. [66] Such a displacement can be facilitated by factors like a high salt concentration, low pH or high ethanol composition in solvent. Adsorbed DNA would then uncoil sufficiently to expose its bases and maximize the contact points

with the AuNPs surface, creating an exclusion zone for other incoming DNAs for further adsorption until these zones overlap. (Figure 4.10)

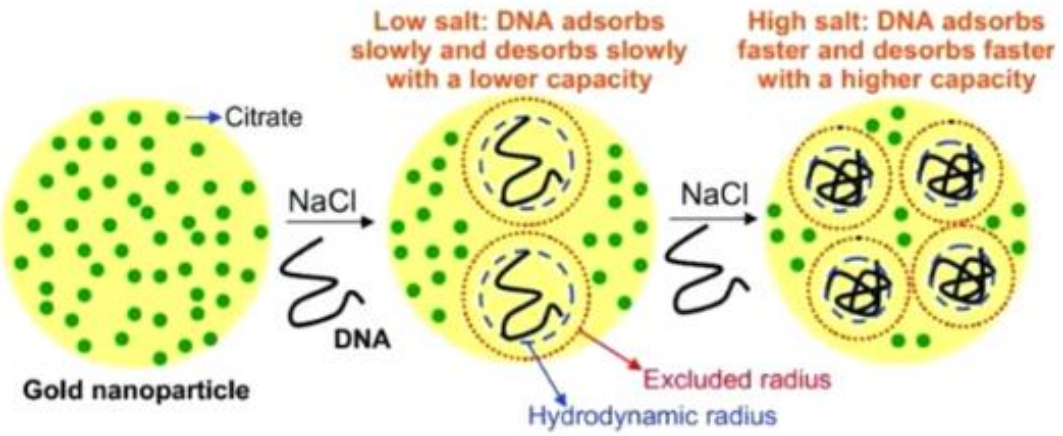

Figure 4.10 Schematics showing the DNA adsorption process. [66]

4.1.4 Design of experiment

In this work, based on our previous finding that urinary Spm can act as a biomarker towards prostate cancer, our effort in developing a rapid sensing kit using AuNPs and DNA towards this analyte is reported. It was inspired by an interesting article reported by Liu *et al.* about the use of ssDNA-capped AuNPs for achieving a sensitive and selective Spm sensing based on a non-crosslinking mechanism. [67] Tetravalent cationic Spm was reported to shield the negative charges of adsorbed DNAs, resulting in the aggregation of AuNPs and shift of absorption band. A lot of unanswered questions were not mentioned in the manuscript so in this report we performed a more comprehensive study on this phenomenon. Different factors' effect was investigated during the optimization

study. Apart from the sensing purpose, we also performed a deeper study on the role of DNA aptamer on the sensor, since the base sequence interestingly is not affecting much the aggregation process, as reported by Liu *et al*. [67] Figure 4.11 shows the expected schematic diagram of the sensing approach.

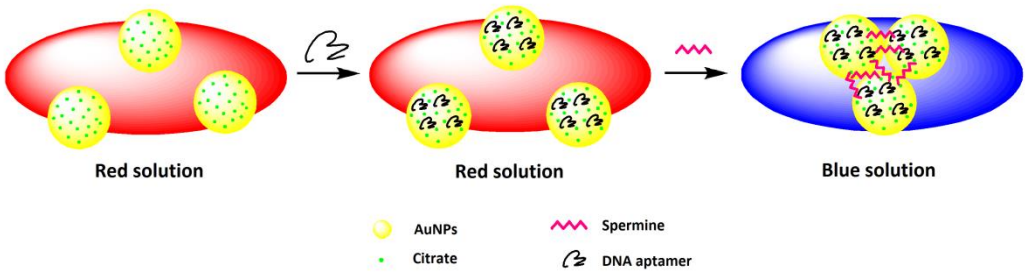

Figure 4.11 Schematic diagram of the developed aptasensor. DNA was adsorbed onto AuNPS by displacing the original citrate surfactants. Later addition of positively charged Spm would induce the aggregation of DNA capped AuNPs, resulting in a surface plasmonic change in its absorbance.

4.2 Experimental section

4.2.1 Materials and Instruments

All chemicals were acquired either from Aldrich (Hong Kong, China) or Meryer (Shanghai, China). DNA aptamers (12mer: **CGA CAA CCA CAA**; 24mer: **CGA CAA CCA CAA CAC ACA ATC TGA**; 36mer: **CGA CAA CCA CAA CAC ACA ATC TGA CGA CAA CCA CAA**) were obtained from Invitrogen (Hong Kong, China). Britton-Robinson (BR) buffer was self-prepared by mixing

equal molar ratio of phosphoric acid, boric acid and acetic acid. The pH was then tuned to specific value using sodium hydroxide solution and a calibrated FiveEasy F20 Benchtop meter (Mettler-Toledo, Hong Kong, China). Artificial urine was prepared according to a recipe previously reported: 1.87g of sodium chloride, 1.13g of potassium chloride, 1.2og of dihydrogen sodium phosphate, 0.50g of creatinine, 4.50g of urea and 12.5mg of human serum albumin were added in a 250 mL volumetric flask and the volume was completed with Milli-Q water. [68] All standard solutions were also prepared in water. For urine samples, they were collected from Princes of Wales Hospital, The Chinese University of Hong Kong under the permission of its ethic committee. Details are mentioned in Chapter three.

The transmission electron microscope (TEM) images of as-prepared AuNPs were captured using a JEOL Model JEM-2011 (JEOL, Beijing, China). Dynamic Light Scattering (DLS) and zeta-potential data were measured by a Zetasizer Nano-ZS90 System (Malvern Instruments, Shanghai, China). The UV-Vis absorption spectra were recorded using a Cary 8453 UV-Vis Spectrometer (Agilent, Hong Kong, China). Isothermal Titration Calorimetry measurement was achieved using MicroCal PEAQ-ITC Automated System (Malvern Instruments, Shanghai, China). For urine sample analysis, liquid chromatographic separation was achieved by an Agilent 1290 Infinity Quaternary LC System while mass analysis was done by an Agilent 6460 Triple Quadrupole mass spectrometer equipped with an Agilent Jet Stream technology electrospray ionization source (Agilent, Hong Kong, China). All the incubations were performed on a KS-260 Basic Orbital Shaker at 1000rpm (IKA, Hong Kong, China).

4.2.2 Synthesis of citrate-AuNPs

Three different sizes (4nm, 13nm, 27nm) of AuNPs were prepared. For 4nm citrate-AuNPs, the synthesis was performed according to a previous published literature by our group using the Natan's method. [69] Briefly, chloroauric acid solution was mixed with trisodium citrate solution at room temperature. Freshly-prepared sodium borohydride solution was then added and left for 2hr without stirring. For 13nm and 27nm AuNPs, the synthesis was done by the well-known Turkevich method mentioned above, where trisodium citrate was used as both the reducing agent and capping ligands under refluxing condition. Final size as determined from TEM was 4.09±0.65nm, 12.8±1.3nm and 27.2±4.2nm by counting 100 individual AuNPs. (Figure 4.12) Concentration was calculated to be 114.54nM, 14.15nM and 1.53nM for 4, 13 and 27nm AuNPs respectively using equations suggested by Liu *et al.* [70] 4nm AuNPs were employed for majority of experiments, and different batches' absorbance and wavelength of plasmonic band did not show significant deviations.

Equation 1: $$N = \pi\rho D^3 / 6M = 30.89602D^3$$

where N = Average number of gold number in each nanoparticle, ρ = density for fcc gold, M = atomic weight of gold, D = Average diameter of AuNPs obtained from TEM

Equation 2: $$C = N_{total} / NVN_A$$

where C = Molar concentration of AuNPs, N_{total} = total number of gold atoms calculated from initial $HAuCl_4$, V = Volume of solution (in L), N_A = Avogadro's constant

(A)

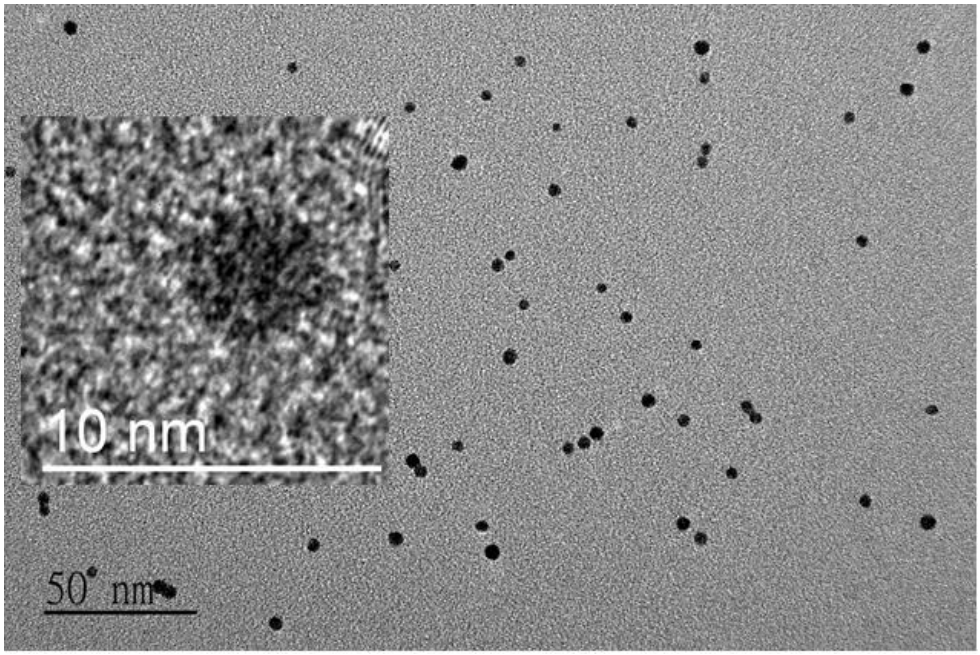

(B)

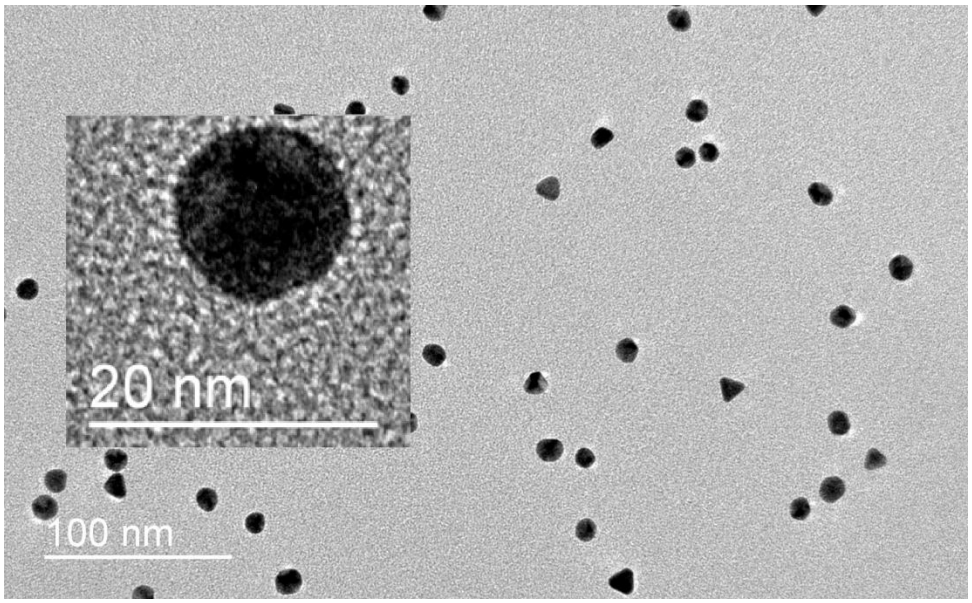

(C)

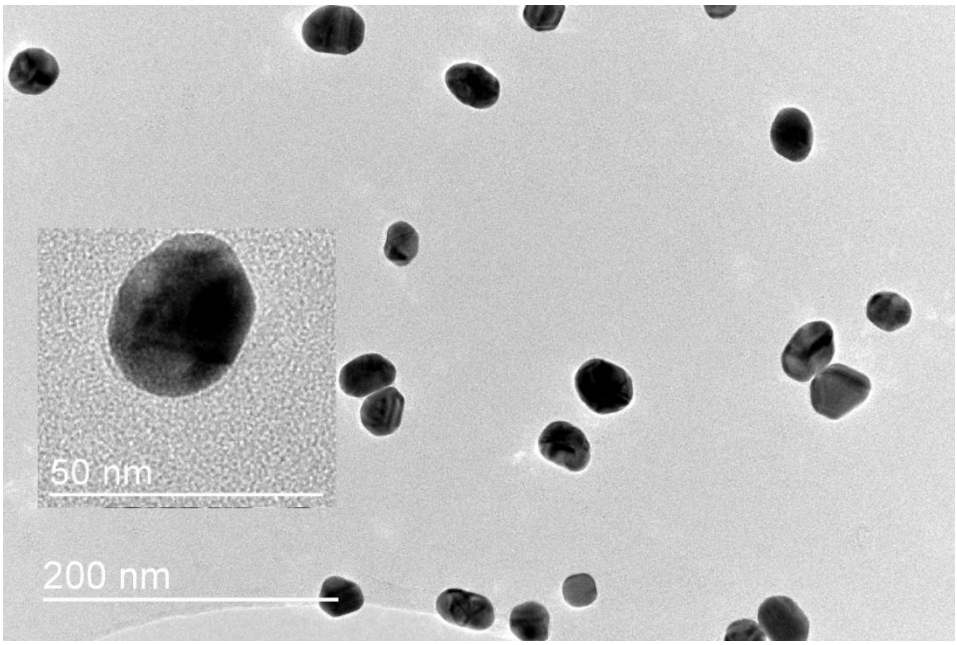

Figure 4.12 TEM images of citrate-AuNPs. (A) 4nm (B) 13nm (C) 27nm. Inset: Magnified TEM image.

4.2.3 Quantitative detection of spermine by AuNPs

In blank solvent, 80nM as-prepared 4nm AuNPs was vortex-mixed with 25nM DNA aptamer inside 4mM BR buffer (pH=3.29) for selective adsorption to take place. SPM standard/urine sample solution was then added and incubated for 60 min. The mixture was then ready for UV-Vis absorption, DLS and zeta-potential measurements. In complicated matrices like artificial urine and clinical urine, DNA concentration was raised to 100nM to provide a better protection.

4.2.4 Optimization of working conditions

Parameters including the AuNPs size (4, 13, 27nm), DNA aptamer concentration (12.5, 25, 50, 100 and 200nM), DNA length effect (12mer, 24mer

and 36mer), pH (3.29, 4.96, 6.99, 8.98 and 11.0) and length of incubation time were studied and optimized based on the sensitivity towards Spm obtained from the slope of corresponding calibration graph.

4.2.5 Sample pretreatment procedures

The clinical urine samples were thawed naturally and centrifuged for 5 min at 13000 rpm and room temperature. Then it was pre-treated with ultrafiltration (Amicon Ultra-15, MWCO = 3000Da) before use to remove any undesired interfering large molecules (e.g. proteins). For artificial urine, it was two-fold diluted before use without any further pre-treatments.

4.2.6 Isothermal titration calorimetry (ITC)

For the study of interactions between DNA capped AuNPs and Spm, the AuNPs was firstly pre-concentrated using Amicon Ultra-15 30K centrifugal filter (Millipore, Hong Kong, China). Free citrate ligands inside stock solution should also be removed during this step. Afterwards, 0.5μM AuNPs and different concentration of DNA aptamer (0, 0.5, 1 & 3μM) were mixed and placed inside the sample cell. 0.25mM Spm solution was then gradually added for recording the temperature change per injection (2μL per injection in 150s interval at 25˚C).

For the study of interactions between citrate and polyamine analogs, 1mM trisodium citrate solution was placed into sample cell. Different polyamine analogs solution was then injected independently for recording the temperature under the

above-mentioned conditions. Similarly, for the study of interactions between DNA and polyamine analogs, 10μM DNA solution was placed in to the sample cell followed by addition of different polyamine solution.

In both cases data was fitted by the binding model of one site of binding and analyzed by the MicroCal PEAQ-ITC Analysis software to obtain the stoichiometry, dissociation constant, change of enthalpy, entropy and Gibbs free energy.

4.3 Results and discussion

Sensitive and specific sensing towards Spm was achieved by the current developed aptasensor via two stages according to Zhang's binding model abovementioned. The first stage, as demonstrated in Figure 4.11, is the selective adsorption of DNA aptamer onto surface of citrate-AuNPs, which is facilitated by a low pH working condition. Citrate ligands are being displaced since DNA can adopt an extended conformation to strengthen the binding with AuNPs surface. This can be viewed from our DLS results in Figure 4.13. With more DNA, the hydrodynamic size of AuNPs became smaller and smaller due to the displacement of citrate layer by a more compact DNA molecule. The better stabilization effect by DNA also accounts for that decrease in Z-average value in acidic condition, which can make AuNPs aggregate. Such a protection effect against aggregation can be viewed in Figure 4.14, which clearly shows that the aggregation slows down at higher DNA capping condition. The second stage is the addition of positively charged Spm which induces further DNA adsorption by shielding the

negative charges on both AuNPs and DNA aptamer, and as results weakens the repulsion force for AuNPs aggregation. The extent of aggregation would allow an indirect quantitation of Spm content in a convenient and fast manner.

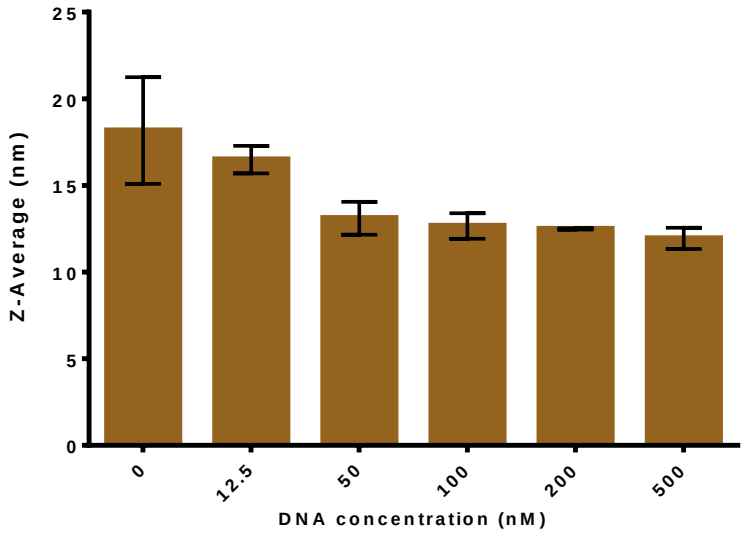

Figure 4.13 Effect of DNA adsorption on DLS results of AuNPs. (AuNPs: 80nM in 4mM BR-buffer, pH=3.29)

To further study the driving force of citrate displacement by DNA, it was well studied before that the presence of salt would screen the charge repulsion between negatively charged AuNPs and DNA. [66] In our case, the AuNPs are used directly without any clean-up. Therefore a lot of free citrate molecules and side products from sodium borohydride would act as such screening sources for DNA adsorption. A proof-of-concept experiment was performed to remove these free salts by ultrafiltration. It was found that without them, DNA cannot attach and the AuNPs would aggregate immediately upon addition of acidic BR buffer for

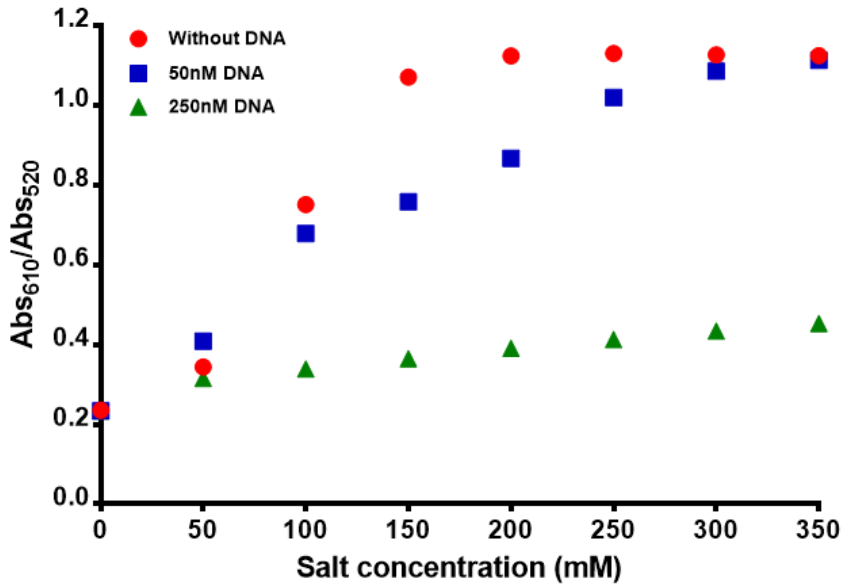

Figure 4.14 DNA protection effect against AuNPs aggregation at different salt concentration.

protonating the citrate groups, even in the presence of DNA. And vice versa, when stock AuNPs solution was used, aggregation did not happen. This confirms the importance of free citrate and other salts for the aptasensor to function properly.

Working conditions was optimized carefully by studying the calibration graphs of Spm in each case. The slope which reflects the sensitivity and the linear working range were used as the criterion in deciding the optimal case in each factor being studied.

The first parameter we studied was the size effect of AuNPs. As being illustrated in Figure 4.15, by taking logarithm on the absorbance ratio at the blue region (e.g. 610nm in our study) and their plasmonic peaks' wavelength, the sensitivity becomes greater and linear range become narrower with the increase of

AuNPs size. Considering the fact that most urine samples are having urinary SPM content in the range of 0-15μM, 4nm AuNPs seemed to be the best choice for later experiments by providing the widest and most appropriate linear working range. And to explain such an observation of trend, it was believed that the number of AuNPs was smaller in cases of larger AuNPs, thereby more easily getting aggregated as induced by the same amount of SPM being added into the AuNPs solution.

The second parameter being studied was the DNA concentration. Basically in all cases the curves showed a linear range initially, which then gradually leveled off. (Figure 4.15 and Table 4.1) Also with more DNAs, a wider linear working range was obtained with a compensation of sensitivity. Due to the nature of single stranded DNA easily being adsorbed onto AuNPs, in this method it omitted the need to prepare DNA-AuNPs through tedious target-mediated reactions for surface modifications. Flexibility was therefore provided to users to tune the working range according to their wills easily by changing the DNA amount added for incubation. Finally, 25nM was chosen as the optimal concentration which gave the best sensitivity and a linear range from 0-6μM.

The third parameter studied was pH. (Figure 4.17 and Table 4.2) Our results showed that the aptasensor worked better in acidic medium, which is essential to maintain Spm (pKa = 7.90, 8.83, 9.97 and 10.79) in its +4 charge state. Finally pH 3.29 was chosen as the optimal value.

For the effect of DNA length, we got similar conclusions as Zhang *et al.* that a longer aptamer adsorbs with a higher stability and protects AuNPs better

from aggregation. (Figure 4.18) [66] When considering the absorbance change at 610nm, 24-mer was slighter greater than the others so it was chosen.

The last parameter was the incubation time which was optimized by monitoring the aggregation kinetics. Upon addition of Spm, the absorbance at 512nm decreased immediately indicating the further adsorption of DNAs onto AuNPs surface. Concurrently the absorbance at 610nm increased indicating the aggregation was taking place. Finally it was determined that 40 minutes was enough for reaching an equilibrium state. (Figure 4.19-4.20)

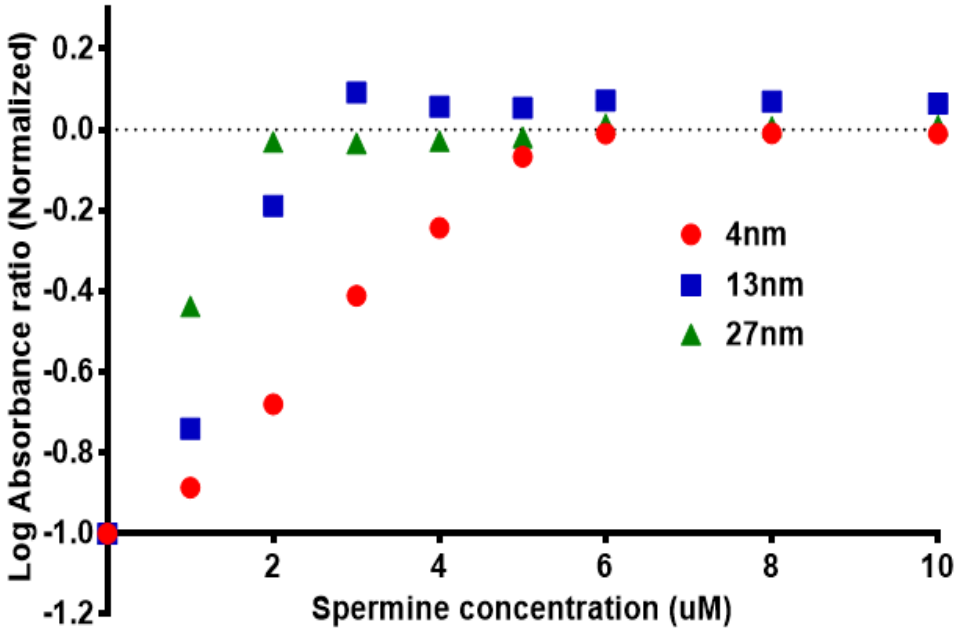

Figure 4.15 AuNPs size effect on calibration graph of spermine. (DNA concentration: 25nM; pH=3.29; AuNPs concentration: 80nM for 4nm, 2.38nM for 13nm, 0.24nM for 27nm; concentration was chosen such that they gave similar absorbance value at their plasmonic peak; Plasmonic peak wavelength: 512nm for 4nm, 523nm for 13nm, 532nm for 27nm)

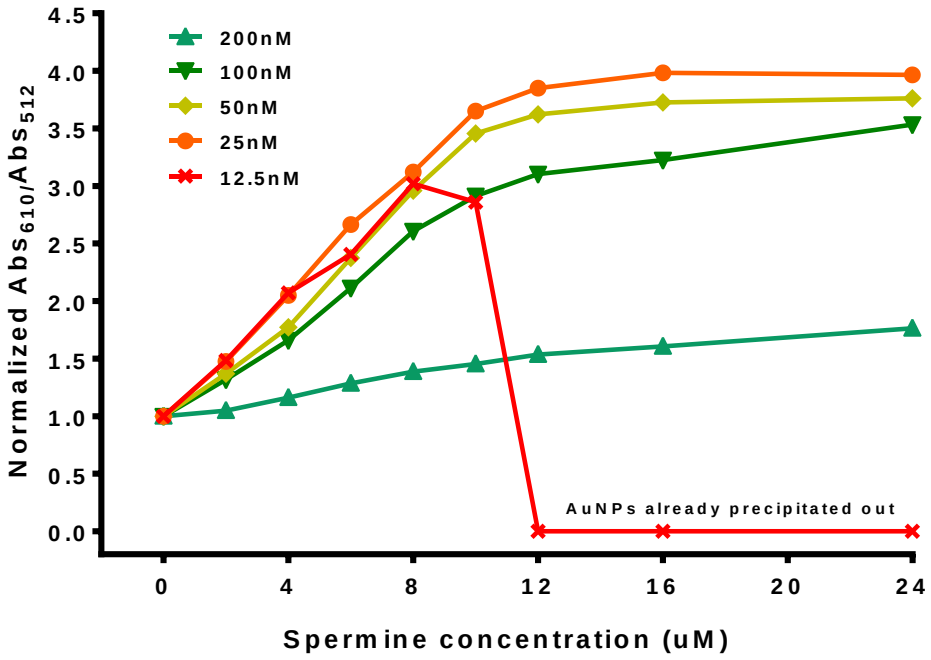

Figure 4.16 DNA effect on Spm calibration graph.

DNA concentration (nM)	Equation	R^2	Linear range
12.5	y = 0.2305x + 1.0134	0.9975	0-4µM
25	y = 0.2657x + 0.9893	0.9988	0-6µM
50	y= 0.2258x + 0.9987	0.9968	0-10µM
100	y = 0.1972x + 1.0578	0.9959	0-10µM
200	y = 0.0529x + 0.9981	0.9926	0-16µM

Table 4.1 Summarized results on the linear equation, R^2 and linear range of Spm calibration graphs at different DNA concentration.

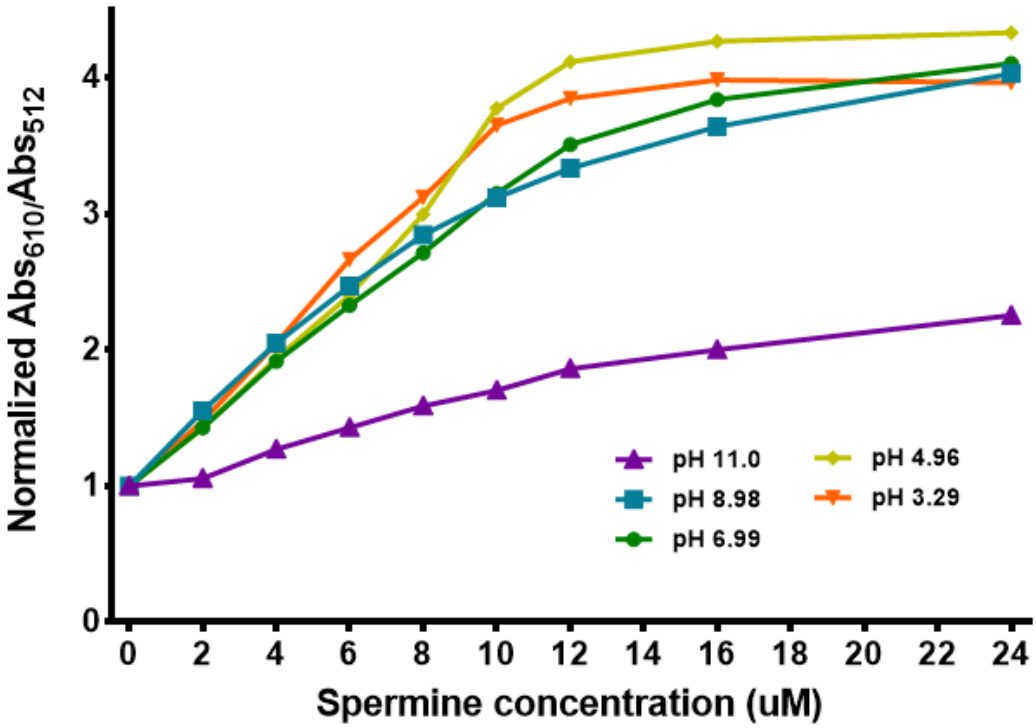

Figure 4.17 pH effect on Spm calibration graph.

pH	Equation	R^2	Linear range
3.29	y = 0.2657x + 0.9893	0.9988	0-6µM
4.96	y= 0.2510x + 0.9708	0.9944	0-10µM
6.99	y = 0.2021x + 1.0845	0.9945	0-12µM
8.98	y = 0.2321x + 1.0862	0.9914	0-8µM
11.0	y = 0.0822x + 0.8323	0.9996	2-8µM

Table 4.2 Summarized results on the linear equeation, R^2 and linear range of Spm calibration graphs at different pH.

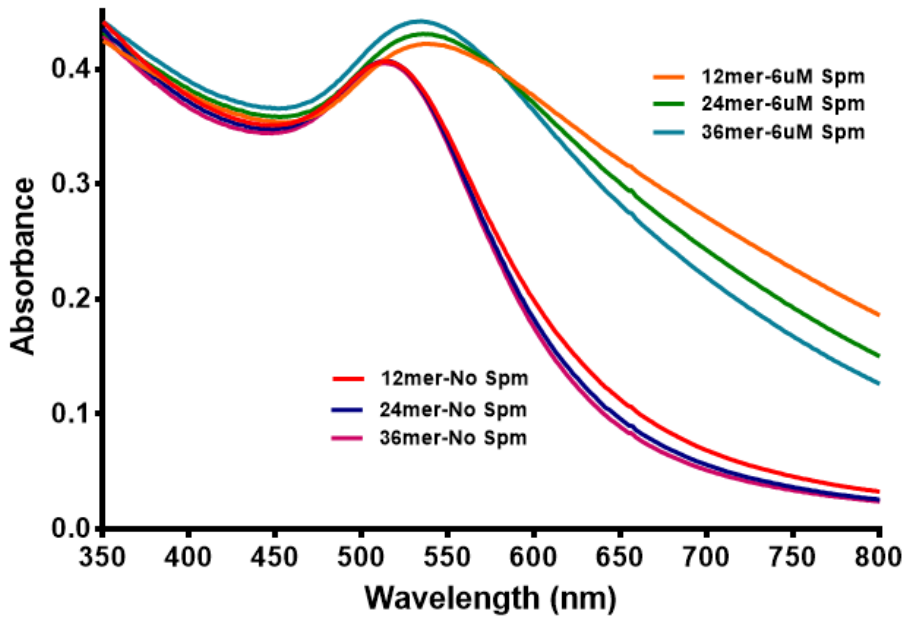

Figure 4.18 Absorption spectrum showing DNA length effect in the presence and absence of spermine.

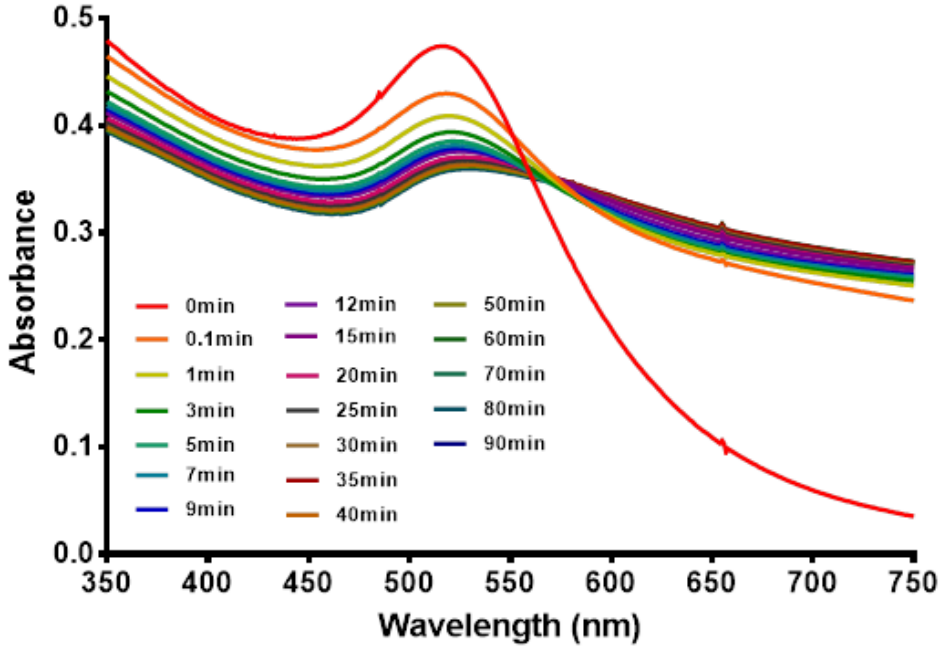

Figure 4.19 Kinetics for Spm induced aggregation of DNA-AuNPs. (AuNPs: 80nM; DNA: 25nM; Spm: 6μM)

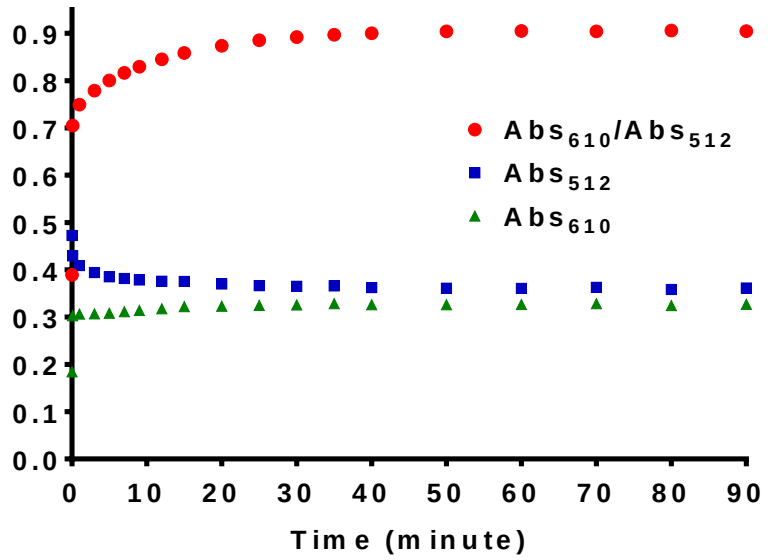

Figure 4.20 Change of Abs_{610}, Abs_{512} and Abs_{610},/Abs_{512} against time.

Under the final optimal conditions in a blank matrix, by taking logarithm on the absorbance ratio, a linear SPM calibration curve from 0-5μM could be fitted by the least square linear regression. (Figure 4.21) The equation was y = 0.1029x - 0.4941, with limit of detection (LOD) calculated to be 15.25nM (3.09ng/ml) by using the equation LOD = 3σ / k of SPM-free AuNPs solution, where k is the slope of curve. DLS and zeta-potential were also measured under the described conditions. (Figure 4.22) The hydrodynamic size increased with an elevating Spm concentration for causing a larger degree of aggregation. But unlike the results from Liu *et al.* for 13nm AuNPs, our results showed that the zeta-potential of 4nm AuNPs did not show any trends of change instead of gradually restoring to a more positive level. [67] This might be due to most Spm molecules being embedded in the core of aggregates.

During the optimization of DNA concentration, it was interesting to observe a drop of sensitivity towards Spm when more DNA was added for adsorption during the assay. This contradicted to the previous suggestion that Spm induced aggregation occurred through DNA molecules via an ion-bridging effect and non-crosslinking mechanism. [67] To gain more information, we conducted a control experiment in the absence of DNA. Surprisingly, the Spm induced aggregation process could still be observed and it exhibited the fastest initial kinetics rate when compared to other conditions performing in the presence of different amount of DNA. (Figure 4.23) It seemed that the presence of citrate groups originally capped on AuNPs could not be neglected and they contributed significantly to the aggregation process.

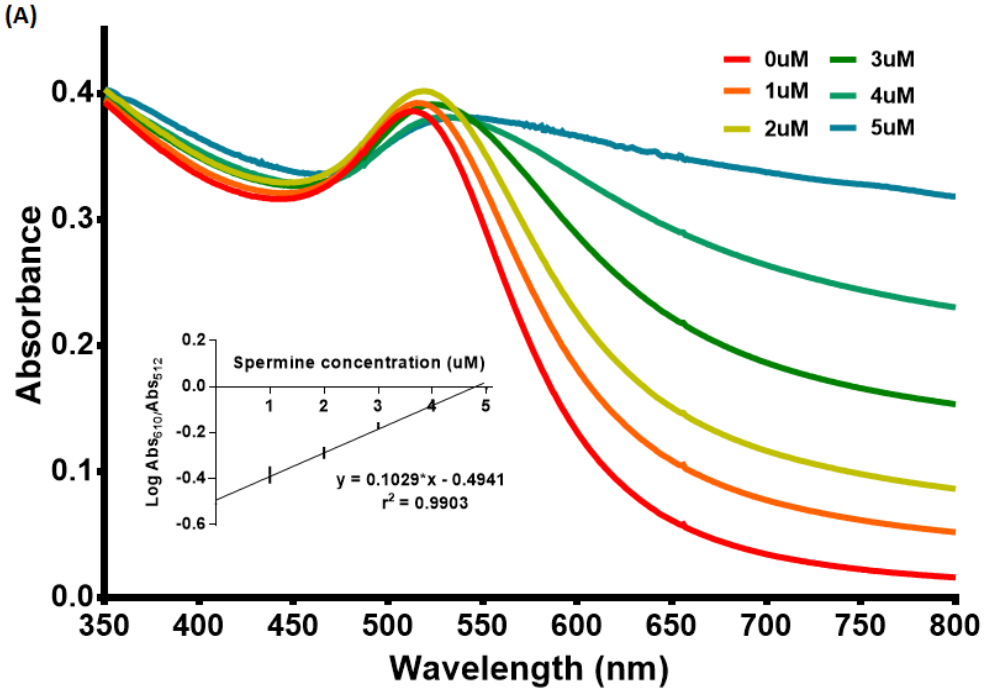

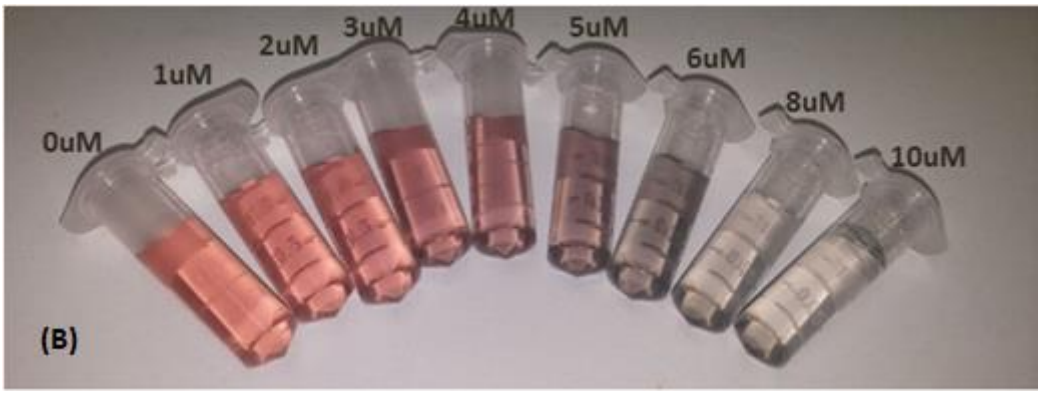

Figure 4.21 (A) The Spm induced aggregation on DNA capped AuNPs in blank matrix - The absorption spectra of DNA capped AuNPs upon addition of Spm solution. (0-5µM) Inset: Plot of normalized Abs_{610}/Abs_{512} vs Spm concentration. (B) The photo of AuNPs solution color with different extent of Spm induced aggregation. (0-10µM)

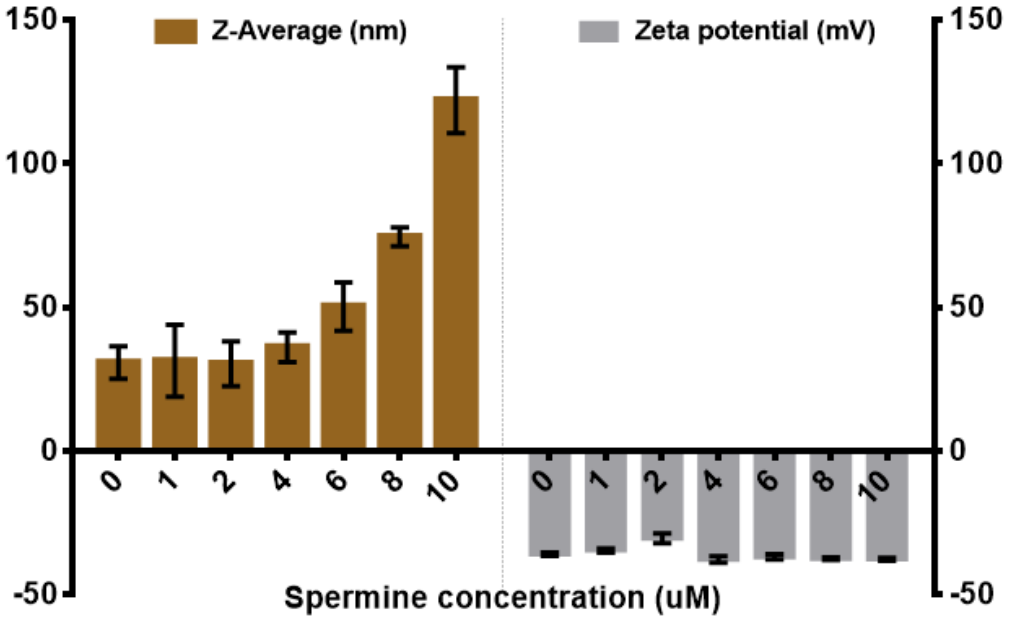

Figure 4.22 DLS and zeta-potential measurements showing Spm induced aggregation of DNA-AuNPs.

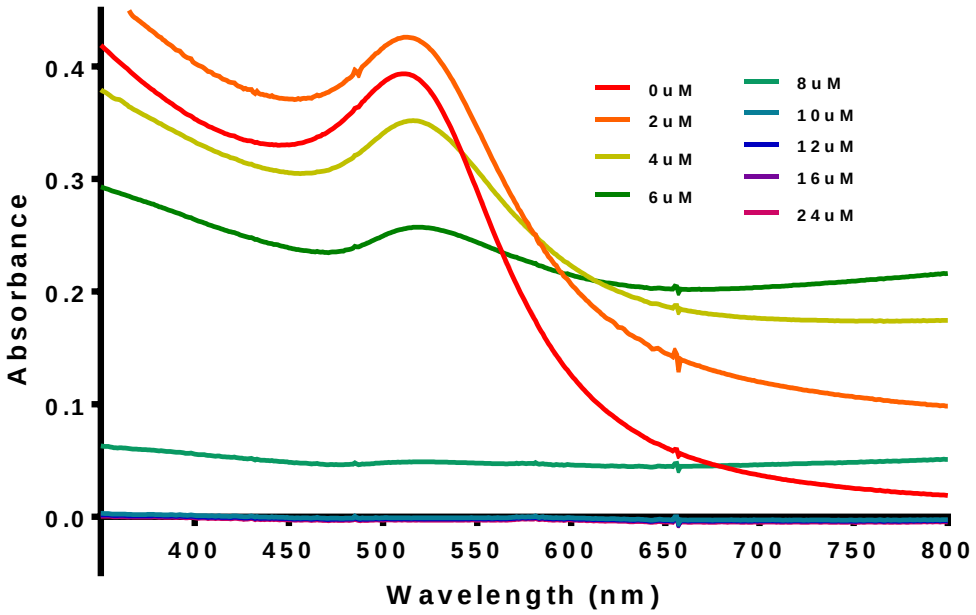

Figure 4.23 Absorption spectrum showing Spm induced aggregation in the absence of DNA at different concentration of Spm. (0-24µM)

To have a deeper insight into the mechanism, several ITC experiments as suggested in the above experimental section were performed: Same amount of citrate-AuNPs was mixed with four different concentration of DNA (0, 0.5, 1 and 3µM) separately. Spm solution was then added gradually for measuring the temperature change in each injection. The data of each case are shown respectively in Figure 4.24-4.27 and the overall results are summarized in Table 4.3 below:

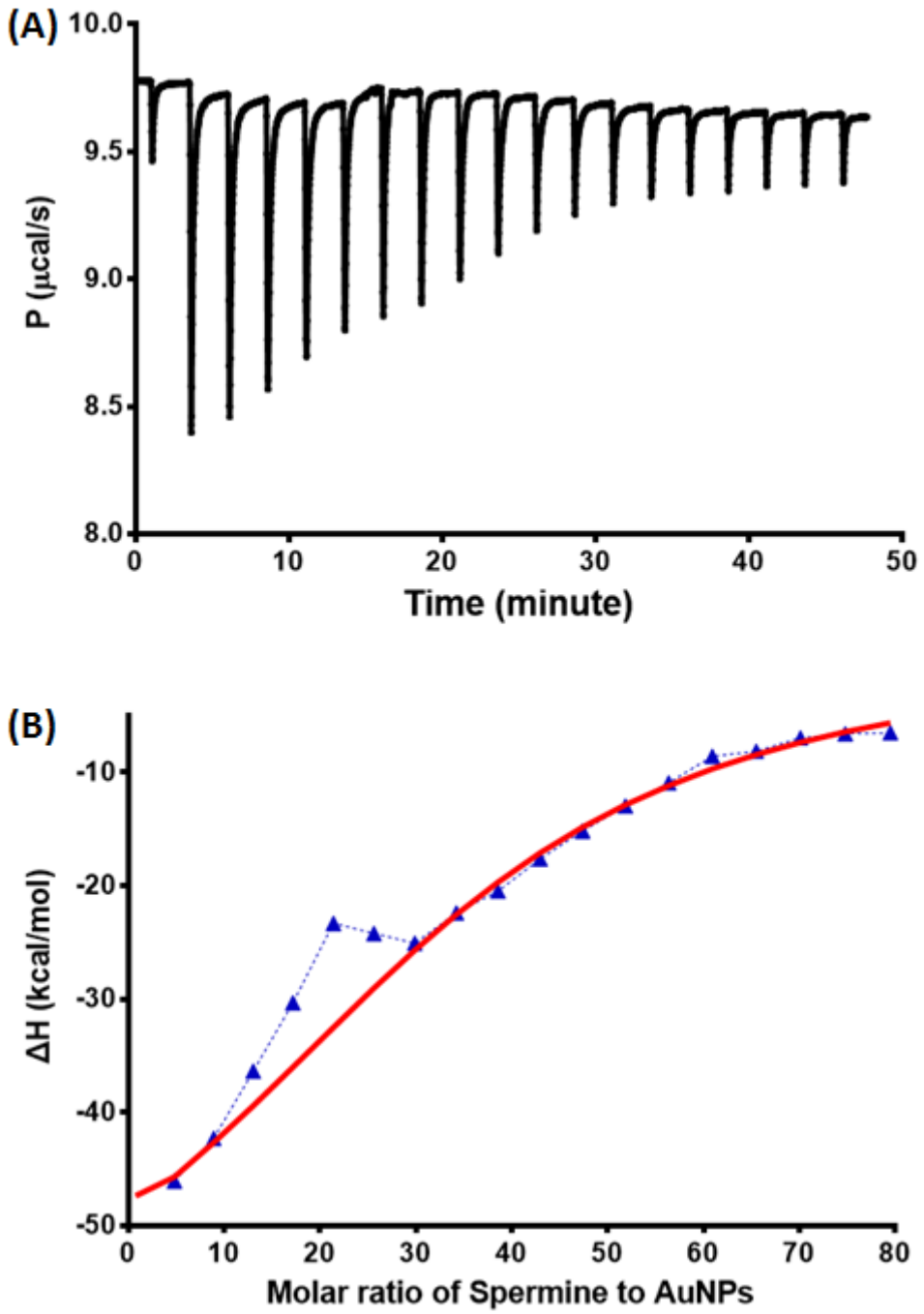

Figure 4.24 (A) The heat flow of each injection of Spm solution to AuNPs solution as a function of time at 0µM DNA concentration. (B) The corresponding integration of each peak in (A) as a function of molar ratio of Spm to AuNPs.

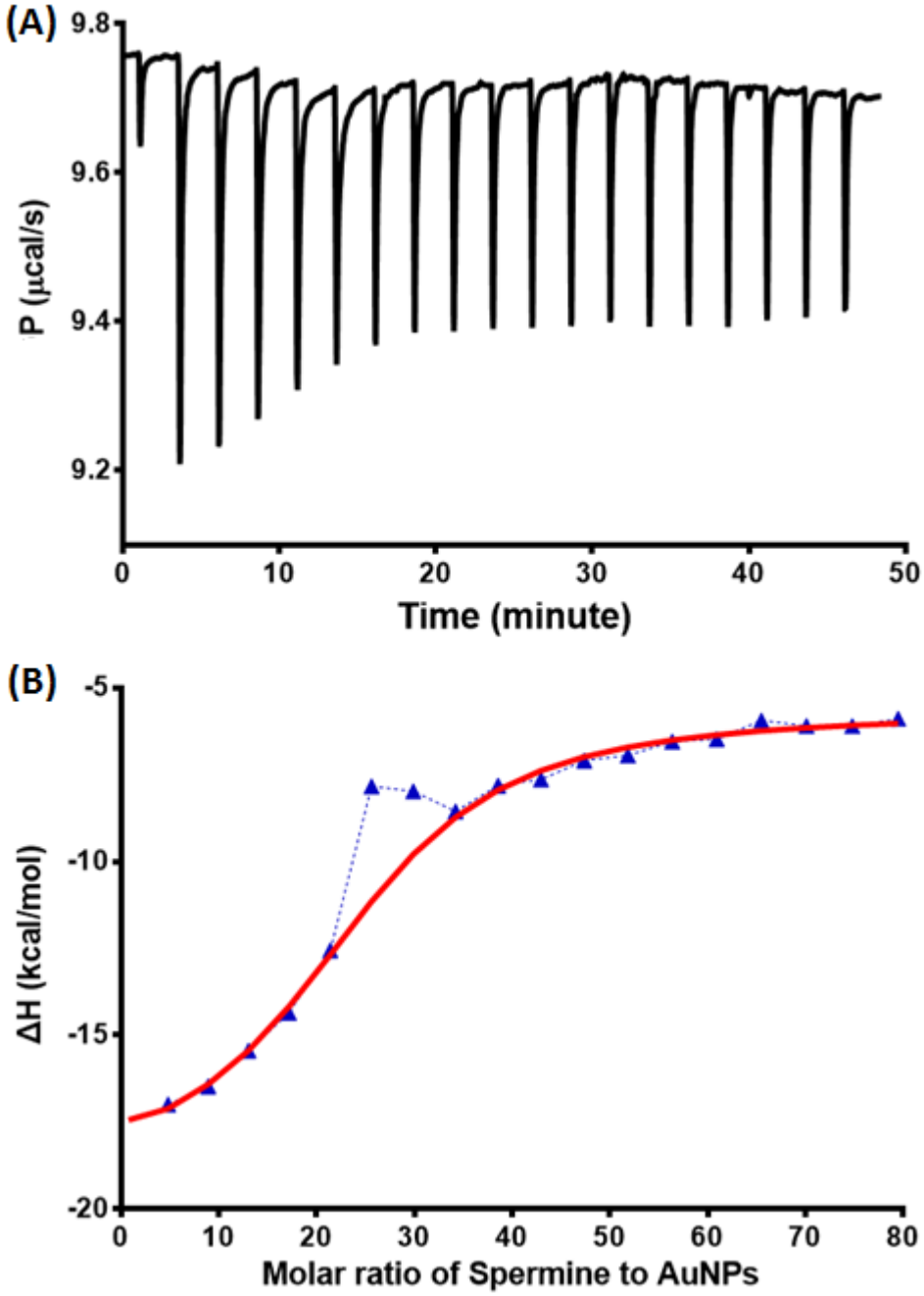

Figure 4.25 (A) The heat flow of each injection of Spm solution to AuNPs solution as a function of time at 0.5µM DNA concentration. (B) The corresponding integration of each peak as a function of molar ratio of Spm to AuNPs.

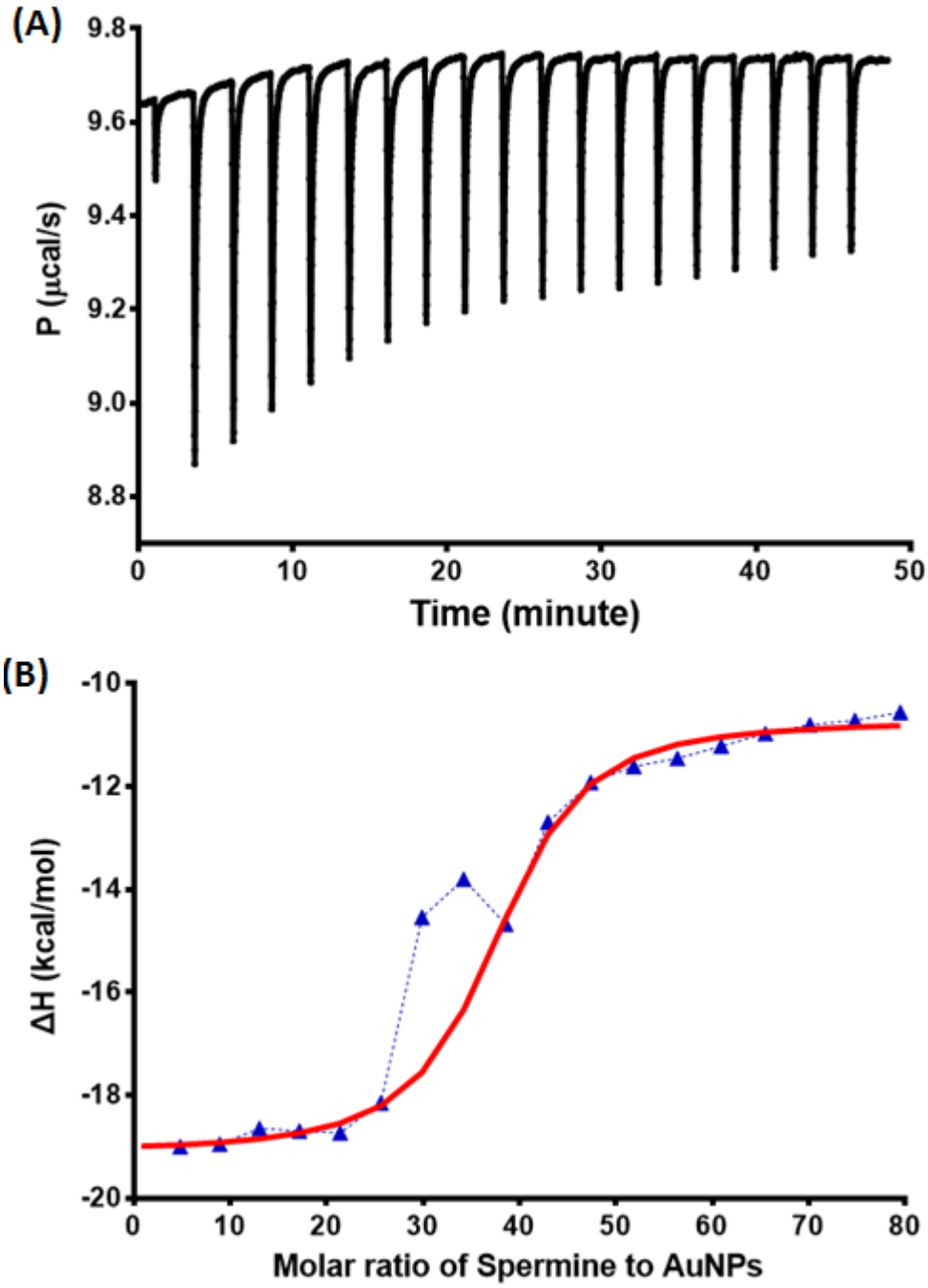

Figure 4.26 (A) The heat flow of each injection of Spm solution to AuNPs solution as a function of time at 1µM DNA concentration. (B) The corresponding integration of each peak as a function of molar ratio of Spm to AuNPs.

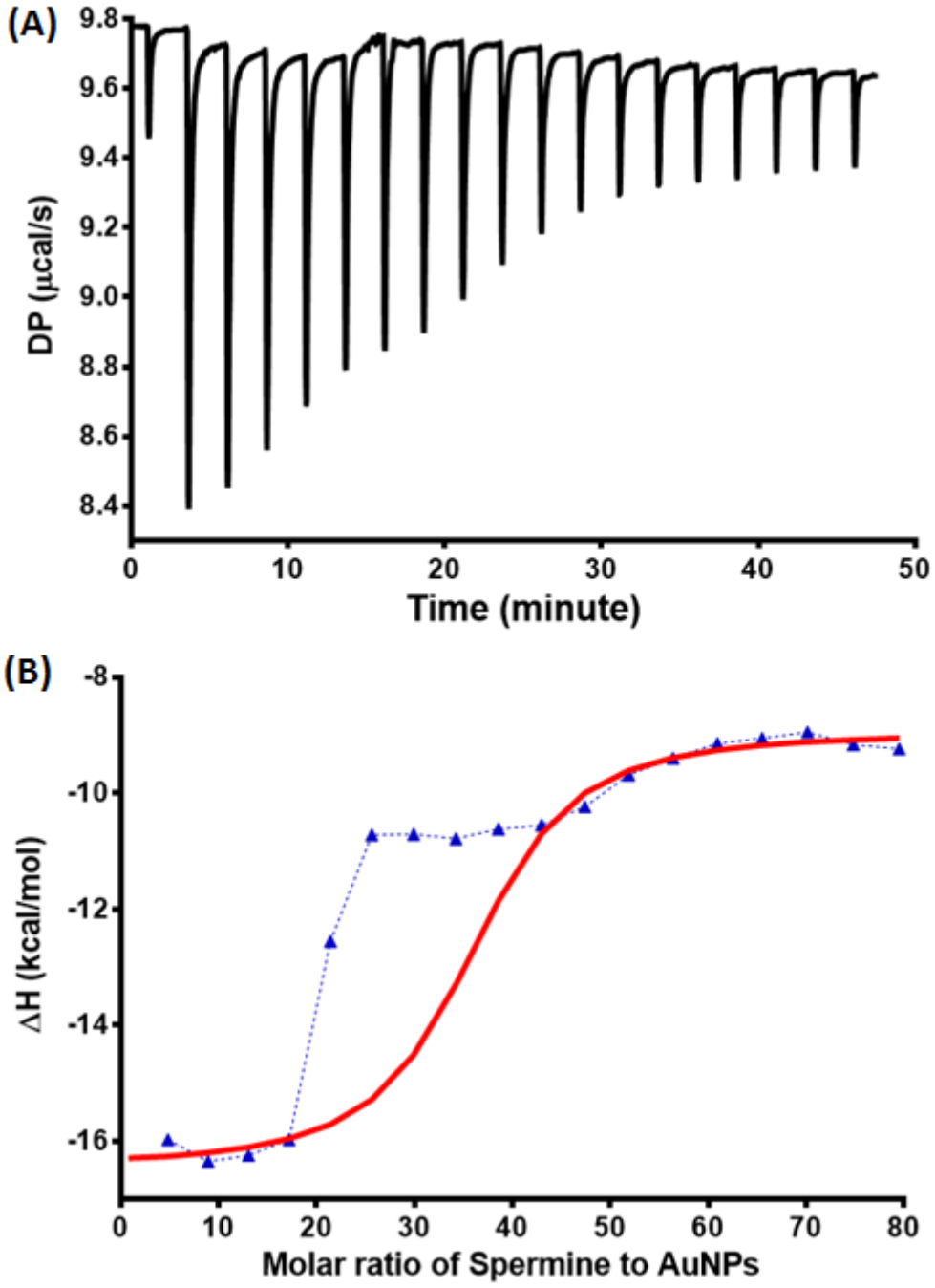

Figure 4.27 (A) The heat flow of each injection of Spm solution to AuNPs solution as a function of time at 3µM DNA concentration. (B) The corresponding integration of each peak as a function of molar ratio of Spm to AuNPs.

DNA concentration (μM)	N (sites)	K_D (M)	ΔH (kcal/mol)	ΔG (kcal/mol)	TΔS (kcal/mol)
0	10	8.13×10^{-6}	-67.9	-6.95	-61.0
0.5	10	2.03×10^{-6}	-13.4	-7.77	-5.68
1	10	3.45×10^{-6}	-8.40	-8.82	0.418
3	10	4.72×10^{-7}	-7.52	-8.63	1.12

Table 4.3 Thermodynamic parameters of the binding of Spm to AuNPs at different DNA concentration. (0-3μM) (K_D: dissociation constant; ΔH: enthalpy change; ΔG: Gibbs free energy change; T: temperature in Kelvin (298K); ΔS: entropy change)

In each case the binding isotherm showed an extra enthalpic peak deviating from the fitting model. Rautaray *et al.* had a similar observation before during their study of the interactions between calcium ions and aspartic acid-capped AuNPs. [71] They suggested that the peak was due to the aggregation of AuNPs as a consequence of negative charges on aspartic acid groups being neutralized by the positively charged calcium ions. This statement seemed reasonable when being applied in our case. We could observe the enthalpic peak indeed gradually shifted to a higher molar ratio of Spm to AuNP when more DNAs were being added, implying that the AuNPs aggregation was only initiated at a higher concentration of Spm. This matched well with the results from UV-Vis absorption measurements which revealed the decline of sensitivity towards Spm at high DNA concentration.

Analyzing the thermodynamic parameters carefully, we knew that Spm induced aggregation of AuNPs mainly happened via an enthalpy-driven electrostatic/hydrogen-bonding interaction with both DNAs and citrates as reflected from the comparatively large negative values of ΔH. The entropy component gradually became more favorable as the DNA concentration increased, but it was still weak and enthalpy remained as the major driving force. Similarly Morgan *et al.* reported long time ago that spermine interacts with DNA primarily through electrostatic interaction, while minor non-electrostatic interactions are also present, which is similar to results of our later ITC experiment on DNA and different polyamine analogs. [72] Therefore, the gradual drop of ΔH strength with increasing DNA concentrations implied the weakening of such electrostatic/hydrogen-bonding interactions. From these results, we hypothesized Spm interacting with AuNPs electrostatically primarily through the surface citrate ligands, but not through the DNA aptamers mainly. The role of DNA in the current developed aptasensor was to displace surficial citrate ligands for providing a better protection, and concurrently to control the extent of the major citrate-Spm interaction, AuNPs' aggregation rate and therefore the analytical performance of the aptasensor.

To further confirm the importance of surface citrate during aggregation, another ITC experiment was performed to study the interactions of polyamine analogs with pure citrate and DNA solution separately. While there are three carboxylate groups in free citrate ligand for interacting with Spm, the conformation is different when being capped onto AuNPs. On average there may

be only one free carboxylate group available for each citrate ligand for interaction, according to the proposed configurations by Park *et al.* (Figure 4.6) Despite this structural difference, the cross-reactivity sequence determined from UV-Vis absorption measurements of AuNPs (Spm > Spd > His > Put = Arg = Tyr = Cad = Orn = Crea = Control) was quite similar to that of the ΔH strength sequence obtained from the ITC profile of free citrate (Spm > Spd > His > Put > Arg > Tyr = Cad = Orn = Crea = Control), but not to that of the DNA. (See Table 4.4 and 4.5 for the summarized thermodynamics data of free citrate and DNA obtained from ITC, Figure 4.28 for selectivity data obtained from UV-Vis spectroscopy, Appendix for ITC spectrum) This result might indirectly imply the importance of surface citrates in achieving aggregation.

Analyte	**Fitness of binding model**	**N (sites)**	**K_D (M)**	**ΔH (kcal/ mol)**	**ΔG (kcal/ mol)**	**TΔS (kcal/ mol)**
Spermine	Good	1.40×10^{-2}	1.26×10^{-6}	-36.9	-8.05	-28.8
Spermidine	Good	3.80×10^{-2}	2.11×10^{-6}	-18.4	-7.74	-10.7
Histamine	Moderate	9.96	6.56×10^{-3}	-15.6	-2.98	-12.7
Putrescine	Good	4.10×10^{-2}	1.41×10^{-6}	-14.5	-7.98	-6.54
Arginine	Poor	3.68	3.65×10^{-3}	-6.45	-3.33	-3.13
Tyramine	Poor	0.102	3.88×10^{-6}	-0.24	-7.38	7.14
Cadaverine	Cannot be fitted	N/A	N/A	N/A	N/A	N/A
Ornithine	Cannot be fitted	N/A	N/A	N/A	N/A	N/A
Creatinine	Cannot be fitted	N/A	N/A	N/A	N/A	N/A
Control (water)	Cannot be fitted	N/A	N/A	N/A	N/A	N/A

Table 4.4 Thermodynamic parameters of the binding of free citrate to different polyamine analogs.

Analyte	Fitness of binding model	N (sites)	K_D (M)	ΔH (kcal/ mol)	ΔG (kcal/ mol)	TΔS (kcal/ mol)
Spermine	Good	3.65	1.10×10^{-6}	-7.83	-8.13	0.308
Spermidine	Good	4.01	1.11×10^{-6}	-4.44	-8.13	3.69
Histamine	Good	6.31	1.27×10^{-5}	-3.61	-6.68	3.07
Putrescine	Good	3.77	3.97×10^{-6}	-7.29	-7.37	0.08
Arginine	Good	2.44	1.42×10^{-5}	-4.59	-6.61	2.03
Tyramine	Good	10.0	3.06×10^{-5}	-13.6	-6.16	-7.46
Cadaverine*	Good	6.31	9.33×10^{-6}	1.06	-6.86	7.93
Ornithine	Cannot be fitted	N/A	N/A	N/A	N/A	N/A
Creatinine	Cannot be fitted	N/A	N/A	N/A	N/A	N/A
Control (water)	Cannot be fitted	N/A	N/A	N/A	N/A	N/A

* Cadaverine interacted with DNA following an endothermic pathway.

Table 4.5 Thermodynamic parameters of the binding of DNA to different polyamine analogs.

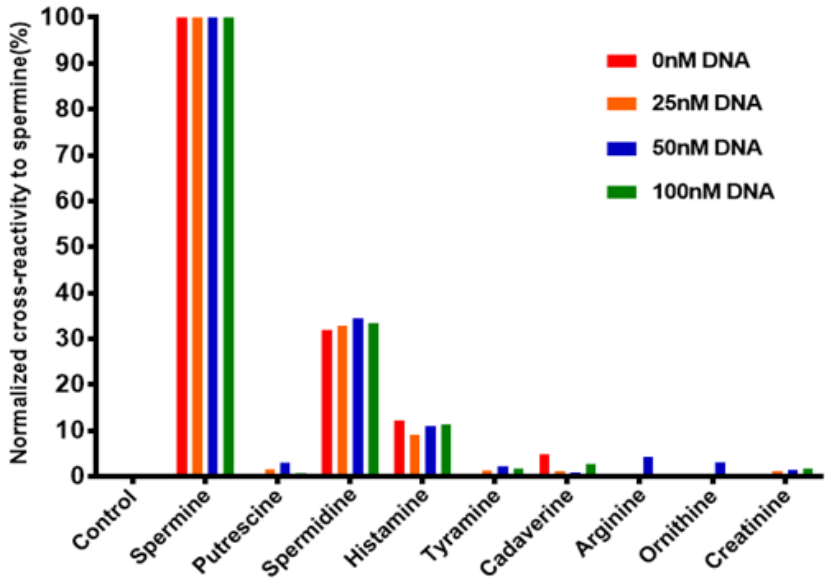

Figure 4.28 Selectivity profile of the current aptasensor at different DNA concentration. (0-100nM) In each case control (only water) and Spm were normalized to 0 and 100% respectively. (Polyamines concentration used = 5μM)

To further show that DNA only play a minor role in the interactions with Spm in causing aggregation, we tried to monitor the selectivity profile of AuNPs at different DNA concentrations. Cross-reactivity of each polyamine analogs were determined by comparing the Abs_{610}/Abs_{512} to that of Spm. The thought behind this experiment was that citrate and DNA should both have their own selectivity profile towards different polyamine analogs, as revealed from the ITC experiments done before. Upon modulating their capping ratio by adding more DNAs for displacing citrate, we expected to see some trends of change on the overall selectivity profile of AuNPs. After normalization, however; we could observe from Figure 4.27 that there was not much difference among the tested conditions. It means that DNA indeed had only weak or insignificant interactions with Spm and other polyamine analogs in causing any changes in the overall selectivity of AuNPs. Therefore we suspected citrate to be the key component in spermine-induced aggregation of AuNPs. This also explains why Liu *et al.* reported a similar aggregation phenomenon of DNA capped AuNPs using two DNAs with widely different base sequences, despite DNA-polyamine interaction was reported to be affected by factors like DNA conformation, base composition and sequence. [67, 73] Another proof-of-concept experiment also indirectly indicated the importance of citrate groups: strong acid was added to DNA-AuNPs before adding SPM. It was found that SPM could not induce AuNPs aggregation anymore in such an extreme acidic condition. We suspected it was due to the complete protonation of citrate groups for further interaction with SPM, or even detachment from the surface of AuNPs.

To demonstrate that the current developed aptasensor was fitted for its intended purpose for detecting SPM content, its applicability was being validated in one of the most SPM-content concerning sample: human urine. Artificial urine was prepared to mimic clinical urine during early investigation. Unfortunately, under the described optimal condition, the aptasensor failed to work properly since artificial urine is having a high salt concentration which could effectively screen negative charges for aggregation, and AuNPs could not tolerate it even in the absence of SPM. The origin of such an undesired aggregation was a result of insufficient AuNPs protection by the surfactants. Clearly addition of only 25nM DNA was not enough for working in such complicated matrix and to provide further protection, the working DNA concentration was elevated to 250nM. Figure 4.29 showed the titration profile of DNA-AuNPs absorption spectrum against artificial urine with different dilution factor. With more matrix components, which were mainly inorganic salts, the absorbance of plasmonic peak declined gradually owing to the greater extent of DNA adsorption. Results showed that 250nM DNA was enough to protect AuNPs from aggregation up to two-fold diluted artificial urine.

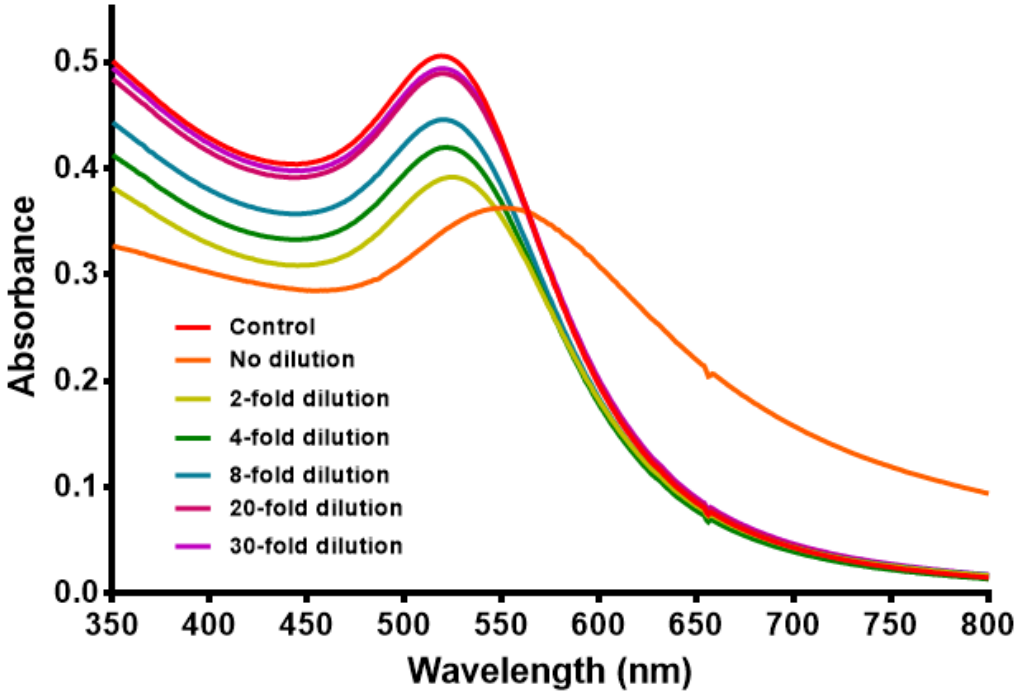

Figure 4.29 Absorption spectrum of DNA-AuNPs upon addition of artificial urine with different dilution factor.

SPM was spiked into artificial urine and Figure 4.30 showed the absorption spectrum and corresponding calibration curve. Surprisingly, AuNPs responded to SPM with a totally different mechanism compared to that in blank matrix. As revealed from the absorption pattern, with a higher SPM concentration, the plasmonic peak declined gradually similar to the previous titration study of artificial urine matrix. It confirmed that SPM also helped to screened negative charges like salts and induced DNA adsorption. [74] Therefore a greater extent of DNA adsorption and even AuNPs precipitation were observed upon addition of SPM. Both of them accounted for the drop of plasmonic band. Figure 4.31 summarizes the two sensing mechanisms of our developed aptasensor.

The decrease was also found to correlate with SPM concentration with a linear relationship. A wider linear calibration curve from 0-18μM could be obtained which matched perfectly with that of general urinary SPM content. Spike analysis in artificial urine by a matrix-match calibration approach gave both satisfactory recovery and reproducibility. [75-76] (Table 4.6)

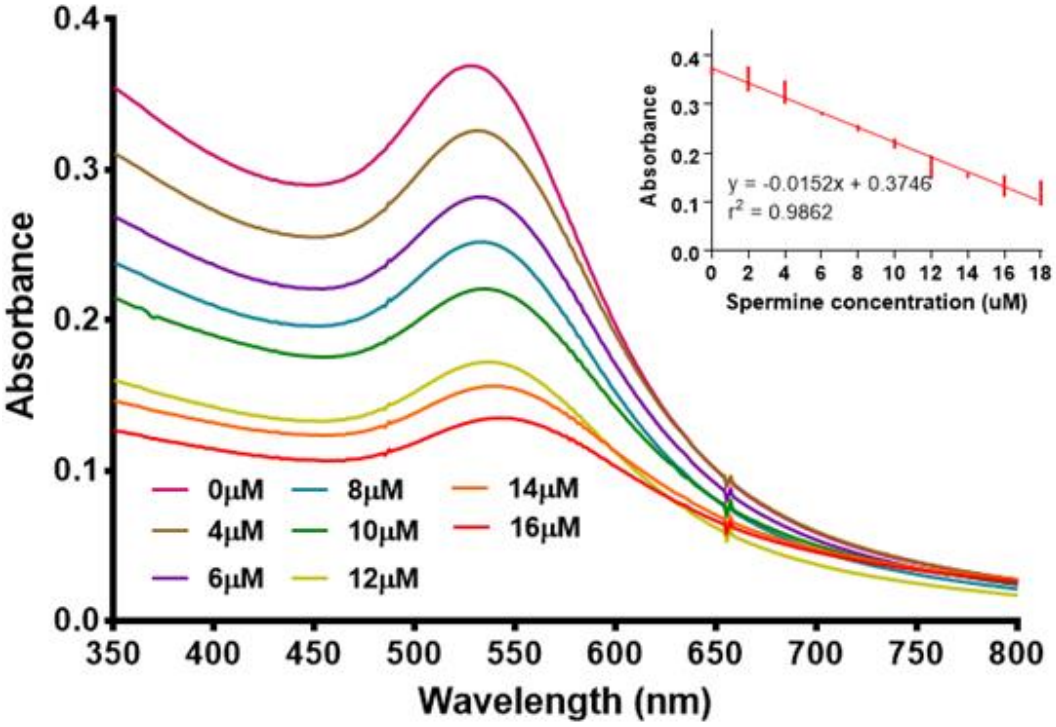

Figure 4.30 The SPM induced aggregation on DNA-AuNPs in artificial urine matrix - The absorption spectra of DNA-AuNPs upon addition of SPM solution. (0-18μM) Inset: Plot of Abs_{512} vs SPM concentration.

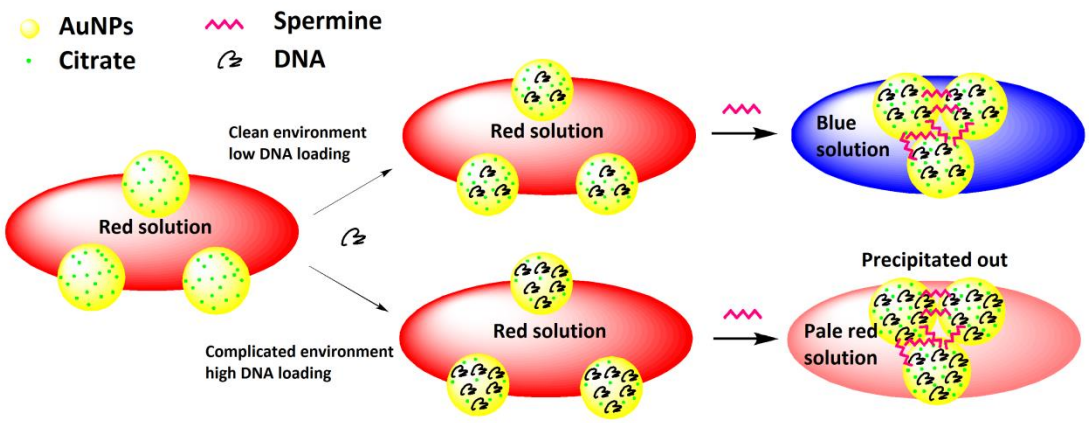

Figure 4.31 Schematic diagram of the developed aptasensor for SPM sensing via two different pathways. Different amount of DNA was adsorbed onto AuNPs by displacing the original citrate surfactants. Later addition of positively charged SPM would induce either the aggregation of DNA-AuNPs which resulted in a red shift of plasmonic peak, or the precipitation of DNA-AuNPs which resulted in a decline of plasmonic band absorbance.

To further demonstrate the applicability of the aptasensor for a fast urinary SPM screening, three clinical urine samples from cancerous patients were selected for further spike analysis. Before that, common urinary components (Urea, uric acid, glutathione, Human Serum Albumin, calcium salt and creatinine) were tested to check if they interfered seriously with SPM sensing. (Figure 4.32) Results showed that only human serum albumin would cause slight AuNPs aggregation since protein is also a highly charged molecule. Therefore all the clinical urine samples were passed through Amicon centrifugal filter to remove any large protein molecules. SPM was then spiked into pre-treated urine and analyzed by the

aptasensor again by a matrix-match calibration approach. The good accuracy values further confirmed the successful applicability of the aptasensor in real samples. (Table 4.6)

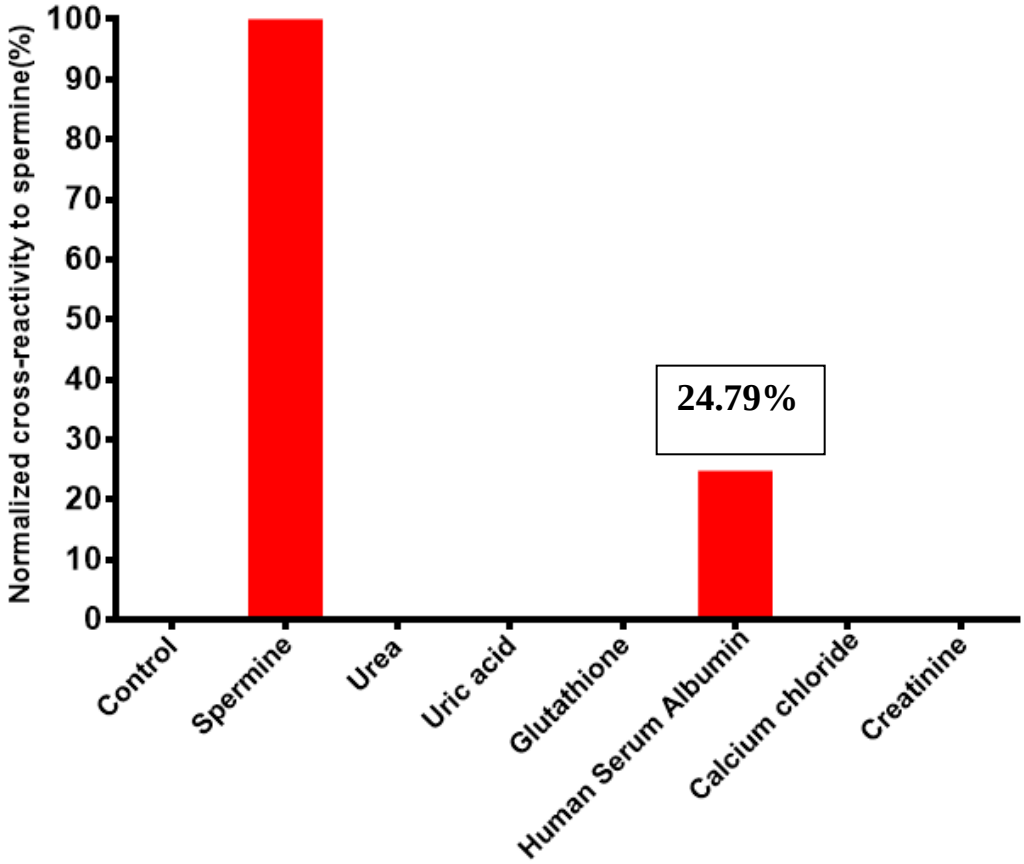

Figure 4.32 Cross-reactivity of urinary components to spermine by developed aptasensor. In each case control (water) and spermine were normalized to 0 and 100% respectively. (Concentration used = 4µM)

Sample	Amount spiked (μM)	Average recovery (%)	Relative standard deviation (%)
Artificial urine	2.0	87.90	5.46
	4.0	100.61	0.07
	6.0	94.76	2.65
	8.0	106.70	2.01
Urine 1	3.0	98.80	9.52
Urine 2	3.0	121.98	7.76
Urine 3	3.0	104.09	4.21

Table 4.6 Determination of spiked SPM in artificial urine and clinical urine specimen. (n=3)

4.4 References

1. Rodriguez, M. B. R., da Silva Carneiro, C., da Silva Feijó, M. B., Júnior, C. A. C., & Mano, S. B. (2014). Bioactive amines: aspects of quality and safety in food. *Food and Nutrition Sciences*, *2014*.
2. Santos, M. S. (1996). Biogenic amines: their importance in foods. *International Journal of Food Microbiology*, *29*(2), 213-231.
3. Silva, T. M., Sabaini, P. S., Evangelista, W. P., & Gloria, M. B. A. (2011). Occurrence of histamine in Brazilian fresh and canned tuna. *Food Control*, *22*(2), 323-327.
4. Balamatsia, C. C., Paleologos, E. K., Kontominas, M. G., & Savvaidis, I. N. (2006). Correlation between microbial flora, sensory changes and biogenic amines formation in fresh chicken meat stored aerobically or under modified atmosphere packaging at 4 C: possible role of biogenic amines as spoilage indicators. *Antonie van Leeuwenhoek*, *89*(1), 9-17.
5. Cohen, G., Laloush, M., & Karpas, Z. (2014). Biogenic amines in bread as indicators of spoilage. *International Journal for Ion Mobility Spectrometry*, *17*(3-4), 125-129.
6. Martuscelli, M., Arfelli, G., Manetta, A. C., & Suzzi, G. (2013). Biogenic amines content as a measure of the quality of wines of Abruzzo (Italy). *Food Chemistry*, *140*(3), 590-597.
7. Veciana-Nogues, M. T., Mariné-Font, A., & Vidal-Carou, M. C. (1997). Biogenic amines as hygienic quality indicators of tuna. Relationships with

microbial counts, ATP-related compounds, volatile amines, and organoleptic changes. *Journal of Agricultural and Food Chemistry*, *45*(6), 2036-2041.

8. Fleisher, J. H., & Russell, D. H. (1975). Estimation of urinary diamines and polyamines by thin-layer chromatography. *Journal of Chromatography A*, *110*(2), 335-340.
9. Khuhawar, M. Y., Memon, A. A., Jaipal, P. D., & Bhanger, M. I. (1999). Capillary gas chromatographic determination of putrescine and cadaverine in serum of cancer patients using trifluoroacetylacetone as derivatizing reagent. *Journal of Chromatography B: Biomedical Sciences and Applications*, 723(1), 17-24.
10. Fujihara, S., Nakashima, T., & Kurogochi, Y. (1983). Determination of polyamines in human blood by electron-capture gas—liquid chromatography. *Journal of Chromatography B: Biomedical Sciences and Applications*, *277*, 53-60.
11. Muskiet, F. A., Van den Berg, G. A., Kingma, A. W., Fremouw-Ottevangers, D. C., & Halie, M. R. (1984). Total polyamines and their non-alpha-amino acid metabolites simultaneously determined in urine by capillary gas chromatography, with nitrogen-phosphorus detector; and some clinical applications. *Clinical Chemistry*, *30*(5), 687-695.
12. Kamei, S., Ohkubo, A., Saito, S., & Takagi, S. (1989). Polyamine detection system for high-performance liquid chromatography involving enzymic and chemiluminescent reactions. *Analytical Chemistry*, *61*(17), 1921-1924.
13. Vandenabeele, O., Garrelly, L., Ghelfenstein, M., Commeyras, A., & Mion, L. (1998). Use of 2-chloroethylnitrosourea, a new type of pre-column derivatizing

agent for the measurement of biogenic amines, by high-performance liquid chromatography with ultraviolet detection. *Journal of Chromatography A*, 795(2), 239-250.

14. Du, M., Flanigan, V., & Ma, Y. (2004). Simultaneous determination of polyamines and catecholamines in PC-12 tumor cell extracts by capillary electrophoresis with laser-induced fluorescence detection. *Electrophoresis*, *25*(10-11), 1496-1502.
15. Byun, J. A., Lee, S. H., Jung, B. H., Choi, M. H., Moon, M. H., & Chung, B. C. (2008). Analysis of polyamines as carbamoyl derivatives in urine and serum by liquid chromatography–tandem mass spectrometry. *Biomedical Chromatography*, *22*(1), 73-80.
16. Liu, R., Bi, K., Jia, Y., Wang, Q., Yin, R., & Li, Q. (2012). Determination of polyamines in human plasma by high-performance liquid chromatography coupled with Q-TOF mass spectrometry. *Journal of Mass Spectrometry*, *47*(10), 1341-1346.
17. Draisci, R., Cavalli, S., Lucentini, L., & Stacchini, A. (1993). Ion exchange separation and pulsed amperometric detection for determination of biogenic amines in fish products. *Chromatographia*, *35*(9-12), 584-590.
18. Casella, I. G., Palladino, G. A., & Contursi, M. (2008). Determination of aliphatic amines by cation-exchange chromatography with suppressed conductivity detection after solid phase extraction. *Journal of Separation Science*, *31*(21), 3718-3726.

19. Sadain, S. K., & Koropchak, J. A. (1999). Condensation nucleation light scattering detection for biogenic amines separated by ion-exchange chromatography. *Journal of Chromatography A*, *844*(1), 111-118.

20. Tombelli, S., & Mascini, M. (1998). Electrochemical biosensors for biogenic amines: a comparison between different approaches. *Analytica Chimica Acta*, *358*(3), 277-284.

21. Liu, J., Yang, X., & Wang, E. (2003). Direct tris (2, 2'-bipyridyl) ruthenium (II) electrochemiluminescence detection of polyamines separated by capillary electrophoresis. *Electrophoresis*, 24(18), 3131-3138.

22. Jornet-Martinez, N., González-Béjar, M., Moliner-Martínez, Y., Campins-Falco, P., & Pérez-Prieto, J. (2014). Sensitive and selective plasmonic assay for spermine as biomarker in human urine. *Analytical Chemistry*, 86(3), 1347-1351.

23. Tu, J., Sun, S., & Xu, Y. (2016). A novel self-assembled platform for the ratiometric fluorescence detection of spermine. *Chemical Communications*, 52(5), 1040-1043.

24. Kim, T. I., & Kim, Y. (2016). Analyte-directed formation of emissive excimers for the selective detection of polyamines. *Chemical Communications*, 52(70), 10648-10651.

25. Chopra, S., Singh, J., Kaur, H., Singh, A., Singh, N., & Kaur, N. (2015). Colorimetric Detection of Spermine by the Cu^{II} Complex of Imine-Based Organic Nanoaggregates in Aqueous Medium. *European Journal of Inorganic Chemistry*, 2015(26), 4437-4442.

26. Malik, A. H., Hussain, S., & Iyer, P. K. (2016). Aggregation-Induced FRET via Polymer–Surfactant Complexation: A New Strategy for the Detection of Spermine. *Analytical Chemistry*, 88(14), 7358-7364.
27. Kim, T. I., Park, J., & Kim, Y. (2011). A Gold Nanoparticle-Based Fluorescence Turn-On Probe for Highly Sensitive Detection of Polyamines. *Chemistry–A European Journal*, 17(43), 11978-11982.
28. Rawat, K. A., Bhamore, J. R., Singhal, R. K., & Kailasa, S. K. (2016). Microwave assisted synthesis of tyrosine protected gold nanoparticles for dual (colorimetric and fluorimetric) detection of spermine and spermidine in biological samples. *Biosensors and Bioelectronics*.
29. Chow, C. F., Kong, H. K., Leung, S. W., Chiu, B. K., Koo, C. K., Lei, E. N., ... & Wong, W. Y. (2010). Heterobimetallic Ru (II)− Eu (III) Complex as Chemodosimeter for Selective Biogenic Amine Odorants Detection in Fish Sample. *Analytical Chemistry*, 83(1), 289-296.
30. Satrijo, A., & Swager, T. M. (2007). Anthryl-doped conjugated polyelectrolytes as aggregation-based sensors for nonquenching multicationic analytes. *Journal of the American Chemical Society*, *129*(51), 16020-16028.
31. Louis, C., & Pluchery, O. (2012). *Gold nanoparticles for physics, chemistry and biology* (pp. 106-124). London: Imperial College Press.
32. Eustis, S., & El-Sayed, M. A. (2006). Why gold nanoparticles are more precious than pretty gold: noble metal surface plasmon resonance and its enhancement of the radiative and nonradiative properties of nanocrystals of different shapes. *Chemical Society Reviews*, *35*(3), 209-217.

33. Huang, X., & El-Sayed, M. A. (2010). Gold nanoparticles: optical properties and implementations in cancer diagnosis and photothermal therapy. *Journal of Advanced Research*, *1*(1), 13-28.

34. Mie, G. (1908). A contribution to the optics of turbid media, especially colloidal metallic suspensions. *Annals of Physics*, 25, 377-445.

35. Njoki, P. N., Lim, I. I. S., Mott, D., Park, H. Y., Khan, B., Mishra, S., ... & Zhong, C. J. (2007). Size correlation of optical and spectroscopic properties for gold nanoparticles. *The Journal of Physical Chemistry C*, *111*(40), 14664-14669.

36. Alex, S., & Tiwari, A. (2015). Functionalized gold nanoparticles: synthesis, properties and applications—a review. *Journal of Nanoscience and Nanotechnology*, *15*(3), 1869-1894.

37. Turkevich, J., Stevenson, P. C., & Hillier, J. (1951). A study of the nucleation and growth processes in the synthesis of colloidal gold. *Discussions of the Faraday Society*, *11*, 55-75.

38. Kettemann, F., Birnbaum, A., Witte, S., Wuithschick, M., Pinna, N., Kraehnert, R., ... & Polte, J. (2016). The missing piece of the mechanism of the Turkevich method: The critical role of citrate protonation. *Chemistry of Materials*.

39. Wuithschick, M., Birnbaum, A., Witte, S., Sztucki, M., Vainio, U., Pinna, N., ... & Polte, J. (2015). Turkevich in new robes: key questions answered for the most common gold nanoparticle synthesis. *ACS Nano*, *9*(7), 7052-7071.

40. Zhao, P., Li, N., & Astruc, D. (2013). State of the art in gold nanoparticle synthesis. *Coordination Chemistry Reviews*, *257*(3), 638-665.

41. Kumar, S., Gandhi, K. S., & Kumar, R. (2007). Modeling of formation of gold nanoparticles by citrate method. *Industrial & Engineering Chemistry Research*, *46*(10), 3128-3136.

42. Park, J. W., & Shumaker-Parry, J. S. (2014). Structural study of citrate layers on gold nanoparticles: role of intermolecular interactions in stabilizing nanoparticles. *Journal of the American Chemical Society*, *136*(5), 1907-1921.

43. Patungwasa, W., & Hodak, J. H. (2008). pH tunable morphology of the gold nanoparticles produced by citrate reduction. *Materials Chemistry and Physics*, *108*(1), 45-54.

44. Rohiman, A., Anshori, I., Surawijaya, A., & Idris, I. (2011, December). Study of colloidal gold synthesis using Turkevich method. In *THE 4TH NANOSCIENCE AND NANOTECHNOLOGY SYMPOSIUM (NNS2011): An International Symposium* (Vol. 1415, No. 1, pp. 39-42). AIP Publishing.

45. Kim, J. H., Lavin, B. W., Burnett, R. D., & Boote, B. W. (2011). Controlled synthesis of gold nanoparticles by fluorescent light irradiation. *Nanotechnology*, *22*(28), 285602.

46. Ojea-Jiménez, I., Romero, F. M., Bastús, N. G., & Puntes, V. (2010). Small gold nanoparticles synthesized with sodium citrate and heavy water: insights into the reaction mechanism. *The Journal of Physical Chemistry C*, *114*(4), 1800-1804.

47. Kasthuri, J., Veerapandian, S., & Rajendiran, N. (2009). Biological synthesis of silver and gold nanoparticles using apiin as reducing agent. *Colloids and Surfaces B: Biointerfaces*, *68*(1), 55-60.

48. Newman, J. D. S., & Blanchard, G. J. (2006). Formation of gold nanoparticles using amine reducing agents. *Langmuir*, *22*(13), 5882-5887.

49. Sarma, T. K., Chowdhury, D., Paul, A., & Chattopadhyay, A. (2002). Synthesis of Au nanoparticle–conductive polyaniline composite using H_2O_2 as oxidising as well as reducing agent. *Chemical Communications*, (10), 1048-1049.

50. Brown, K. R., Fox, A. P., & Natan, M. J. (1996). Morphology-dependent electrochemistry of cytochrome c at Au colloid-modified SnO2 electrodes. *Journal of the American Chemical Society*, *118*(5), 1154-1157.

51. Bakr, O. M., Wunsch, B. H., & Stellacci, F. (2006). High-yield synthesis of multi-branched urchin-like gold nanoparticles. *Chemistry of Materials*, *18*(14), 3297-3301.

52. Kim, D. K., Hwang, Y. J., Yoon, C., Yoon, H. O., Chang, K. S., Lee, G., ... & Yi, G. R. (2015). Experimental approach to the fundamental limit of the extinction coefficients of ultra-smooth and highly spherical gold nanoparticles. *Physical Chemistry Chemical Physics*, *17*(32), 20786-20794.

53. Balan, L., Melinte, V., Buruiana, T., Schneider, R., & Vidal, L. (2012). Controlling the morphology of gold nanoparticles synthesized photochemically in a polymer matrix through photonic parameters. *Nanotechnology*, *23*(41), 415705.

54. Novikov, S. M., Sánchez-Iglesias, A., Schmidt, M. K., Chuvilin, A., Aizpurua, J., Grzelczak, M., & Liz-Marzán, L. M. (2014). Gold spiky nanodumbbells: anisotropy in gold nanostars. *Particle & Particle Systems Characterization*, *31*(1), 77-80.

55. Hernández, J., Solla-Gullón, J., Herrero, E., Aldaz, A., & Feliu, J. M. (2007). Electrochemistry of shape-controlled catalysts: Oxygen reduction reaction on cubic gold nanoparticles. *The Journal of Physical Chemistry C*, *111*(38), 14078-14083.

56. Lundén, H., Liotta, A., Chateau, D., Lerouge, F., Chaput, F., Parola, S., ... & Lopes, C. (2015). Dispersion and self-orientation of gold nanoparticles in sol–gel hybrid silica–optical transmission properties. *Journal of Materials Chemistry C*, *3*(5), 1026-1034.

57. Khlebtsov, N., & Dykman, L. (2011). Biodistribution and toxicity of engineered gold nanoparticles: a review of in vitro and in vivo studies. *Chemical Society Reviews*, *40*(3), 1647-1671.

58. Nehl, C. L., Liao, H., & Hafner, J. H. (2006). Optical properties of star-shaped gold nanoparticles. *Nano Letters*, *6*(4), 683-688.

59. Chen, Y., Gu, X., Nie, C. G., Jiang, Z. Y., Xie, Z. X., & Lin, C. J. (2005). Shape controlled growth of gold nanoparticles by a solution synthesis. *Chemical Communications*, (33), 4181-4183.

60. dos Santos Jr, D. S., Alvarez-Puebla, R. A., Oliveira Jr, O. N., & Aroca, R. F. (2005). Controlling the size and shape of gold nanoparticles in fulvic acid colloidal solutions and their optical characterization using SERS. *Journal of Materials Chemistry*, *15*(29), 3045-3049.

61. Carnerero, J. M., Jimenez-Ruiz, A., Castillo, P. M., & Prado-Gotor, R. (2016). Covalent and non-covalent DNA-Gold Nanoparticles interactions: New avenues of research. *ChemPhysChem*.

62. Zeng, S., Yong, K. T., Roy, I., Dinh, X. Q., Yu, X., & Luan, F. (2011). A review on functionalized gold nanoparticles for biosensing applications. *Plasmonics*, *6*(3), 491-506.

63. Gourishankar, A., Shukla, S., Ganesh, K. N., & Sastry, M. (2004). Isothermal titration calorimetry studies on the binding of DNA bases and PNA base monomers to gold nanoparticles. *Journal of the American Chemical Society*, *126*(41), 13186-13187.

64. Li, H., & Rothberg, L. (2004). Colorimetric detection of DNA sequences based on electrostatic interactions with unmodified gold nanoparticles. *Proceedings of the National Academy of Sciences of the United States of America*, *101*(39), 14036-14039.

65. Liu, J. (2012). Adsorption of DNA onto gold nanoparticles and graphene oxide: surface science and applications. *Physical Chemistry Chemical Physics*, *14*(30), 10485-10496.

66. Zhang, X., Servos, M. R., & Liu, J. (2012). Surface science of DNA adsorption onto citrate-capped gold nanoparticles. *Langmuir*, *28*(8), 3896-3902.

67. De Liu, Z., Zhu, H. Y., Zhao, H. X., & Huang, C. Z. (2013). Highly selective colorimetric detection of spermine in biosamples on basis of the non-crosslinking aggregation of ssDNA-capped gold nanoparticles. *Talanta*, *106*, 255-260.

68. Á lvarez, A., Costa, J. M., Pereiro, R., & Sanz-Medel, A. (2012) Reusable phosphorescent probes based on molecularly imprinted polymers for the

determination of propranolol in urine. *Sensors and Actuators B: Chemical*, 168, 370-375.

69. Gu, Y. J., Cheng, J., Lin, C. C., Lam, Y. W., Cheng, S. H., & Wong, W. T. (2009). Nuclear penetration of surface functionalized gold nanoparticles. *Toxicology and Applied Pharmacology*, *237*(2), 196-204.
70. Liu, X., Atwater, M., Wang, J., & Huo, Q. (2007). Extinction coefficient of gold nanoparticles with different sizes and different capping ligands. *Colloids and Surfaces B: Biointerfaces*, *58*(1), 3-7.
71. Rautaray, D., Mandal, S., & Sastry, M. (2005). Synthesis of hydroxyapatite crystals using amino acid-capped gold nanoparticles as a scaffold. *Langmuir*, 21(11), 5185-5191.
72. Morgan, J. E., Blankenship, J. W., & Matthews, H. R. (1986). Association constants for the interaction of double-stranded and single-stranded DNA with spermine, spermidine, putrescine, diaminopropane, N 1-and N 8-acetylspermidine, and magnesium: Determination from analysis of the broadening of thermal denaturation curves. *Archives of Biochemistry and Biophysics*, *246*(1), 225-232.
73. Bagheryan, Z., Noori, A., Bathaie, S. Z., Yousef-Elahi, M., & Mousavi, M. F. (2016). Preparation of a new nanobiosensor for the determination of some biogenic polyamines and investigation of their interaction with DNA. *Biosensors and Bioelectronics*, *77*, 767-773.
74. Gracie, K., Moores, M., Smith, W. E., Harding, K., Girolami, M., Graham, D., & Faulds, K. (2016). Preferential attachment of specific fluorescent dyes and

dye labeled dna sequences in a surface enhanced raman scattering multiplex. *Analytical Chemistry*, 88(2), 1147-1153.

75. Xiong, A., Li, Y., Yang, L., Gao, J., He, Y., Wang, C., & Wang, Z. (2009). Simultaneous determination of senecionine, adonifoline and their metabolites in rat serum by UPLC–ESIMS and its application in pharmacokinetic studies. *Journal of Pharmaceutical and Biomedical Analysis*, 50(5), 1070-1074.
76. Tsoi, T. H.; Wong, W. T. (2015) A simple, highly sensitive, high throughput and organic solvent-free screening method for melamine by microsphere-based flow cytometry immunoassay. *Analytical Methods*, *7(14)*, 5989-5995.

4.5 Appendix

Technique	Derivatization	Target polyamines	Reference
Thin layer chromatography	Dansylated derivatives	Put, Cad, Spd, Spm	[8]
GC with flame ionization detector	Trifluoroacetylacetone derivatives	Put, Cad	[9]
GC with electron capture detector	Heptafluorobutyric derivatives	Put, Spd, Spm	[10]
GC with nitrogen phosphorus detector	Methyl-heptafluorobutyryl derivatives	Dap, Put, Cad, Spd, Spm, Ipt , Pt , and Spm acid 1	[11]
Chemiluminescence based HPLC	Requires enzymatic oxidation for generating H_2O_2	Put, Cad, Spd, Spm	[12]
HPLC with UV detector	2-chloroethylnitrosourea derivatives	Put, Cad, His	[13]
Capillary electrophoresis with laser induced fluorescence detection	Fluorescein isothiocyanate derivatives	Put, Spd, Spm	[14]
LCMS	Carbamylated derivatives	Dap, Put, Cad, N-actPut, N-actCad, Spd, Spm, N-actSpm,	[15]
Q-TOF MS	Benzoyl chloride derivatives	Dap, Put, Cad, Spd, Spm	[16]
Ion exchange chromatography with pulsed amperometric detection	/	Put, Cad, Spd, His	[17]
Ion exchange chromatography with suppressed conductivity detection	/	Put, Cad, His, Spd, Spm, Me, Pr, 2-B, n-B, Ag, Tyr	[18]
Ion exchange chromatography with condensation	/	Put, Cad, His	[19]

nucleation light scattering detector			
Indirect fluorescence based HPLC	/	Put, Spd, Cad, His, Br	[20]
Capillary electrophoresis with electro-chemiluminescence detection	/	Put, Cad, Spd, Spm	[21]

Table A4.1 Summary of classical polyamines detection techniques. (Put: Putrescine; Spd: Spermidine; Spm: Spermine; Cad: Cadaverine; Dap: 1,3-Diaminopropane; Ipt: Isoputreanine; Pt: Putreanine; Spm acid 1: N-(3-aminopropyl)-*N*-(2-carboxyethyl)-1 4-Diaminobutane; *N*-actPut: *N*-acetylputrescine; *N*-actCad: *N*-acetylcadaverine; *N*-actSpm: *N*-acetylspermine; Me: Methylamine; Pr: Propylamine; 2-B: 2-Butylamine; n-B: *N*-Butylamine; Ag: Agmatine; Tyr: Tyramine; Br: Benzylamine)

Technique	Target polyamines	Reference
Naked gold nanoparticles (AuNPs)	Spm	[22]
Self-assembled platform of squaraine-embedded micelles	Spm	[23]
Analyte-directed formation of emissive excimers	Spm	[24]
Copper (II) Complex of imine-based organic nanoaggregates	Spm	[25]
Aggregation induced fluorescence resonance energy transfer via polymer-surfactant complexation	Spm	[26]
AuNPs Based Fluorescence Turn-On Probe	Spm, Spd	[27]
Tyrosine-AuNPs	Spm, Spd	[28]
Ruthenium(II)−Europium(III) heterobimetallic complexes	Put, Spd, His	[29]
Anthryl-doped conjugated polyelectrolytes	Put, Spd, Spm	[30]

Table A4.2 Recent advances in polyamines detection.

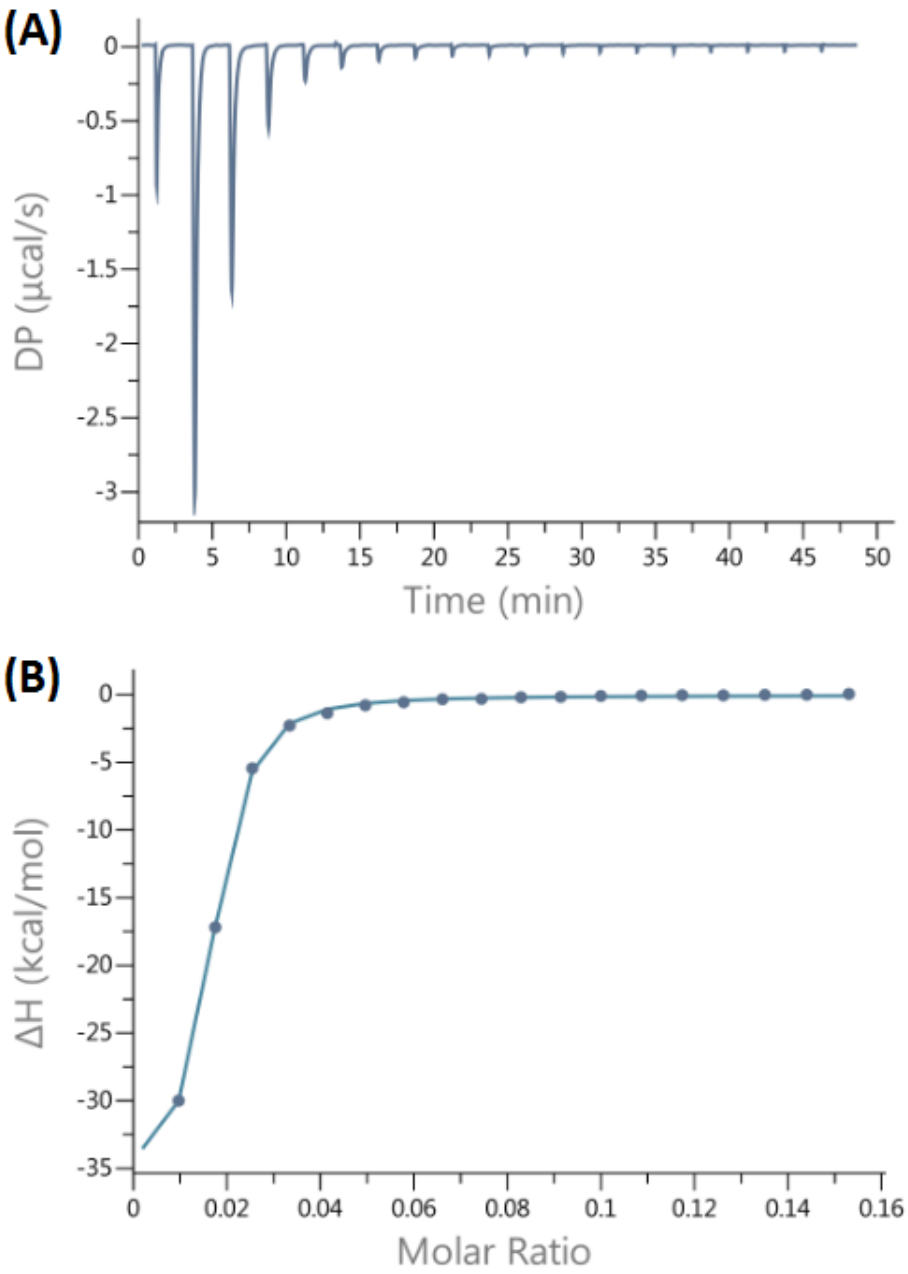

Figure A4.1 (A) The heat flow of each injection of Spm solution to citrate solution as a function of time. (B) The corresponding integration of each peak as a function of molar ratio of Spm to citrate.

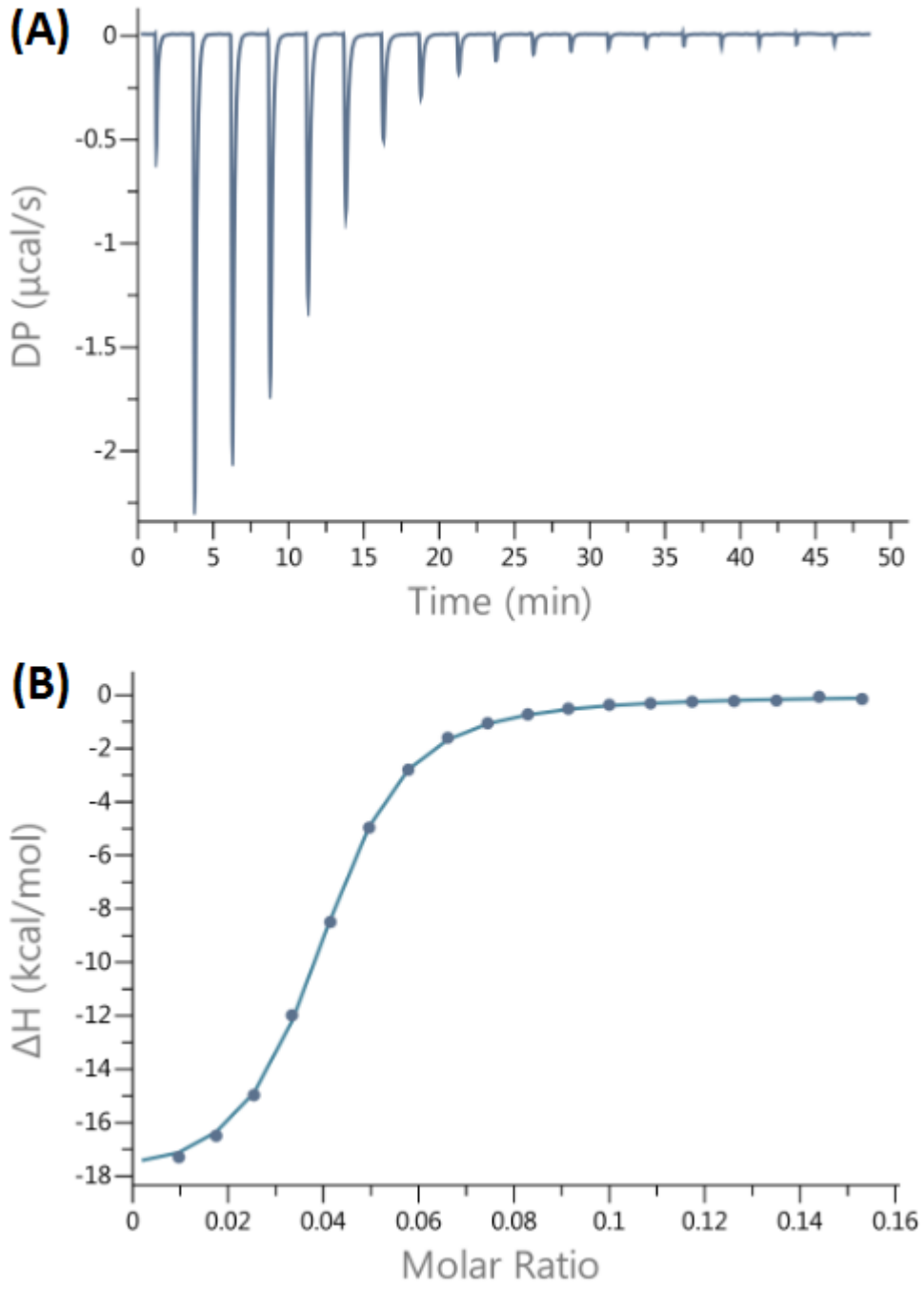

Figure A4.2 (A) The heat flow of each injection of Spd solution to citrate solution as a function of time. (B) The corresponding integration of each peak as a function of molar ratio of Spd to citrate.

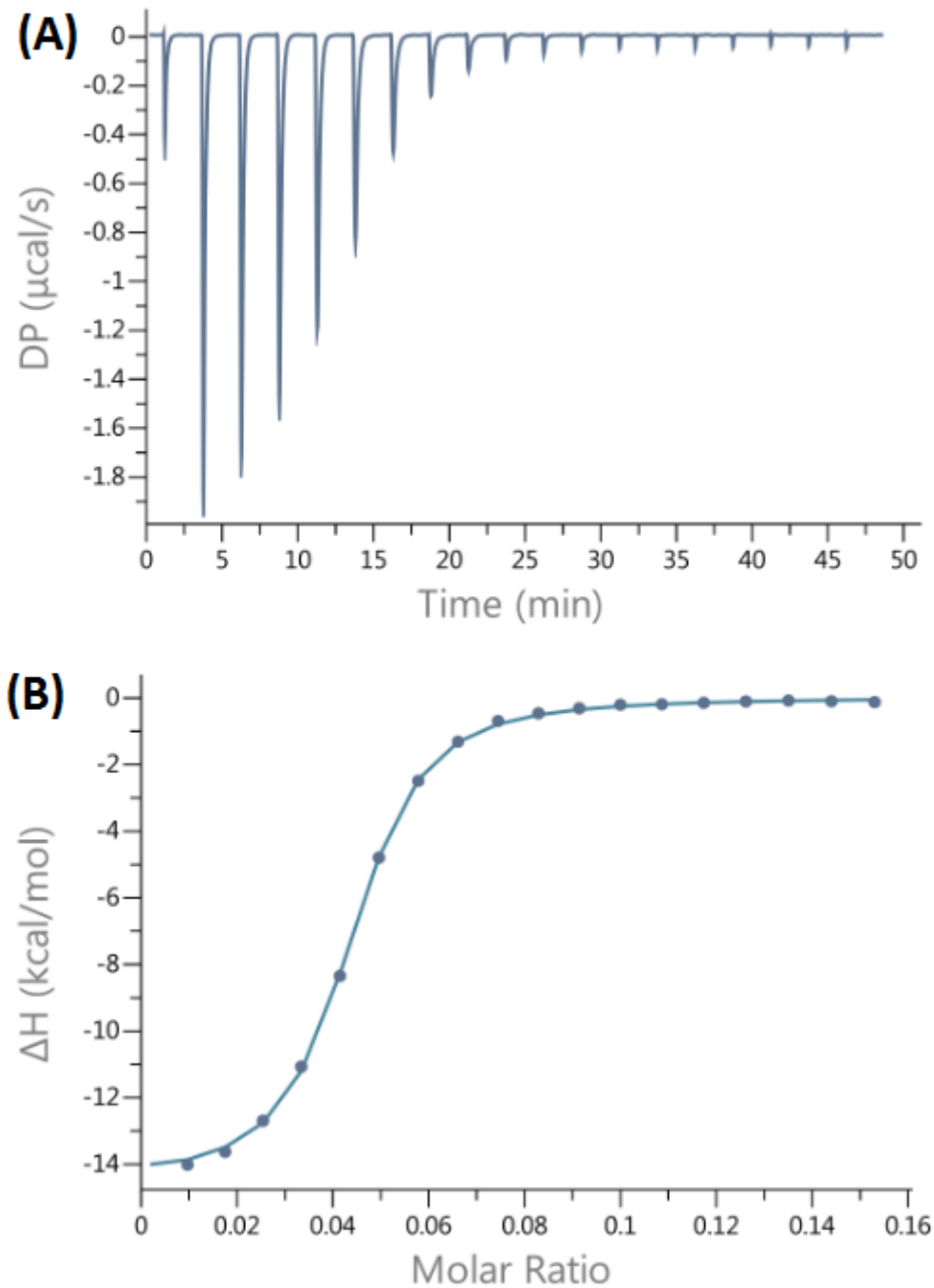

Figure A4.3 (A) The heat flow of each injection of Put solution to citrate solution as a function of time. (B) The corresponding integration of each peak as a function of molar ratio of Put to citrate.

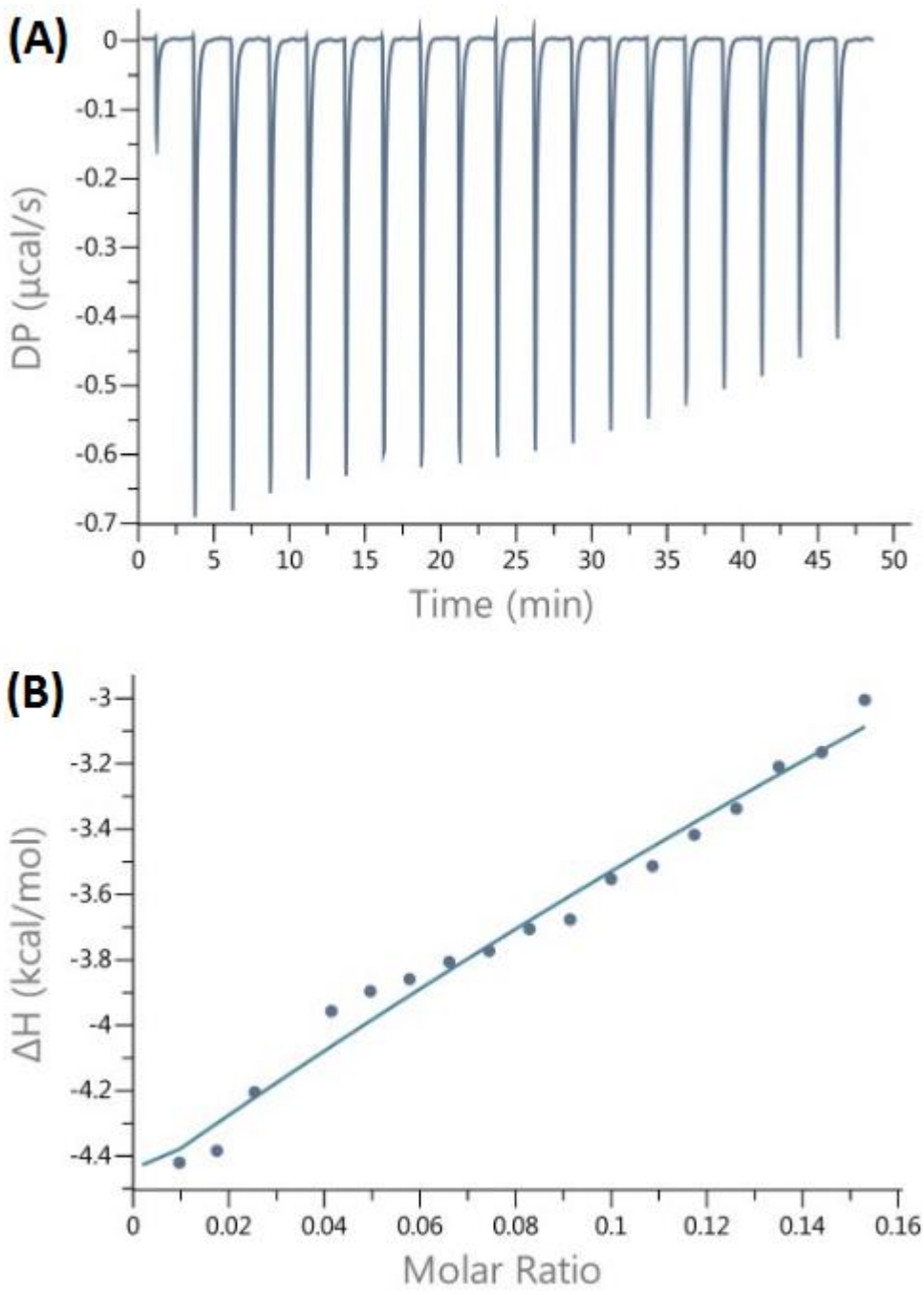

Figure A4.4 (A) The heat flow of each injection of His solution to citrate solution as a function of time. (B) The corresponding integration of each peak as a function of molar ratio of His to citrate.

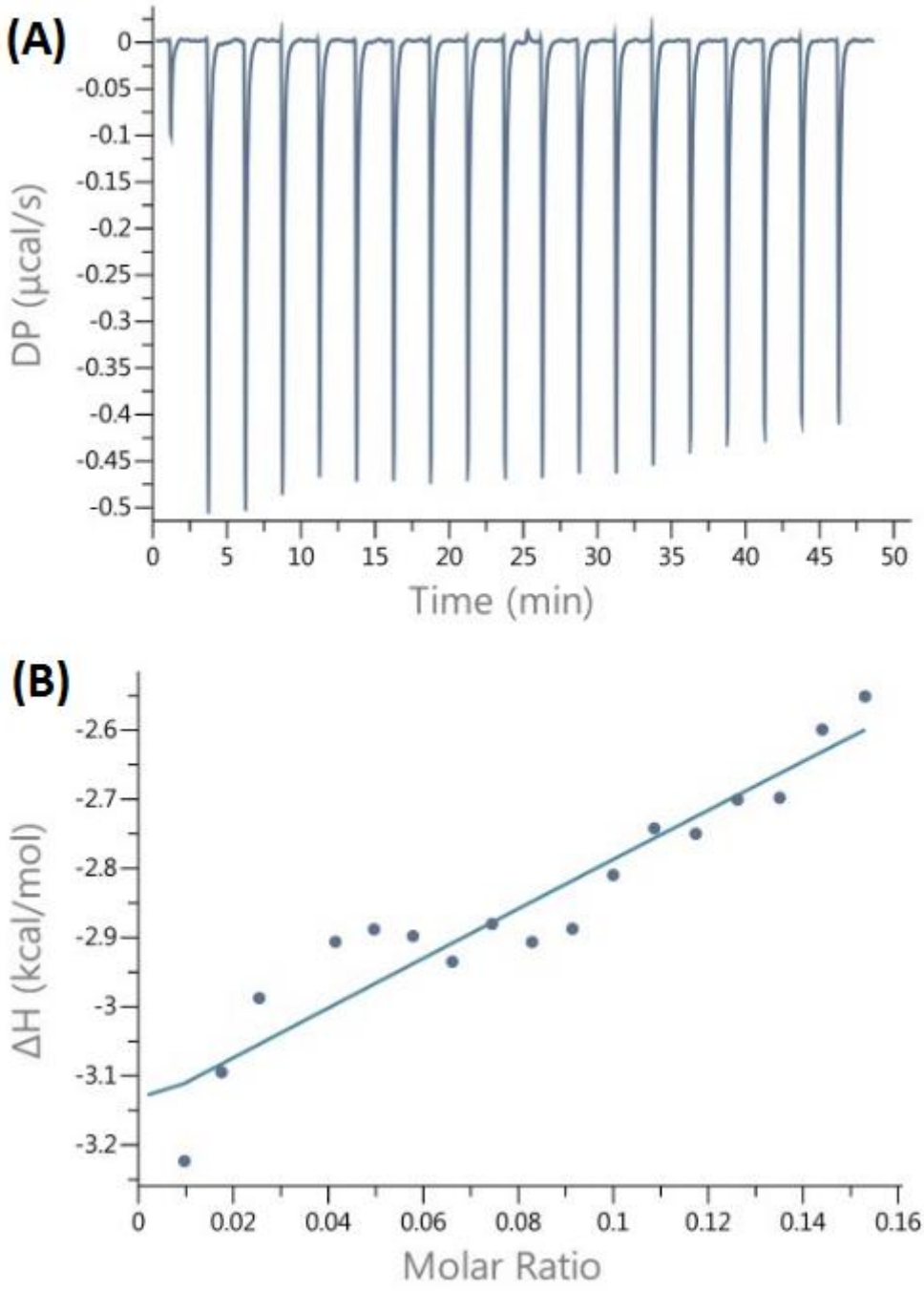

Figure A4.5 (A) The heat flow of each injection of Arg solution to citrate solution as a function of time. (B) The corresponding integration of each peak as a function of molar ratio of Arg to citrate.

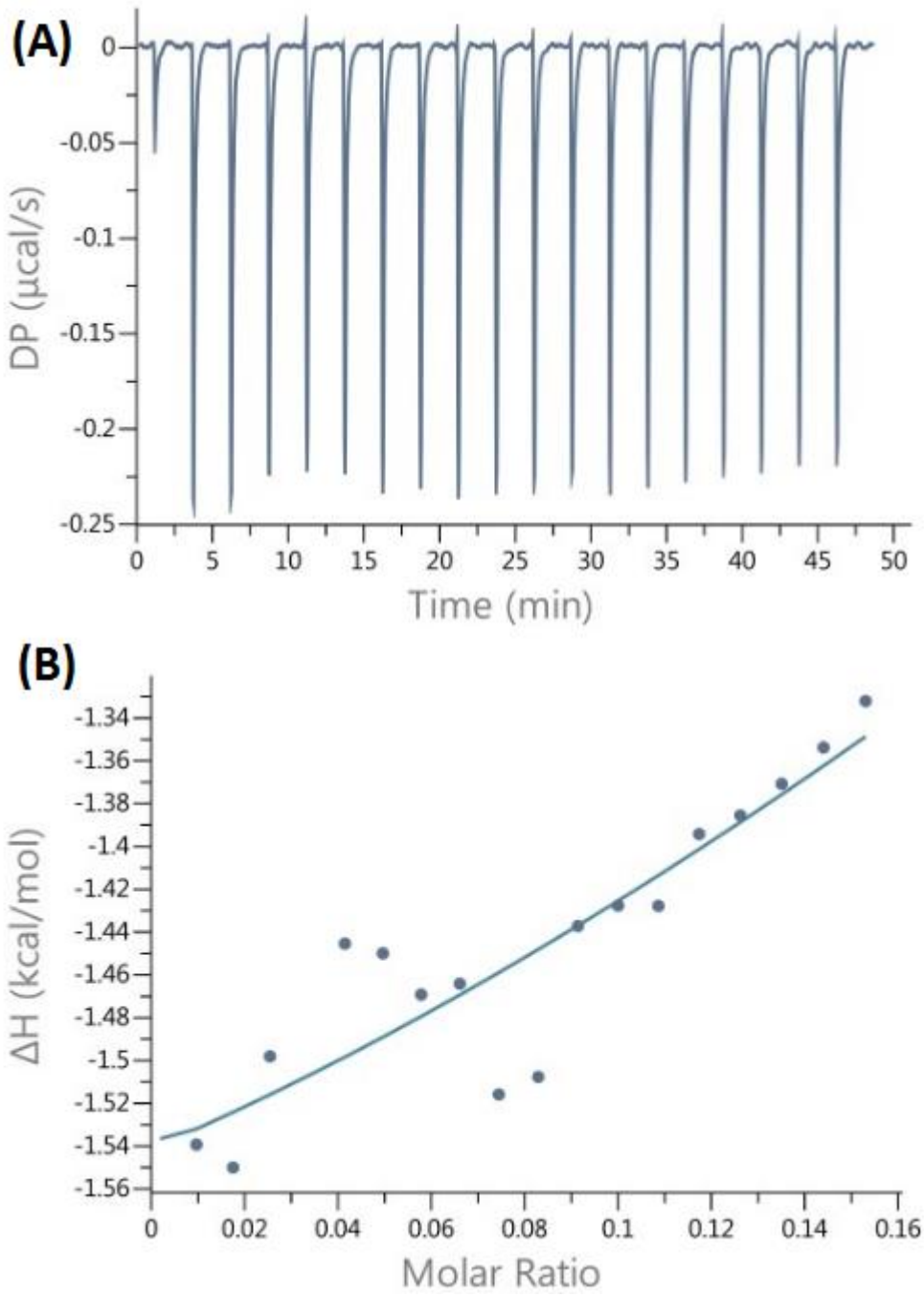

Figure A4.6 (A) The heat flow of each injection of Tyr solution to citrate solution as a function of time. (B) The corresponding integration of each peak as a function of molar ratio of Tyr to citrate.

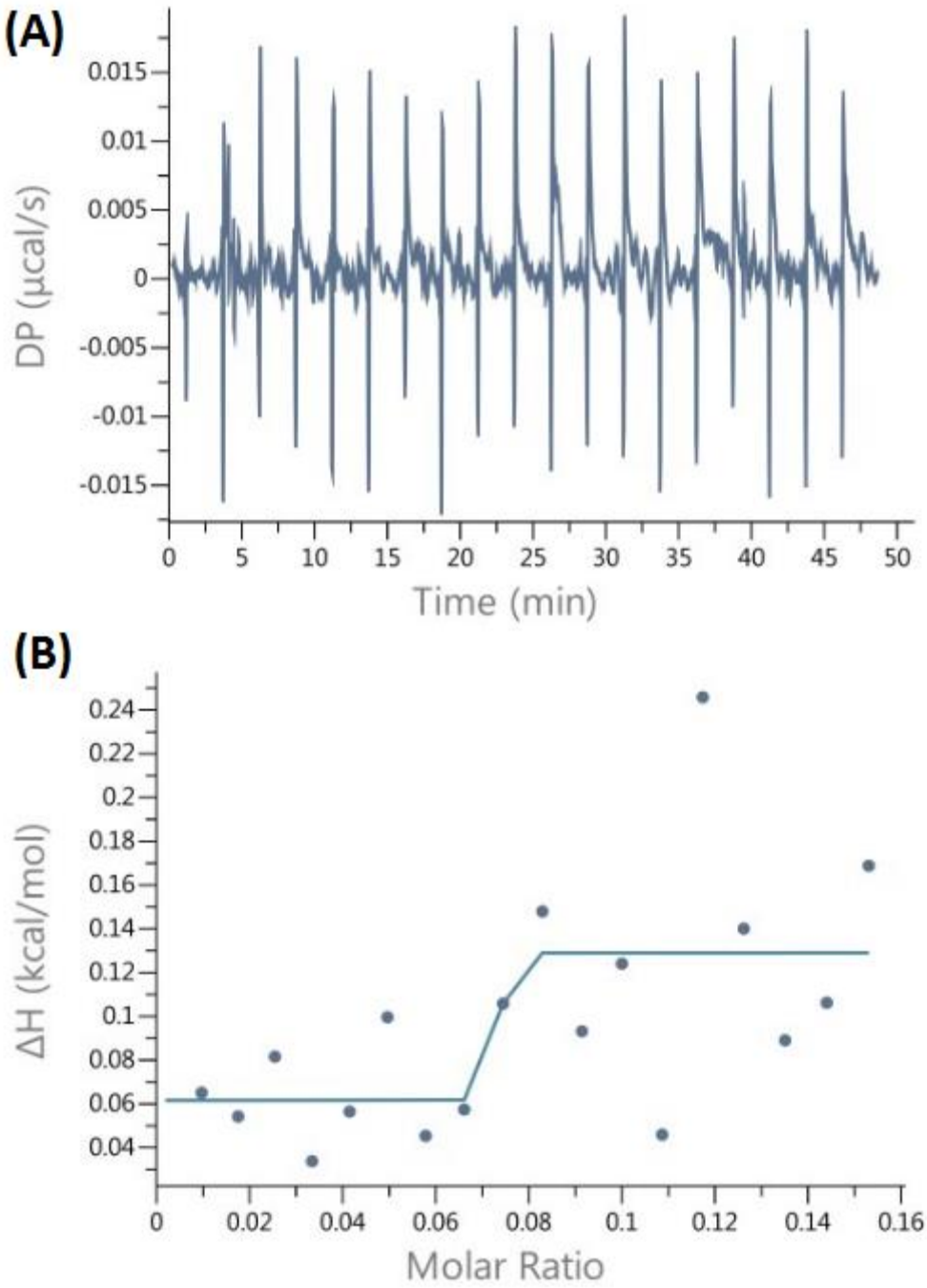

Figure A4.7 (A) The heat flow of each injection of Cad solution to citrate solution as a function of time. (B) The corresponding integration of each peak as a function of molar ratio of Cad to citrate.

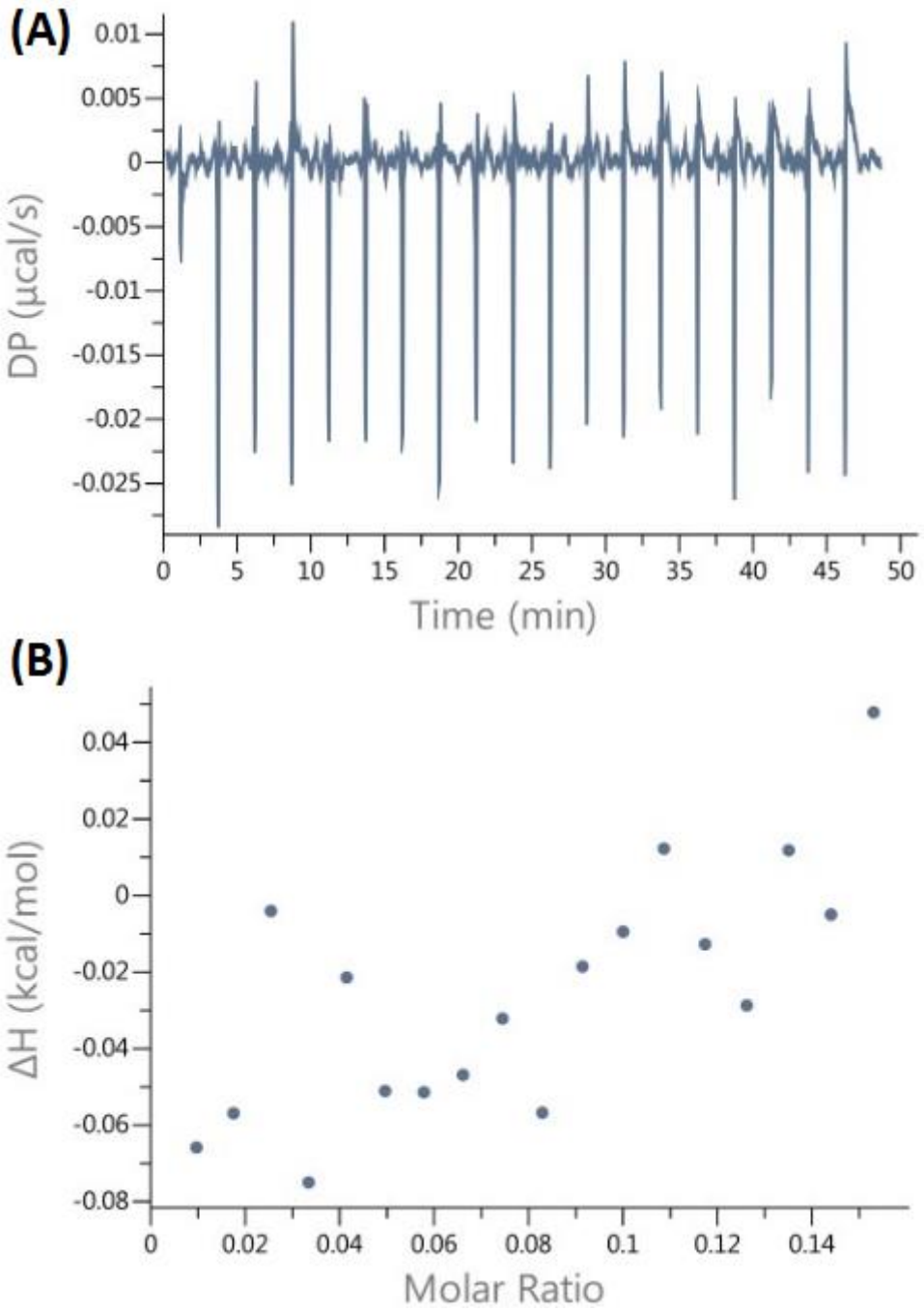

Figure A4.8 (A) The heat flow of each injection of Crea solution to citrate solution as a function of time. (B) The corresponding integration of each peak as a function of molar ratio of Crea to citrate.

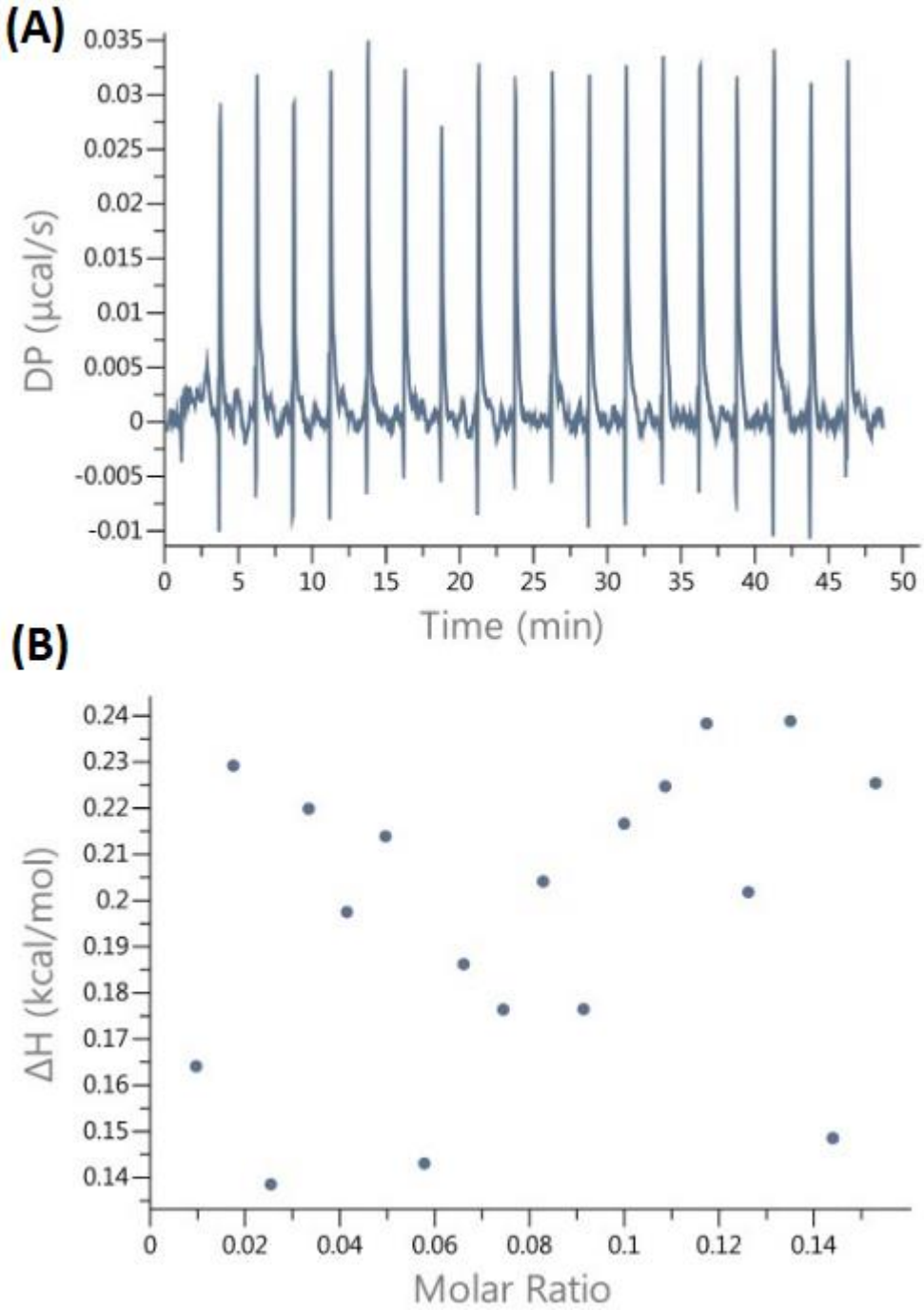

Figure A4.9 (A) The heat flow of each injection of Orn solution to citrate solution as a function of time. (B) The corresponding integration of each peak as a function of molar ratio of Orn to citrate.

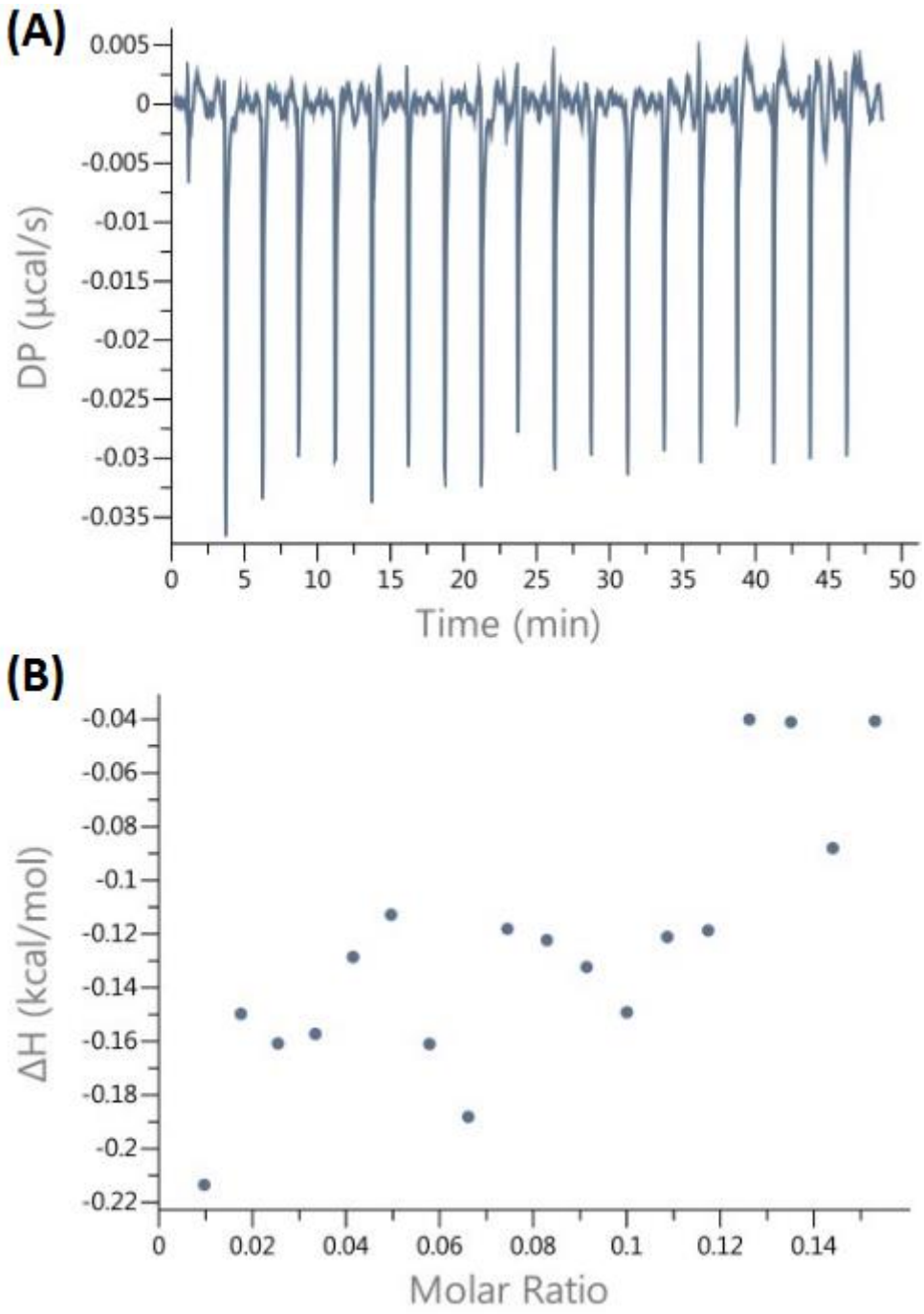

Figure A4.10 (A) The heat flow of each injection of control (water) to citrate solution as a function of time. (B) The corresponding integration of each peak as a function of molar ratio of control (water) to citrate.

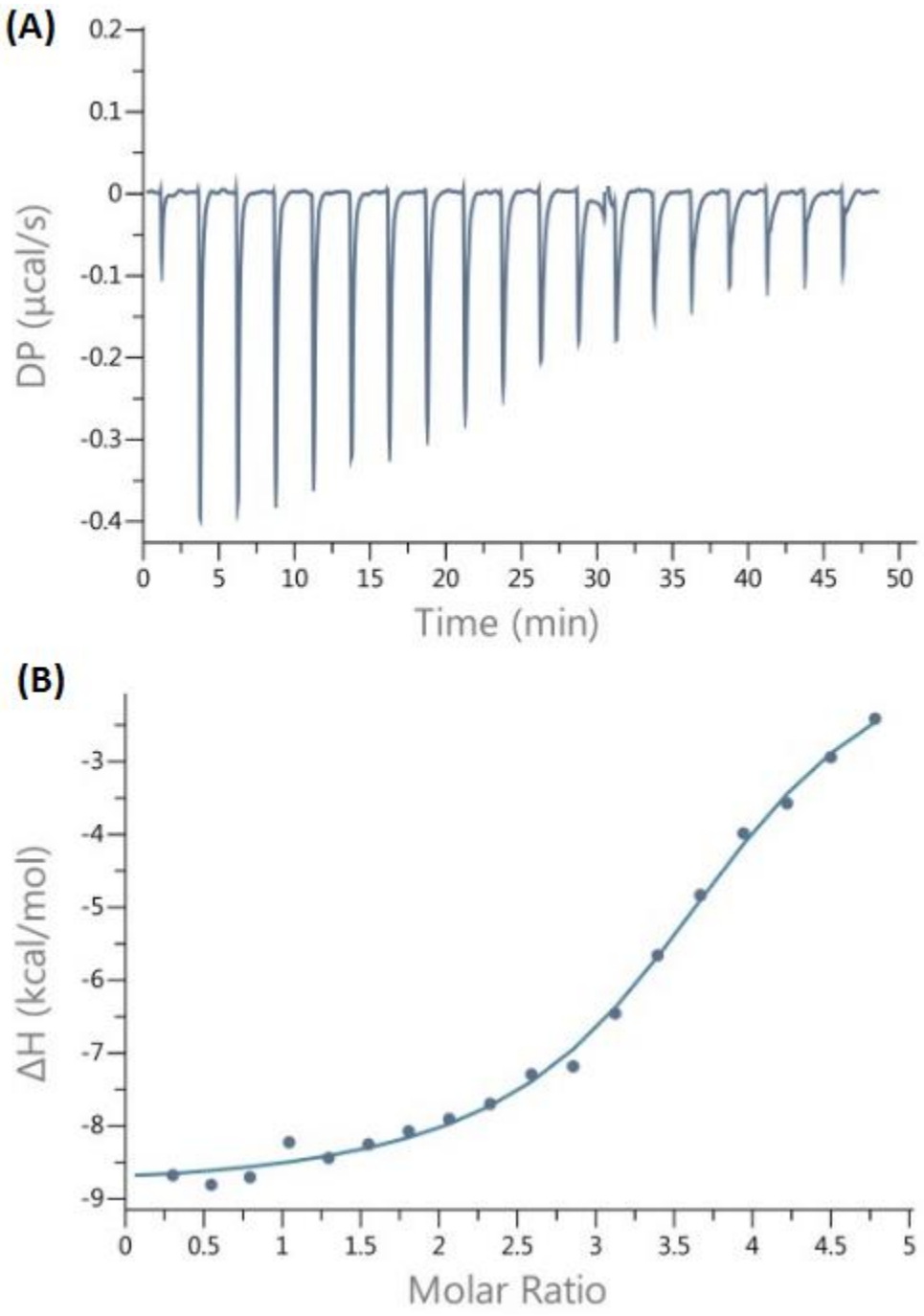

Figure A4.11 (A) The heat flow of each injection of Spm to DNA solution as a function of time. (B) The corresponding integration of each peak as a function of molar ratio of Spm to DNA.

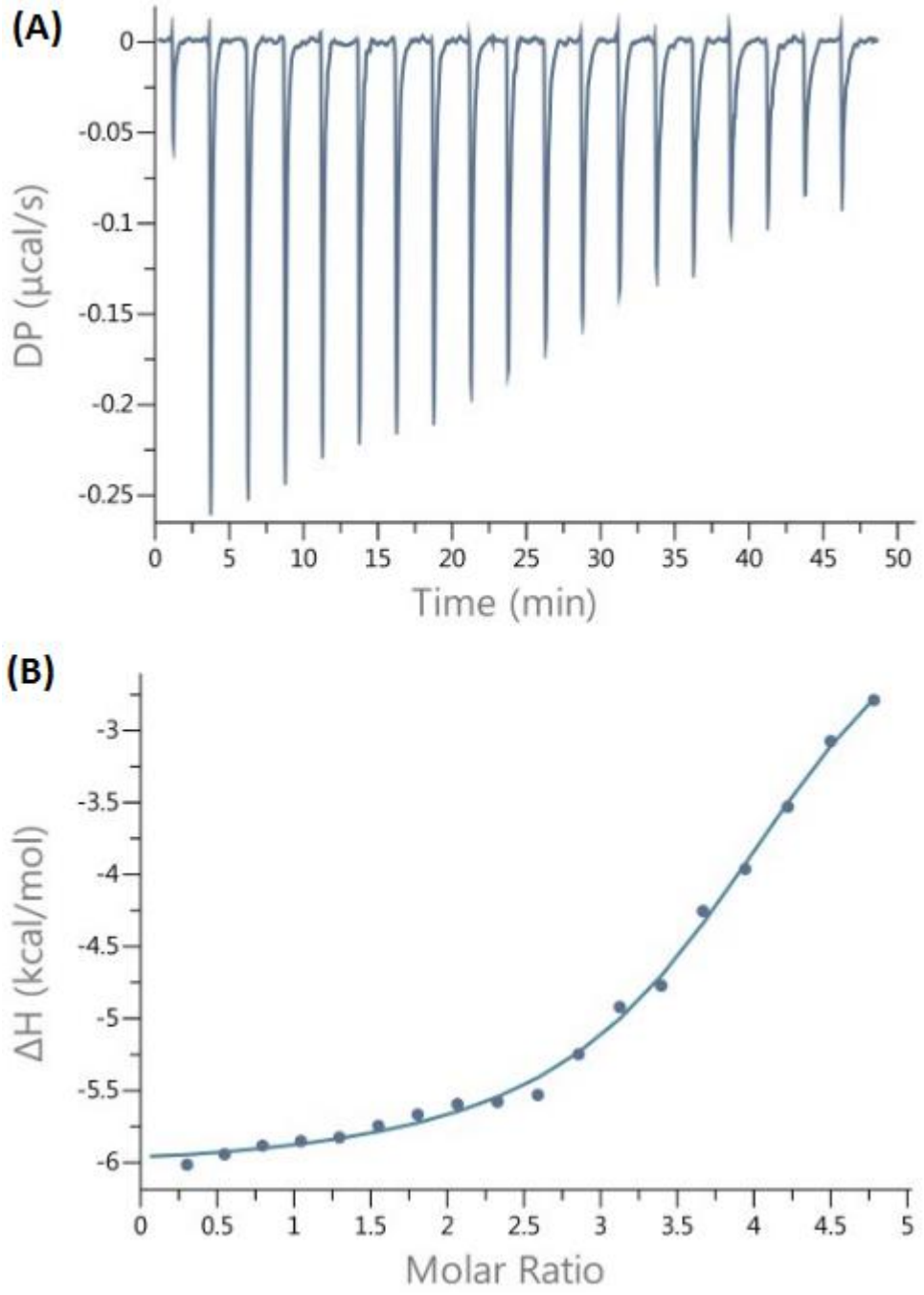

Figure A4.12 (A) The heat flow of each injection of Spd to DNA solution as a function of time. (B) The corresponding integration of each peak as a function of molar ratio of Spd to DNA.

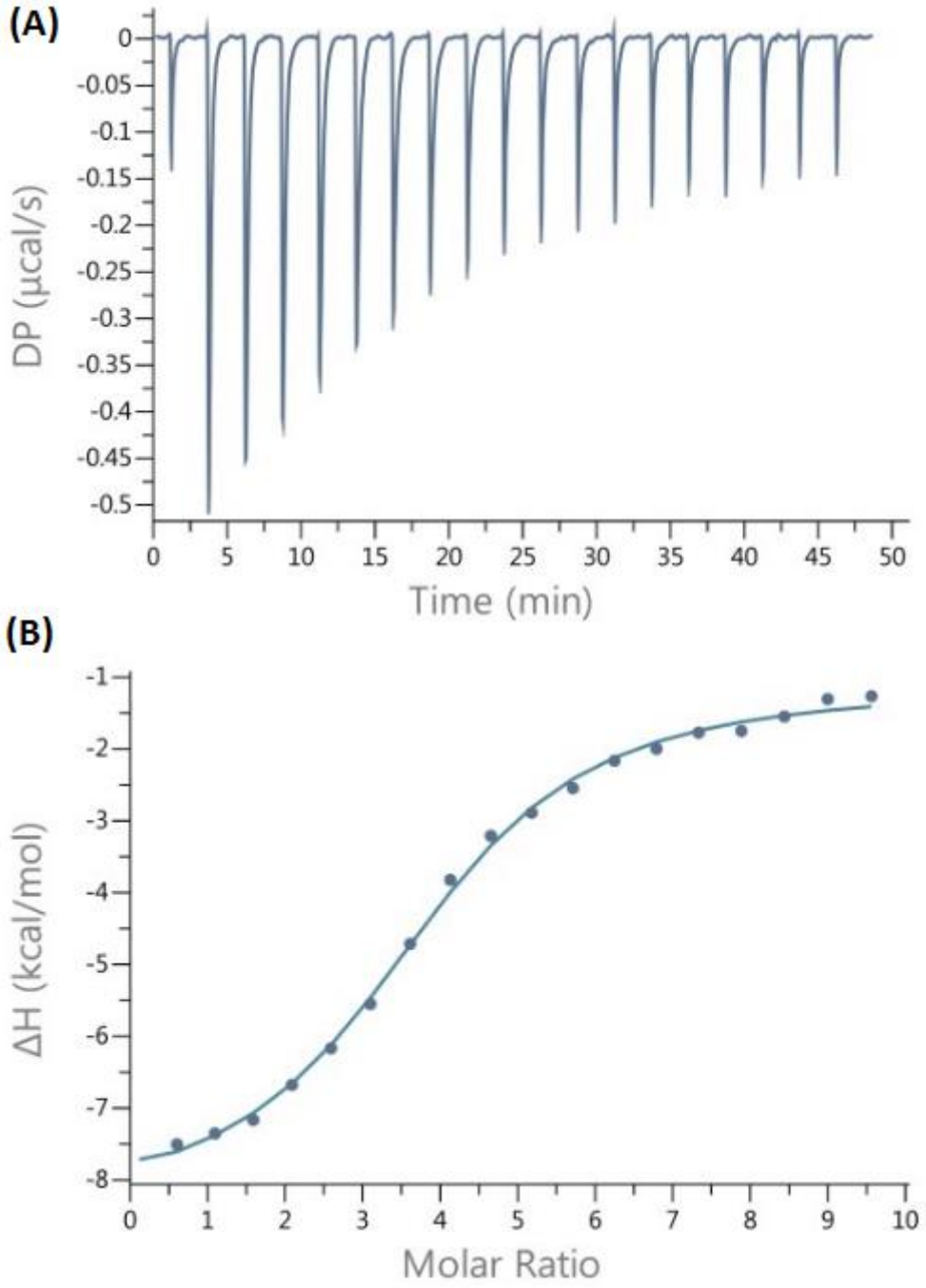

Figure A4.13 (A) The heat flow of each injection of Put to DNA solution as a function of time. (B) The corresponding integration of each peak as a function of molar ratio of Put to DNA.

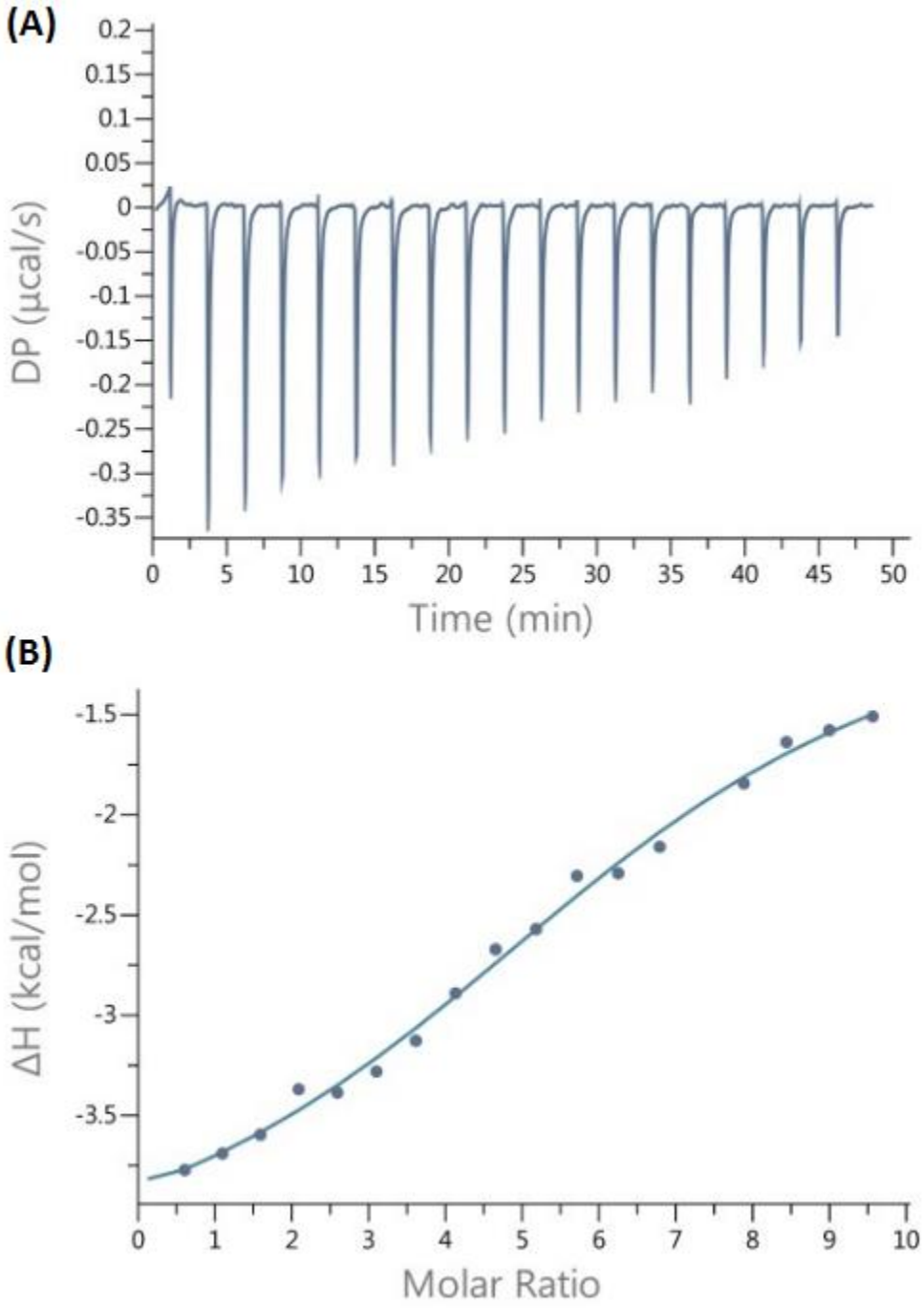

Figure A4.14 (A) The heat flow of each injection of His to DNA solution as a function of time. (B) The corresponding integration of each peak as a function of molar ratio of His to DNA.

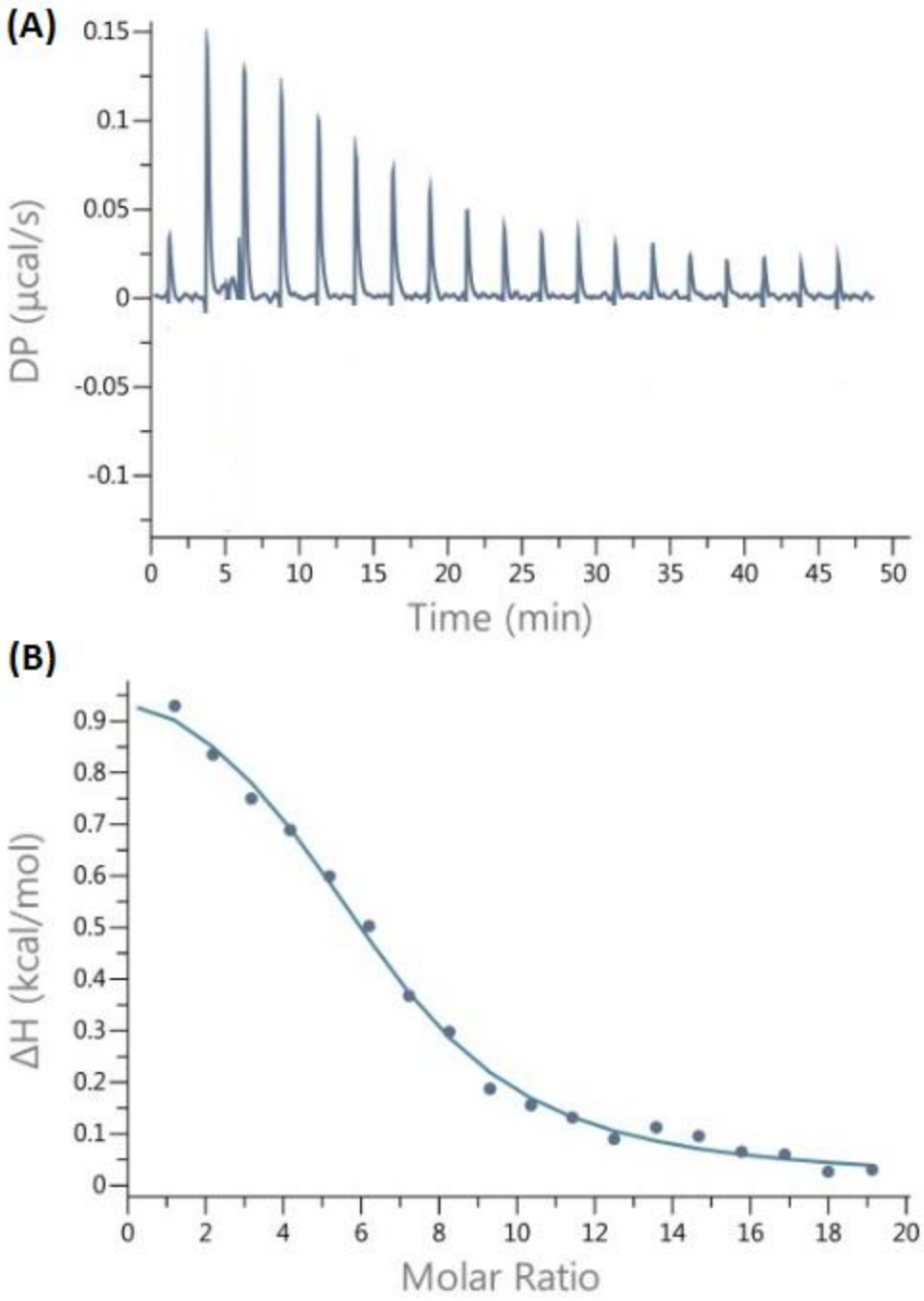

Figure A4.15 (A) The heat flow of each injection of Cad to DNA solution as a function of time. (B) The corresponding integration of each peak as a function of molar ratio of Cad to DNA.

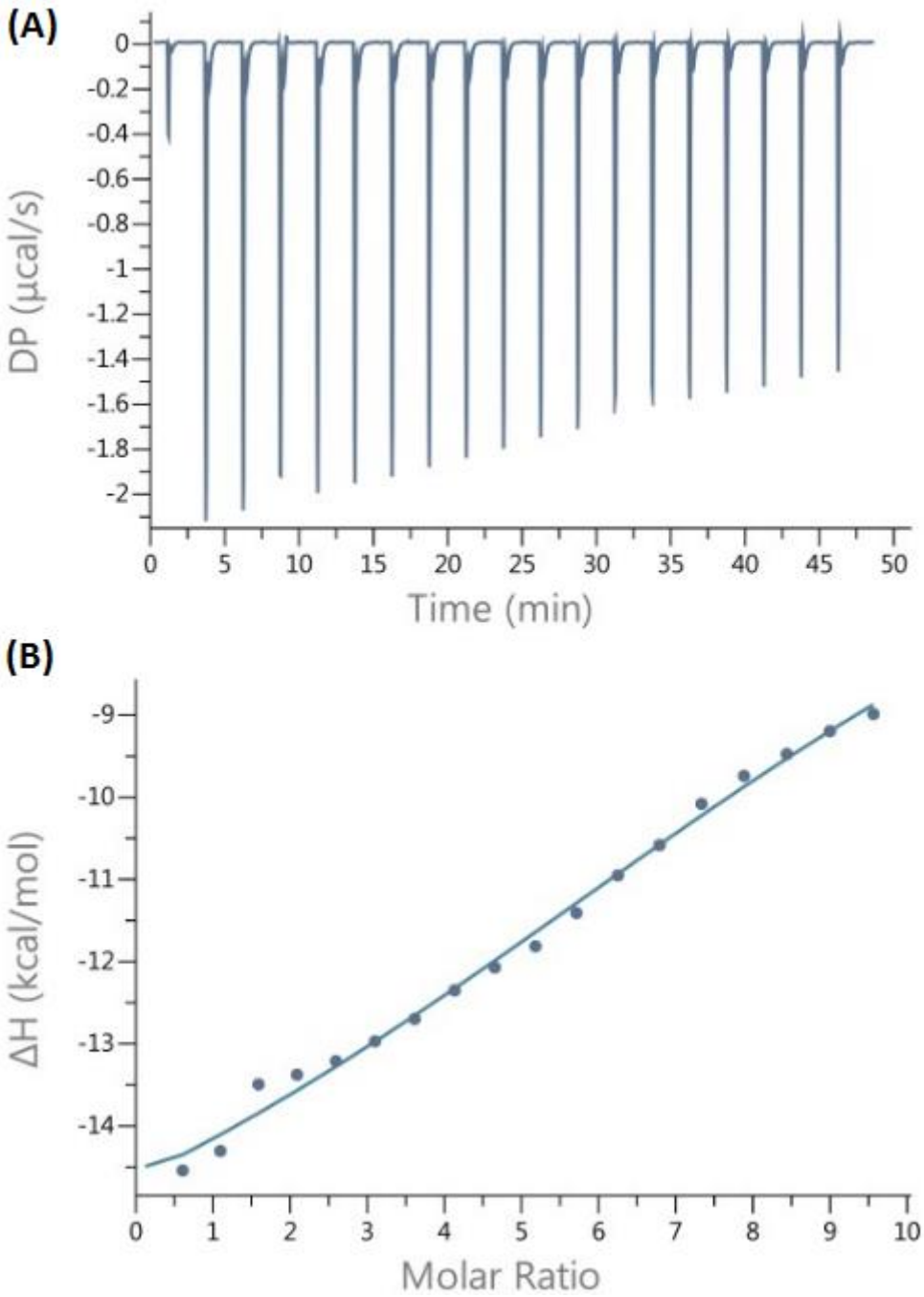

Figure A4.16 (A) The heat flow of each injection of Tyr to DNA solution as a function of time. (B) The corresponding integration of each peak as a function of molar ratio of Tyr to DNA.

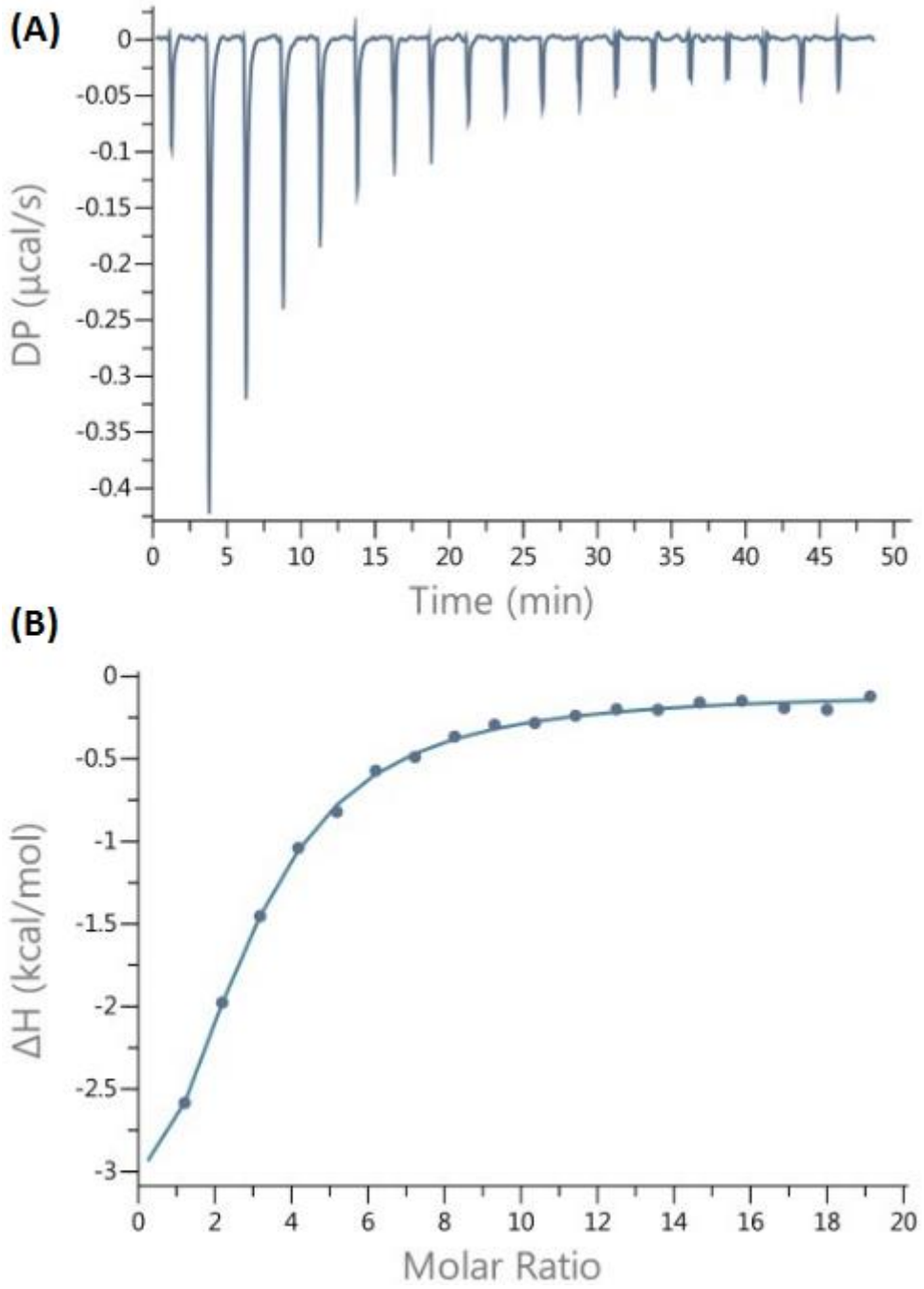

Figure A4.17 (A) The heat flow of each injection of Arg to DNA solution as a function of time. (B) The corresponding integration of each peak as a function of molar ratio of Arg to DNA.

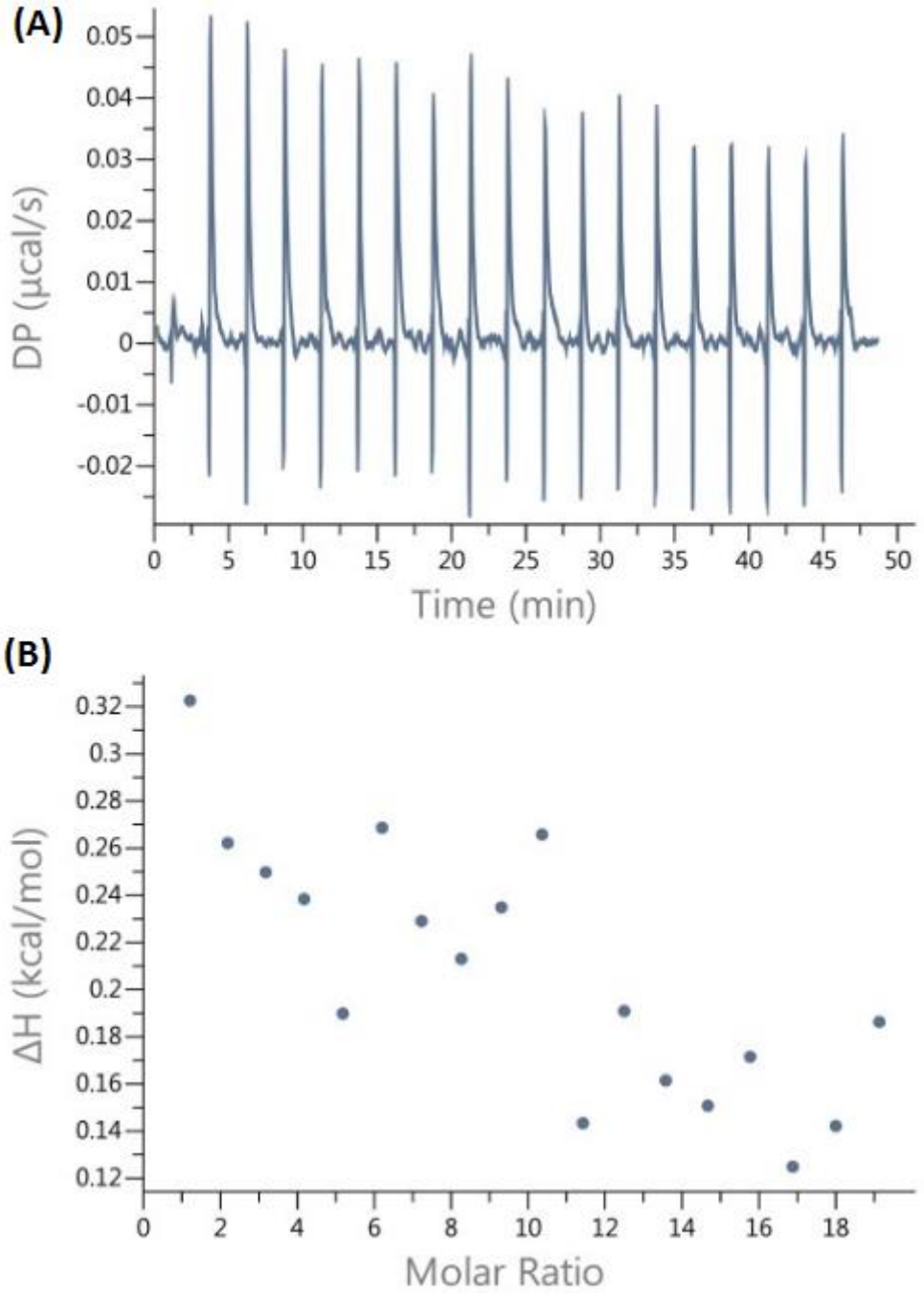

Figure A4.18 (A) The heat flow of each injection of Orn to DNA solution as a function of time. (B) The corresponding integration of each peak as a function of molar ratio of Orn to DNA.

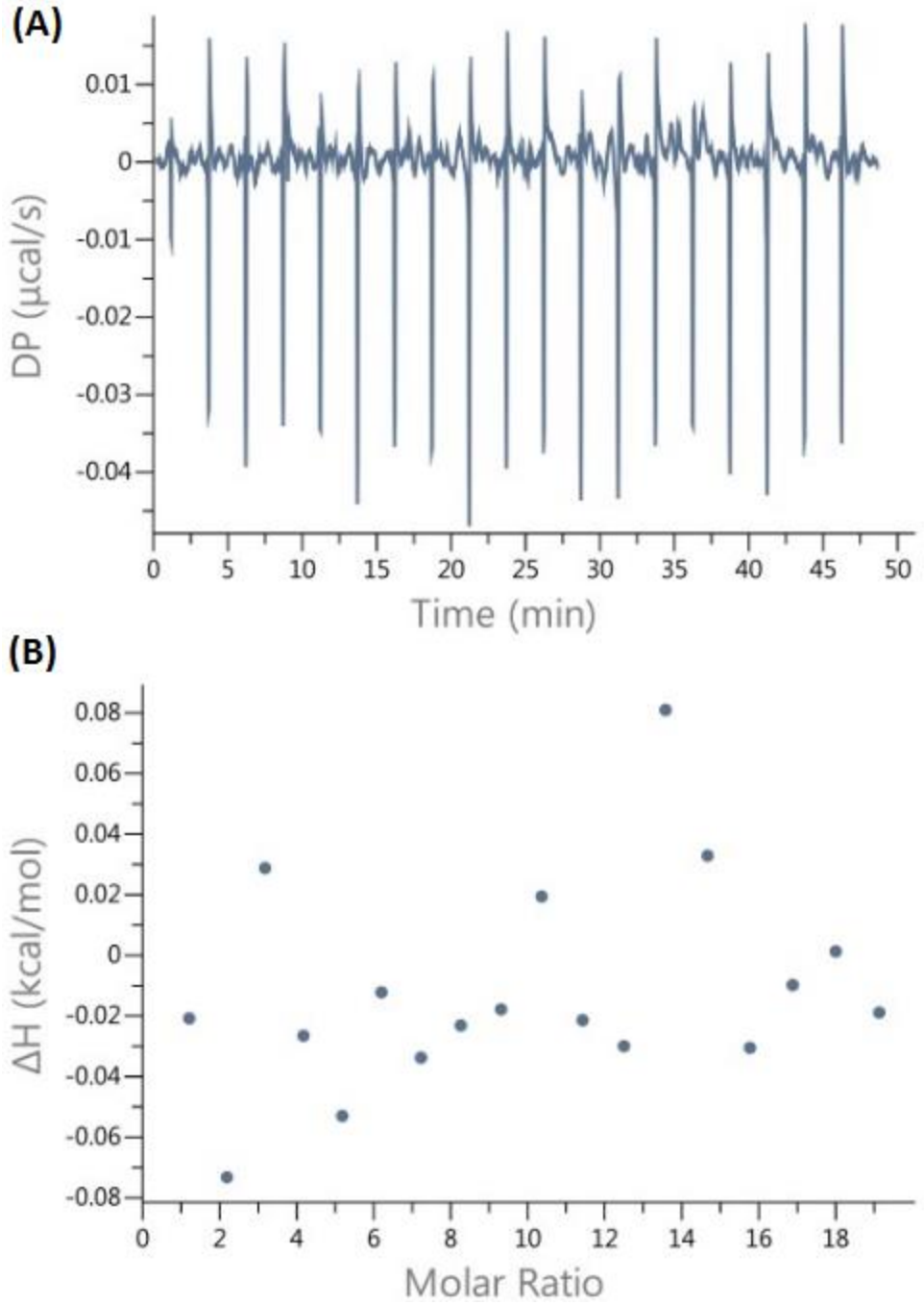

Figure A4.19 (A) The heat flow of each injection of Crea to DNA solution as a function of time. (B) The corresponding integration of each peak as a function of molar ratio of Crea to DNA.

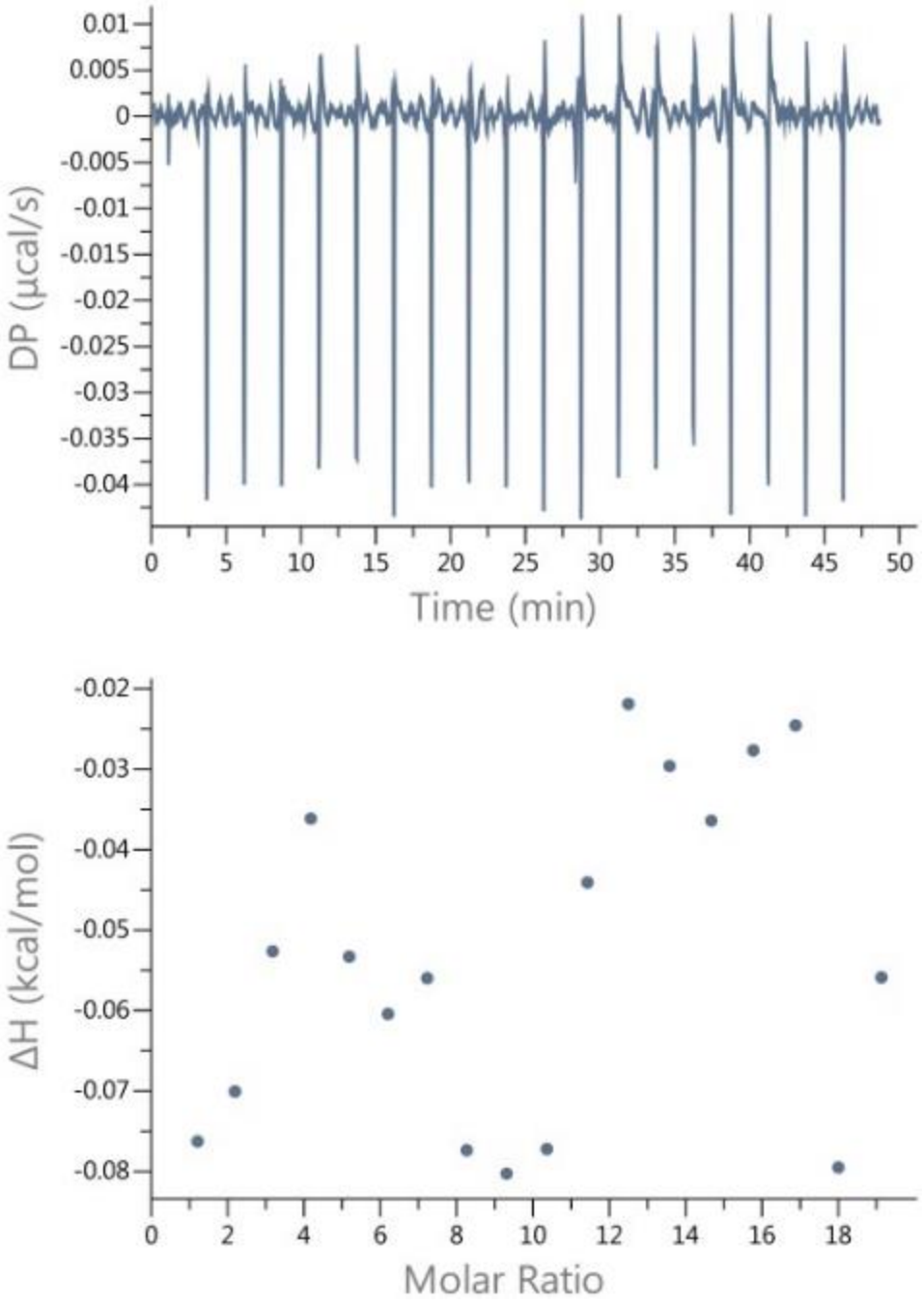

Figure A4.20 (A) The heat flow of each injection of control (water) to DNA solution as a function of time. (B) The corresponding integration of each peak as a function of molar ratio of control (water) to DNA.

CHAPTER FIVE: CONCLUSIONS AND FUTURE WORKS

To conclude on the basis of this dissertation work, two novel bio-sensing platforms for the screening of milk contaminants and prostate cancer were successfully being developed. For the former area, in Chapter Two, our effort in developing a screening method towards MEL based on the flow cytometry principle was described. It has the properties of simple, high throughput, highly sensitive and organic solvent-free. A good sensitivity and limit of detection were demonstrated to be 7.58 and 0.70ng/ml respectively. The method was validated to show it was fit for its intended purpose of screening MEL in infant formula powder, demonstrating good spike recoveries for fortified levels ranging from 0.1 to 10μg/g in six different brands. 96 samples could be analyzed within four hours. The properties of this microsphere-based assay also enable its future modification into a more efficient multi-class infant formula contaminant/adulterant screening method. We also foresee its application in other kinds of MEL-concerning matrices e.g. pet food, by employing similar matrix-match calibration approach.

For the screening of prostate cancer, in Chapter Three the potential roles of the three main urinary polyamines as PCa biomarkers were firstly evaluated. Urinary Spm demonstrated usefulness in diagnosing PCa, in particular for patients with elevated serum PSA level, upon comparison of their levels in cancerous and non-cancerous cases. Results were comparable to the gold standard reference method TRUSPB with a good AUC value of 0.83±0.03. Relative sensitivity and specificity were 84.85% and 67.68% respectively. This work takes a step towards tackling the current medical challenge of poor specificity of the serum PSA test.

To further confirm its usefulness, future work will be focused on several ways: enlarging the validation group through collecting urines from multi-center; performing a continuous follow-up monitoring on Spm level of suspected PCa patients and collecting post-prostate massage urines which more specifically reflects the situation of prostate rather than whole body as a proof-of-concept experiment.

Last but not least, in Chapter Four, a smart and flexible aptasensor for Spm sensing simply by using the very common citrate-AuNPs and DNA aptamer for adsorption were reported. Depending on the situation, users could flexibly tune the DNA concentration and the AuNPs would respond to concentration Spm via two different pathways: When working in a comparatively clean matrix, a low DNA loading concentration was sufficient to protect AuNPs such that it could provide a high sensitivity for Spm sensing. DNA-AuNPs will respond to it through the red-shifting of plasmonic band as the result of aggregation. When working in a complicated matrix like artificial urine, a high DNA loading concentration could provide a better protection to AuNPs. The absorbance of plasmonic band would decrease gradually with a higher Spm concentration, which were accounted by a greater extent of DNA adsorption as well as precipitation of AuNPs. Different factors' effects were also comprehensively studied. Comparing to the target-mediated crosslinking mechanism, the use of non-thiolated DNA for preparing DNA-AuNPs was more easy, convenient and cost-effective. Good applicability in complicated urine matrices was also proven by the

satisfactory results obtained in spike analysis. We foresee this novel approach to be a fast and practical kit towards Spm for secondary prostate cancer screening. Possible future works include the development of a better pre-treatment approach on urine samples such that the kit can be a point of care fast detection kit but not just a laboratory-based method, and modification of the type of surficial ligands on AuNPs to modulate the aptasensor's performance. (Figure 5.1) A comprehensive clinical urine samples analysis by standard addition approach for determining original urinary Spm content is also to be carried out.

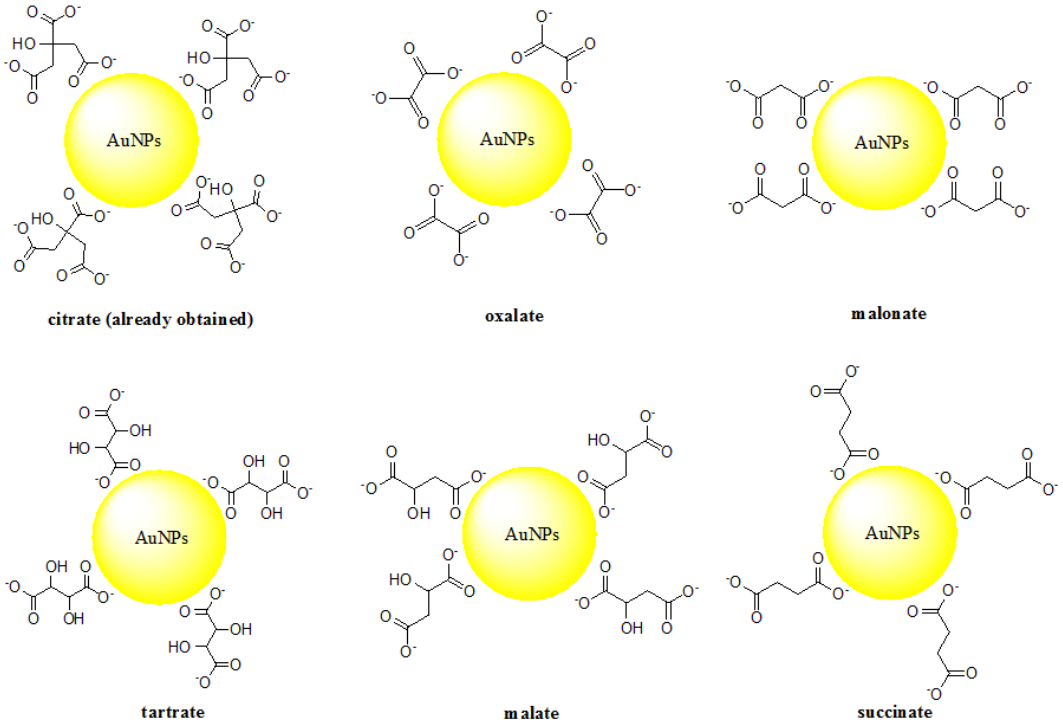

Figure 5.1 Proposed AuNPs with different surfactants for Spm interaction.

Taken into consideration that Spm is a multi-cationic ion with a small and linear shape, the design of our aptasensor only rely on its cationic characteristics.

To develop a fast and non-invasive cancer screening test, another direction is to develop a sensing system incorporating its structural characteristics. One research direction is to tailor make a metal organic framework (e.g. lanthanide metal ion based) such that the framework will contain lots of cationic coordination sphere for spermine penetration specifically. Such penetration into the framework and subsequent coordination with lanthanide ions is predicted to provide a change in absorbance of organic linker as well as lanthanide emission, thus providing an interesting dual sensing approach towards this novel biomarker.